Structural characterization of reaction intermediates of HECT-mediated ubiquitin transfer

Dissertation

der Mathematisch-Naturwissenschaftlichen Fakultät

der Eberhard Karls Universität Tübingen

zur Erlangung des Grades eines

Doktors der Naturwissenschaften

(Dr. rer. nat.)

vorgelegt von

Dipl. Biol. Magnus Jäckl

aus Tettnang

Tübingen 2018

Gedruckt mit der Genehmigung der Mathematisch-Naturwissenschaftlichen Fakultät der Eberhard Karls Universität Tübingen.

Tag der mündlichen Qualifikation:	29.10.2018
Dekan:	Prof. Dr. Wolfgang Rosenstiel
1. Berichterstatter:	Dr. Silke Wiesner
2. Berichterstatter:	Prof. Dr. Thilo Stehle

Summary

The ubiquitination reaction is a post-translational modification in which the small protein ubiquitin (Ub) is attached to a substrate protein. The attachment of Ub onto a substrate generates a signal for the cell e.g. leading to the degradation of the substrate by the proteasome. Ub fulfils therefore a wide array of cellular functions and regulatory circuits. The Ub reaction is mediated by an enzymatic cascade involving three enzymes called E1, E2 and E3.

HECT (Homologues to E6-AP) -type-ubiquitin E3 ligases define the specificity for the substrate protein as well as determine the Ub chain linkage. Hence, HECT ligases control the output signal of the ubiquitination reaction. The HECT domains consist of two lobes. The C-lobe contains the catalytic cysteine (Cys) which forms an intermediate Ub-thioester during the Ub reaction. However, the N-lobe possesses a ubiquitin binding surface (UBS) which is involved in the Ub-reaction by binding the Ub non-covalently.

The C-lobe can adopt various orientations with respect to the N-lobe. This flexibility of the C-lobe is essential during the Ub transfer reaction and is also involved in HECT domain inhibition. Mutations in HECT E3s are linked to various human diseases i.e. cancer where HECT E3s either act as oncoproteins or tumor suppressors. Therefore, it is important to understand the mechanistic details and regulation of the Ub transfer mediated by the HECT E3 ligases.

Here, I present a method to form disulfides mimicking intermediates of the ubiquitination reaction of HECT domains utilizing chemically activated ubiquitin. With this method it is possible to bypass the highly instable thioester between the catalytic cysteine and the C-terminus of the Ub. This enables the study of otherwise unstable and inaccessible intermediates of the ubiquitination transfer reaction on a structural level by biophysical methods e.g. NMR spectroscopy.

With this method in hand, I was able to study the first step of the HECT mediated Ub transfer in which the Ub is bound to the catalytic cysteine of the HECT domain. This enabled the discovery of a β-sheet augmentation during Ub transfer between the HECT C-lobe and the C-terminus of Ub. Of note, I was able to show for the first time that this β-sheet augmentation is conserved among the different HECT E3 families.

In addition, I could identify a novel auto-inhibition mechanism of the Huwe1 HECT domain in which the non-covalent Ub binding surface (UBS) of the Huwe1 HECT domain is blocked by the Huwe1 HECT domain C-lobe. Moreover, I was able to show that during the thioester formation a large rearrangement in the HECT domain occurs which subsequently allows the binding of Ub to the UBS of Huwe1. Hence, the thioester intermediate adopts an open conformation. Furthermore, I identified residues on the C- and N-lobe interface responsible for the auto-inhibition. Mutations of those residues resolve the auto-inhibition and are able to accelerate the ubiquitination reaction. In contrast, mutations in the UBS impair Huwe1 activity thereby providing further evidence of the importance of the UBS during ubiquitination.

The data presented here enable new insights into the mechanism of the Ub-transfer mediated by the HECT E3 ligases and furthermore lead to a better understanding of the Ub reaction.

Zusammenfassung

Ubiquitinierung ist eine posttranslationale Modifikation, bei der Ubiquitin kovalent mit einem Substratprotein verknüpft wird. Ist Ubiquitin (Ub) an ein Substratprotein gebunden, kann dies ein Signal für die Zelle z.B zum Abbau des markierten Substratproteins durch das Proteasom sein. Die Ubiquitinierung spielt, durch ihren Signal- und den damit einhergehenden Regulationscharakter, eine entscheidende Rolle in einer Vielzahl von zellulären Prozessen. Bei der Übertragung von Ubiquitin auf ein Substratprotein sind drei Enzyme beteiligt: E1, E2 und E3.

Hierbei haben die HECT E3 Ligasen (E3s) eine besondere Bedeutung. Sie sind nicht nur für die Substratspezifität verantwortlich, sondern legen auch die Verknüpfung von Ubiquitin fest. Daher kontrollieren HECT-Ligasen das Endergebnis der Ubiquitinierung, welches wiederum das Schicksal des Substrats definiert. Die HECT-Ligasen besitzen eine HECT-Domäne, diese kann wiederum in zwei Einheiten unterteilt werden. Die C-Einheit mit dem katalytischen Cystein, welches eine intermediäre Thioesterbindung mit Ub ausbildet, sowie der N-Einheit mit einer nicht-kovalenten Ubiquitin-Bindungsstelle (UBS). Die C-Einheit ist durch einen Linker mit der N-Einheit verbunden, wodurch beide Einheiten hoch flexible gegenüber einander sind. Diese Flexibilität ist nicht nur notwendig bei der Ub-Transfer-Reaktion sondern spielt auch eine entscheidende Rolle bei der Inhibierung der HECT-Ligasen. In einer Vielzahl von Studien wurde ein Zusammenhang mit fehlerhafter Expression oder Mutation von HECT-E3-Ligasen und verschiedenen Krankheiten, unter anderem Krebs, festgestellt. Daher ist es unabdingbar, die mechanistischen Details, die der Ubiquitinierungsreaktion zu Grunde liegen, sowie deren Regulation lückenlos aufzuklären.

Um sich die mechanistischen Grundlagen der Ubiquitinierungsreaktion detailliert anschauen zu können, muss der instabile Thioester, der während des Ub-Transfers auf die HECT-E3-Ligase entsteht, umgangen werden. In dieser Arbeit konnte ich den Thioester durch eine Disulfidbindung zwischen Ub und HECT-Domäne imitieren. Dafür habe ich eine Methode etabliert und verfeinert, bei der Ubiquitin chemisch aktiviert wird und nachfolgend eine Disulfidbrücke mit der HECT-Domäne bildet. Mittels dieser Disulfide konnte ich die sonst unzugänglichen Reaktionsintermediate auf struktureller Ebene mit der Hilfe von biophysikalischen Methoden, wie z.B. NMR-Spektroskopie, untersuchen. Dadurch war es mir möglich den ersten Schritt der

Ubiquitinierungsreaktion, den Transfer des Ub auf das katalytische Cystein der C-Einheit der HECT-Domäne, im Detail zu betrachten. Hier konnte ich zeigen, dass die Interaktion zu Bildung eines zusätzlichen β-Faltblatts seitens des Ub führt. Desweitern konnte ich durch NMR-Spektroskopie, Kristallographie und Mutationsstudien zeigen, dass diese Interaktion zwischen den verschieden HECT Familien konserviert ist.
Im letzten Teil meiner Doktorarbeit habe ich mich mit der HECT-Domäne der HECT Ligase Huwe1 auseinandergesetzt. Hier konnte ich durch NMR-Spektroskopie nachweisen, dass die UBS von der Huwe1 HECT-Domäne für Ub nicht zugänglich ist und durch die C-Einheit der HECT-Domäne blockiert wird. Dies stellt einen bis dahin unbekannten Autoinhibitionsmechanismus der Huwe1 HECT-Domäne dar. Des Weiteren konnte ich zeigen, dass eine starke Konformationsänderung während der Thioesterbildung zwischen der C- und N-Einheit der Huwe1 HECT-Domäne auftritt. Durch diese Konformationsänderung kann nun Ub an die UBS binden und die Huwe1 HECT-Domäne nimmt eine offene Konformation ein. Desweitern lässt sich die Konformationsänderung und Öffnung der HECT-Domäne durch Mutationen in der Bindungsoberfläche zwischen der C- und N- Einheit hervorrufen. Diese Mutationen führen zu einer Reaktionsbeschleunigung der Ub-Reaktion. Im Gegensatz dazu beeinträchtigen Mutationen in der UBS die Ub-Reaktion. Dies wiederum hebt die Bedeutung der UBS während der Ubiquitinierungsreaktion hervor.

Insgesamt gesehen helfen die in dieser Doktorarbeit vorgestellten Ergebnisse die Ub-Reaktion und die zugrundeliegenden mechanistischen Details besser zu verstehen.

Table of Contents

Summary 1

Zusammenfassung 3

Table of Contents 5

List of abbreviations and symbols 11

Table of Figures 15

List of Tables 19

1. Introduction 20

1.1. Ubiquitin 20

1.1.1. The mechanism of ubiquitin conjugation 20

1.1.2. Cellular functions of ubiquitination 21

1.1.3. Ubiquitin and the proteasome 25

1.2. E3 ligases 27

1.2.1. The classification of the E3 ligases 27

1.2.2. RING E3-ligases 28

1.2.2. RBR-domain E3-ligases 28

1.2.3. HECT E3-ligases 29

1.3. The HECT E3-ligase in detail 30

1.3.1. The catalytic mechanism of HECT domains 30

1.3.2. HECT E3 families 34

1.3.3. Nedd4 family 36

1.3.4. HERC-family 37

1.3.5. SI(ngle) HECT-familiy 38

1.3.6. Regulation of the HECT-type E3 ligases 39

2. Aims and significance of the project 41

3. Nuclear magnetic resonance spectroscopy: A tool to study protein interactions and structure 43
3.1. Basics of NMR spectroscopy 43
3.2. HSQC experiment 46
3.3. TROSY experiment 47
3.4. Methyl TROSY HMQC experiment 47
3.5. Protein-protein interaction studies by NMR spectroscopy 47
3.6. Observing conformational changes by NMR spectroscopy using paramagnetic relaxation enhancement (PRE) 50
3.7. Methyl resonance assignments 52
4. X-ray crystallography 53
4.1 The protein crystal 53
4.2. X-ray diffraction 53
5. Results 56
5.1. Disulfide formation as a powerful tool to study reaction intermediates in HECT-mediated ubiquitin transfer 56
5.1.1. Introduction 56
5.1.2. Results 59
5.1.3. Workflow for the DTNB-catalysed formation of disulfide bonds between Ub and ubiquitination enzymes 59
5.1.4. Validation of the reaction products by SDS-PAGE 62
5.1.5. DTNB catalysed disulfide formation is a versatile tool to study reaction intermediates of the ubiquitination pathway 62
5.1.6. Crystallographic analysis of HECT reaction intermediates mimicked through disulfide formation 64
5.1.7. NMR analysis of HECT reaction intermediates mimicked through disulfide formation 66
5.1.8. Discussion 70

5.2. β sheet augmentation – a common theme in ubiquitin HECT-domain interaction 72
5.2.1. Contribution 72
5.2.2. Introduction 72
5.2.3. Results 72
5.2.4. The Huwe1 HECT domain forms preferentially K6- and K48-linked Ub chains 72
5.2.5. The Huwe1 HECT domain does not interact with Ub in a non-covalent manner 74
5.2.6. The Huwe1 C-lobe~Ub^{D} complex is highly similar to Nedd4 family E3s 75
5.2.8. Interfering with β-strand formation disrupts thioester formation 78
5.2.9. The sequence of the C-terminal tail modulates ligation activity 82
5.2.10 Discussion 85
5.3. The Huwe1 HECT domain is auto-inhibited by interactions of the N- and C-lobe 87
5.3.1. Contribution 87
5.3.2. Introduction 87
5.3.3. Results 88
5.3.4. Ub does not interact with the UBS of the Huwe1 HECT domain 88
5.3.5. The isolated N-lobe of the Huwe1 HECT domain is able to bind Ub in a non-covalent manner 89
5.3.6. Mutations in the ubiquitin binding surface affect Huwe1 activity 91
5.3.7. Thioester formation enables monomeric Ub to bind to the Huwe1 UBS 93
5.3.8. The free Huwe1 HECT domain adopts a closed conformation in solution 98
5.3.9. The thioester induced rearrangement of the C-lobe can by mimicked by small organic compounds or mutations of the catalytic cysteine 103
5.3.10. The thioester mimicking mutants interact with Ub in a non-covalent manner 106

5.3.11. Structural rearrangement and non-covalent Ub-UBS binding of the Huwe1 HECT domain 107
5.3.12. The open state can be induced by mutations in the N-lobe of the Huwe1 HECT domain 111
5.3.13. Reorientation of the C-lobe leads to an acceleration of auto-ubiquitination for Y162A single mutant of the Huwe1 HECT domain 114
5.3.14. Discussion 116
6. General discussion 119
7. Materials 125
7.1. Equipment 125
7.2. Consumable 126
7.3. Chemicals 127
7.4. Enzymes 128
7.5. Buffers and Media 128
8. Methods 130
8.1. Molecular biology 130
8.1.1. PCR amplification 130
8.1.2. QuikChange™ mutagenesis 131
8.1.3. Restriction free cloning 131
5.1.4. Digestion with DpnI 132
8.1.5. Transformation into chemically competent *E. coli* cells 132
8.1.6. Isolation of plasmid DNA 132
8.1.7. DNA sequencing 132
8.2. Protein biochemistry 133
8.2.1. Sodium dodecyl sulfate polyacrylamide gel electrophoresis (SDS-PAGE) 133
8.2.2. Coomassie staining 134
8.2.3. Recombinant protein expression 134

8.2.4. Unlabelled protein expression 134
8.2.5. Isotopic labelling 135
8.2.6. Protein purification by affinity chromatography 135
8.2.7. Dialysis and TEV protease cleavage 136
8.2.8. Gel filtration chromatography 136
8.2.9. Chemical induced disulfide formation 137
8.2.10. Labelling of ubiquitin with Fluorescein 138
8.3. Functional assays 138
8.3.1. Ubiquitylation assays 138
8.3.2. Thioester assays 139
8.4. Structural biology and biophysics 139
9. Appendix 151
9.1. Huwe1 C352 HECT domain disulfides ^{1}H ^{13}C-methyl TROSY spectra 151
9.2. Superimpose of Smurf2 C-lobe ~UbG76C 152
9.2. Huwe1 HECT domain (WT) ^{1}H,^{15}N-TROSY NMR titration experiments 153
9.3 Huwe1 C352 HECT domain ^{1}H,^{15}N-TROSY NMR titration experiments 154
9.4. Smurf2 (WT) HECT domain ^{1}H,^{15}N-TROSY NMR titration experiments 155
9.4. Huwe1 N-lobe ^{1}H ^{13}C-methyl TROSY NMR titration experiments 156
9.5. Huwe1 C532 HECT ~Ub G76C and Ub ^{1}H ^{13}C-methyl TROSY NMR titration experiments 157
9.6. Paramagnetic relaxation enhancement (PRE) experiments with Huwe1 HECT mutants 158
9.7. ^{1}H ^{13}C-methyl TROSY NMR spectra of the Huwe1 C352 HECT and the isolated C- and N-lobe of Huwe1. 159
9.8. Spectra of Huwe1 C352 HECT ~UbG76C and different mutation of the catalytic cysteine in the Huwe1 HECT domain 160
9.9. Huwe1 C352K HECT NMR titration experiments 161

9.10. NMR titration experiments with mutations of the Huwe1 HECT in the N-lobe 162
9.11. Line shape fitting analysis of Huwe1 HECT N-lobe 163
9.12. Plasmids 164
9.13. Protein sequences 166
9.14. Primers 167
10. References 169
11. Acknowledgments 180

List of abbreviations and symbols

Table 1: Abbreviations and symbols used in this thesis

Abbreviation	Full form
aa	Amino acid
Ala (A)	Alanine
Arg (R)	Arginine
Asn (N)	Asparagine
Asp (D)	Aspartic acid
ATP	Adenosine triphosphate
C-lobe	C-terminal lobe
CSP	Chemical shift perturbation
Cys (C)	Cysteine
DNA	Deoxyribonucleic acid
dNTPs	Deoxynucleotides
DTT	Dithiothreitol
E. coli	Escherichia coli
ER	Endoplasmic reticulum
FD	Fast digest
FID	Free induction decay
FT	Fourier transformation
FL	Full length
GF	Gel filtration
Glu (E)	Glutamic acid
Gln (Q)	Glutamine
Gly (G)	Glycine
h	Hour(s)
HA	Hemagglutinin
His (H)	Histidine
HMQC	Heteronuclear multiple quantum coherence
hs	*homo sapiens*
HSQC	Heteronuclear single quantum coherence
Hz	Hertz
IM	Isoleucine/Methionine
IPTG	Isopropyl β-D-1-thiogalactopyranoside
Ile (I)	Isoleucine

kb	Kilobases/1000 nt
kDa	Kilo Dalton
K_d	Dissociation constant
k_{off}	Dissociation rate
k_{on}	Association rate
L	Ligand
LB	Luria Broth
Leu (L)	Leucine
Lys (K)	Lysine
Met (M)	Methionine
mM	Millimolar
min	Minute (s)
ms	Millisecond
MW	Molecular weight
µM	Micromolar
µs	Microsecond
nM	Nanomolar
NMR	Nuclear magnetic resonance
N-lobe	N-terminal lobe
N-terminus	Amino terminus
Ni-NTA	Ni^{2+}-nitrilotriacetic acid
o/n	over night
OD	Optical density
PAGE	Polyacrylamide gel electrophoresis
PCR	Polymerase chain reaction
PD10	Protein desalting column
Phe (F)	Phenylalanine
Pro (P)	Proline
PTM	Post-translational modification(s)
RE	Restriction enzyme
SDS	Sodium dodecysulfate
SEC	Size-exclusion chromatography
Ser (S)	Serine
SI(ngle)	Single HECT
TEV	Tobacco etch virus
Thr (T)	Threonine

TROSY	Transverse relaxation optimized spectroscopy
Trp (W)	Tryptophan
Tyr (Y)	Tyrosine
UBS	Ubiquitin binding surface
UPS	Ubiquitin proteasome system
Val (V)	Valine
WT	Wild type
w.r.t.	with respect to

Names of Domains and Proteins

BH3	Bcl-2 (B-cell lymphoma 2) homology 3
DUBs	Deubiquitylating enzymes
E1	Ubiquitin-activating enzyme
E2	Ubiquitin-conjugating enzyme
E3	Ubiquitin ligase
E6AP	E6-associated protein
HACE1	HECT domain and ankyrin repeat-containing E3 ubiquitin-protein ligase 1
HECT	Homologous to the E6-AP C terminus
HECW1	HECT, C2 and WW domain-containing protein 1
HECW2	HECT, C2 and WW domain-containing protein 1
HERC	HECT and RDL containing protein
HOIP	HOIL-1L interacting protein
HOIL-1L	Heme-oxidized IRP2 ubiquitin ligase 1
HUWE1	HECT, UBA and WWE domain-containing protein 1
IBR	In between RINGs
Itch	E3 ubiquitin-protein ligase Itchy homolog
LUBAC	Linear ubiquitin chain assembly complex
Nedd4	Neuronal precursor cell-expressed developmentally downregulated gene 4
Nedd4L	Nedd4-Like
NF-κB	Nuclear factor kappa-light-chain-enhancer of activated B cells
RBR	RING between RINGs
RING	Really interesting new genes (s)

Rsp5	Reverses SPT-phenotype protein 5
Smurf1	Smad ubiquitin regulatory factor 1
Smurf2	Smad ubiquitin regulatory factor 2
TGF-β	Tumor grow factor β
TNFα	Tumor necrosis factor α
UIM	Ubiquitin-interacting motif
Ub	Ubiquitin
UBA	Ubiquitin-associated
Ub^A	Acceptor ubiquitin
Ub^D	Donor ubiquitin
UBD	Ubiquitin binding domain
UBL	Ubiquitin-like

Table of Figures

Figure 1: Overview of different cellular processes which are regulated by ubiquitination pathways 20
Figure 2: Overview of the ubiquitination reaction 21
Figure 3: The different types of ubiquitination 21
Figure 4: Ubiquitin contains different interaction surfaces 22
Figure 5: Compact or open conformation of Ub chains 23
Figure 6: Mechanism of the RING E3 ligases 28
Figure 7: Mechanism of the RBR E3 ligases 28
Figure 8. Mechanism of the HECT E3 ligase. 29
Figure 9. The orientations of the C-lobe w.r.t to the N-lobe in HECT domains 30
Figure 10: The structure of the HECT domain 31
Figure 11: HECT domain-mediated Ub transfer 32
Figure 12: Schema of the reaction mechanism of the HECTs 33
Figure 13: Overview of the domain architecture of the HECT E3 ligase family 35
Figure 14: Different regulation mechanisms of the HECT domains known to date 39
Figure 15: The effect of the external magnetic field onto the spin 44
Figure 16: Transformation of the FID into a frequency signal 45
Figure 17: J-couplings constants in proteins 46
Figure 18: Chemical shift perturbation experiment 48
Figure 19: The exchange rate information is contained in the line shape of the cross peak of an NMR spectrum 50
Figure 20: Paramagnetic effects on NMR spectra 51
Figure 21: Comparison of the natural thioester bond with the disulfide mimic 57
Figure 22: Chemical reaction of the Ellman's agent 58
Figure 23: Workflow for the DTNB-catalyzed formation of Ub-protein disulfides 61
Figure 24: SDS-PAGE of a HECT-Ub disulfide. 62
Figure 25: X-ray structure of a disulfide between ubiquitin and the HECT domain 64
Figure 26: The structure of the Huwe1 HECT N113C : Ub G76C complex is highly similar to the Rsp5 HECT : UbV R5.4 and WWP1 HECT : UbVP2.3 complex 65
Figure 27: NMR analysis of the Huwe1 HECT-Ub disulfides mimicking different steps along the Ub ligation pathway 68

Figure 28: Ub chain specificity and functional characterization of the Huwe1 HECT domain ... 73
Figure 29: The structure of the Huwe1 C-lobe~Ub complex is highly similar to Nedd4 family HECT~Ub intermediates ... 76
Figure 30: Mutations in the C-lobe~Ub^{D} interface interfere with thioester formation ... 78
Figure 31: Mutations in the C-lobe~Ub^{D} interface of Smurf2 and Huwe1 interfere with auto-ubiquitination formation ... 79
Figure 32: Structural characterisation of the Pro mutants of Smurf2 and Huwe1. ... 81
Figure 33: The length and composition of the HECT C-terminal tail is important for isopeptide formation ... 83
Figure 34: Truncation or mutation of the HECT C-terminal tail does not impair thioester formation ... 84
Figure 35: Ubiquitin interacts with the Smurf2 HECT domain ... 88
Figure 36: The ubiquitin binding surface (UBS) is highly conserved in the HECT domain family ... 89
Figure 37: Comparison of the obtained Huwe1 N-lobe CSP with the Huwe1 HECT C352K / N113C:Ub G76C complex. ... 91
Figure 38: Mutation of the UBS in Huwe1 HECT interferes with ubiquitination activity 93
Figure 39: Thioester formation and subsequent Ub titration induces CSPs not only in the C-lobe but also in the N- / C- lobe interface and in the UBS ... 95
Figure 40: The reorientation of the HECT domain is reversible ... 97
Figure 41: Per-residue quantification of the obtained PREs for the Huwe1 HECT cysteine mutants ... 99
Figure 42: Paramagnetic relaxation enhancement (PRE) experiments to probe the conformation of the C-lobe w.r.t to the N-lobe of the Huwe1 HECT domain ... 101
Figure 43: The isolated C- and N-lobe of Huwe1 HECT show similar chemical shift perturbations as the whole HECT domain during the thioester formation at the catalytic cysteine ... 102
Figure 44: Mutation of the catalytic cysteine induce conformational changes in the Huwe1 HECT domain that are similar to the Huwe1 HECT C352 ~ Ub G76C disulfide ... 104
Figure 45: A mutation of the Huwe1 HECT catalytic cysteine mimics the conformational change that occurs upon thioester formation and is able to bind Ub in a non-covalent manner ... 106

Figure 46: The structure of the Huwe1 HECT N113C / C352K : Ub G76C complex shows differences in the C-N-lobe as well as the Ub-UBS interfaces in comparison to the Huwe1 HECT structure 5lp8 107
Figure 47: The Huwe1 HECT N113C /C352K : UbG76C mimic, the isolated N-lobe of Huwe1 as well as the mutant Huwe1 C352K HECT are able to bind Ub in a non-covalent fashion.. 109
Figure 48: The Huwe1 HECT N113C / C352K : UbG76C mimic shows the similar CSPs in C-N-lobe as the Huwe1 N113C / C352 HECT ~UbG76C : UbG76C mimic 110
Figure 49: The open state can also be induced by mutants in the N-lobe 113
Figure 50: The mutations in the N-lobe can enhance Huwe1 auto-ubiquitination..... 115
Figure 51: Ubiquitin binding mediated by the Huwe1 HECT domain. 118
Figure 52: Inhibition of the Nedd4 family in comparison to Huwe1..... 122
Figure 53: Known genetic alterations in the HECT domain of Huwe1..... 123

Figure A 1: Complete spectra of the ^{1}H ^{13}C-methyl labelled Huwe1 HECT domain disulfides 151
Figure A 2: Structure overlay of the two copies of Smurf2 C-lobe ~UbG76C form the asymmetric unit. 152
Figure A 3: NMR titration experiments with ^{15}N-labeled Huwe1 HECT WT domains and Ub.. 153
Figure A 4: NMR titration experiments with ^{15}N-labeled Huwe1 HECT C352 domains and Ub. 154
Figure A 5: NMR titration experiments with ^{15}N-labeled Smurf2 HECT WT domains and Ub.. 155
Figure A 6: NMR titration experiments with IM-labelled Huwe1 HECT N-lobe and Ub. 156
Figure A 7: NMR titration experiments with IMVLA-labelled Huwe1 C 352 HECT ~Ub G76C and Ub. 157
Figure A 8: Paramagnetic relaxation enhancement (PRE) experiments to probe the conformation change of the Huwe1 HECT domain..... 158
Figure A 9: The isolated C- and N-lobe of Huwe1 HECT show similar chemical shift perturbations during the thioester formation. 159

Figure A 10: Mutation of the catalytic cysteine induce conformational changes in the Huwe1 HECT domain that are similar to the Huwe1 HECT C352 ~ Ub G76C disulfide. 160
Figure A 11: The mutations of the Huwe1 HECT mimic the conformational change that occurs upon thioester formation and are able to bind Ub in a non-covalent manner... 161
Figure A 12: Titration experiments with Huwe1 HECT mutants in the N-lobe and Ub. 162
Figure A 13: Line shape fitting analysis of the Huwe1 HECT N-lobe interaction with the Ubiquitin. 163

List of Tables

Table 1: Abbreviations and symbols used in this thesis 11
Table 2: Overview of the different substrates and main Ub linkage for the HECT family 36
Table 3: Spin properties of the isotopes used in biological NMR spectroscopy 43
Table 4: Disulfides formed in the Wiesner laboratory by chemical activation of ubiquitin 63
Table 5: Dissociation constants (K_D values) determined by NMR titration experiments with monomeric Ub and subsequent line shape analysis for the isolated Huwe1 HECT N-lobe 91
Table 6: Equipment 125
Table 7: Consumables 126
Table 8: Chemicals 127
Table 9: Enzymes 128
Table 10: Composition of buffers and media 128
Table 11: Standard Kapa-HiFi PCR-protocol 131
Table 12: Gel recipe for polyacrylamide separating gels 133
Table 13: Gel reipe for polyacrylamide stacking gel 133
Table 14: Coomassie staining solution 134
Table 15: Constructs which were used for NMR experiments 143
Table 16: Buffer and crystallization conditions of the X-ray constructs. 146
Table 17: Statistics of X-ray data collection and model refinement for the Huwe1 HECT N113 / C352K : Ub G76C complex[1] 147
Table 18: Statistics of X-ray data collection and model refinement for the Smurf2 C-lobe~Ub G76C complex[1] 148
Table 19: Statistics of X-ray data collection and model refinement for the Huwe1 HECT C-lobe~Ub G76C complex[1] 149
Table 20: Submitted plasmids into the local database related to this thesis.. 164
Table 21: List of primes used during these projects. 167

1. Introduction

1.1. Ubiquitin

Ubiquitin (Ub), a 76 amino acid (aa) protein which is highly conserved among eukaryotes, was discovered in 1978 by A. Hershko and A. Ciechanover [1]–[3]. For this discovery and their subsequent research of the functions of Ubiquitin, A. Hershko and A. Ciechanover were awarded with the Noble prize in 2004 together with Irwin Rose.

Initially, Ub was linked to the protein degradation. However, nowadays, it is known that Ub is involved in the regulation of almost all cellular functions (**Figure 1**) including transcription, DNA repair, protein stability, signal transduction, protein trafficking, endocytosis, lysosomal and proteasomal degradation of proteins and cell cycle control [3]–[8].

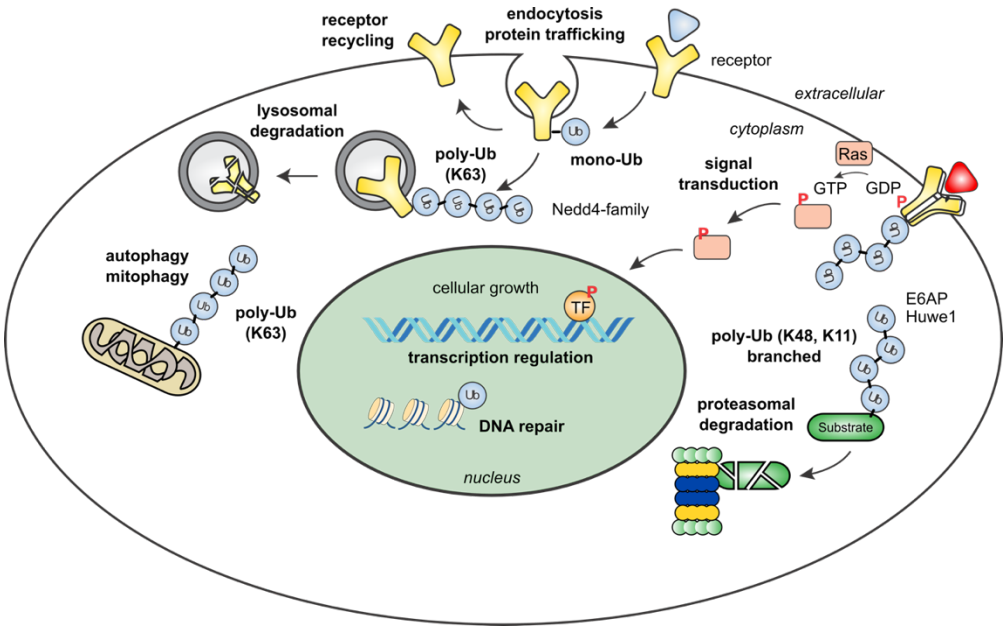

Figure 1: Overview of different cellular processes which are regulated by ubiquitination pathways.

1.1.1. The mechanism of ubiquitin conjugation

In order to fulfil its vast number of functions, ubiquitin is attached as a posttranslational modification (PTM) to a target protein. This attachment to a target protein or substrate is accomplished by an enzymatic cascade involving the consecutive action of three enzymes. In the first step, the C-terminus of Ub is activated by the Ub-activating enzyme (E1) in an ATP-dependent manner (**Figure 2**).

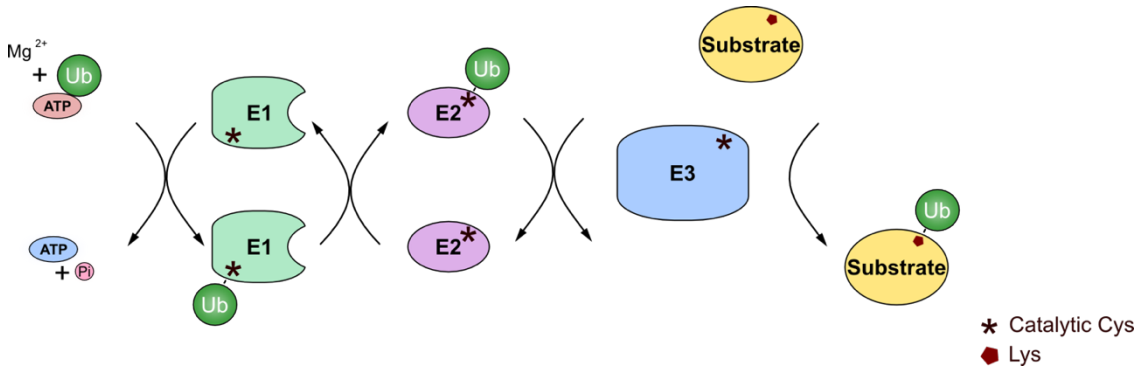

Figure 2: Overview of the ubiquitination reaction. The initial step is the activation of Ub in an ATP dependent manner by the Ub activating enzyme (E1). Next the transfer of Ub from the E1 to the Ub-conjugating enzyme (E2) takes place. In the final step the formation of the isopeptide bond between Ub and the substrate is mediated by the Ub ligase (E3).

In the ubiquitination reaction, Ub is bound *via* a thioester to the catalytic cysteine of the E1. Next, the E1~Ub intermediate binds to the Ub-conjugating enzyme (E2), and in a transesterification reaction Ub is transferred from the E1 to the catalytic cysteine of the E2. Then the loaded E2 binds to the Ub ligase (E3). In this final step, Ub is attached *via* an isopeptide linkage to the target protein (**Figure 2**). This linkage occurs between the carboxyl group of the C-terminal glycine of Ub and the lysine ε-amino group of the target protein [3]. Of note, Ub itself can function as a substrate in a ubiquitination reaction thereby forming Ub-chains.

1.1.2. Cellular functions of ubiquitination

Each type of ubiquitination is linked to a cellular function. Based on the topologies of the attached Ub moieties, ubiquitination can be categorized into monoubiqutination and multimonoubiquitionation as well as homogenous, mixed or branched ubiquitin chains (**Figure 3**).

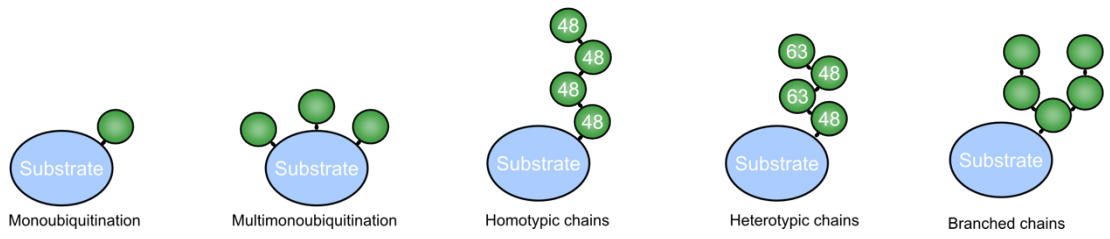

Figure 3: **The different types of ubiquitination.** The variety of different ubiquitination types are depicted as monoubiquitination, multimonoubiquitination as well as different Ub chain types. Ub chains can be homotypic (only one linkage present), heterotypic (different linkages) or branched. The figure is adopted from Rape *et al.*, 2012 [7].

In the case of monoubiquitination, one Ub molecule is attached to a specific lysine of the target protein (**Figure 3**). Monoubiquitination is mainly involved in membrane trafficking, endocytosis and viral budding (**Figure 1**) [4], [7], [9]–[11]. If the target protein is modified on multiple lysine residues with Ub the reaction is called multimonoubiquitination, one example for this is the epidermal growth factor receptor (EGFR).

In order to form Ub chains, Ub can be ubiquitinated at eight positions (**Figure 4** A). This leads to polyubiquitin chains which generate a myriad of signals in the cell. For chain formation, seven lysines (6, 11, 27, 29, 33, 48 and 63) and the N-terminal Met of the Ub are available (**Figure 4** A). Ub consists of a compact β-grasp fold with a flexible carboxyl-terminal (C-t) tail. The surface of Ub contains interaction patches (**Figure 4** B) [7], [8]. Those hydrophobic surfaces can be recognized by several proteins in different processes [12].

Each linkage type adopts a different conformation leading to compact or open chains. These conformations allow Ub to present its four interaction surfaces in different ways which results in the respective chain type being recognized by specific proteins (**Figure 4** B). [4], [7], [9]–[11].

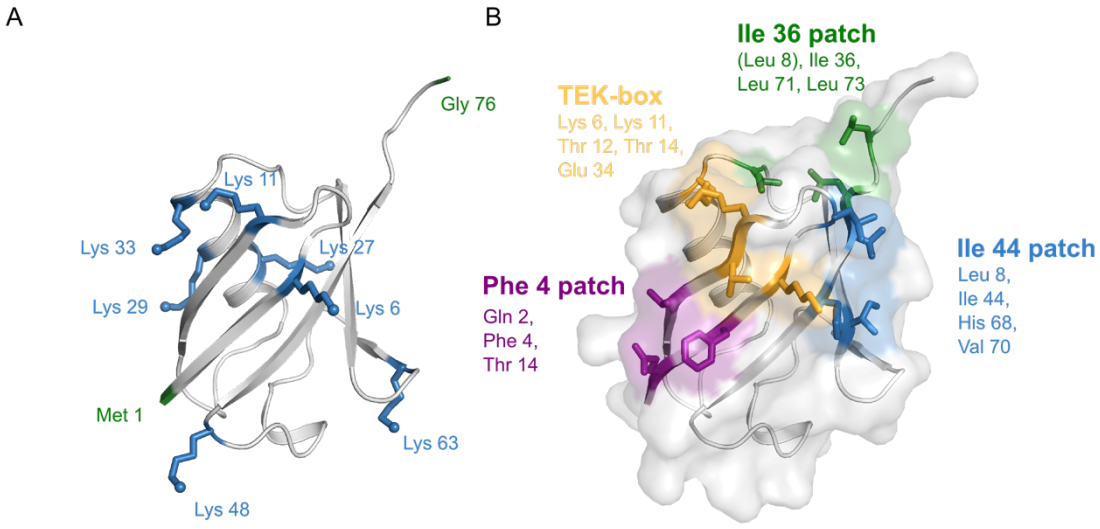

Figure 4: Ubiquitin contains different interaction surfaces. (A) Cartoon representation of ubiquitin (PDB: 1ubq) All Lys residues are shown in light blue and represented as sticks. In green the C-terminal Gly and the N-terminal Met which are involved in the ubiquitin reaction. **(B)** The different binding surfaces of Ub are shown as cartoon and surface

representation of ubiquitin (PBD: 1ubq), in sky blue the Ile44 patch, in green the Phe4 patch, in magenta the Ile 36 patch and in light orange the TEK-box. The figure is adopted from Rape *et al.*, 2012 [7].

Met1 and K63 linked polyubiquitin results in an extended conformation in which the Ile36 patch and the Ile44 patch of ubiquitin are accessible for interactions with binding partners (**Figure 5** A) [7]. The recognition of the Met1 and K63 specific chain linkages are known to play an essential role in inflammatory and immune responses mediated by the regulation of the transcription factor NF-κB (nuclear factor "kappa-light-chain-enhancer" of activated B-cells) [4], [13]. The linear Met1-linked chains are exclusively assembled by the linear ubiquitin chain assembly complex (LUBAC), a Ring between Ring (RBR) E3 ligase [14], [15].

In contrast, Lys 48 linked Ub chains adopt a compact conformation in which, either the Ile36 patch is presented for interaction, while the Ile44 patch is blocked by the formed linkage between the K48 and C-terminus of Ub (**Figure 5** B) [7], or, the Ile44 and the Ile36 patch are presented if the Ile36 interacts with the Ile44 patch (**Figure 5** B) [7]. This leads in both cases to a compact conformation [7]. Therefore, K48 linked chains can present the Ile36 patch as well as the Ile44 patch depending on the interaction of the patches (**Figure 5** B) [7].

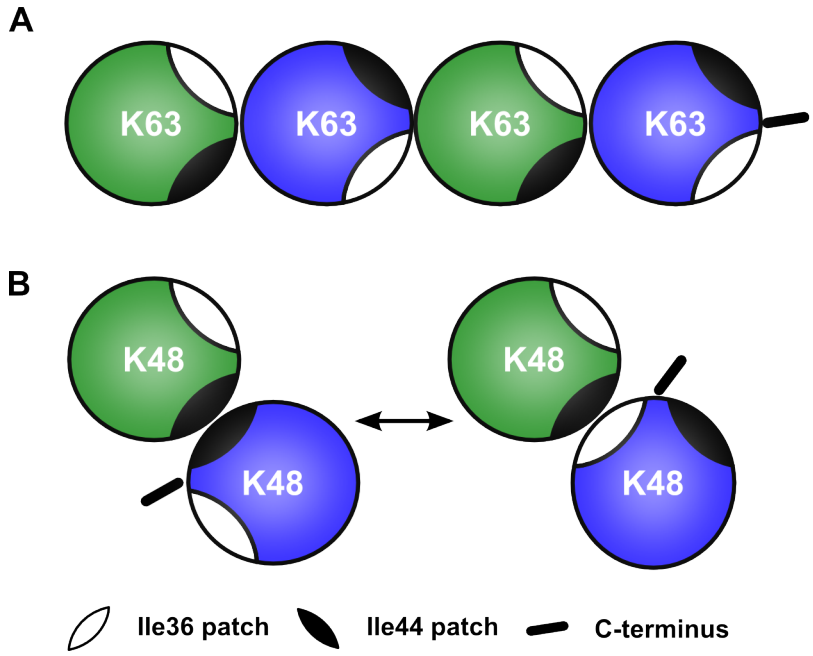

Figure 5: Compact or open conformation of Ub chains. (A) A K63 Ub chain adopts an extended conformation where the Ile36 and Ile44 patches are accessible for interaction. **(B)** A K48 Ub chain adopts a compact conformation which can either present the only the Ile36 patch or the Ile36 and K48 patch depending of the interaction of the patches. The figure is adopted from Rape *et al.*, 2012 [7]

The K48 linkage is the most common in eukaryotic cells [7]. The main function of K48 Ub chains is to serve as signal for the degradation of target proteins *via* the proteasome (**Figure 1**) since the inhibition of the proteasome leads to an increase in the level of proteins linked to K48 Ub chains [3].

K63 Ub chains also adopt an open conformation like the Met1 chains and play a role in the lysosomal proteolysis [7], [16], [17]. K63 Ub chains are related to the NF-κB transcription factor, DNA repair, innate immune response, clearance of damaged mitochondria and protein sorting [7], [16]–[18].

Ub-chains with K6, K11, K27, K29 or K33 linkage types are called atypical because their function and structure is not well defined in comparison to K48 and K63 chains [19]. In addition, their role in the cell is not fully understood [19]. It is known that K6 Ub chains are involved in proteasomal degradation [20], [21], whereas the K11 Ub chains are not only linked to proteasomal degradation but also relevant for cell cycle regulation [4]. For K27, K29 and K33 there is even less information available then for the K6 and K11 Ub chains. It was shown that K29 Ub chains inhibit the Wnt signaling pathway [4], while K33 Ub chains are associated with post-Golgi protein trafficking [7], [17].

An additional layer of complexity is added to the recognition of Ub chains by the presence of heterotypic and branched Ub chains (**Figure 3**). Branching allows the change of the signal function e.g. homotypic K11 chains are unable to interact with the proteasome whereas in a branched structure with K48 linkage the chains are recognized by the proteasome [17], [22]. With branched Ub chains the cell is able to increase the local concentration of Ub which then leads to a strong proteolytic activity [4]. Recent data suggest that any non-degradative Ub-chain can be transformed into a degradation signal if the chain undergoes branching with K11 or K48 linkage or short K48 linked chains [7], [12], [21]. This function is proposed as the "ubiquitination threshold" model [12].

Moreover, combination of ubiquitination with other PTMs further enhances the complexity of the ubiquitin system [12]. For example, the phosphorylation of Ub at Ser65 affects the Val70 residue of the Ile44 patch and thereby the conformational state of the K48 chain [23]. Besides phosphorylation, other PTMs such as Ub-like proteins (UBL) like SUMO or acetylation affect the Ub-topology [12]. The modifications of Ub itself together with the numerous combinations of these modifications enables the entire system to

generate an unlimited amount of different output signals and further studies are necessary to provide detailed analysis of the underlying components.

To read and interpret this system, the cell relies on decoding proteins which are able to interpret the signal and act accordingly to it. This role is accomplished by the Ub receptors and ubiquitin binding proteins (UBPs). The UBPs contain one or several Ubiquitin Binding Domains (UBDs) [24]. Currently, there are 20 different families of UBDs known. Of note, UBDs often occur in tandem repeats and are present in hundreds of human proteins [19]. Usually, UBDs recognize one or more of the interaction surfaces of Ub like the Ile44 patch, Ile36 patch, the Phe4 patch, the Asp58 patch, and the TEK box (**Figure 4** B) [19]. The UBD-based decoding of the Ub chain type is based on the distance difference between the Ub molecules within a chain and therefore the accessibility of different patches for interaction with different UBDs [7], [25], [26]. Yet, the recognition mechanism of each specific Ub linkages is not fully understood.

To inactivate the Ub signal the Ub is removed by the deubiquitinating enzymes (DUBs), a specific group of cysteine protease enzymes [2], [7]. The DUBs cleave the isopeptide bond either within the Ub-chain or at the end. An essential function of DUBs is the recycling of Ub to provide a sufficient level of free Ub in the cell [12]. Of note, several DUBs are known to be specific for one Ub linkage type and often show a "writing and erasing" functions together with E3s [26]. Here, the E3s generate or "write" the "ubiquitin code" [4], [7] which consists of mono-, multi- or poly ubiquitin of different Ub chain types [4], [7]. In contrast, the DUBs "erase" the ubiquitin code from the target proteins and control therefore the ubiquitin dependent signal by the distinct linkage, topology and length of the Ub chain [26]

1.1.3. Ubiquitin and the proteasome

The main task of the Ub system is to prime proteins for degradation by the proteasome. Misfolded proteins are often eliminated by the evolutionarily conserved ER-associated degradation (ERAD) pathway. The pathway to degraded cytosolic proteins is the chaperone-mediated autophagy (CAM) *via* lysosome pathway [27]. In the ERAD pathway, the misfolded protein is re-translocated into the cytosol, ubiquitinated and degraded *via* the proteasome (**Figure 1**) [22], [28]–[31]. The 26S proteasome consists of two distinct sub-complexes, the 20S core particle (CP) and the 19S regulatory particle (RP). The 20S

CP has a barrel-shaped structure consisting of four heptameric rings. This barrel is formed by two outer α- and two inner β-rings [29], [32], [33]. In this barrel, the outer alpha rings form a pore which functions as a gate for the substrate [29], [32], [33]. The gate regulates the catalytic chamber by the entrance of the substrate to the pore [29], [32], [33]. The opening of this gate and subsequently the activation of the 20S CP is facilitated by the interaction of the 19S RP with the 20S CP [29], [32], [33]. Ubiquitinated substrate can directly be recognized by ubiquitin receptors located in 19S RP subunits. In addition, substrate recruitment to the proteasome is also mediated by shuttle factors. Before the degradation of the substrate takes place the polyubiquitin chains are removed by DUBs and the substrate is funneled through the 19S RP and the alpha ring pore into the catalytic chamber. The catalytic chamber which is formed by the two heptametric beta rings is located in the center of the 20S CP. Finally, the substrate is degraded using a nucleophilic threonine hydroxyl group at the N-terminus of the beta subunits. The polypeptide chain is cleaved into shorter fragments which can differ in length. However, the biochemical mechanism that determines the length of the fragment is not fully understood [22], [32].

Defects in the Ub-proteasome system (UPS) can have severe effects. A common result of proteasome deregulation is cancer or neurodegenerative diseases [34]. In both scenarios, the Ub ligases play a crucial role because of their key function as promotor of the Ub transfer to the substrate. The Ub ligase Huwe1 is e.g. involved in the regulation and stability of the tumor suppressor p53 [18]. The tumor suppressor p53 plays a role in the DNA repair response of the cell. p53 promotes the transcription of the *Mouse double minute 2* (*MDM2*) gene. This results in the expression of the Ub-ligase MDM2 which ubiquitinates p53 and leads to the degradation of p53 *via* the proteasome. This negative feedback loop allows the regulation of p53 levels. If the ubiquitination site of p53 is mutated this leads to an increase of MDM2 expression which induces tumor development in muscles [34], [35]. Another important signal pathway in which UPS related miss-regulation leads to the susceptibility for cancer is NF-κB [34]. This factor is the major regulator of cell survival and cell death pathways. Aberrant NF-κB signaling is related to a number of cancer types like prostate, breast, lung, pancreatic or skin cancer [34], [36], [37]. Here, several key steps in the pathway are regulated by the Ub-system [34].

Also, in neurodegenerative diseases, as in Alzheimer it was shown that the UPS shows a reduced efficiency [34], [38]. This leads to the aggregation of TAU protein [34]. TAU

aggregates are found in the brain tissue of Alzheimer patients [34]. As a consequence of the aggregation, the neurons and synapses lose their function which leads to the degeneration of cognitive functions [34]. It is still unclear why the UPS is impaired [34], [39]. As described above, the UPS is involved in a huge variety of crucial cellular processes, therefore the UPS system plays an essential role in the cell.

1.2. E3 ligases

In the last step of the Ub-reaction the Ub ligase (E3) mediate the Ub transfer to the target protein. They function not only as a mediator of Ub transfer but also determine the chain specificity and therefore the fate of the target protein. In addition, they are responsible for the substrate specificity. Therefore, the E3 ligases play an essential role in the Ub-transfer-system. Since they are associated with several pathological disorders, E3s are considered attractive targets for therapeutic manipulations [40]. There are around 600 E3s encoded in the human genome. This large number reflects the high abundance of potential target proteins which are recognised by the E3s [13], [40].

1.2.1. The classification of the E3 ligases

The E3 ligases are subdivided into three classes based on their structural organisation and mechanism [40]. The largest subfamily is represented by the Really Interesting New Genes (RING family) which contains a RING domain as catalytic domain. This subclass includes also called the U-box E3s [40]. The two other classes are the Homologous to the E6AP (E6-associated protein) C-Terminus (HECT) E3s and the RING between RINGs (RBR) E3s.

These subclasses differ in the mechanism how Ub is transferred to the target protein and in their structures (see below). All three subclasses have in common that they form an isopeptide bond between the C-terminal glycine of Ub and the ε-amino group of a lysine of the target protein. The RING E3s act as a scaffold and bind the E2 and the target protein simultaneously and mediate the Ub transfer between the E2 and the target protein. In contrast to RING E3s, the HECT and RBR E3s ubiquitinate the target protein in a two-step reaction [40]. Here, the Ub is transferred in a transthiolation reaction to the catalytic cysteine of the E3 and then passed from the E3 to the target protein [40]–[42].

1.2.2. RING E3-ligases

The RING-containing E3s are the prevalent Ub-ligase in humans with around 500 members [15]. The RING E3 ligases act as a scaffold bringing the E2~Ub and the target protein together (**Figure 6**). The transfer of Ub occurs directly from the E2 to a lysine residue of the target. The RING domains are zinc finger domains able to bind two zinc ions and comprise 40-60 residues [15]. The conserved cysteines of the zinc finger motif play no role in the Ub-transfer because they are not surface exposed. This argues for a scaffold function because no thiol-based catalytic intermediate can be formed. Also is the RING-domain too far from the active site of the E2 to participate in the catalysis reaction [43]. For target protein recruiting the RING E3 ligase contains several substrate interaction sites [43]. During the catalytic cycle, the E2~Ub adopts a closed conformation whereas in a free state the E2~Ub is highly dynamic and shows an open conformation. This closed conformation of the bound E2~Ub positions the C-terminus of the Ub for the transfer to the target protein [43]. Therefore, the Ub chain type of the reaction is defined by the E2. On the other side, the RING domain selects the target protein and positions the target protein. Hence, the RING domain defines which lysine is accessible for ubiquitination [41], [42].

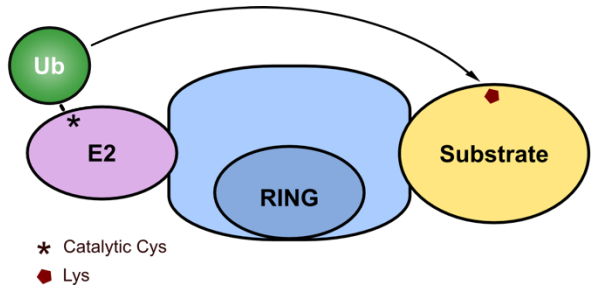

Figure 6: Mechanism of the RING E3 ligases. Schematic representation of the Ub transfer from the E2 to the substrate mediated by RING E3 ligases.

1.2.2. RBR-domain E3-ligases

Until today, the 14 known RBR E3s regulate diverse cellular processes in humans. The best studied member of the RBR E3s is Parkin which is associated with mitophagy [44]. The RBR ligases are defined by their two RING domains (RING 1 and 2). These two domains are connected *via* an inbetween RING domain (IBR) (**Figure 7**). The RING1 domain acts similar to the canonical RING domains and binds the

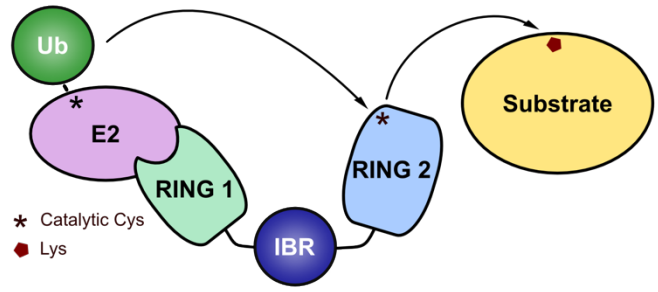

Figure 7: Mechanism of the RBR E3 ligases. Schematic representation of the Ub transfer from the E2 to the substrate mediated by the RING in between RING E3 ligase (IBR= In between Ring domain).

E2 loaded with Ub (**Figure 7**). Whereas the RING2 domain contains an essential catalytic cysteine which receives the Ub from the E2~Ub and forms a thioester intermediate (**Figure 7**). Therefore, the catalytic function of RING2 domain is similar to the activity of the HECT E3s (see below). Thus, the RBR class is a hybrid between the RING and HECT domain ligase on a mechanistic level. However, the target ubiquitination in the RBRs uses a different catalytic mechanism. One of the best investigated RBR E3s, the linear ubiquitination assembly complex (LUBAC), generates linear Ub chains [45]. This complex consists of HOIL-1L, HOIP and Sharpin and has been reported to activate the NF-κB response by the ligation of linear Ub-chains between the C-terminus of the donor Ub and the first methionine of the acceptor Ub [41], [42], [44], [46], [47].

1.2.3. HECT E3-ligases

From the 600 known human E3s only around 28 E3s belong to the HECT E3 ligase family. The key signature of this family is the C-terminal domain of approximately 350 amino acids which was first characterized in the E6-associated protein (E6-AP) [48]. Therefore, the class of these E3s is named after the first described member, the E6-AP domain, Homologous to the E6-AP Carboxyl Terminus (HECT). The reaction cycle of HECT domains consists of two steps. In the first step the Ub is transferred to the HECT E3 and in the final step the Ub is transferred from the HECT to the lysine of the target protein (**Figure 8**).

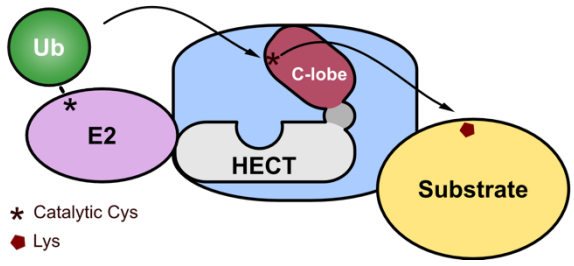

Figure 8. Mechanism of the HECT E3 ligase. Schematic representation of the Ub transfer from the E2 to the substrate mediated by the HECT E3 ligase.

1.3. The HECT E3-ligase in detail

1.3.1. The catalytic mechanism of HECT domains

The HECT domain is a bilobal domain that consists of an N- and a C-terminal lobe (**Figure 9**). The lobes are connected *via* a short hinge loop. The linker allows the C-lobe to adopt different orientations w.r.t. the N-lobe (**Figure 9**). This flexibility of the linker is essential for the activity of HECT domains [13], [40], [49]–[52].

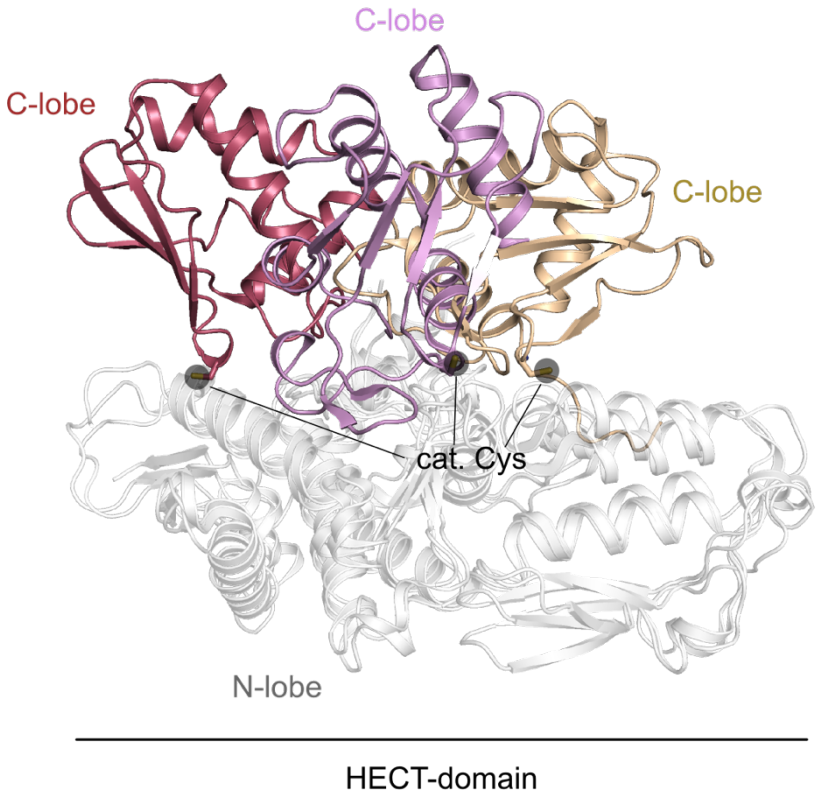

Figure 9. The orientations of the C-lobe w.r.t to the N-lobe in HECT domains. Superposition of different HECT domains in cartoon representation are shown to highlight the flexibility of N- and C-lobe. The C-lobes are coloured according to the HECT domain (red, E6-AP, PDB:1d5f), (purple, Nedd4L, PDB:2oni), (gold, Huwe1, PDB:5lp8) whereas the N-lobes are aligned to each other and coloured in white to show the different conformations of the C-lobe and therefore the conformational flexibility of HECT domains. The catalytic cysteines of the different HECT domains are marked with a grey cycle.

The C-lobe contains the conserved catalytic cysteine residue, which interacts during the transfer reaction with Ub (**Figure 10**) [40]. Additionally, the last amino acid of the C-lobe C-terminus plays an important but yet not entirely clarified role in the catalysis [50], [53], [54]. The N-lobe is associated with the recruitment of the E2~Ub thioester (**Figure 10**). Moreover, a subclass of HECT-E3s possesses a surface which allows the binding of Ub in

a non-covalent manner. This ubiquitin binding site (UBS) is located at the N-lobe of the HECT domain (**Figure 10**).

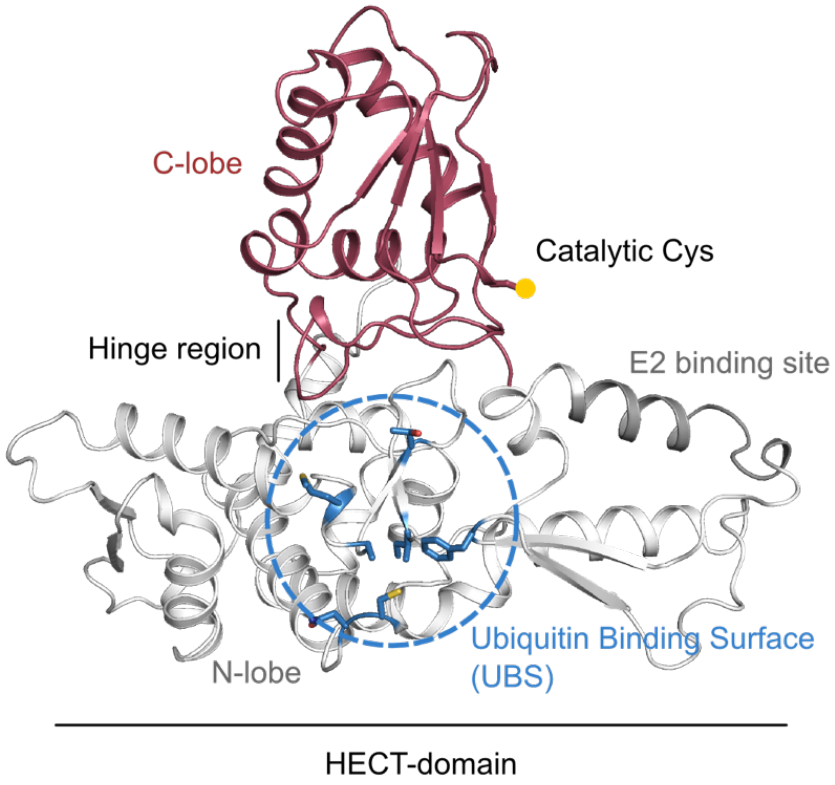

Figure 10: The structure of the HECT domain. The most relevant characteristics of HECT domains are shown. The Nedd4 HECT domain (PBD: 4bbn) is shown as cartoon and different regions of the protein are highlighted. The N-lobe is coloured in light grey, the C-lobe is coloured in red, the ubiquitin binding surface (UBS) is represented in blue sticks and marked by a cycle, the catalytic cysteine as yellow sphere, the E2 binding site is coloured in dark grey.

Mutations in the UBS have strong effects on polyubiquitin chain elongation whereas the transthiolation step between E2 - E3 and monoubiquitination are not affected [51] Therefore, the UBS is essential for the chain formation. In contrast to the catalytic activity located in the HECT domain, recognition of the target protein is mediated by domains or motifs located in the extended regions N-terminal of the catalytic HECT domain [40].

The HECT E3 enzymes catalyse the Ub transfer in a two-step reaction. At first the trans-thioesterification reaction takes place. Here, the E2~Ub binds to the HECT domain and transfers the Ub to the conserved catalytic cysteine of the C-lobe forming a thioester bond between the C-terminal glycine of Ub and the catalytic cysteine of the HECT domain. In the last step the thioester of the HECT~Ub is nucleophilically attacked by the ε-amino group of the lysine of a target protein and formation of the isopeptide bond takes place (**Figure 11**) [40].

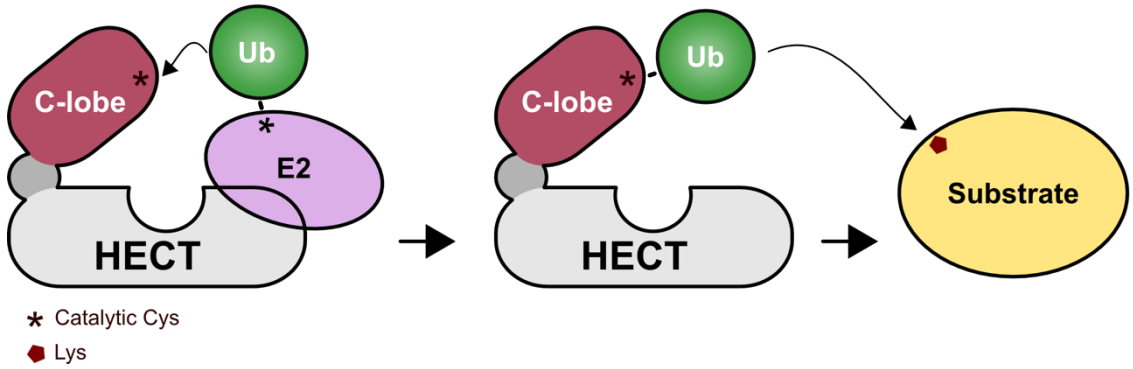

Figure 11: HECT domain-mediated Ub transfer. The E2~Ub binds to the HECT domain. Thereafter the Ub is transferred to the catalytic cysteine (asterisk) under the formation of a thioester bond. In the final step Ub is transferred from HECT to a Lys of a substrate.

However, the chemical basis of the isopeptide formation is unclear. One of the open questions is how the deprotonation of the primary amino group of lysines and N-terminal methionines from the Ub and substrates is facilitated. Interestingly, the HECT domain has the ability to perform this catalytic cycle without an additional target and is able to use the HECT domain itself as substrate in an auto-ubiquitination reaction [40], [41].

Several structures of HECT E3s show that the C-lobe adopts different positions w.r.t. the N-lobe (**Figure 9**). This flexibility is necessary to allow the transfer of Ub from the E2 to the HECT E3 due to the large distance (between 50 and 16 Å) which was observed between the catalytic cysteine of the HECT E3 and the E2 [13]. Until today only one structure captures the pre-transthiolation state. The structure of Nedd4-2 HECT domain in complex with an E2~Ub (PDB: 3jw0) [49]. Here, the E2~Ub thioester is bound to the N-lobe side of the HECT E3. The C-lobe is rotated around the hinge region towards the catalytic cysteine of the E2. By convention the Ub which binds on the C-lobe is referred as donor Ub (Ub^D) whereas the Ub that attacks the thioester with its Lys side chain and subsequently is modified with the Ub^D is the acceptor Ub (Ub^A). It is unknown where the where the Ub^A binds on the HECT domain [40]. During the E2 binding, the C-lobe binds the Ub^D and brings both the catalytic cysteines of the E2 and the E3 in close proximity to each other which promotes the formation of the HECT~Ub intermediate [40], [49]. After the transthiolation reaction, the interaction between the C-lobe and the Ub^D of the HECT~Ub^D intermediate is maintained. This was shown by the crystal structure of Nedd4 HECT~ Ub^D:Ub^A (PDB: 4bbn) and the Nedd4 homolog of *S. cerevisiae*, Rsp5, in complex

with Ub^D and Sna3, a Rsp5 substrate (PDB: 3jw0) [18]. In the next step the Ub^D is placed close to the lysine of the target and transferred (**Figure 12**).

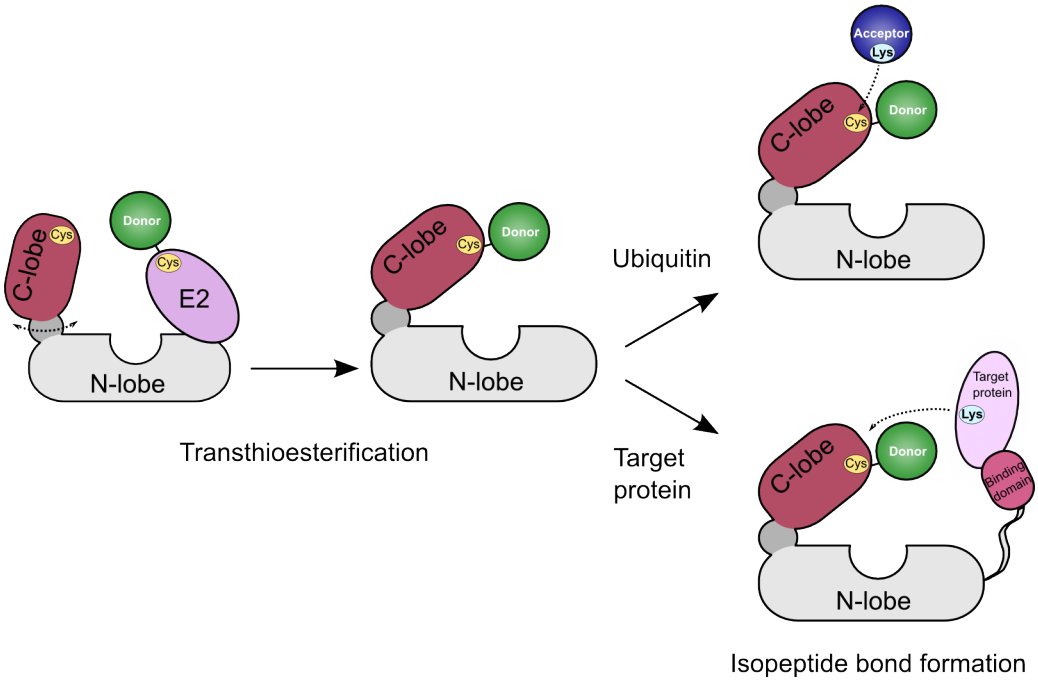

Figure 12: Schema of the reaction mechanism of the HECTs. E2~Ub binds to the HECT domain (Of note the C-lobe and the N-lobe are flexible to each other). During a transthioesterification the Ub is transferred to the catalytic cysteine of the HECT domain. The HECT domain loaded with the donor Ub is attacked either by a primary amine of an acceptor Ub or target protein under the formation of an isopeptide bond. The figure is adapted from Lorenz *et al.,* 2018 [40].

It was shown that a conserved phenylalanine at the -4 position (-4 Phe) of the C-terminus of HECT domain is crucial for isopeptide formation [49], [54]. The structure of Rsp5 in complex with Ub and Sna3 highlight the role of the -4 Phe [49]. In this structure, the phenylalanine acts as an anchor to lock the C-lobe in a position which is suitable for the ubiquitination of target proteins. It was shown that the C-lobe adopts a conformation which is rotated 130° around the hinge region in comparison to the Nedd4 HECT~Ub^D:Ub^A structure [49], [50]. The -4 Phe is conserved among all the HECT E3s. Biochemical data showed that the -4 Phe is essential for the ubiquitination reaction. However, it is not required for thioester formation and therefore does not affect the transthiolation step i.e. the transfer of Ub between the E2 and E3. Moreover, the binding grove for this Phe is conserved in the Nedd4 family, suggesting that the anchoring of the C-lobe is required for the ligation reaction in the entire family of the HECT E3s [42].

The UBS was shown to be important for the Ub chain elongation. With this surface the Ub interacts *via* the hydrophobic Ile44 patch. This interaction is based on the hydrophobic interaction of Ile44 with a phenylalanine residue in the loop between the beta 5 and beta 6 sheets of the HECT domain. For example, mutation of Phe707 in Nedd4 abolishes the Ub chain elongation [50]. Therefore, this contact is crucial for the Ub chain elongation whereas the thioester formation is not affected by this mutation. However, the exact role of the UBS is still under discussion. The best established model suggests that the UBS serves as a binding site for ubiquitinylated substrates thereby promoting processivity [50]–[53].

However, until today it has been difficult to pinpoint the structural determinants of HECT E3 Ub chain elongation. In addition, the question how the chain specificity is achieved is incompletely understood [40]. However, it was shown that the exchange of the last 60 residues of the C-lobe from Rsp5 to E6-AP can shift the chain specificity from K48 to K63 [55]. Moreover, in the Nedd4-2 HECT domain, a C-tail substitution leads to a change of linkage specificity [40], [50]. This suggests that the C-lobe is necessary to determine the linkage type [40], [50]. However, further studies are necessary to investigate the underlying mechanisms of these processes in greater detail.

1.3.2. HECT E3 families

The HECT E3s are classified by their N-terminal domain composition into three groups: the Nedd4 family, the HERC family and the other or SI(ngle) HECT E3s (**Figure 13**) [13]. In short, the presence of regulator of chromosome condensation 1 (RCC1)-like domains (RLDs) defines members of the HERC family (**Figure 13**) as well as the presence of C2 and protein-protein interaction WW domains defines members of the Nedd4 family (**Figure 13**). In contrast, SI(ngle) family members do not share a common N-terminal domain architecture (**Figure 13**). An overview of the main Ub linkage type and the substrates and function of the different HECT families is given in Table 2.

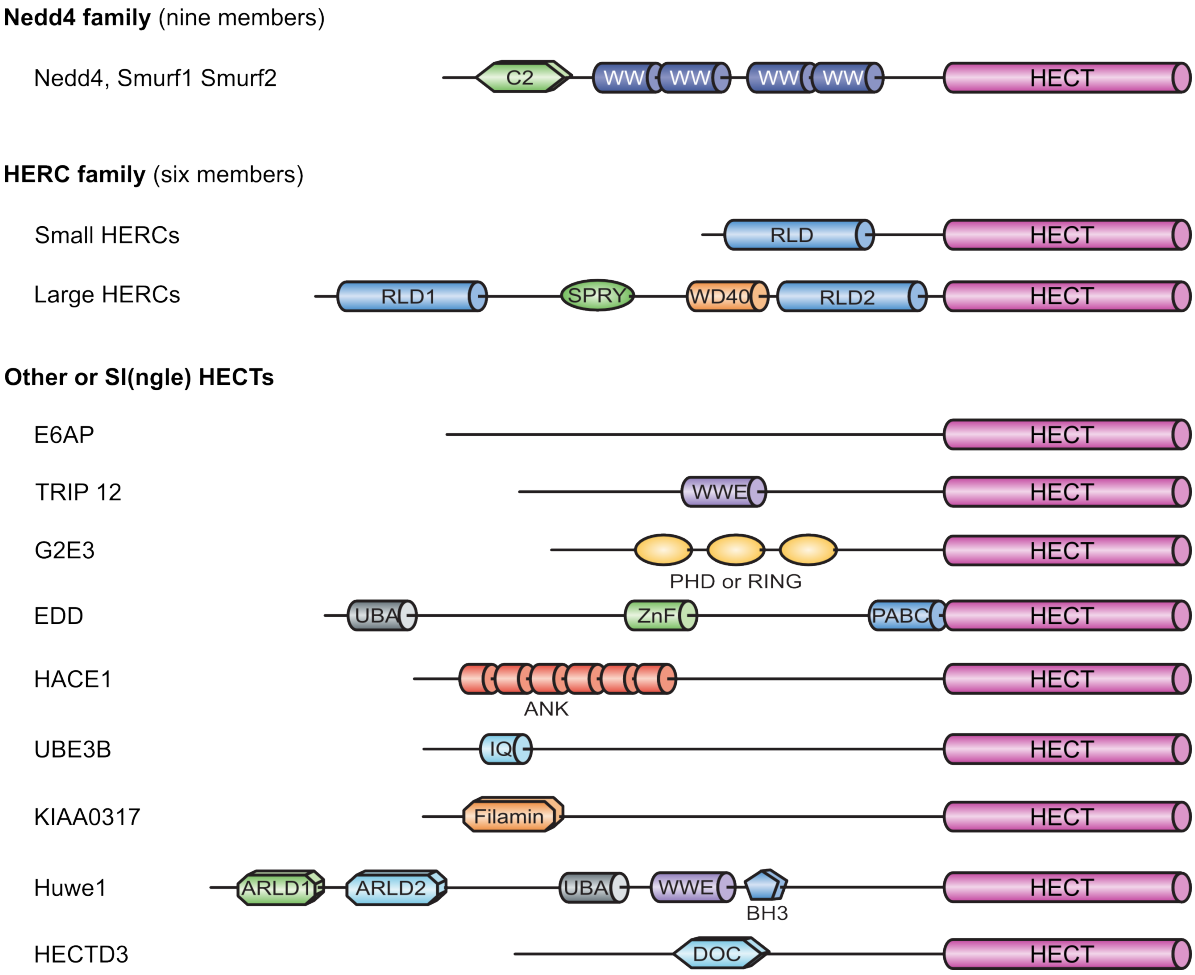

Figure 13: Overview of the domain architecture of the HECT E3 ligase family. All human HECT E3 ligases share the HECT domain on the C-terminus. The Nedd4 family and the HERC family are clearly defined by their N-terminal domains. The Nedd4 family have a characteristic N-terminal C2 domain and two to four protein-protein interaction WW domains. The HERC family consists of one or more regulator of chromosome condensation 1 (RCC1)-like domains (RLDs). The HERC family can be divided into two groups: small HERCs with one single RLD and the large HERCs with contain more than one RLD and also additional domains like SPRY or WD40. The other or SI(ngle) HECTs contain a myriad of different domains at the N-terminus (as shown). For example, Huwe1 possesses an Arm repeat- like domain (ARLD1 and 2), a ubiquitin associated domain (UBA), a WWE domain for protein-protein interaction and a BH3 substrate binding domain. Other HECT E3s in this family possess a different N-terminal domain composition and contain domains such as ANK, ankyrin repeats; PABC, PABP (Poly(A)-binding protein) C terminus and ZnF, zinc finger domains. The figure is adapted from Rotin *et al.*, 2009 [13].

Table 2: Overview of the different substrates and main Ub linkage for the HECT family. Table 2 shows the Nedd4 family, the HERC family and two members, E6-AP and Huwe1 from the SI(ngle) HECT family. Here, the main Ub chain type is shown, the substrate and the function of the HECT family [13], [18], [34], [56]–[58].

HECT family	main Ub linkage	Substrate	Function
Nedd4	K63	PTEM, TGFβ, TNFα, WNT, Notch, EGFR, p53/p73/p63, Hippo	Apoptosis, endocytosis, growth arrest
HERC	(K63)	BRAC1, p53, BAK, ARF	membrane trafficking, DNA damage repair, cell growth immune response, degradation
SI(ngle) e.g. E6-AP and Huwe1	K48	p53, Mcl-1, ARF, Myc, Miz	DNA damage repair, proteasomal degradation

1.3.3. Nedd4 family

The Nedd4 family consists of nine members in humans (Nedd4-1, Nedd4-2, Itch, Smurf1, Smurf2, WWP1, WWP2, HECW1 and HECW2). Another well studied Nedd4 HECT E3 is Rsp5, a Nedd4 homologue of *S. cerevisae*. All the Nedd4 members share the same domain architecture. They possess a Ca^{2+} dependent membrane targeting C2 domain at the N-terminus, followed by two to four WW domains (**Figure 13**). The WW domain contains two Trp residues. These domains are small protein-protein interactors which recognise proline-tyrosine motifs such as PPxY- or LPxY-motifs. These motifs are present in substrates of Nedd4 family E3s or can be found in adaptor proteins which recruit additional substrates to the Nedd4 family members [40], [50], [53], [59]. The catalytically active HECT domain of around 350 amino acids is located at the C-terminus. Nedd4 family members can monoubiquitinate their substrates, but also form K63 Ub chains. The main physiological function of the Nedd4 family is linked to diverse cellular pathways including TGF-β, TNFα, WNT, Notch, EGFR, p53/p73/p63 and Hippo signalling. Not surprisingly due to their functions in various important signalling pathways, it was shown that some Nedd4 family members act as tumour promoting or suppressing factors [58], [60].

The neural precursor cell-expressed developmentally downregulated gene 4 is the founding member of the Nedd4 family. It is expressed in most tissues and localized in the cytoplasm of the cell. Among other targets, Nedd4 is involved in the regulation of cellular homeostasis by down-regulating ion channels in the brain. Therefore, it has a strong effect on the neural embryonic development and growth [61].

Another well-studied member of the Nedd4 family are the smad (small body size, receptor-regulated mothers against decapentaplegic) ubiquitin regulatory factors (Smurf) proteins. Smurf1 and Smurf2 are antagonists in the TGF-β signalling pathway. They recruit the Smad proteins with the WW domain and regulate the TGF-β pathway by the degradation of these critical players. Even though Smurf1 and Smurf2 display 70% of sequence identity and some redundancy in their substrates, Smurf1 is linked with apoptosis and cancer metastasis whereas Smurf2 is linked with gene expression, DNA damage response and genomic integrity. [61].

1.3.4. HERC-family

The human HERC family contains six members, HERC 1 to 6. The HERC enzymes possess two characteristic domains in their sequence, at the C-terminus the catalytic active HECT domain and a regulator of chromatin condensation1 (RCC1) -like domain (RLD) (**Figure 13**) [56]. The protein family is named after the first two letters of the HECT domain and the RCC1-like domain [62]. The RLD adopts a β-propeller fold and interacts with chromatin. The HERC family can be divided into subgroups: the small and the large HERC group. In the small HERC group (HERC 3 to 6) the RLDs are located ~1000 residues N-terminal of the HECT domain whereas in the large HERC group (HERC 1 and 2) the linker between HECT domain and RLD is ~4800 residues long. In this linker regions different protein domains are present like the guanine nucleotide exchange factor (GEF) which interacts with small GTPases (**Figure 13**). The HERC family is linked to different cellular functions like membrane trafficking, DNA damage repair, cell growth and immune response. Nevertheless, the physiological role of HERCs remains incompletely understood. [13], [40], [56], [62], [63].

1.3.5. SI(ngle) HECT-familiy

The remaining 13 HECT E3s in humans are summarized in the other or SI(ngle) HECT family (**Figure 13**). They show no conserved domain architecture in their N-terminal region as described before in the Nedd4 or HERC families [13]. The best studied members of this family are E6-AP, HUWE1, HACE1, TRIP12 and UBR5 [13], [18]. They all play an important role in the human physiology and are therefore also linked to severe diseases like cancer or neuronal dysfunctions. E.g. the Angelman syndrome, which is caused by a mutation in the E6-AP gene [53], [64]. Of note, the first described member of this family is E6-AP [48], [65]. In contrast to the Nedd4 family which primarily synthesizes K63 Ub-chains, the members of the SI(ngle) HECT family assemble Ub chains of various linkages including K48 as well as K11 linked Ub-chains and are therefore connected to the proteolytic pathway by the proteasome [4], [50], [64].

Noteworthy, the HECT, UBA and WWE domain-containing protein 1 (Huwe1 also known as MULE, ARF-BP1, Lasu1 or HECTH9) is able to assemble not only K48 but also K6, K11 and K63 poly-Ub-chains [66]–[69]. N-terminal of its HECT domain, Huwe1 possesses two Armadillo-like repeat domains, a Ub associated (UBA) domain, a UIM (Ub interacting motif), a WWE protein interaction domain and a BH3 motif (**Figure 13**) [70]–[72]. The Huwe1 BH3 motif interacts preferentially with the substrate myeloid cell leukemia-1 (Mcl-1) [73]. Mcl-1 plays a role in the early response of cell survival or death and is upregulated in tumours [74]. Huwe1 is the only known HECT ligase which possesses a BH3 binding motif for Mcl-1 and regulates the cytoplasmic level of Mcl-1 by proteasomal degradation [74]. The regulation of Mcl-1 by Huwe1 is an initial step for apoptosis in a cell damage event [75]. Huwe1 is also involved in the cell survival by the regulation of p53 levels in the nucleus *via* the proteasome [76]. In the nucleus p53 acts as a transcription factor to initiate DNA repair mechanisms [76]. If the level of p53 is increasing and not down regulated by Huwe1 leads to an apoptosis signal and an inhibition of Huwe1 in the cytoplasm. This has also an effect on the regulation of Mcl-1 in the cytoplasm. Therefore, both, Mcl-1 and p53 levels are regulated by Huwe1 [76].

Besides the involvement in apoptosis and DNA damage repair, Huwe1 is linked to the regulation of tumour suppressors such as ARF, Myc and Miz1 by proteasomal degradation [72], [73], [77], [78].

Since the SI HECT family includes E3 proteins with diverse N-terminal domain organisations, this suggests that these regions act as interaction hubs for various

signalling factors, anchoring regions or substrate targeting sites. Moreover, the information about the structure and mechanistic behaviour of SI family members is scarce in contrast to the Nedd4 family [40].

1.3.6. Regulation of the HECT-type E3 ligases

The E3s define the specificity of the reaction by selecting the target protein and the type of ubiquitination they perform. This empowers them to regulate various signalling pathways in the cell. Because of this high impact on the cell physiology, the HECT E3s possess various intrinsic regulation mechanisms [40], [60]. Regulation mechanisms of HECT E3s share that they restrict the flexibility of the C-lobe w.r.t. to the N-lobe which is essential for the transthiolation reaction between the HECT E3 and the E2~Ub thioester[42], [79].

The first evidence of auto-inhibition was found in Smurf2. Here the HECT domain is inhibited by the C2 domain at the N-terminus of the protein. The C2 domain interacts with a surface that overlaps with the UBS and locks the C-lobe in a catalytically incompetent conformation. Thereby the C2 domain interferes with the thioester formation (**Figure 14** A) [79]. The inhibition state of Smurf2 can be released by binding of Smad7 to the WW domains of Smurf2 which leads to a release of the C2 domain from the HECT domain and an activation of the HECT domain [80]. Similar mechanisms were found for the Nedd4-1 and -2 HECT enzymes. Here the C2 domain binds Ca^{2+} ions which leads to an activation of the HECT domains [59], [79], [81], [82].

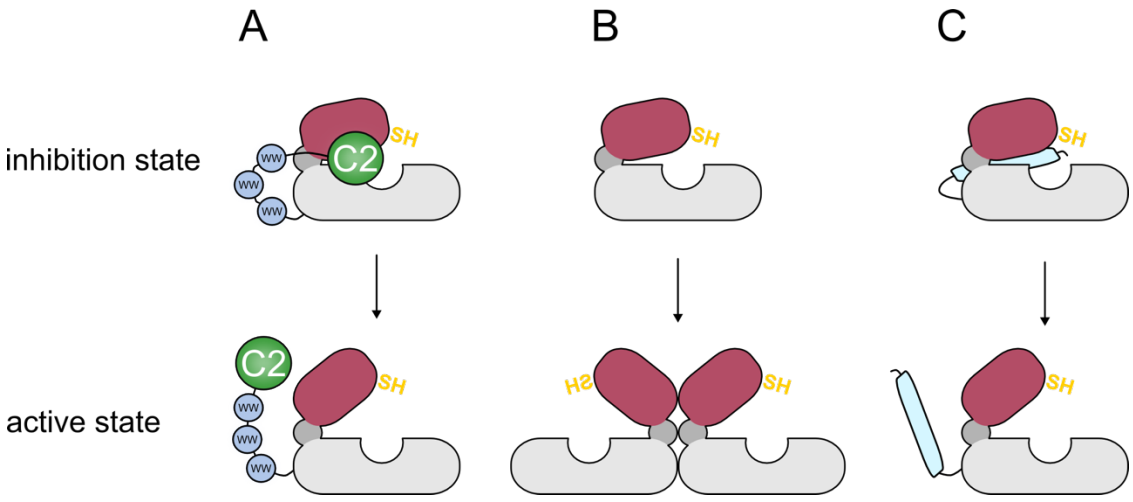

Figure 14: Different regulation mechanisms of the HECT domains known to date. (A) Scheme of the regulation mechanism of the Nedd4 family. The C2-domain is locking the C-lobe in a position where the transfer reaction is

inhibited. The C2 domain is released by phospholipid binding at the cell surface leading to the UBS being accessible [81]. **(B)** Scheme of the regulation of Rsp5 by oligomerization. Upon dimerization, the activity of the HECT domain is restored [40], [83]. **(C)** Scheme of the regulation of the Huwe1 HECT domain by an additional N-terminal helix. The N-terminal helix locks the C-lobe in an orientation where the transfer reaction is inhibited. How Huwe1 is activated is under speculation [70]. Adopted from Distel *et al.*, 2018 [108]

Another type of regulation is the formation of HECT domain oligomers which also reduces the flexibility of the two lobes [40], [83]. This affects the flexibility of the C-lobe by locking the C-lobe in a position where the catalytic cysteine is not accessible for the transthiolation. The ability to self-associate and to form trimers in cells was shown for E6-AP [84]. E6-AP trimer represents the active state of the E3 (**Figure 14** B). This trimerization can be inhibited by phosphorylation. However, the details of this mechanism have to be investigated in more detail. For Rsp5 it was shown that the HECT domain forms oligomers in the absence of the α1-helix [40], [83]. This oligomerization leads to an inactivation of the HECT domain.

For Huwe1, a similar model as for Rsp5 was proposed [40], [70]. Here, the α1-helix acts as a conformational switch which leads to the formation of an auto-inhibited, dimeric state of the Huwe1 HECT domain by an asymmetric structure (**Figure 14** C). This auto-inhibited dimeric state can be released by the activation segment located ~50 residues N-terminal of the α1-helix [40], [70]. In short, this segment can interact with the α1-helix. This interaction leads to a release of the α1-helix from the HECT domain. This dissociation of the α1-helix and the HECT domain releases the dimeric state of the Huwe1 HECT domain and activates Huwe1 HECT [40], [70].

The high impact of the E3 ligases on cellular events makes them targets for therapeutic treatment. Therefore, it is indispensable to reveal the molecular mechanisms of the ubiquitination, the specificity of the chain formation and the regulation mechanism of HECT domains. This holds the key for a better understanding of diseases and the investigation for treatments [40], [85], [86].

2. Aims and significance of the project

The aim of this thesis is to address open questions in the field of the Ub transfer mediated by the HECT E3s. Since HECT E3s are involved in a variety of biological processes connected with severe disease such as cancer and Alzheimer's, it is necessary to study the HECT-mediated Ub ubiquitination on a structural and function level in greater detail. This can help to enlighten the role of the HECT E3s and will help to identify promising therapeutic approaches in a variety of diseases [40], [58], [60], [87].
The focus of this thesis is to determine the mechanisms underlying Ub transfer in HECT domains outside the well-studied Nedd4-family and to decipher commonalities and differences in the catalytic mechanisms between the Nedd4 family and the SI(ngle) HECT family. To this end, I used the Nedd4 family member Smurf2 and Huwe1 as a member of the SI(ngle) HECT family. Of note, Smurf2 and Huwe1 also synthesize different Ub chain types (K63 and K48, respectively). Therefore, they have different functions in the cell, but nevertheless possess a highly conserved HECT domain.

In the first part of my thesis I established chemical cross-linking as a method to mimic different intermediates along the catalytic pathway of HECT domains. This included the formation of E2~Ub and HECT~Ub thioester intermediates, but also a mimic of a HECT-acceptor Ub complex. This method allows for the study of otherwise labile HECT reaction intermediates by NMR spectroscopy and X-ray crystallography to gain structural insights into the HECT-mediated Ub transfer.

Secondly, the stabile formation of HECT~Ub intermediates allowed the investigation of the interaction between the C-lobe of the HECT domain and donor Ub the first step in the HECT E3 mediated Ub transfer. To this end, different HECT domain C-lobe~Ub^D intermediates where compared to investigate whether the C-lobe:Ub^D interaction is conserved among the HECT E3s or whether the orientation of the donor Ub may be a determinant of Ub chain specificity.

In the last part of my thesis I addressed the conformational dynamics of the Huwe1 HECT domain and its role in non-covalent Ub binding. Based on sequence alignments, the Huwe1 HECT domain possesses a UBS. Despite being able to form poly-Ub chains, we

found that the Huwe1 HECT domain interacts with Ub very weakly in a non-covalent manner in comparison to the Nedd4 family members [88]. Hence, the question arises whether an auto-inhibition mechanism in the Huwe1 HECT domain may block the UBS and that it is released during catalysis.

3. Nuclear magnetic resonance spectroscopy: A tool to study protein interactions and structure

3.1. Basics of NMR spectroscopy

NMR is a powerful technique to study the structure and the function of proteins on an atomic level in solution [89]. This section will give an overview of the basic principles of NMR spectroscopy. The basis of the NMR spectroscopy is the spin of atomic nuclei, a quantum mechanical property that is associated with a small magnetic moment.

Depending on the isotope atomic nuclei can have a spin (I) of zero or a discrete integer or half-integer number (0, ½, 1, $^3/_2$, …). Nuclei with a spin of zero (e.g. ^{12}C and ^{16}O) do not possess a magnetic moment and cannot be probed by NMR spectroscopy. In contrast if the spin is greater than 0 (e.g. ^{1}H and ^{15}N) the isotopes can be used for NMR spectroscopy. If the nuclei have I > ½ the nuclei also possess an electric quadrupole moment which leads to a shortening of the lifetimes of the magnetic states and results in line broadening. Therefore, the nuclei in the most used isotopes in NMR spectroscopy have a spin ½. All isotopes used in the field of NMR spectroscopy are listed in

Table **3**. All atoms of biomacromolecules except for S and O are thus amenable to NMR spectroscopy.

Table 3: Spin properties of the isotopes used in biological NMR spectroscopy [90].

Nucleus	I	γ in $(T\ s)^{-1}$	Abundance in %
^{1}H	1/2	2.675×10^8	99.99
^{2}H	1	4.107×10^7	0.012
^{13}C	1/2	6.728×10^7	1.07
^{14}N	1	1.934×10^7	99.63
^{15}N	1/2	-2.713×10^7	0.37
^{17}O	5/2	-3.628×10^7	0.038
^{19}F	1/2	2.518×10^8	100
^{31}P	1/2	1.083×10^8	100

The nuclear spin is associated with a magnetic momentum (μ) which leads to an interaction of the nuclei with an external magnetic field (B_0). If there is no external magnetic field applied all spins are oriented randomly. The magnet of the NMR

spectrometer generates a strong external magnet field along the z-axis. The spins of a sample that is placed into the B_0 field will interact with this field. For nuclei with spin ½ two orientations are possible. a parallel (α) and anti-parallel (β) orientation to the B_0 field (**Figure 15**). The α state is slightly more populated because of its lower energy. A small excess of the spins will be therefore be aligned along the z-axis. It is this net magnetic moment that is used in NMR experiments.

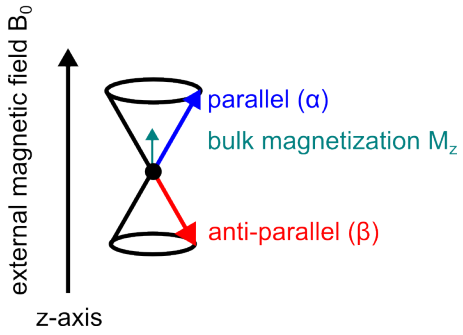

Figure 15: The effect of the external magnetic field onto the spin. In the schema the external magnetic field (B_0) and the z-axis is shown. In blue the parallel and in red the anti-parallel state of the spin after the B_0 field is applied. In cyan the arsing bulk magnetization along the z-axis.

This state where the bulk magnetic momentous aligned along the z-axis is called the equilibrium state. Furthermore, the individual spins precess around the B_0 field. This rotation of the spins is described by the Larmor frequency. During the rotation of the spin around the B_0 field all spins add up to a bulk magnetization M which is aligned along the B_0 field (M_z). The M_z magnetisation can be manipulated by an applied magnetic field B_1. For the induced B_1 field electromagnetic waves are used which are in the radio frequency spectrum range. The B_1 field is generated by a coil and is applied vertical to the B_0 field. If the applied radio frequency pulse is applied at the Lamor frequency it interacts constructively with the nuclear spins and the magnetic moment is rotated to the xy-plane This is then called a 90° pulse. After the 90° pulse the magnetic moment rotates in the xy-plane. Through this rotation an electric current is induced in the same coil that is used for the application of the B1 field and this current is detected as the NMR signal The magnetization then starts to relax back to the z-axis which leads to an exponential decline of the electric current over time. This declining signal is also called the free induction decay (FID). The information which is contained in the FID is converted by a Fourier transformation (FT) into a frequency domain spectrum (**Figure 16**).

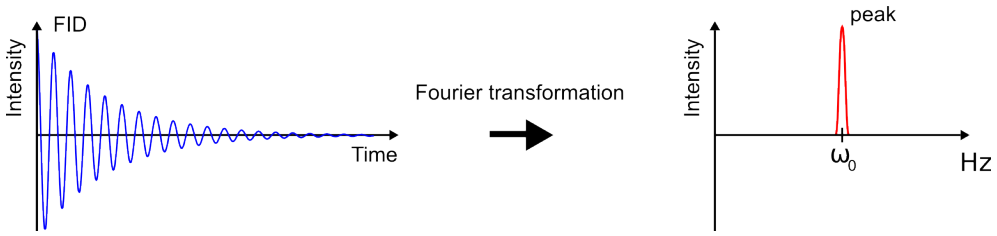

Figure 16: Transformation of the FID into a frequency signal. Shema of the detected signal which decays over time (free induction decay, FID). After Fourier transformation (FT) the FID is converted to a frequency signal.

An NMR spectrum shows a unique set of peaks. Each peak originating from one nucleus. The precession frequency and therefore the position in the spectrum depend on the chemical environment of each atom. The chemical environment of the atoms is influenced by shielding effects or charges in proximity (e.g. solvent exposure, secondary structure, aromatic ring currents, bond torsion angles etc.). Those effects result in a local magnetic field and therefore a slightly different resonance frequency for each atom in a molecule which results then in an individual peak in an NMR spectrum.

Relaxation or the return of the magnetisation (coherence) from $M_{x,y}$ to M_z involves two processes. The longitudinal relaxation T_1 is the realignment of the bulk magnetisation with the B_0 field when no B_1 field is present. The Brownian motion of the molecules induces the random reorientation of the nuclei and therefore the realignment of the spin to the B_0 field. The second relaxation process is the transversal relaxation T_2 which describes the decay of the transverse components of the $M_{x,y}$ magnetization. Here, the phase coherence of the spins is lost over time. The precession frequency of a given atom depends on the orientation of the molecule in the B_0 field. Molecular tumbling leads to an averaging of this precession frequency, but this averaging is incomplete. Therefore the spins of the same atom in different molecules do not rotate at the same frequency $a_{x,y}$ plane. The T_1 relaxation induces also T_2 relaxation whereas the T_2 relaxation can occur without T_1 relaxation.

Another aspect of NMR spectroscopy is the possibility to gain information about the distance between the nucleus as well as the angels of a spin system connected through chemical bonds. This information is contained in the J-coupling (**Figure 17**).

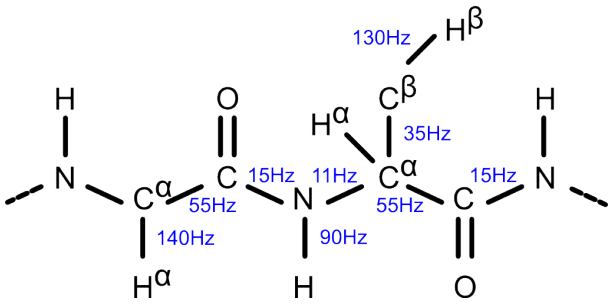

Figure 17: J-couplings constants in proteins. The solid black lines represent J-couplings between the different nucleus. In blue the J-coupling constants for the different chemical bound between the nucleus. The figure was adapted from van de Ven [91]

In protein NMR the J-coupling is used to transfer magnetization from one nucleus to another. This correlation spectrum holds the information about the connectivity between the nuclei. The so called NOESY experiment allows to transfer magnetization through space to other nuclei nearby. This information can then be used to determine the structure of proteins or for the investigation of folding or conformation events and ligand interaction [92] [93].

3.2. HSQC experiment

The heteronuclear single quantum coherence (HSQC) experiment is used for proteins smaller up to approximately 30 kDa. This experiment is normally performed on ^{15}N and/or 13C isotopically labelled proteins. The HSQC experiment correlates the proton chemical shift with the covalently bound nitrogen atoms by the ^{1}J-coupling of the HN-bond (Figure 17). In a HSQC spectrum each peak corresponds to a backbone amide, with the exception of proline that does not possess an amide proton and histidine, arginine, tryptophan, asparagine and glutamine that also possess sidechain amides. This results in a two-dimensional spectrum (2D) with a ^{1}H axis and an axis for a heteronucleus which is usually ^{15}N or ^{13}C. At first a ^{15}N HSQC heteronuclear spectrums is acquired to obtain information about structural changes or aggregation. If a protein is folded the individual peaks are distinguishable and well-dispersed in comparison to a protein aggregate. Binding events can be observed by the change of the chemical environment of the spin upon ligand binding or domain rearrangements which lead to the change of the resonance frequency. This change of the frequency can than by observed by NMR spectroscopy and allows for e.g. the investigation of ligand binding to a protein.

3.3. TROSY experiment

The transverse relaxation-optimized spectroscopy (TROSY) is a technique to study proteins that are larger than 30 kDa. The main problems for the study of larger proteins are that the residue number increases which leads to more signal overlap in the spectra and the rotational correlation time (τ_C) is longer with the increase of the molecular weight of the protein. This leads to a shorter transverse spin relaxation (T_2) time. The result of a longer (τ_C) and a shorter (T_2) is line broadening for the observed peaks. The increased peak density and the longer rotational correlation time lead to stronger signal overlap. To overcome this problem the TROSY pulse sequence is designed to select the slowest relaxing component of the magnetization. This leads to a single sharp peak and improves the spectral resolution and the sensitivity which is necessary to study large protein or complexes [94], [95].

3.4. Methyl TROSY HMQC experiment

Another possibility to study intermediate (40 kDa) or large (up to MDa) proteins by NMR spectroscopy is to use the favourable spectroscopic properties of methyl-groups (CH_3). The protons of the CH_3-groups rotate fast around the C-C bond and are organized in a threefold symmetry around the carbon atom. The behaviour of the methyl resonance leads to excellent relaxation properties which are preserved by the methyl TROSY heteronuclear multiple quantum coherence (HMQC) experiment. The result of this experiment is a well-resolved and sensitive NMR spectrum [92]. To implement the NMR-active methyl groups into the residues of the protein metabolic precursors are used. Ile-δ, Val-γ Leu-δ, Met-ε and Ala-β are currently the most frequently used methyl groups [96]. The methyl-groups distribute evenly within the protein and therefore can serve as reporters for protein-ligand interaction. Also, the high sensitivity of the methyl-groups to changes in the chemical environment and the reduced peak density in the spectra make them a good tool for studying intermediate (40 kDa) or large (MDa) proteins [97], [98].

3.5. Protein-protein interaction studies by NMR spectroscopy

NMR is a tool that allows for the investigation of protein-protein interactions at atomic resolution and therefore gives insights into the interaction surface and the binding affinities of the interaction. In a 2D NMR spectrum the peak and therefore the observed

nucleus reflect a unique chemical environment, this fingerprint spectrum of a protein can be used in NMR-spectroscopy. If a ligand is added in a stepwise manner to the protein the chemical environment of the interacting residues is changed, and this leads to chemical shift perturbation (CSPs) (**Figure 18**).

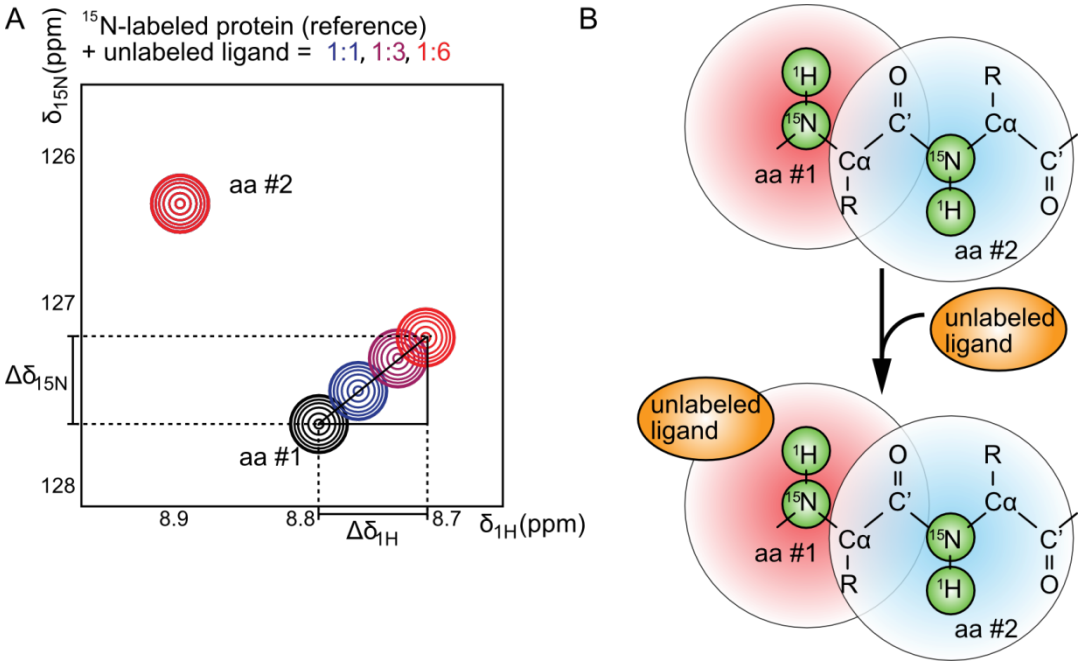

Figure 18: Chemical shift perturbation experiment. (A) Spectra of a ^{15}N-labeled protein during an NMR titration experiment. The amino acid (aa #1) shows CSPs after unlabelled ligand is added because the chemical environment is affected. Whereas, the residue aa #2 shows no effect because the chemical environment is not affected by the ligand binding. The observed changes in the proton and nitrogen dimension can be used to quantify the strength of the protein ligand interaction. **(B)** Shows the chemical environment of protein residues during the ligand binding. The chemical environment of aa #1 and aa #2 are represented by red and blue circles. The ligand is shown as an orange sphere, whereas the observed protons and nitrogen are shown as green circles. The figure is adapted from Renschler *et al.,* 2018 [99].

The CSPs are often correlated with the amount of structural change due to ligand binding Therefore, large CSPs induced during titration of the ligand indicate a more structural changes upon interaction between the protein and the ligand. If a methyl or backbone assignment and a structure of the protein is available, the observed CSP can be mapped onto the structure according to their shift distance which is the difference between the reference cross peak and the cross peak of the last titration step. Thereby the binding surface of the protein ligand interaction can by visualized.

The binding equilibrium between a free protein (P) and a free ligand (L) can be described by:

Equation 1:

$$P + L \rightleftharpoons PL$$

P and L form the protein-ligand complex (PL). The kinetics of this process can also be described by the association and dissociation constant (k_{on} and k_{off}). The k_{on} and k_{off} rate lead to the exchange rate (k_{ex}).

Equation 2:

$$k_{ex} = k_{on}[L] + k_{off}$$

where [L] is the ligand concentration. Through this definition the dissociation constant K_d can be determined by:

Equation 3:

$$K_d = \frac{k_{off}}{k_{on}} = \frac{[P][L]}{[PL]}$$

Depending on the nature of the interaction between the protein and the ligand there are different exchange regimes at constant K_d values. This can be observed by the line shape during NMR titration experiments. If the interaction is in the slow exchanging regime the peak of the unbound state disappears while the peak of the bound state starts to appear in the spectra. The slow exchange regime is encountered when the difference of the frequency $\Delta\omega$ between bound and unbound state is much larger then k_{ex} ($k_{ex} << \Delta\omega$). In contrast if the binding takes place in the fast exchange regime ($k_{ex} >> \Delta\omega$) the peaks show a constant shift during the titration until saturation is reached. The intermediate exchange regime shows shifts and a decrease in peak intensity depending on $\Delta\omega$ (**Figure 19**).

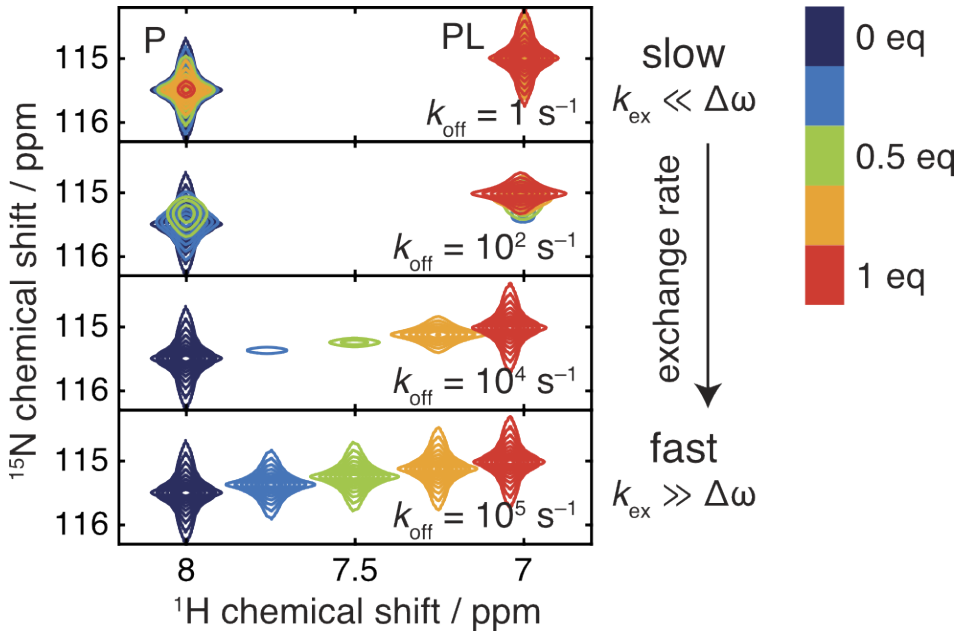

Figure 19: The exchange rate information is contained in the line shape of the cross peak of an NMR spectrum. During NMR ligand titration to a labelled protein, the line shape of the peaks is affected by the change of the chemical environment upon ligand binding. Here, P represents the unbound and PL the bound state. k_{ex} is the exchange rate and $\Delta\omega$ the frequency difference between P and PL. Here, the ligand concentration is increased step wise form 0 (dark blue) to 1 (red). The figure was adapted from Waudby *et al.*, 2016 and was simulated with the parameters: K_d = 2 µM, $\Delta\omega_H$ = 4400 Hz, $\Delta\omega_N$ = 220 Hz, [P] = 1 mM, data recorded at 700 MHz [100].

3.6. Observing conformational changes by NMR spectroscopy using paramagnetic relaxation enhancement (PRE)

In the presence of an unpaired electron of a paramagnetic compound the R1 and R2 relaxation rates of the nucleus in proximity is increased. The increase in the R2 relaxation rate is called paramagnetic relaxation enhancement (PRE) and leads to a line broadening and therefore to the loss of intensity of the effected peaks. One of the common techniques is the measurement of the relaxation rate in a sample with an oxidized paramagnetic substance and compare the result with the reduced form. This approach is more demanding in terms of measurement time and a simple alternative is to compare the signal intensities of the reduced state with the oxidized stat of the spin label. In an HMQC faster R2 relaxation due the PRE is the oxidised state leads to signal losses during the magnetization transfer steps and also increases the linewidth in the direct and indirect dimension. Both of these effects lead to a reduced signal intensity of the nuclei are close to the spin label and are therefore affected by the PRE. The increase of the R2 relaxation due the PRE decreases with the r^{-6} (r=distances between the nucleus and spin label) and can therefore be used to determine distances in proteins. The PRE-effect the spin of the

sample extends approximately 25Å from the center of the spin label [93]. Due to this long range, the PRE-effect is well suited for the study of domain orientations in proteins. In contrast NOE cross peaks are only observed up to about 6Å. Interdomain contacts in multidomain proteins can be determined by labelling on domain with a spin label and mapping the affected nuclei onto the structure of other domains [101] (**Figure 20**).

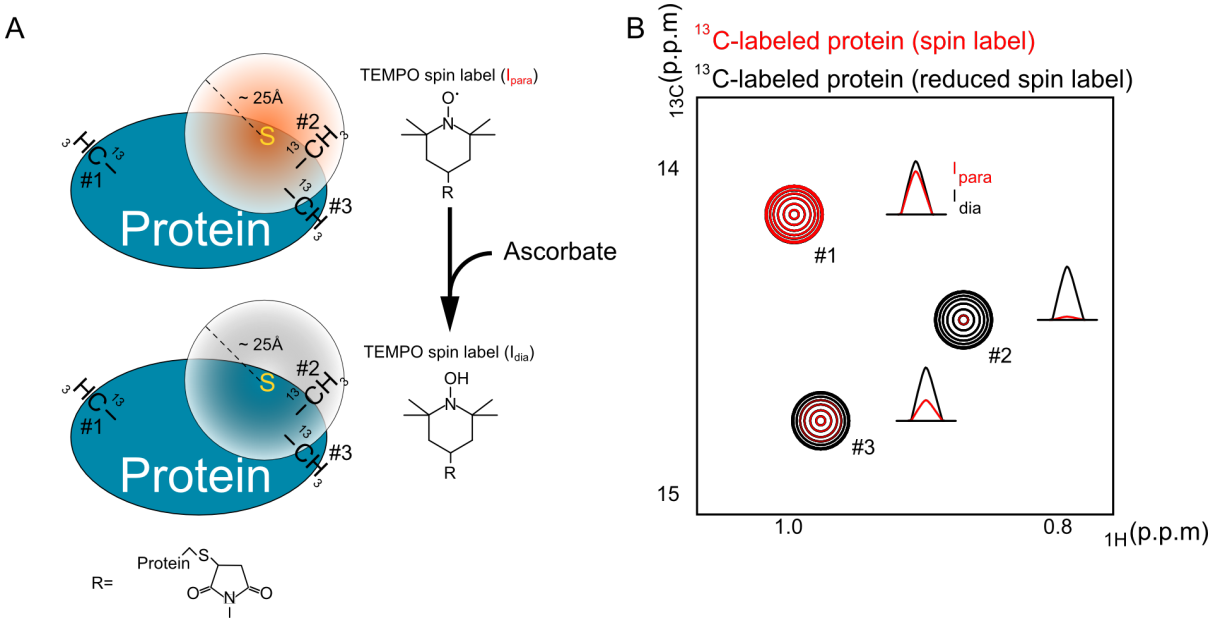

Figure 20: Paramagnetic effects on NMR spectra. (A) Methyl-labelled protein with spin label. The paramagnetic state of the spin label bound to a cysteine is shown as a sphere in orange. Residues in range of around 20 Å are affected by the paramagnetic relaxation enhancement. The residue 1# is not in spatial proximity to the spin label. In contrast, residue 2# and #3 are close to the spin label and experience a PRE that leads to a reduction of the signal intensity. By adding a reducing agent such as ascorbate, the spin label is reduced, and the paramagnetic effect is removed. **(B)** Shows the corresponding NMR spectra to **(A)** here, are the intensities of the peaks with and without the paramagnetic effect are shown. The residue #3 is partially affected by the spin leading to a reduction in peak intensity, residue #2 is close to the spin label and the signal is not visible in the oxidized state to rapid R2 relaxation. Residue #1 is more then 25Å away from the spin label and its peak intensity is thus not affected. Comparison of the peak intensities in the oxidized and reduced state therefore yields information about the distances of the residues to the spin label. This information can be used to determine the orientation of domain in a protein in solution.

Different methods have been developed to attach the spin labels to the protein. Therefore, different applications are present to link the spin label onto the protein. One method is the binding of copper(II) or lanthanoid(III) ions to a short peptide sequence at the N-terminus of the protein [102] [93]. Another possibility is to use nitroxide radicals like TEMPO. These labels can have a functional contain reactive groups like 4-maleimido which can be used to specifically link the spin label to side to cysteine chains [93].

Labelling of lysine residues using e.g. N-Hydroxysuccinimde derivatives is also possible but usually less preferable due the high numbers of lysine residues in most proteins [93].

3.7. Methyl resonance assignments

To gain detailed information about the residues which are present in the NMR spectra as peaks it is necessary to assign the peaks of the spectra. For small sized proteins 3D-NMR experiments are sufficient to assign the peaks of the spectrum. For proteins ≥ 30kDa the conventional 3D experiments are insufficient because of the line broadening. Therefore, two strategies can be used. The first one is to fragment the protein into smaller parts e.g. domains to gain better NMR-spectroscopic properties of the sample and assign these parts of the protein. At the end all assignments of the fragments are transferred to the full-length protein. In the methyl labelled approach the methyl groups of the amino acids Ile, Val, Met, Leu and Ala are labelled in a deuterated background by adding precursors of the amino acids during protein expression [96]. Only the methyl groups are $^{1}H^{13}C$-labelled in this approach while the rest of the protein is $^{2}H^{12}C$ labelled. Therefore, the ^{13}C-HMQC spectra shows only the cross peaks of the labelled methyl groups. This allows a drastic reduction of peak density of the NMR spectra in comparison to a ^{15}N labelled proteins. As mentioned above the ^{1}H and ^{13}C nuclei of the methyl group also possess very favourable relaxation properties, which allows their observation even in large biomolecular complexes up to the MDa range. One of the commonly used labelling schemes is to label only the methyl groups of the amino acids Ile and Met. Ile and Met are often distributed uniformly over a protein. Therefore, Ile and Met are well suited as reporters for interaction events or domain rearrangement in a protein [92], [103]. In addition, this approach allows the mutation of single residues to NMR-invisible amino acids. Through comparison between the wild type (WT) and mutant spectra the signal of the mutated residue can be easily identified [92], [103] This approach can be used *vice versa* where NMR-invisible residues are mutated to NMR-visible residues. This allows to map an interaction surface in more detail and one can also obtain information about residues which are crucial for the interaction between ligand and protein [104].

In this thesis all of the previously describe NMR techniques where used to investigate the interaction and the structural mechanism between the HECT E3 domains and Ub.

4. X-ray crystallography

To gain insights into the mechanism of a protein function it becomes necessary to the examine the three-dimensional structure of the protein of interest on the atomic level.
One of the commonly used methods for protein structure determination is X-ray crystallography. For this method, the protein of interest is crystallized and a single crystal is subsequently exposed to a X-ray beam resulting in a diffraction pattern [106]. The diffraction patter relives the positions of the atoms in the protein crystal and therefore holds the raw data of the three-dimensional structure of the protein [105].

4.1 The protein crystal

The smallest motif of the protein with in a crystal, is called the asymmetric unit cell [105]. The asymmetric unit forms the unit cell and furthermore the crystal lattice by the application of crystallographic symmetry operators [105]. The unit cell is described by the length of the three axes a, b, and c and the angels between those axis α, β and δ [105]. In a protein crystal the three symmetry operations translation, rotation and screw axis and a combination of translation and rotation are allowed and define the space group of the crystal [105]. Thereby, the space group holds the complete information of the crystallographic symmetry operations so that by a known space group and known content of the asymmetric unit all atom positions in a crystal are defined [105].

4.2. X-ray diffraction

The basic of crystallography is the specific diffraction pattern which is generated by the exposure of the protein crystal to X-ray waves. Here, the X-ray radiation is scattered by the electrons in the crystal [105]. This obtained diffraction pattern holds information about the electron density and therefore the positions, chemical bounds and torsion angels of the atoms in the crystal [105]. Based on the symmetry pattern of the reflection, the space group can be determined [105]. The positions of the reflections to each other furthermore encode information about the unit cell angels and dimensions [105]. The diffraction patter can only be observed if the scattered waves of the crystal are in phase and interfere constructively this leads then to a reflection [105]. Destructive property of

the scattered wave leads to a eradication of the wave and no refection [105]. Bragg's law describes the conditions of this constructive interference of the scattering wave characteristics of the scattering wave [105].

Equation 4:

$$n\lambda = 2d \sin\theta$$

Here, n corresponds to any integer. λ is the wavelength of the beam, d represents the space between the diffracting planes and θ is the reflection angle. Is Bragg's law fulfilled the X-ray waves interfere constructively and lead to a reflection pattern. Whereas, the wave leads to a destructive interference when the Bragg's law is not fulfilled.

The electron distribution in the unit cell is linked by Fourier transformation to the amplitude and phase of the scattered x-ray beams. Phase and amplitude of a given scattered beam form together the structure factor $\mathbf{F}_{khl}$. The structure factor $\mathbf{F}_{khl}$ is used to describe the scattered, reciprocal diffraction pattern and contains all the information about the atomic scattering contributions from to the unit cell. By Fourier transformation, the information of the reciprocal space is extracted from the structure factor $\mathbf{F}_{khl}$. After the Fourier transformation, the electron density of the real space is obtained. In order to generate this electron density map, the phase of the wave have to be known which is crucial to determine the structure factor $\mathbf{F}_{khl}$. However, the diffraction pattern contains no phase information this lack of information is known as the phase problem. One of the common methods to overcome this problem is molecular replacement. In molecular replacement a homologous protein structure can be used as search model to determine the atom position and orientation in the unit cell of the protein of interest. From this solution, initial phases are then back-calculated and used with the measured amplitudes in a Fourier transformation to generate the electron density map. The phased density is now used to model the protein of interest into the electron density map. Subsequently, the phases are improved by a convergent iterative process named model refinement. There, rounds of manual and computational model improvement alternate with back calculation of phase information from the improved model. These are then used to generate a new electron density map that is subsequently used for model improvement.

In this thesis x-ray crystallography together with molecular replacement has been used to solve the structures of the Huwe1 C352 HECT C-lobe~Ub G76C, Smurf2 C716 HECT C-lobe~Ub G76C and Huwe1 N113C / C352K : UbG76C complexes.

5. Results

5.1. Disulfide formation as a powerful tool to study reaction intermediates in HECT-mediated ubiquitin transfer

5.1.1. Introduction

One of the challenging tasks in the structural biology is the fact that proteins are often part of complex assemblies in which PTMs are of crucial importance [107]. To obtain detailed information on these protein interactions, the structural biologist relies more and more on the ability of protein engineering to reproduce the complex protein network in the test tube [107]. One of the common protein modifications is the attachment of the 76 amino acid short protein ubiquitin. This protein is involved nearly in all of biological processes in eukaryotes [13]. The transfer of Ub is mediated by the ubiquitination systems which is composed of three enzymes E1, E2 and E3 [13], [40]. In the last step HECT E3s recognize the substrate or target protein and modify it with ubiquitin [108]. Therefore, the HECT E3s are specific for ubiquitin signaling in the cell [13], [40]. Nevertheless, the details of HECT mediated ubiquitin transfer are poorly understood. A major obstacle to study the transfer mechanism on a structure level is the instability of reaction intermediates, in particular the thioesters formed during the transfer reaction of the ubiquitin to the HECT E3 [40], [108]. To investigate the structure and function of HECT-mediated Ub transfer we thus sought to bypass the instability of thioesters and to specifically mimic other catalytic steps such as the nucleophilic attack of the thioester by the acceptor Ub.

In order to specifically cross-link certain subunits of a protein complex, a number of biological and chemical tools are available. One powerful tool for protein ligation and modification is the utilization of cysteine chemistry. Cysteines contain a sulfhydryl group which has a strong nucleophilic character and can therefore be used for selective chemical reactions [107]. These reactions can be classified in three categories: cysteine alkylations, desulfurization and oxidations reactions [107]. In the cysteine alkylation reaction, the cysteine sulfhydryl group participates in a nucleophilic substitution at an electrophilic center e.g. present in iodoacetamide or maleimide. This leads to a covalent bond between the Cys containing protein and the electrophilic agent [107]. These

reagents can contain a fluorophore like fluorescein or a paramagnetic relaxation enhancement (PRE) label such as 4-maleimido-TEMPO [93], [107]. In addition, this approach holds the opportunity of native chemical ligation of proteins [109].

In the first step of the reaction, a thioester is attacked by a cysteine and undergoes a trans-thioesterification reaction. Next, an S to N acyl shift occurs, forming a peptide bond between the attacking cysteine and the carboxyl group of the thioester [107]. Subsequently, the cysteine can by transformed into an alanine *via* a desulfurization reduction catalyzed by metals or Tris(2-carboxyethyl)phosphine (TCEP) [107].

Cysteine oxidation is associated with the formation of disulfide bonds for example between proteins. Since we wanted to fuse proteins and due to the chemical similarity of the disulfide bond to the native thioester, I used the oxidation of cysteines to substitute the instable thioester intermediate (**Figure 21**).

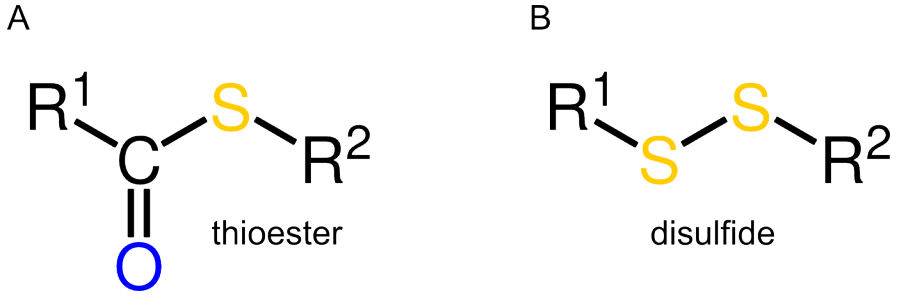

Figure 21: Comparison of the natural thioester bond with the disulfide mimic. (A**)** Thioester **(**B**)** Disulfide

Such disulfides have previously been successfully implemented to mimic the natural thioester between E1~, E2~ and E3~Ub intermediates for structural characterization [50], [110]–[112]. To apply this strategy successfully and thus generate a disulfide bond between proteins all solvent exposed Cys residues in the binding partner of Ub have to be mutated to avoid unspecific disulfide bond formation. Usually, dialysis in non-reducing conditions with a catalytic amount of Cu^{2+} ions [50], [110] have been used to form the disulfide adducts. The drawback of this strategy is the time-consuming reaction and purification of the disulfide [50]. Another problem that can occur with this strategy is that some proteins precipitate in the presence of Cu^{2+} ions. A possibility to overcome the drawbacks of dialysis driven disulfide formation is the chemical activation of one of the utilized components.

Ellman's reagent, 5,5'-dithiobis-2-nitrobenzoic acid (DTNB), is a commonly used agent to identify unmodified thiol groups [113], [114]. The DTNB reacts with the free thiol group of a cysteine to a thiobenzoic cysteine and releases a 2-nitro-5-thiobenzoic acid (NTB) (**Figure 22** A).

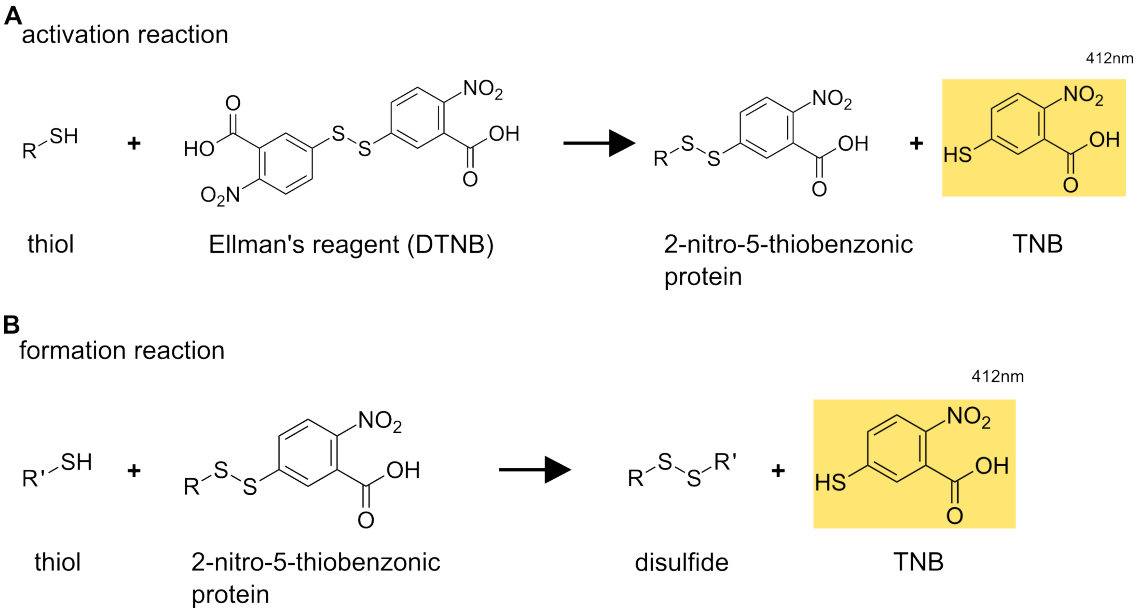

Figure 22: Chemical reaction of the Ellman's agent. (A) Chemical activation of a thiol-group by the Ellman's reagent under the formation of a disulfide bond and the yellow side product 2-nitro-5-thiobenzoic acid (TNB). **(B)** Formation reaction of the disulfide bond and the yellow side product 2-nitro-5-thiobenzoic acid.

The UV absorption of TNB at 420nm can be used to determine the amount of free thiol groups [114]. Following the activation, a disulfide bridge can be formed between a free thiol group and the 2-nitro-5-thiobenzoic cysteine (**Figure 22** A). [115]. The described chemical reaction is suitable for the disulfide formation between proteins (**Figure 22** B). One benefit of this technique is the short reaction time that is needed to form the disulfide bridge between two components. One of the drawbacks of the disulfide bond formation is its susceptibility to the presence of reducing agents [107].

Here I present an approach for the selective and rapid formation of disulfides between Ub and E2 enzymes or HECT domains, based on the chemical activation of a Ub mutant carrying a Cys by DTNB. An advantage of this method in comparison to the dialysis method is the immobilization of His-tagged Ub on Ni^{2+}-NTA-beads. This allows the direct purification of the formed disulfide from the Ni^{2+}-NTA column. Moreover, this approach is not only limited to E3 ligases, but it can be used to link different proteins to Ub e.g. E2, a substrate or another Ub to mimic a variety of steps during HECT-mediated Ub transfer

and specific linkages in poly-Ub chains. In addition, this approach should also be applicable to all proteins related to the Ub-reaction and transfer like E1 enzymes [111] de-ubiquitinating enzymes (DUB) or Ub-like modifiers. In the end, this method is suitable for the study of a series of Ub intermediates which are formed during the ubiquitination reaction. Furthermore, this method can be used to study other protein interactions that involve one cysteine and are stable as single cysteine mutants.

During my studies, I used this method to form and purify different reaction intermediates of the Ub transfer of HECT domains for structural and biophysical characterization by NMR spectroscopy and X-ray crystallography.

5.1.2. Results

5.1.3. Workflow for the DTNB-catalysed formation of disulfide bonds between Ub and ubiquitination enzymes

To establish a method that is suitable for the generation of a large variety of ubiquitination reaction intermediates, I developed a protocol (**Figure 23**) where Cys mutants of Ub are chemically activated and ligated to a ubiquitination enzyme or a substrate *via* disulfide formation. To this end, a His-tagged Cys mutant of Ub is immobilized on Ni-NTA beads (**Figure 23** A). To fully reduce the thiol group of the Ub, the column is washed with buffer A (20 mM NaP, pH 7.8 150 mM NaCl, 1 mM DTT) containing DTT as reducing reagent (**Figure 23** B). After this step, the Ub is activated with buffer B (20 mM NaP, pH 7.8 150 mM NaCl) containing 50 mM Ellman's reagent (5,5`-dithiobis-(2-nitrobenzoicacid); DTNB) (**Figure 23** C). DTNB reacts with the thiol in Ub to 2-nitro-5-thiobenzoic Ub and 2-nitro-5-thiobenzoic acid (TNB) (**Figure 22**). The product of this reaction is a chemically activated Ub. Since TNB absorbs light at 412 nm and has a yellow colour it is easy to visually follow the reaction. Therefore, occurrence of a yellow colour is an indication of a successful reaction.

Next, the Ni-NTA beads loaded with 2-nitro-5-thiobenzoate Ub are washed with buffer C (20 mM NaP, pH 7.8, 150 mM NaCl; degassed and Argon purged) to remove all unreacted DTNB and TNB (**Figure 23** D). In the subsequent step, the untagged protein that should be fused to Ub is applied to a desalting column to remove any DTT and to exchange the buffer to buffer C (**Figure 23** E). At the same time, the buffer exchanged protein is directly eluted from the desalting column onto the Ni-NTA column with the 2-nitro-5-thiobenzoic

Ub. The thiol of the untagged protein reacts with the 2-nitro-5-thiobenzoic Ub releasing TNB. Again, this reaction can be followed by the appearance of a yellow colour of the TNB indicating a successful formation of the disulfide bond between the protein of interest and Ub. Afterwards, the disulfide is wash with buffer D (20mM NaP, pH 6.4, 150mM NaCl; degassed and Argon purged) to remove all TNB (**Figure 23** F). Then, Ni-NTA bound proteins are eluted with buffer D supplemented with increasing concentrations of imidazole (**Figure 23** G). The eluted proteins are applied to size exclusion chromatography (SEC) (**Figure 23** H) in order to remove side products like di-Ub or dimers of the untagged protein that also form during the reaction. The best yield for the desired disulfide bond between Ub and e.g. a HECT domain was achieved by a 3-fold excess of His-tagged Ub over the HECT domain.

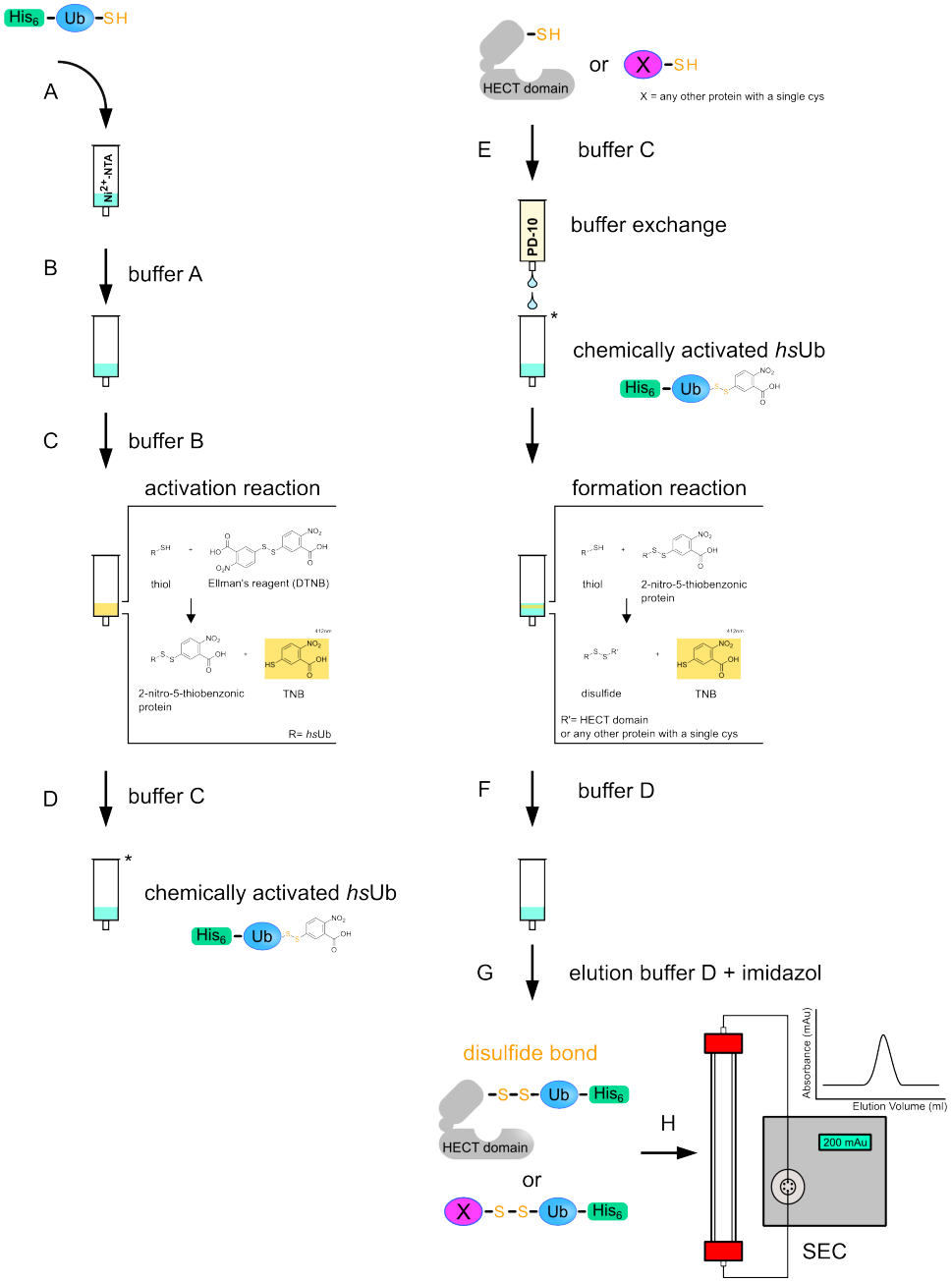

Figure 23: Workflow for the DTNB-catalyzed formation of Ub-protein disulfides. (A) His-tagged Ub containing a single Cys is immobilized on Ni-NTA beads (Qiagen). **(B)** The beads are washed with buffer A (20 mM NaP, pH 7.8 150 mM NaCl, 1 mM DTT) to fully reduce all cysteines in Ub. **(C)** Ub is activated with buffer B (20 mM NaP, pH 7.8 150 mM NaCl, 50 mM Ellman's reagent (5,5`-dithiobis-(2-nitrobenzoic acid); DTNB). Ub is chemically activated to 2-nitro-5-thiobenzoic Ub. Due to the characteristic absorbance of the side product 2-nitro-5-thiobenzoic acid (TNB) at 412nm (yellow) the reaction can be controlled visually. **(D)** The column is washed with buffer C (20 mM NaP, pH 7.8, 150 mM NaCl; degassed and Argon purged) to remove all unreacted DTNB and TNB. **(E)** The HECT domain or any other protein X with a single cysteine is buffer exchanged with a desalting column (PD-10, Qiagen) into buffer C and directly eluted onto the Ni-NTA column containing the activated Ub. Successful disulfide formation is indicated by the formation of yellow TNB. **(F)** The column is washed with buffer D (20mM NaP, pH 6.4, 150mM NaCl; degassed and Argon purged) to remove free TNB. **(G)** The disulfide is then eluted with increasing imidazole concentrations in buffer D. (H) In a final step, the HECT-Ub or protein-Ub disulfides are purified by size exclusion chromatography (SEC).

5.1.4. Validation of the reaction products by SDS-PAGE

To monitor disulfide formation and assess the purity of the final sample a SDS-PAGE was performed (**Figure 24**). Samples were loaded on SDS gels with and without DTT in the sample buffer. DTT reduces the disulfide bond and therefore the untagged protein and the Ub run separately on the SDS-PAGE in comparison to the sample loaded without DTT. This simple approach allows an easy and fast verification of the formed disulfide.

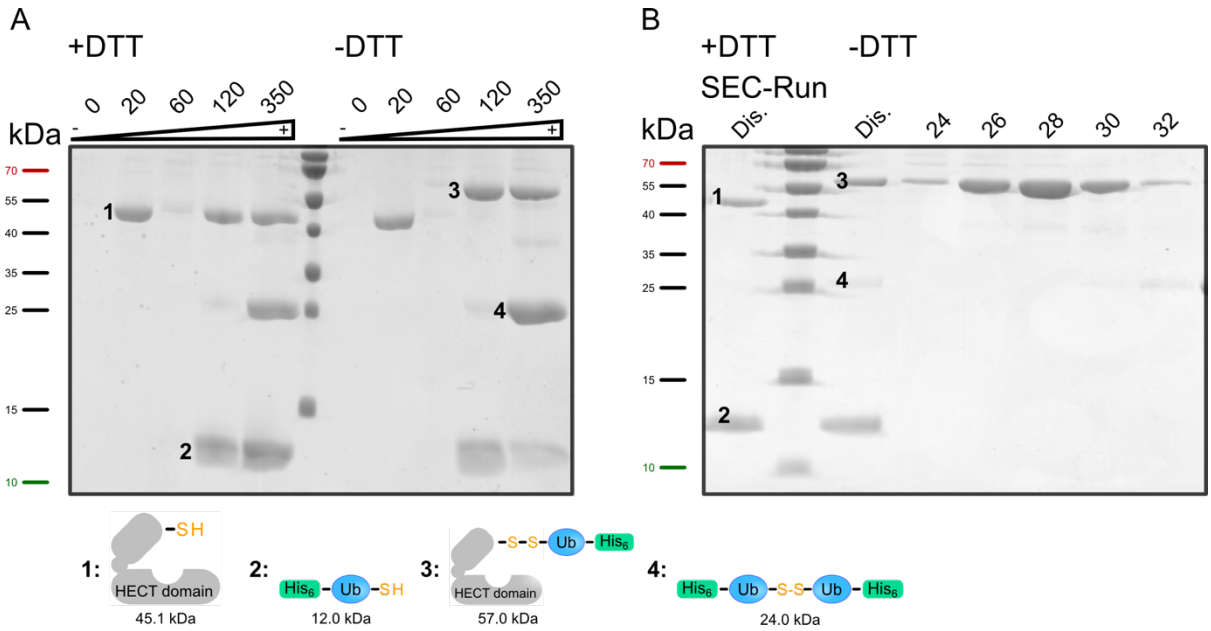

Figure 24: SDS-PAGE of a HECT-Ub disulfide. (A) Shows the SDS-PAGE during the formation of the disulfide bond between the HECT domain and Ub G76C loaded with and without DTT to show the successful formation of the disulfide bond. The top panel shows an increasing concentration of Imidazole in mM which was used to separate the disulfide from the side products in a stepwise elution from the Ni-NTA-beads. **(B)** SDS-PAGE after a SEC run with the purified disulfide with and without DTT to show the successful formation of the disulfide bond. At the top panel the SEC input consisting of disulfide (Dis.) (from (A), 120mM Imidazole elution) is loaded as a control. The numbers on the top reflect the positions of fractions from the SEC. The numbers at the bottom reflect the different reaction products during disulfide formation and purification steps with the corresponding molecular mass.

5.1.5. DTNB catalysed disulfide formation is a versatile tool to study reaction intermediates of the ubiquitination pathway

With this newly established technique, I and other lab members were able to generate different reaction intermediates of the ubiquitination pathway ranging from E2~Ub thioester mimics to complexes of HECT domains with an acceptor Ub (**Table 4**). This demonstrates the straightforward easiness and adaptability of the developed approach to investigate reaction intermediates of the ubiquitination pathway.

Table 4: Disulfides formed in the Wiesner laboratory by chemical activation of ubiquitin. Table 4 shows all disulfides formed to date using the technique of chemical activation of Ub. Single Cys enzyme mutants are denoted by the presence of the name tag "only" in combination with the respective single Cys, e.g. Ube2T C86 only indicates the Ube2T mutant in which only C86 is remaining. The Huwe1 HECT ½ Δ α1 refers to a mutation where the first half of the N-terminal helix α1 is truncated.

Catalytic intermediate	Ubiquitination enzyme	Enzyme variant	Ubiquitin variant	Biophysical Characterization	Experimenter
Mono-ubiquitination	E2	Ube2T C86A/K91C	Ub G76C	NMR	Hyz. K
Thioester	E2	Ube2T C86 only	Ub G76C	NMR	Hyz. K
Thioester	E2	Ubc4 C86 only	Ub G76C	SEC / NMR	Anders, S.; Schütz-Stoffregen, M.
Thioester	E2	UbcH7 C86 only	Ub G76C	SEC	Jäckl, M.
Thioester	E3	Huwe1 C-lobe C352 only	Ub G76C	NMR and X-ray	Stohäker, T.; Stollmaier, C.; Jäckl, M.
Thioester	E3	Smurf2 C-lobe C716 only	Ub G76C	NMR and X-ray	Stollmaier, C.; Jäckl, M.
Thioester	E3	Rsp5 C-lobe C777 only	Ub G76C	NMR	Stollmaier, C.
Thioester	E3	Huwe1 HECT C352 only	Ub G76C	NMR and X-ray	Strohäker, T.; Jäckl, M.
Thioester	E3	Huwe1 HECT C352 only	Ub I44A/G76C	NMR and X-ray	Jäckl, M.
Thioester	E3	Huwe1 HECT ½ Δ α 1 C352 only	Ub G76C	NMR	Jäckl, M.
Thioester	E3	Huwe1 HECT F192A/C352 only	Ub G76C	NMR	Jäckl, M.
Thioester	E3	Huwe1 HECT A349F/C352 only	Ub G76C	NMR	Jäckl, M.
Thioester	E3	Smurf2 HECT C716 only	Ub G76C	NMR	Jäckl, M.
Thioester	E3	Rsp5 HECT C777 only,	Ub G76C	NMR	Stollmaier, C.
Thioester	E3	Huwe1 HECT M328V/C352 only	Ub G76C	NMR	Tholen, J.
Thioester and non-covalent Ub binding	E3	Huwe1 HECT N113C/C352 only	2*Ub G76C	NMR	Jäckl, M.
Thioester and acceptor binding	E3	Rsp5 C-lobe C777 only	diUb G76C	NMR	Stollmaier, C.
Thioester and acceptor binding	E3	Rsp5 HECT C777 only,	diUb G76C	NMR	Stollmaier, C.
Acceptor binding	E3	Huwe1 HECT C352 only	Ub K11C	NMR	Jäckl, M.
Acceptor binding	E3	Huwe1 HECT C352 only	Ub K48C	NMR	Jäckl, M.
Acceptor binding	E3	Rsp5 HECT cat. Cys only,	Ub K63C	NMR	Stollmaier, C.
Acceptor binding	E3	Huwe1 HECT C352 only	Ub K63C	NMR	Jäckl, M.
Non-covalent Ub binding	E3	Huwe1 HECT Y117C/C352K	Ub G76C	NMR	Jäckl, M.
Non-covalent Ub binding	E3	Smurf2 HECT E87C/C715K	Ub G76C	NMR and X-ray	Jäckl, M.
Non-covalent Ub binding	E3	Huwe1 HECT E83C/C352K	Ub G76C	NMR	Jäckl, M.
Non-covalent Ub binding	E3	Huwe1 HECT N113C/C352K	Ub G76C	NMR and X-ray	Jäckl, M.

5.1.6. Crystallographic analysis of HECT reaction intermediates mimicked through disulfide formation

As a useful method to structurally characterize the ubiquitination reaction intermediates mimicked by disulfide formation, I used NMR-spectroscopy and X-ray crystallography as biophysical method. I was able to solve the crystal structures of the disulfides for the Huwe1 HECT N113C / C352K and Ub G76C (**Figure 25** A) as a mimic of non-covalent Ub binding by molecular replacement at 2.9 Å (Sup. **Table 17**). Clear electron density of the disulfide bond was present in the structure and was verified using iterative-built OMIT maps to check for model bias [116] (**Figure 25**, B). Of note, the sulfur atoms of the disulfides have similar B-factors as their surrounding atoms (**Figure 25**, C) thereby indicating a well-ordered environment of the disulfides. Taken together, the OMIT map and the B-factors show that the disulfide bond is formed properly (**Figure 25**). Most importantly, no steric distortions were observed for the region surrounding the disulfide bridges demonstrating that disulfide linkage is a valid tool to mimic ubiquitination reaction intermediates. Therefore, I was able to show that the DTNB catalysed disulfide formation generates stable disulfides between a variety of HECT domains and ubiquitins that allows for the study of otherwise unstable intermediates of the Ub transfer pathway of HECT domains. In addition, the analysis of these disulfide complexes is not only limited to X-ray crystallography but can be also performed by other biophysical methods which require stable proteins such as NMR spectroscopy.

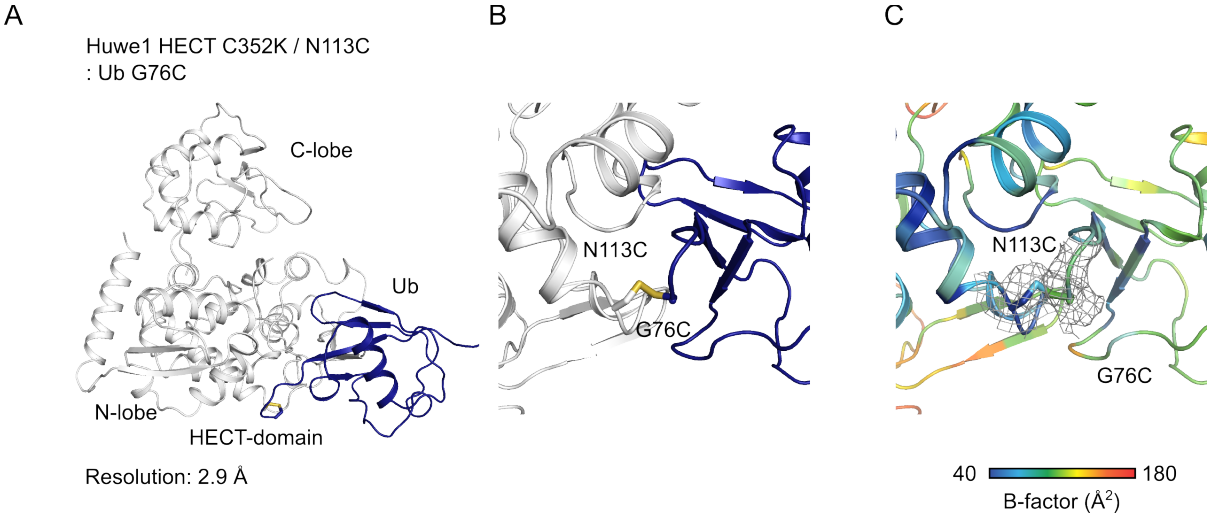

Figure 25: X-ray structure of a disulfide between ubiquitin and the HECT domain. (A) Ribbon representation of the Huwe1 HECT N113C / C352K : Ub G76C disulfide mimicking non-covalent Ub binding with the HECT domain in white and the Ub in blue on the left. **(B)** A close up of the disulfide bond between the HECT domain and Ub represented in sticks is shown in the centre panel. **(C)** The atoms are coloured according to their B-factors from blue to red with

ranging from 40 - 180 Å^2. The iteratively built OMIT electron density map [116] of the disulfide bond is shown as 2Fo-Fc map contoured at a sigma level of 1.0 to highlight the presence of the disulfide bond in the crystal structure.

Previously, the Rsp5 HECT: UbV R5.4 (PBD: 5hpl) and WWP1 HECT : UbVP2.3 (PBD: 5hpt) complexes where published [117]. Both of these structures show a similar orientation of the non-covalently bound Ub as the Huwe1 HECT N113C / C352K : Ub G76C complex (**Figure 26** A, B). Therefore, I aligned the Rsp5 HECT: UbV R5.4 and WWP1 HECT : UbVP2.3 complexes with the Huwe1 HECT N113C / C352K : Ub G76C complex to determine the backbone root-mean square deviation (RMSD). The RMSD measures the average distance between the backbone atoms of a superimposed structure. Therefore, a high degree of structural similarity is reflected by a low RMSD. Here, the superimposed Rsp5 HECT: UbV R5.4 shows an RMSD of 2.55 Å and the WWP1 HECT : UbVP2.3 an RMSD of 2.46 Å with the Huwe1 HECT N113C/C352K : Ub G76C complex (**Figure 26** B). Hence, the RMSD reflects the high similarity between Huwe1 HECT N113C/C352K : Ub G76C disulfide and Rsp5 HECT: UbV R5.4 and WWP1 HECT : UbVP2.3 complexes.

In conclusion, I was able to show that the Huwe1 HECT domain UBS interacts highly similar as the Rsp5 HECT and WWP1 HECT domain with Ub. Therefore, the DTNB catalysed disulfide formation is able to generate HECT : Ub complexes which reflect different steps of the HECT domain Ub transfer pathway.

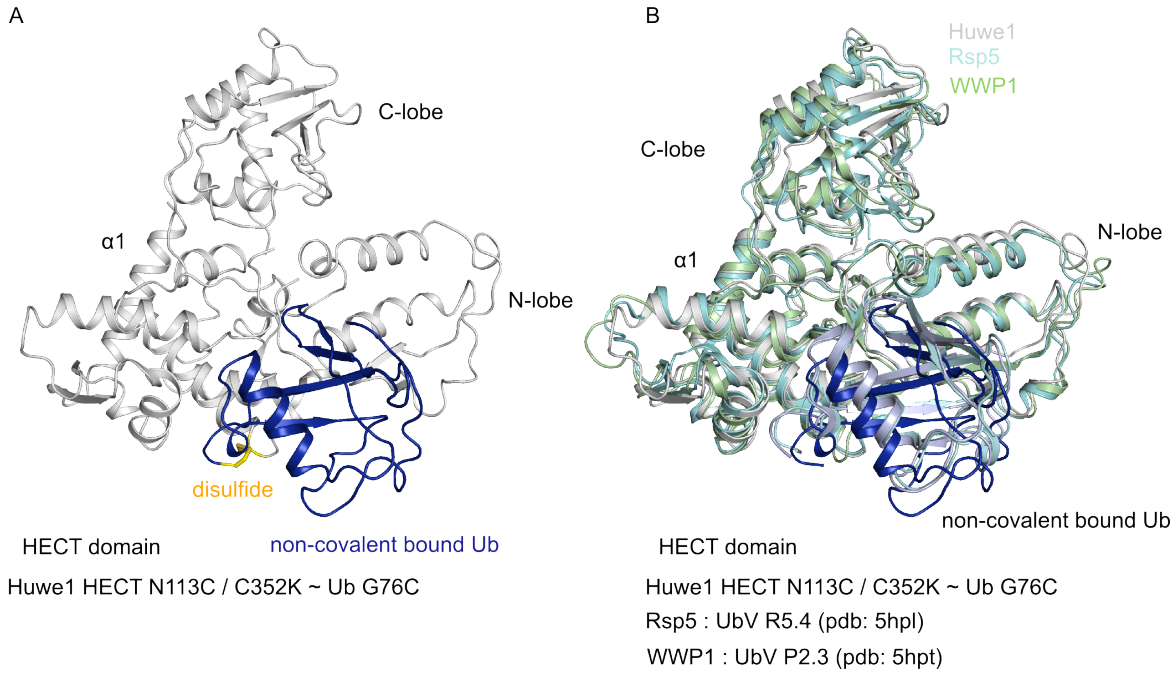

Figure 26: The structure of the Huwe1 HECT N113C : Ub G76C complex is highly similar to the Rsp5 HECT : UbV R5.4 and WWP1 HECT : UbVP2.3 complex. (A) Ribbon representation of the x-ray structure of the Huwe1 HECT

N113C/C352K : Ub G76C disulfide with Huwe1 shown in white and Ub G76C coloured in blue. The disulfide bridge (Huwe1 HECT N113C/C352K : UbG76C) is depicted as sticks. **(B)** Overlay of the crystal structures of the Huwe1 HECT N113C/C352K (white):UbG76C (blue) with Rsp5 HECT: UbV R5.4 (cyan) (PBD: 5hpl) and WWP1 HECT : UbVP2.3 (light green) (PBD: 5hpt) complex [117].

5.1.7. NMR analysis of HECT reaction intermediates mimicked through disulfide formation

Apart from crystallographic studies I analysed several different Huwe1 HECT-Ub disulfides by comparing the NMR spectra of the disulfides with those of the individual components, i.e. the HECT domain and Ub. To investigate structural rearrangements and interactions during thioester formation, I generated Huwe1 HECT ~ Ub G76C disulfides to mimic the transthiolation reaction between the Ub C-terminus (G76C) and the catalytic cysteine (C352) of the HECT domain (**Figure 27** A, **Figure A 1**). In order to avoid non-covalent binding of Ub to the UBS, I used a Ub mutant (I44A) in the background of the G76C mutant. The I44A mutation is known to abolish non-covalent Ub binding to HCT domains [50], [55].

With the HECT-Ub disulfide in hands, I recorded $^{1}H,^{13}C$-methyl TROSY NMR spectra of the HECT domain in comparison to the HECT C352 ~ Ub I44A/G76C disulfide (**Figure 27** A left). Of note, several pronounced CSPs of residues in the C-lobe in close proximity of the catalytic Cys were observed (M157, I331 and M328). However, we also observed that residues experiencing CSPs were distributed almost all over the HECT domain indicating that large conformational changes occur upon thioester formation (**Results 5.3**).

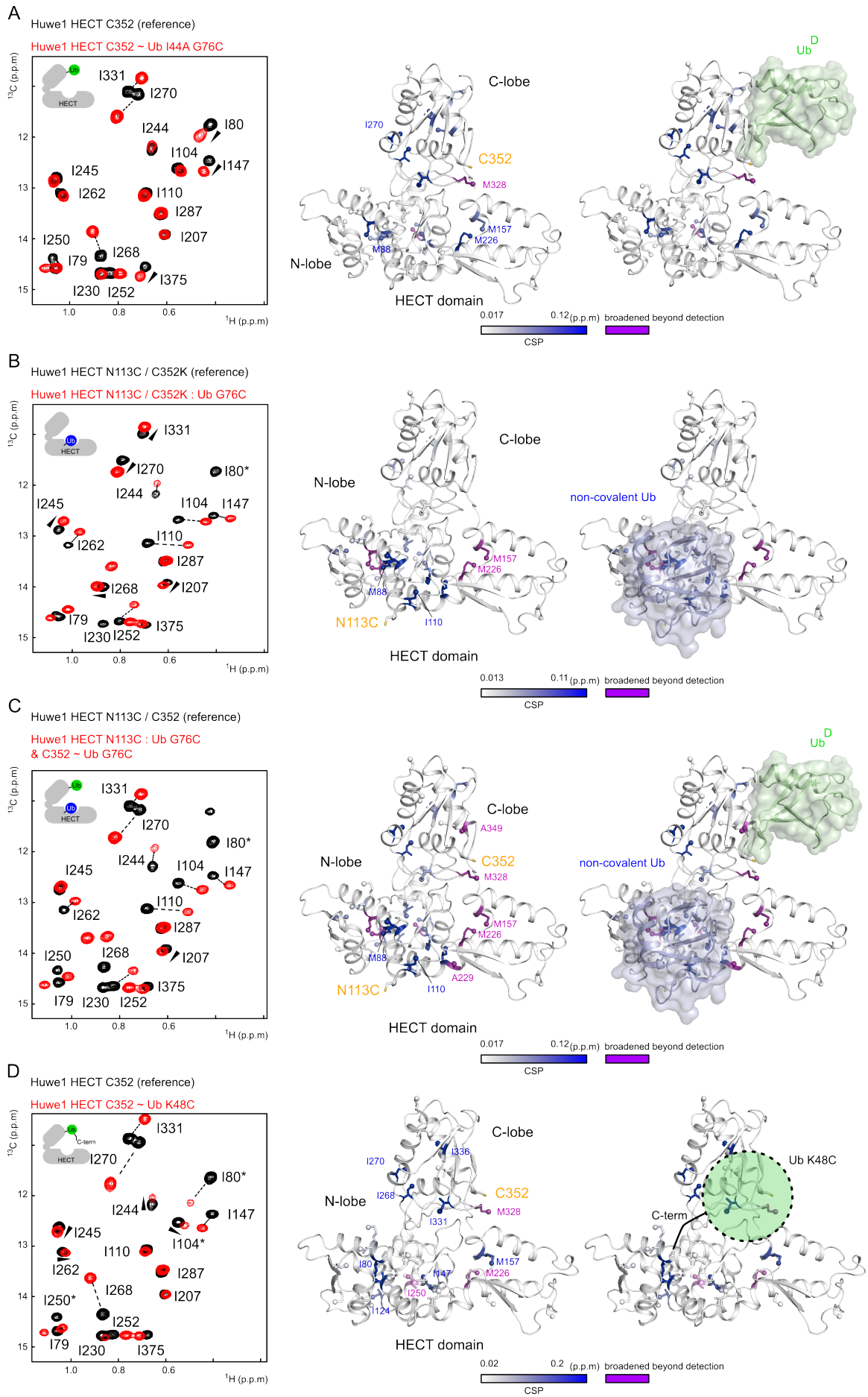
A
Huwe1 HECT C352 (reference)
Huwe1 HECT C352 ~ Ub I44A G76C
I331
I270
I80
I244
I104
I147
I245
I262
I110
I287
I207
I250
I268
I79
I375
I230
I252
HECT
Ub
^{13}C (p.p.m)
^{1}H (p.p.m)
C-lobe
N-lobe
HECT domain
I270
C352
M328
M157
M226
M88
Ub^{D}
0.017
0.12 (p.p.m)
broadened beyond detection
CSP
B
Huwe1 HECT N113C / C352K (reference)
Huwe1 HECT N113C / C352K : Ub G76C
I80*
C-lobe
N-lobe
non-covalent Ub
N113C
I110
0.013
0.11 (p.p.m)
C
Huwe1 HECT N113C / C352 (reference)
Huwe1 HECT N113C : Ub G76C
& C352 ~ Ub G76C
A349
A229
D
Huwe1 HECT C352 (reference)
Huwe1 HECT C352 ~ Ub K48C
C-term
I104*
I250*
I336
I268
I124
Ub K48C
0.02
0.2

Figure 27: NMR analysis of the Huwe1 HECT-Ub disulfides mimicking different steps along the Ub ligation pathway. (A) left, NMR experiments with ^{1}H ^{13}C-methyl IM labelled Huwe1 HECT domain as indicated. Overlay of a representative region of the ^{1}H ^{13}C-methyl TROSY spectra of a single Cys mutant of the Huwe1 HECT domain (black) as reference and a disulfide between the respective Huwe1 HECT domain and a Ub mutant. Arrowheads and dotted lines indicate the direction of the chemical shift perturbations in comparison to the reference spectra (black).
In the left corner of the spectra the catalytic state is represented as cartoon. Middle and right panel, CSPs induced by the formation of the Huwe1 HECT mutant ~ Ub mutant disulfide mapped onto a model of Huwe1 HECT generated by MODELLER [118]. The HUWE1 HECT model is based on the Nedd4 HECT~Ub^{D}:Ub complex (PDB 4bbn) [50]. The CSPs are coloured from white to blue as indicated. Magenta indicates residues broadened beyond detection. The HECT domain is shown in white cartoon representation. The effected amino acids are shown in stick representation and the methyl groups as spheres. **(A)** with the Huwe1 C352 HECT domain and its disulfide with Ub I44A/G76C. **(B)** with the Huwe1 N113C/C352K HECT domain and its disulfide with UbG76C. The CSPs induced by the formation of the Huwe1 HECT N113C/C352C : Ub G76C disulfide can be explained by the presence of a Ub bound to the non-covalent Ub binding surface (blue). **(C)** with the IMA labelled Huwe1 HECT N113C/C352 domain and its double disulfide with Ub G76C at N113C and C352. The CSPs induced by the disulfide can be explained by the presence of the Ub^{D} (green) and the non-covalent bound Ub (blue) in the UBS of the HECT domain. **(D)** with the Huwe1 C352 domain and its disulfide with Ub K48C mimic the attack of the acceptor Ub.

Next, I investigated the interaction of the Huwe1 HECT domain with an Ub residing in its UBS. This step would report on a step in the ubiquitination reaction chain that is important for Ub chain elongation. To this end, I mutated the catalytic Cys to a lysine (C352K) and asparagine 113 which is in close proximity to the UBS to Cys (N113C). With this mutation, Ub G76C was placed into the ubiquitin binding surface *via* DTNB catalysed disulfide formation to mimic non-covalent Ub binding. Comparison of the ^{1}H,^{13}C-methyl TROSY NMR spectra of the HECT N113C/C352K : Ub G76C disulfide and the HECT domain (**Figure 27** B left side, **Figure A 1**) revealed CSPs for methyl groups that map to the expected UBS (I79, I80, M84, M88, I104, I110 and M328), but also of residues remote from the UBS such as I124, I230, I270, I268 and I331. Since the isolated Huwe1 HECT domain is incapable of interacting with Ub in a non-covalent manner (**Results 5.3**) the CSP were mapped on a model of the Huwe1 HECT domain generated by MODELLER [118] using the Nedd4 HECT ~ Ub^{D}: Ub complex (PDB: 4bbn) as template [50] (**Figure 27** B middle panel). The strongest CPSs were observed for residues in the N-lobe of the HECT domain where monomeric Ub is expected to bind [50] (**Figure 27** B right side). In contrast, the CSPs outside the UBS were much smaller, but nonetheless indicate conformational rearrangements occurring upon non-covalent Ub binding (**Figure 27** B middle and right panel).

In order to investigate the entire Huwe1 HECT~Ub^D:Ub intermediate in a manner similar to the Nedd4 HECT ~ Ub^D: Ub complex [50], I introduced N113C mutation in the background of the Huwe1 HECT domain that contained the catalytic Cys (C352) as sole Cys. This mutation allows the formation of a double disulfide of the Huwe1 HECT domain with one Ub G76C serving as donor Ub and the other as non-covalent Ub. The comparison of the $^{1}H,^{13}C$-methyl TROSY NMR spectra of the HECT domain to the HECT ~ Ub : Ub double disulfide (**Figure 27** C left side, **Figure A 1**) shows CSPs originating from both disulfides and can be viewed as an overlay of the effects observed with the HECT C352 ~ Ub I44A/G76C disulfide (thioester mimic) and the Huwe1 HECT N113C / C352K : Ub G76C disulfide (mimic for non-covalent Ub binding). Mapping of the observed CSPs (**Figure 27** C middle panel) recapitulated the individual effects of donor and non-covalent Ub binding demonstrating that these two catalytic steps are largely independent from each other (**Figure 27** A-C middle and right panel). To gain insights into a step further along the catalytic pathway, I probed the effect of an acceptor Ub (Ub^A) attacking the thioester bond between Ub^D and the catalytic cysteine as Huwe1 was shown to catalyse K48 linked Ub chains [7]. Therefore, I cross-linked Huwe1 C352 HECT with a Ub K48C mutant to mimic the acceptor Ub and recorded a $^{1}H,^{13}C$-methyl TROSY NMR spectrum (**Figure 27** D, **Figure A 1**) and mapped the obtained CSPs onto on a model of the Huwe1 HECT domain generated by MODELLER [118] using the Nedd4 HECT ~ Ub^D: Ub complex (PDB: 4bbn) as template [50]. The spectrum of the Huwe1 C352 HECT ~Ub K48C disulfide shows in comparison with the HECT C352 ~ Ub I44A/G76C disulfide similar CSPs in the residues I80, I147, I230, I250, I268, I270, I331 and I375 with respect to the references. Interestingly the residues I147, I268, I270 and I331 are affected stronger in the Huwe1 C352 HECT ~Ub K48C than in the HECT C352 ~ Ub I44A/G76C disulfide. This suggest a strong conformational change of the HECT domain. In sum, I conclude that DTNB catalysed disulfide formation allows for the structural investigation of the complex reaction intermediates formed during Ub chain elongation.

5.1.8. Discussion

Here, I could show that the chemically driven disulfide formation is a remarkable tool to study Ub transfer on a structural level. A major problem of studying ubiquitination reaction interaction intermediates is the presence of the natural formed thioester intermediate between different enzymes of the ubiquitination reaction e.g. E1 ~Ub, E2 ~Ub or E3 ~Ub. This intermediate is necessary for the transfer of the Ub because the thioester stores the energy for the next transfer step in the reaction. Unfortunately, the thioester bond is prone to hydrolysis, and therefore structural studies by biophysical methods like NMR-spectroscopy or X-ray crystallography are difficult to perform. To overcome this instability the chemically similar disulfide bond (**Figure 21**) was used which is stable against spontaneous hydrolysis and can be stored under non–reducing conditions for months. This has been shown for different ubiquitination enzymes like the E3 HECT ligase Nedd4 [50] as well as for different ubiquitination enzymes in our laboratory (**Table 4**). To use this method, all solvent-exposed cysteines of the enzyme of interest have to be removed and only one solvent-exposed cysteine remains. This is one of the drawbacks of this method since not every protein is stable after the substitution of all cysteines. Another issue is that the desired disulfide may have a similar molecular weight as the side products and thus cannot be separated by size-exclusion chromatography. For example, a typical E2~Ub G76C disulfide has a molecular weight of 30 kDa, while the Ub G76C dimer as a side product has a molecular weight of 25 kDa. In this case, other protein purification techniques have to be used. Since the method developed by myself utilizes His-tagged Ub in combination with Ni-affinity chromatography for the DTNB catalysed disulfide formation, it already contains an intrinsic separation step (**Figure 23**) and combination with further downstream purification steps offers numerous possibilities for separating side products. Of note, the Ub itself has to be mutated since WT Ub does not contain native Cys residues. In order to study thioester formation, the C-terminal glycine in Ub was mutated to a cysteine. To study poly-Ub chain formation, the lysine residues that serve as linkage points can be replaced by a cysteine such as K48. This versatility to introduce Cys mutations at any desired position holds the potential to investigate a tremendous amount of different ubiquitination reaction steps and products.

In the approach which I was able to establish in the laboratory of Dr. Silke Wiesner I used Ellman's reagent to chemically activate the thiol group of the Ub mutants. In different wash steps, I could form a disulfide bond between a HECT domain and Ub on a Ni-NTA column (**Figure 23**). Furthermore, I was able to validate the existence of the disulfide bond by SDS-PAGE (**Figure 24**), X-ray crystallography (**Figure 25**) and NMR-spectroscopy (**Figure 27**). Moreover, I could show that the results obtained for the Huwe1 HECT ~ Ub complex with my protocol (**Figure 25, Figure 26**) correlate well with the known structure of the intermediate of HECT E3 ligase Rsp5 HECT and WWP1 (**Figure 26**) [117]. By alignment of the backbone of the Huwe1 HECT N113C / C352K :UbG76C complex with the structure of Rsp5 and WWP1 in complex with Ub [117] I was able to extract the RMSDs (**Figure 26**). Superimposed with the Huwe1 N113C / C352K structure, the RMSDs for Rsp5 is 2.55 Å and the RMSD for WWP1 is 2.46 Å. The low RMSD reflects the high similarity between the structures. This proves the ability of DTNB catalysed disulfide formation to mimic the native conformation of HECT domain reaction intermediates which have been shown in the literature for Rsp5 and WWP1 in complex with Ub [117]. In addition, I could show by NMR-spectroscopy for the Huwe1 HECT N113C/C352 ~ UbG76C : UbG76C and Huwe1 HECT N113C/C352K ~ UbG76C that the obtained CSPs fit to the thioester interaction surface on the C-lobe and to the ubiquitin binding surface on the N-lobe of the HECT domain (**Figure 27** B, C) in solution. With these results, I conclude that the method that I established and the disulfides that I formed are able to reflect different reaction intermediates of the Ub transfer cascade.

Because of its simplicity, this method is now commonly used in the Laboratory of Dr. Silke Wiesner to investigate different reaction intermediates of the Ub-transfer pathway (**Table 4**). Therefore, the method holds the potential to studied short lived interactions like thioesters in the ubiquitination reaction on a structural level with biophysical techniques like NMR-spectroscopy or X-ray crystallography.

In sum, I could establish and improve the technique of the chemical activation and subsequent disulfide formation between the thiol groups of cysteines in proteins in the Wiesner Laboratory.

5.2. β sheet augmentation – a common theme in ubiquitin HECT-domain interaction

5.2.1. Contribution

This work was carried out in collaboration with the research group of Dr. Simona Polo from the Institute FIRC of Molecular Oncology (IFOM), Milan, Italy. Contributions by others are listed in the figure legends. This part of the work is published in the Journal of molecular biology: "β-Sheet Augmentation Is a Conserved Mechanism of Priming HECT E3 Ligases for Ubiquitin Ligation" [88].

5.2.2. Introduction

Structural information on HECT-mediated Ub transfer is available almost exclusively for the K63-specific Nedd4-family ligases. To gain insight into the catalytic mechanism of E3s that do not belong to the Nedd4 family, I investigated the mechanism of thioester formation for Huwe1 (a.k.a. MULE, ARF-BP1, Lasu1 or HECTH9) an K6-, K48- and / or K11-linked chain specific Ub HECT E3 ligase [21], [51], [67], [68], [119] and for Smurf2, a K63- chain specific Ub HECT E3 ligase from the Nedd4 family. By using NMR spectroscopy and X-ray crystallography, I could characterize the catalytic mechanism of the Huwe1 HECT domain and compared it in detail to the Nedd4-family member Smurf2. The findings show that the Huwe1 and Smurf2 C-lobe~Ub^D complexes are not only highly similar on a structural level but also share on a functional level common mechanism of transthiolation and isopeptide formation.

5.2.3. Results

5.2.4. The Huwe1 HECT domain forms preferentially K6- and K48-linked Ub chains

To gain insight into Huwe1 Ub chain specificity, I performed auto-ubiquitination assays with the isolated Huwe1 HECT domain using WT and single Lys Ub mutants (**Figure 28** A).

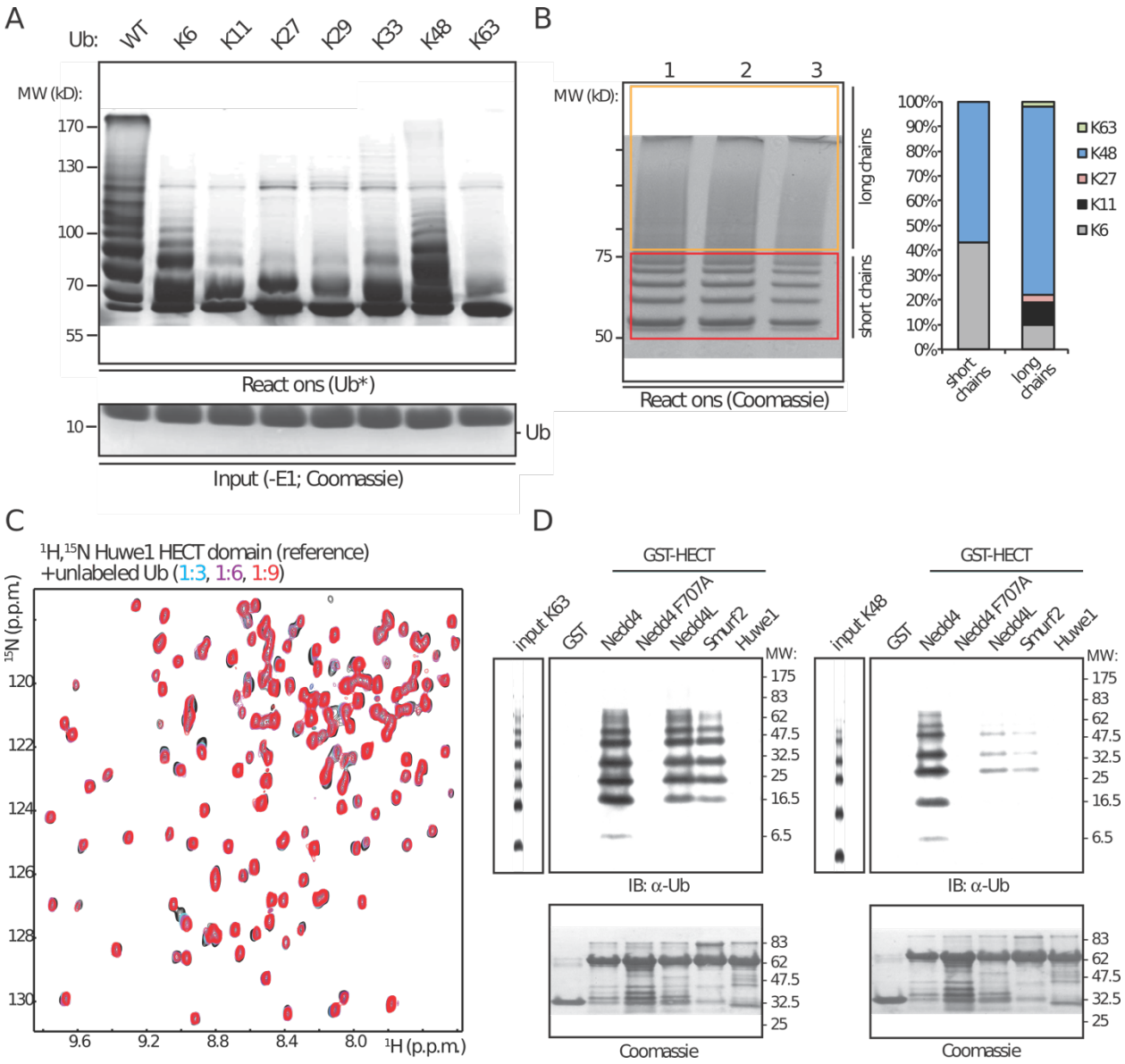

Figure 28: Ub chain specificity and functional characterization of the Huwe1 HECT domain. (A) *In vitro* auto-ubiquitination of the Huwe1 HECT domain in the presence of E1 (Ube1) and E2 (UbcH7) with WT or single Lys Ub mutants as indicated. **(B)** AQUA analysis of poly-Ub chain linkages formed by the Huwe1 HECT domain. Left panel: SDS-PAGE gel of the poly-Ub chains formed by the Huwe1 HECT domain in the *in vitro* auto-ubiquitination reactions used for AQUA analysis. Right panel: AQUA proteomics quantification of the poly-Ub linkages showing the means and s.d. from measurements of the three reactions depicted in the gel on the left. Data of the AQUA analysis were provided by Elena Maspero and Simona Polo. **(C)** Overlay of a representative region of the $^{1}H,^{15}N$-TROSY NMR spectra of the ^{15}N-labelled Huwe1 HECT domain in the absence (black) and presence of increasing stoichiometric amounts of unlabelled monomeric Ub as indicated. The Huwe1 HECT Ub NMR titration experiments were performed by Timo Strohäker. **(D)** GST pull-down assays with commercial K63- (left panel) and K48-linked (right panel) poly-Ub chains and GST-tagged HECT domains or GST alone as indicated. Immunoblot (IB) and Coomassie as indicated. The GST pull-down assays were performed by Elena Maspero in the lab of Simona Polo. Adapted from Jäckl *et al.*, 2018 [88] and printed with the permission of Elsevier.

The most active Ub variant for the Huwe1 HECT domain was the Ub WT, Ub K48- and K6-only. This demonstrates that K6 and K48 are the preferred Lys residues in Ub for poly-Ub chain synthesis by the Huwe1 HECT domain. For more detailed analysis our collaboration partners Elena Maspero and Simona Polo examined the Ub chain type specificity of the Huwe1 HECT domain with absolute-quantification (AQUA) assays [120]. Therefore, they used three independent auto-ubiquitination reactions (**Figure 28** B; left panel) to perform AQUA mass spectrometric analysis and quantified the di-Gly peptide bonds within the formed Ub chains (**Figure 28** B; right panel). The results of the AQUA mass spectrometric analysis reflect the results of the auto-ubiquitination assays with the single Lys Ub mutants, with the Huwe1 HECT domain predominantly producing K48- and K6-linked oligomeric Ub chains. Elena Maspero and Simona Polo could also observe a difference Ub chain composition depending on the length of the poly-Ub chain. Shorter Ub chains contained besides K48-linked chains smaller fractions of K6- and K11-linked chains, whereas longer chains contained mailnly K48 chains (**Figure 28** B; right panel). In sum, these results show that Huwe1 HECT domain prioritizes K6-, K11- and K48-linked poly-Ub chains and thus differs in Ub chain specificity from Nedd4-family members such as Smurf2, Nedd4 and WWP1 [50], [119].

5.2.5. The Huwe1 HECT domain does not interact with Ub in a non-covalent manner

It has been shown for numerous of members of the Nedd4 family that they contain a non-covalent Ub binding surface that promotes Ub chain elongation [51], [52], [55], [117], [119].

To examine whether the Huwe1 HECT domain possesses a non-covalent Ub binding surface Timo Strohäker performed NMR titration experiments with ^{15}N-labelled and partially deuterated Huwe1 HECT domain. He added up to 9-fold stoichiometric excess of WT Ub to the HECT domain and compared the respective ^{1}H,^{15}N-TROSY spectra of the Huwe1 HECT domain (**Figure 28** C). However, even at a large excess of Ub only very few chemical shift changes could be observed.

Moreover, our collaboration partners Elena Maspero and Simona Polo performed a pull-down assay with commercial K63- and K48-linked poly-Ub chains and the GST-tagged HECT domains of Nedd4, Nedd4L, Smurf2 and Huwe1 (**Figure 28** D). As a negative control experiments they used GST and the Nedd4 F707A mutant that is defective in non-

covalent Ub binding [50]. As expected, they found for the HECT domains Nedd4, Nedd4L and Smurf2, which are members of the Nedd4-family an interaction of the HECT domains with K63-linked poly-Ub chains (**Figure 28** D; left panel) and to a lesser extend with K48-Ub chains (**Figure 28** D; right panel). In contrast, the Huwe1 HECT domain and the negative control proteins GST and the Nedd4 F707A mutant were unable to pull down K63- or K48-linked poly-Ub chains. In sum, the NMR analysis and the pull-down assays show that the Huwe1 HECT domain does not interact with Ub in a non-covalent manner in contrast to Nedd4-family HECT domains. The fact that the Huwe1 HECT domain is none-the-less able to synthesize poly-Ub chains points towards a different catalytic mechanism for Huwe1 in comparison to the Nedd4 HECT ligases family.

5.2.6. The Huwe1 C-lobe~Ub^{D} complex is highly similar to Nedd4 family E3s

To gain more detailed information of the catalytic intermediates of the Huwe1 HECT domain in comparison to Nedd4 HECT-type E3s, I characterized the Huwe1 and Smurf2 thioesters on a structural level. For structural analysis, I bypassed the instability of the thioesters by forming chemically similar, yet hydrolysis-resistant disulfides between a G76C mutant that served as donor Ub (Ub^{D}) and a Smurf2 or Huwe1 HECT domain that was Cys-free except for the catalytic Cys residue as described in the result part 5.1.

Unfortunately, the Smurf2 HECT~Ub disulfide was prone to aggregation and did not crystallize. In the crystal structure of the Nedd4 HECT~Ub^{D}:Ub complex the donor Ub showed only limited contacts to the N-lobe [50]. Therefore, I generated disulfides with the isolated Smurf2 and Huwe1 C-lobes and Ub G76C mimicking the donor Ub. I was able to solve the crystal structure of the Smurf2 C-lobe~Ub^{D} complex at 2.5 Å resolution by molecular replacement (**Figure 29** A, Sup. **Table 18**).

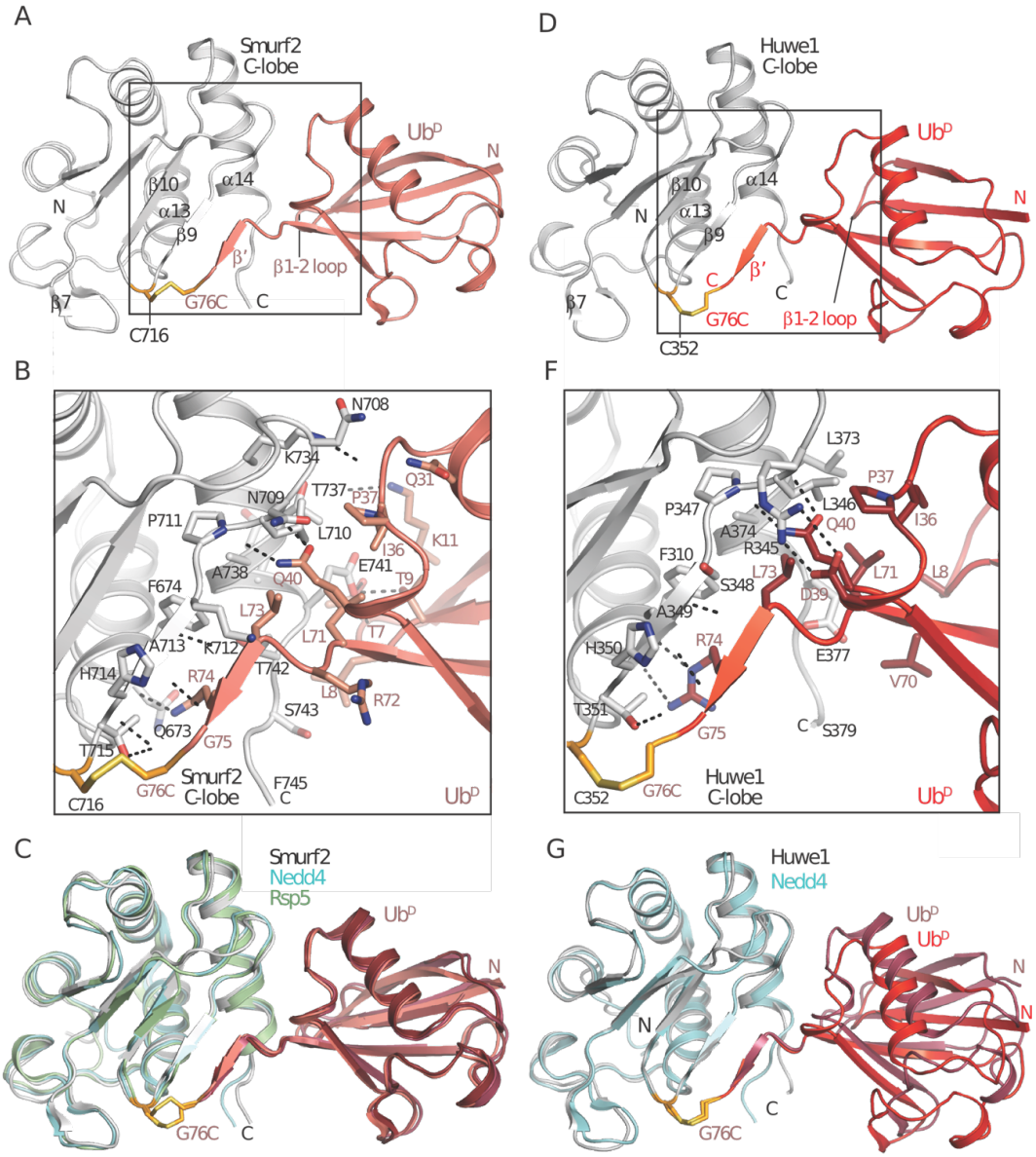

Figure 29: The structure of the Huwe1 C-lobe~Ub complex is highly similar to Nedd4 family HECT~Ub intermediates. (A) Ribbon representation of the X-ray structure of the Smurf2 C-lobe~Ub disulfide. Smurf2 is shown in grey and Ub G76C in salmon. The disulfide bridge (Smurf2 C716 ~ Ub G76C) is depicted in stick representation. The region of the structure used in **(B)** is indicated with a black box. **(B)** Zoom-in on covalent and non-covalent interactions that define the Smurf2 C-lobe~Ub^D complex. Hydrogen bonds are shown with dashed lines. **(C)** Overlay of the crystal structures of the Smurf2 (grey), Nedd4 (cyan) (PDB-ID: 4bbn, [50]) and Rsp5 (green) (PDB-ID: 4lcd, [53]) C-lobe thioester intermediates. **(D)** As **(A)**, but for the Huwe1 C-lobe~Ub disulfide. Huwe1 is shown in grey and Ub G76C in red. The disulfide bridge (Huwe1 C352 ~ Ub G76C) is depicted in stick representation. **(E)** As **(B),** but for the Huwe1 C-lobe~Ub^D complex. **(F)** Overlay of the crystal structures of the Huwe1 (grey) and Nedd4 (cyan) (PDB-ID: 4bbn, [50]) C-lobe thioester intermediates. Adapted from Jäckl *et al.*, 2018 [88] and printed with the permission of Elsevier.

The crystal contained two complexes per asymmetric unit that superimposed with an RMSD of 0.49 Å for the backbone atoms (**Figure A 2**). Residues 73-75 of his C-terminal tail in Ub adopt an extended conformation and form an additional antiparallel β-strand with the β9 strand of the Smurf2 C-lobe (**Figure 29** A, B). In addition, the side chain of R74 in the Ub^D forms hydrogen bonds with the backbone amides of Q673 and F674 in the α13 helix of the Smurf2 C-lobe (**Figure 29** B). The β-sheet augmentation is complemented by two additional non-covalent interaction surfaces. The Ub residues I36-Q40 are involved in an interaction network with the Smurf2 residues N709 and L710 in the loop preceding the β9 strand and with residue T737 at the C-terminal end of the α14 helix. Moreover, the β1-2 loop (T7-T9) in Ub interacts with C-terminal residues of the α14 helix of the Smurf2 C-lobe (E741-T742) (**Figure 29** B). Compared with the Nedd4 HECT~Ub^D:Ub [50] and Rsp5 HECT~Ub^D:Sna3 [53] complexes, the non-covalent interaction networks are highly similar to the Smurf2 C-lobe~Ub^D complex. By the superimposing of the Smurf2 C-lobe~Ub^D complex with Nedd4 HECT~Ub^D:Ub [50] an RMSD of 0.63 Å and for Rsp5 HECT~Ub^D:Sna3 [53] an RMSD of 0.72 Å for the backbone atoms was observed(**Figure 29** C). I thus conclude that the overall architecture and interface composition of the C-lobe~Ub thioester complexes are highly conserved within the Nedd4 family of E3 ligases.

Next, I solved the crystal structure of the Huwe1 C-lobe~Ub^D at 2.8 Å resolution by molecular replacement (**Figure 29** D, Sup. **Table 19**). The crystal contained one complex per asymmetric unit. The Huwe1 C-lobe~Ub^D shows by comparison with the Nedd4 HECT~Ub thioester that the intermolecular contacts are preserved in the additional β-strand between the Ub C-terminus and the C-lobe β9 strand of Huwe1 (**Figure 29** D, E) The similarity of the Huwe1 C-lobe~Ub^D complex and the Smurf2 C-lobe~Ub^D is reflected in a backbone RMSD of 2.18 Å. The high overall RMSD is explained to the fact that the Ub^D of the Huwe1 C-lobe is slightly rotated with respect to the C-lobe of the Nedd4-family structures (**Figure 29** F). Of note, the slightly rotated of the Ub in the Huwe1 C-lobe~Ub^D complex is caused by a symmetry related Huwe1 C-lobe. Here, the Huwe1 C-lobe intercalates with the Ub:C-lobe interface and thereby rotate the Ub slightly in comparison to Nedd4. The RMSD of the C-lobe and Ub^D alone align to the backbone result in an RMSD of 0.80 Å and 0.47 Å. Nevertheless, the hydrogen bond network between the Ub^D and the C-lobe is largely preserved between Huwe1 and Smurf2 (**Figure 29** B, E).

The obtained data show that the structural arrangement of the Ub^D towards the HECT C-lobe is conserved among Nedd4 family members and Huwe1. Therefore β-sheet augmentation seems to be a common conformation occurring during the HECT~Ub thioester formation regardless of the Ub chain specificity of the HECT domain.

5.2.8. Interfering with β-strand formation disrupts thioester formation

To test the importance of non-covalent interactions in β-sheet augmentation during thioester formation, Carsten Stollmaier mutated a conserved Ala in the β9 strand of the Smurf2 (A713) and I mutated the corresponding A349 residue in the Huwe1 HECT domains to prolines (**Figure 30** A).

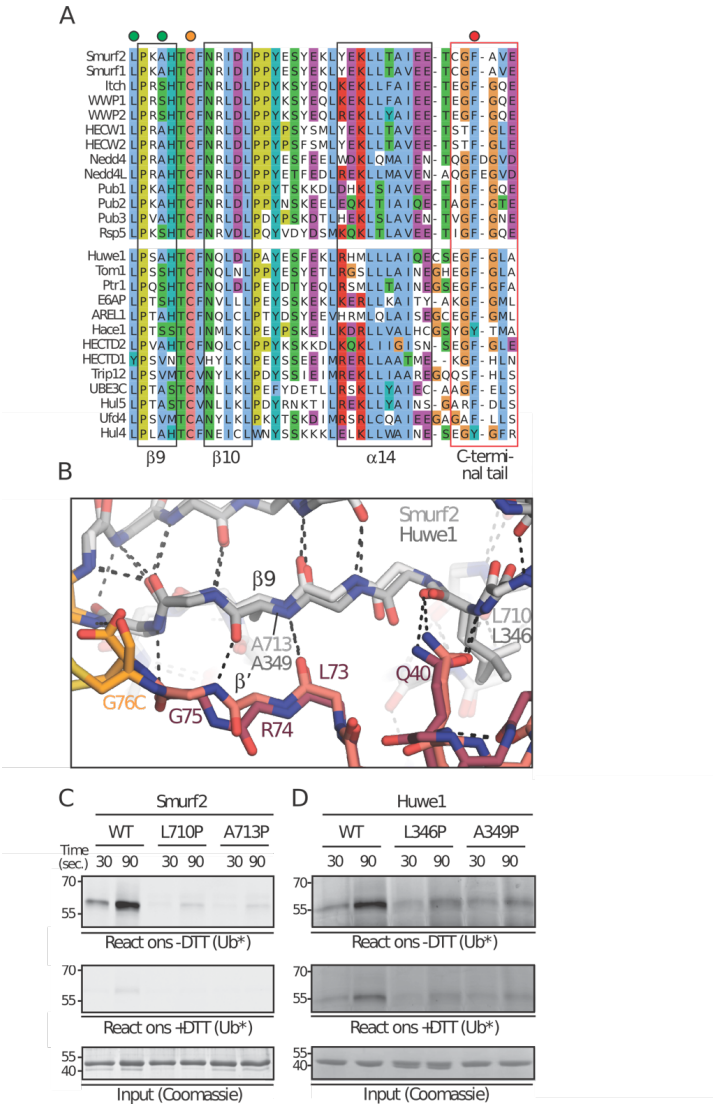

Figure 30: Mutations in the C-lobe~Ub^D interface interfere with thioester formation. (A) Multiple sequence alignment of the C-terminal residues of Nedd4 family (top) and other HECT-type (bottom) Ub ligases. Circles on top of the alignment highlight positions equivalent to L710 (Smurf2) / L346 (Huwe1) and A713 (Smurf2) / A349 (Huwe1)

that form hydrogen bonds *via* their amide nitrogen atoms to the thioester Ub (green), the catalytic Cys (orange) and the -4F residue (red). The four or five (in Nedd4 E3s) C-terminal residues are boxed in red, while secondary structure elements are boxed in black and indicated at the bottom. **(B)** Hydrogen bonding network at the C-lobe~Ub^{D} interface. The Huwe1 and Smurf2 C-lobe~Ub^{D} complexes are shown in stick representation with hydrogen bonds indicated by dashed lines. Residues in the C-lobes that were mutated to prolines in functional assays are labelled along with their hydrogen bonding partners in the Ub^{D}. **(C-D)** Thioester assays with Pro mutants in Smurf2 **(C)** and Huwe1 **(D)**. Transthiolation reactions were performed with bacterially expressed WT and mutant HECT domains as indicated. HECT thioester formation was monitored by using fluorescently labelled Ub (Ub*) after quenching the reaction at different time points by addition of Laemmli buffer without (top) or with (centre) reducing agent. Equivalent levels of HECT domains were confirmed by incubation of the proteins in the absence of E1 and visualised by Coomassie staining (bottom). The Smurf2 thioester assays were performed by Carsten Stollmaier. Adapted from Jäckl et al., 2018 [88] and printed with the permission of Elsevier.

Since prolines lack an amide proton this mutation should destabilize the hydrogen bond network between the Ub^{D} C-terminus and the C-lobe of the HECT~Ub thioester (**Figure 30** B). Indeed, the proline mutations in Smurf2 and Huwe1 HECT domain affected the Ub thioester formation. So, were the proline mutations of Smurf2 and Huwe1 defective in the thioester formation comparison to the WT HECT domain (**Figure 30** C, D). As a consequence, also the auto-ubiquitination was affected. Therefore, the Smurf2 mutants L710P and A713P as well as the Huwe1 mutants L346P and A349P show no auto-ubiquitination (**Figure 31**).

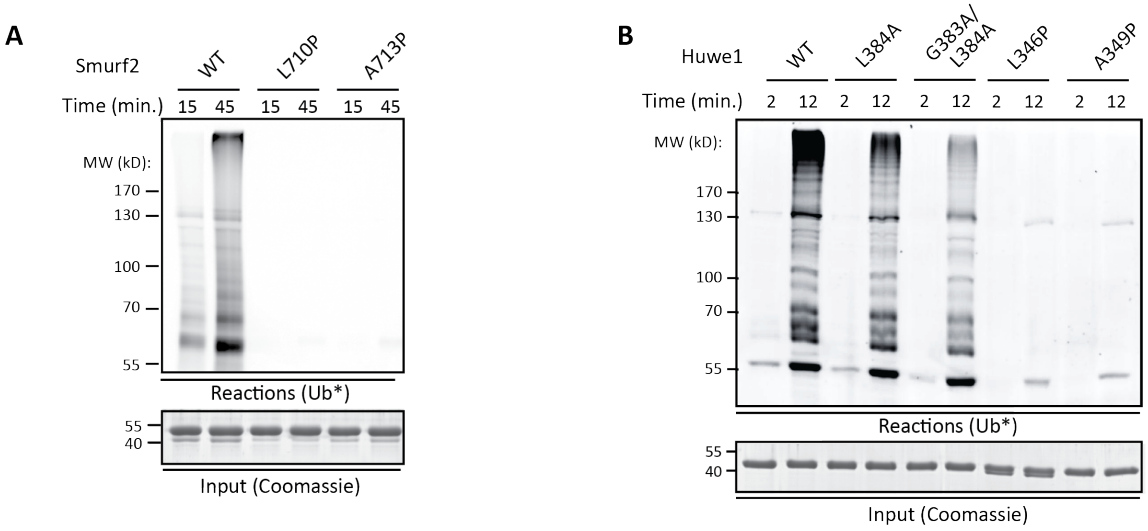

Figure 31: Mutations in the C-lobe~Ub^{D} interface of Smurf2 and Huwe1 interfere with auto-ubiquitination formation. (A) *In vitro* ubiquitination assays of Smurf2 WT and the proline mutants as indicated. **(B)** Huwe1 WT and mutants as indicated. Reaction stopped after the indicated points and loaded onto an SDS-PAGE for analysis. Top panel fluorescently labelled Ub*, bottom panel Coomassie stained SDS-PAGE of the reaction in the absence of E1. The Smurf2 thioester assays were performed by Carsten Stollmaier. Adapted from Jäckl *et al.*, 2018 [88] and printed with the permission of Elsevier.

Therefore, A713 in Smurf2 and A349 in Huwe1 are key residues for thioester formation. This suggests that β-sheet augmentation indeed plays a crucial role in transthiolation as has been suggested for Nedd4 [50]. In the next step, we mutated a conserved L710 in Smurf2 and L346 in Huwe1 to proline to interfere with the non-covalent interactions between the C-lobe and the Ub^D outside of the region of the β-sheet augmentation (**Figure 30** A). The leucine is located in the C-lobe directly N-terminal of the β9 strand. The backbone amide and the carbonyl of the leucine form a hydrogen bonds to the side chain of Q40 in Ub. This hydrogen bond between the leucine and Q40 in Ub is present in both the Huwe1 and the Smurf2 C-lobe~Ub^D crystal structures (**Figure 29** B, E). These mutations had a similar effect as the Ala mutations in the β9 strand. The mutations essentially abolished the E2-E3 transthiolation (**Figure 30** C, D) and consequently poly-ubiquitination activity (**Figure 31**). To verify that all Pro mutants were folded the mutations were validated by NMR spectroscopy. Therefore, a ^{1}H,^{15}N-TROSY spectra were recorded from the WT and compared with the proline mutants for Smurf2 and Huwe1. For all mutants the structural integrity is intact (**Figure 32**).

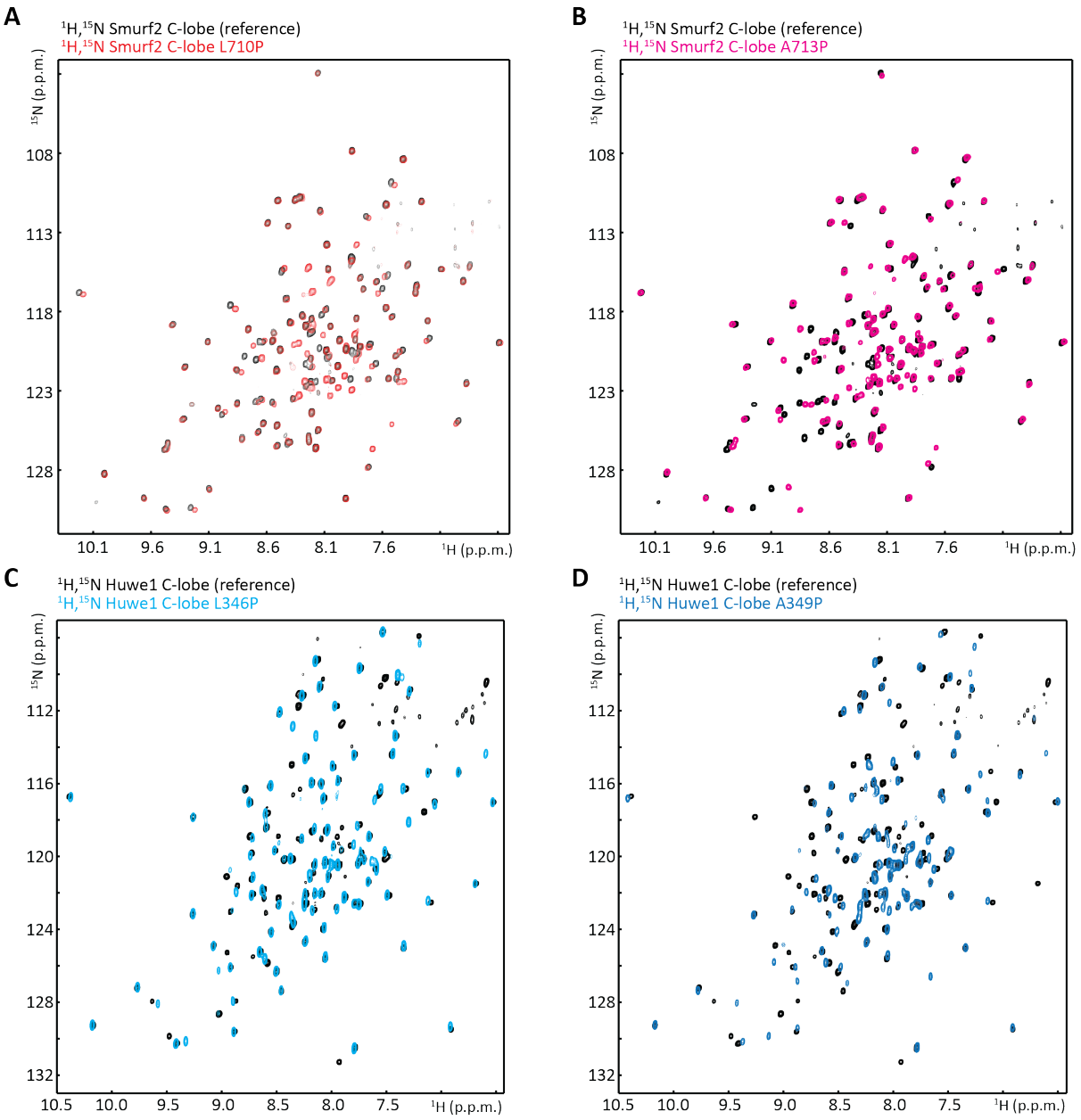

Figure 32: Structural characterisation of the Pro mutants of Smurf2 and Huwe1. $^{1}H,^{15}N$-TROSY spectra the Smurf2 L710P **(A)** and A713P **(B)** and Huwe1 L346P **(C)** and A349P **(D)** mutants as well the respective WT for Smurf2 and Huwe1. The well-dispersed spectra confirm the structural integrity of the mutants. Adapted from Jäckl *et al.*, 2018 [88] and printed with the permission of Elsevier.

In sum, I conclude that the conserved non-covalent contacts formed between the HECT C-lobe and the donor Ub are essential for thioester formation in Huwe1 and Nedd4-family E3s. Also, my data suggest that the interaction between the donor Ub and the C-lobe is shared not only between Smurf2 and Huwe1 but also potentially between other HECT domains regardless of their distinct poly-Ub chain specificities. My results also indicate

that the orientation of the donor Ub alone with respect to the C-lobe is not a determinant of Ub chain specificity.

5.2.9. The sequence of the C-terminal tail modulates ligation activity

The C-terminal tail of HECT domains plays a crucial role for isopeptide formation and Ub chain specificity [50], [53], [54], [79]. The underlying mechanistic details for the isopeptide formation and Ub chain specificity have remained elusive partially because the C-terminal tail of HECT domains were missing in all HECT thioester structures (**Figure 29** A, D) [49], [50], [54] and because no structures of HECT domains in complex with an acceptor Ub are available. For the final step, the isopeptide formation a strictly conserved Phe or Tyr at the -4 position is required relative to the HECT-C-terminus [54]. It is known that the truncations from the C-terminus starting from the "Δ-4F" position show a defect in isopeptide formation but not in the E2-E3 transthiolation [54]. In order to study the effect of amino acid composition of the C-terminal tail in Smurf2 and Huwe1 on transthiolation and poly-ubiquitination activity Carsten Stollmaier generated for the Smurf2 HECT domain mutants where the C-terminus was successively truncated starting from the "Δ-4F" mutant (Δ745-748 mutants in Smurf2) and I generated the equivalent mutants in the Huwe1 HECT domain (Δ382-385 mutants in Huwe1). All our deletion mutants show defectives in the poly-ubiquitination reaction in comparison to the WT (**Figure 33** A, B).

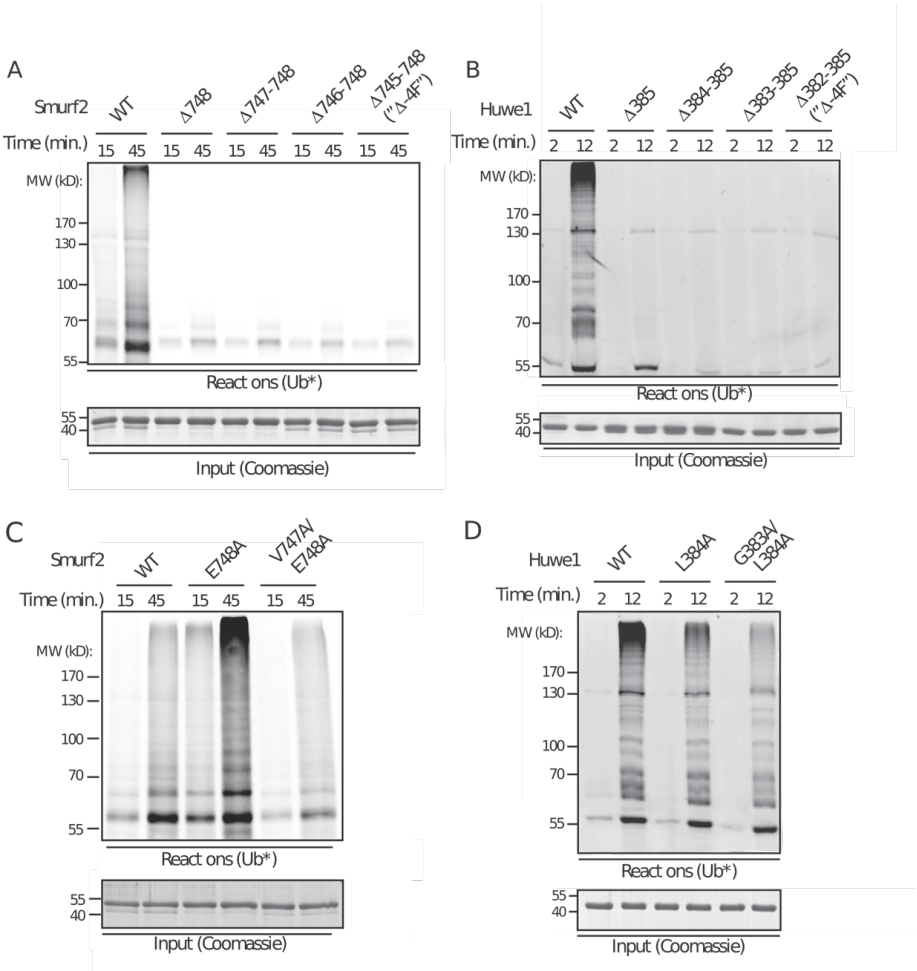

Figure 33: The length and composition of the HECT C-terminal tail is important for isopeptide formation. *In vitro* ubiquitination assay using the indicated bacterially expressed and purified Smurf2 **(A)** or Huwe1 **(B)** WT HECT domains or the indicated HECT truncation constructs. Reactions were stopped after the indicated time points and loaded on an SDS-PAGE gel to analyse HECT auto-ubiquitination activity with fluorescently labelled Ub (Ub*) (top panels). Coomassie staining of the reactions in the absence of E1 enzyme (bottom panel). **(C, D)** as **(A, B)**, but for Ala substitutions of C-terminal residues as indicated. The *in vitro* ubiquitination assay with Smurf2 and Smurf2 mutants where kindly provided by Carsten Stollmaier. Adapted from Jäckl *et al.*, 2018 [88] and printed with the permission of Elsevier.

Next, Carsten Stollmaier generated mutants for Smurf2 (E748A and V747A/E748A) where the C-terminal residues were successively replaced with alanine, I inserted the equivalent mutations into the Huwe1 HECT domain (L384A and G383A/L384A). Of note, the -1 positions in the native Huwe1 sequence is already an Ala, while the same holds true for the -3 position relative to the C-terminus in Smurf2 (**Figure 30** A) Interestingly, substitution of the residue E748 to A in Smurf2 enhanced poly-ubiquitination activity. While the other mutants of the Smurf2 C-terminus led to reduced auto-ubiquitination as

compared to the WT (**Figure 33** C). For the mutants of Huwe1, I observed successively decreasing ubiquitination activity (**Figure 33** D).

To test whether the truncation and substitution mutations play a role in thioester formation, their thioester levels were compared to the WT for both the Smurf2 and Huwe1 HECT domains (**Figure 34** A, B).

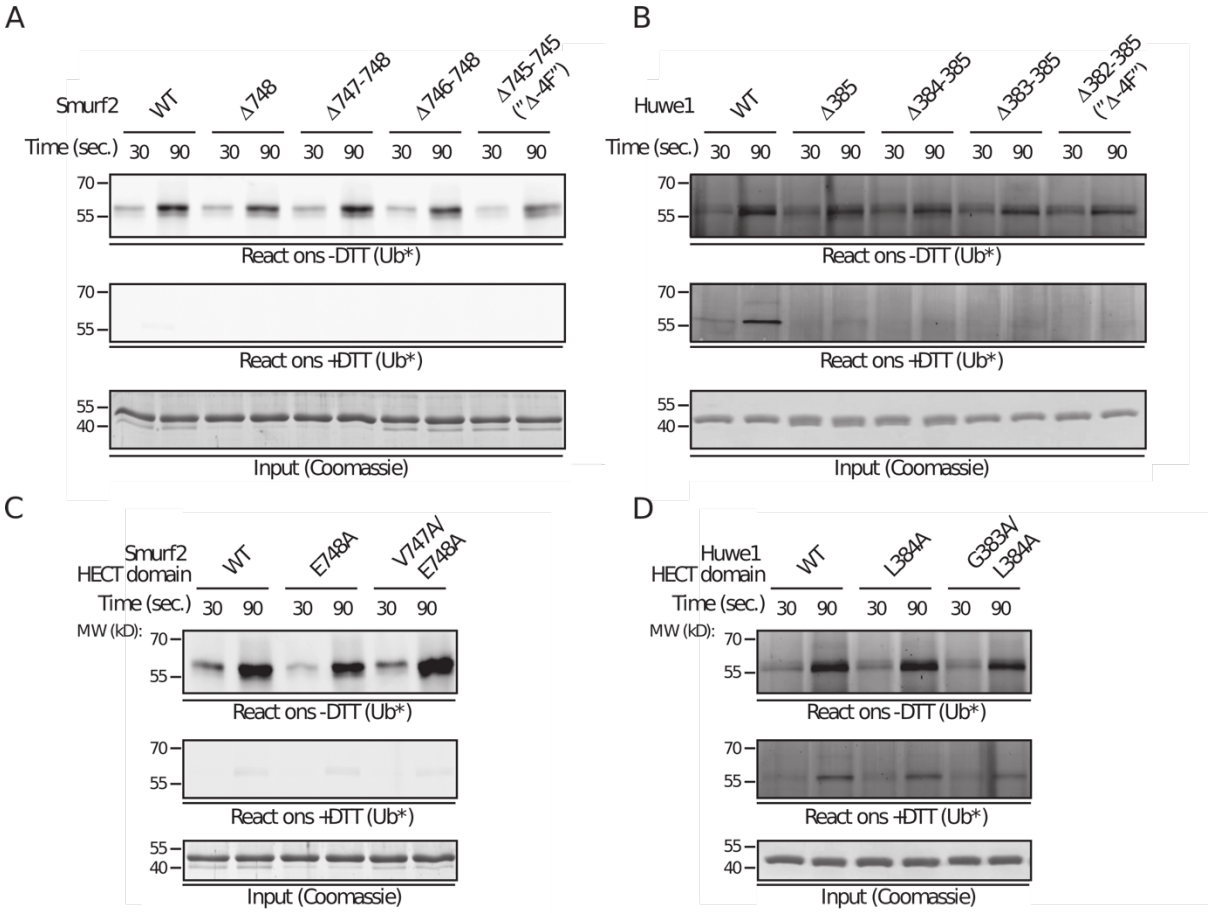

Figure 34: Truncation or mutation of the HECT C-terminal tail does not impair thioester formation. Thioester assays with Smurf2 **(A, C)** or Huwe1 **(C, D)** WT and the indicated mutants of the HECT domains. Transthiolation reactions were performed with WT and mutant HECT domains as indicated. HECT thioester formation was observed by using fluorescently labeled Ub (Ub*). The reaction was quenched at different time points by addition of Laemmli buffer without (top) or with (center) reducing agent. Equivalent levels of HECT domains were confirmed by incubation of the proteins in the absence of E1 and visualized by Coomassie staining (bottom). The *in vitro* ubiquitination assay with Smurf2 and Smurf2 mutants where kindly provided by Carsten Stollmaier. Adapted from Jäckl *et al.*, 2018 [88] and printed with the permission of Elsevier.

For both HECT domains, the truncation and the Ala substitutions of the C-terminal residues have no effect on the thioester formation. Nonetheless, the Ala substitutions mutants of Smurf2 and Huwe1 are tolerated for poly-ubiquitination even though the reaction is weaker with increasing the Ala substitution. In case of the mutation E748A in

Smurf2 this leads to an acceleration of the poly-ubiquitination. In contrast, truncation mutants of Smurf2 and Huwe1 affect the poly-ubiquitination but not the thioester formation. Taken these results together, I conclude that for the C-terminal tail sequence composition of Smurf2 and Huwe1 has no role in the transthiolation reaction but influences Ub ligation irrespective of Ub chain specificity.

5.2.10 Discussion

HECT E3 ligases are important regulators of a variety of biological functions, such as signal transduction, cellular homeostasis or embryonic development. Malfunction e.g. through genetic alterations in HECT E3 ligases therefore play an important role in carcinogenesis [58]. Over the past decade significant progress has been made in the elucidation of the mechanisms underlying HECT-mediated ubiquitination of Nedd4 E3 ligases family. Nevertheless, many general questions remain unresolved. One of these questions is whether the mechanisms underlying Ub transfer are conserved within the entire HECT family or what determines Ub chain specificity in the HECT mediated Ub transfer.

Here, we could show that the mechanisms of thioester formation are conserved between the Smurf2 and the Huwe1 E3 ligase, despite the fact that these enzymes belong to different E3 ligase families and possess different Ub chain specificities. Our functional and structural analyses thus suggest a conserved mechanism underlying the first catalytic step in HECT-mediated Ub transfer. In this step, the E2-E3 transthiolation takes place which involves a β-sheet augmentation and a conserved network of non-covalent interactions between the HECT C-lobe and the donor Ub (**Figure 29**, **Figure 30**). Interfering with this C-lobe~Ub network abolished thioester formation in both Smurf2 and Huwe1 (**Figure 30** C, D).

We were able to show by truncation or substitution of the last residues in the C-terminal tail for Smurf2 and Huwe1, that the C-terminal tail is rather participating in Ub ligation (**Figure 33**) and is not required for transthiolation (**Figure 34**). Our functional assays, together with previous studies show the impact of the individual residues in the C-terminal tail on ubiquitination reaction. The mutation of the C-terminal residues in Huwe1, Rsp5 and E6AP is tolerated but decreases Ub ligation activity (**Figure 33** D) [50],

[53], [54]. In case of Smurf2 the effects on Ub ligation depend on the specific mutation (**Figure 33** C). Interestingly, isopeptide formation in Nedd4 was abolished by mutations of the C-terminal residues [50], [53], [54]. Of note, in Nedd4 and Nedd4L the C-terminal tail contains an additional residue in comparison to other HECT domains (**Figure 30** A). This suggests that the requirement of an acidic residue at the C-terminal position may be more stringent in Nedd4 and Nedd4L than in other HECT domains [53]. Nevertheless, the here obtain results for Smurf2 and Huwe1 suggest that the sequence composition of the C-terminal tails plays an individual role in the HECT mediated ubiquitination reaction and ultimately in Ub chain specificity.

In sum, I could show that the mechanisms underlying thioester formation appear to be highly conserved in HECT domains irrespective of their Ub chain specificities. The Ub ligation and chain specificity seems to be at least partially determined by the individual C-terminal sequences of the HECT domain. I thus speculate that the individual C-terminal sequence of the HECT domains may fine-tune the ubiqiuitination reaction and Ub chain specificity by creating particular binding surfaces with the preferred Lys in the substrate or in the acceptor Ub and / or the N-lobe.

5.3. The Huwe1 HECT domain is auto-inhibited by interactions of the N- and C-lobe

5.3.1. Contribution

This project has been carried out in collaboration with Carsten Stollmaier, Karolina Hyz and Timo Strohäker. Contributions by others are noted in the text and figure legends.

5.3.2. Introduction

It is well established that the activity of Nedd4 family ligases is tightly controlled by auto-inhibitory mechanisms [79], [81], [85], [86], [121]. This was first shown for Smurf2 whose C2 domain at the N-terminus of the protein interacts with the C-terminal HECT domain on a surface located close to the catalytic cysteine. This interaction interferes with Ub thioester formation and blocks non-covalent Ub binding [79], [83]. Similar auto-inhibition mechanisms are found for other members of the Nedd4 family [86], [121]. In addition, it has been shown that the interaction between the C2 and the HECT domains of Nedd4.2 depend on the concentration of Ca^{2+}. A high Ca^{2+} concentration disrupts the interaction between the HECT and the C2 domain and targets the HECT E3 to the plasma membrane [122]. In case of Smurf2 the C2 domain is released by the interaction of Smad7 with the WW domains which activates Smurf2 for ubiquitination [80]. For Itch, another member of the Nedd4 family the auto-inhibitory conformation is abrogated by phosphorylation of residues S199, S232 and T222 which are located between the C2 and the WW domains [108]. These inhibition mechanisms have in common that the mobility of the C-lobe is restricted by the C2 domain and the UBS in the N-lobe of the HECT domain is blocked. Thereby the HECT domain is unable to catalyse the Ub reaction until the inhibition is released e.g. by phosphorylation [79], [81], [86], [121], [123]. For the members of the other HECTs it is not known if a similar inhibition process regulates the Ub-reaction as in the Nedd4 family. Regulation of the E3 Ub ligases is essential for the cellular health because they are key players in the degradation of proteins. [40], [60], [108]. Therefore, the strict regulation of the E3s are necessary for the cellular fate [108]. Hence, the question arises if SI(ngel) HECT family E3s are regulated and if so what are the underlying mechanisms since they contain an N-terminal domain architecture that is distinct from the Nedd4 family. Here, I combined different biophysical techniques to investigate the conformational landscape of the Huwe1 HECT domain during catalysis.

5.3.3. Results

5.3.4. Ub does not interact with the UBS of the Huwe1 HECT domain

Numerous members of the Nedd4 family contain a non-covalent Ub binding surface that promotes Ub chain elongation [51], [52], [55], [117], [119]. To examine whether Huwe1 HECT domain possesses a non-covalent Ub binding surface NMR titration experiments were performed with ^{15}N-labeled Huwe1 HECT domain in the absence and presence of increasing amounts of unlabelled Ub (**Figure 35** A, B, **Figure A 3, Figure A 4**).

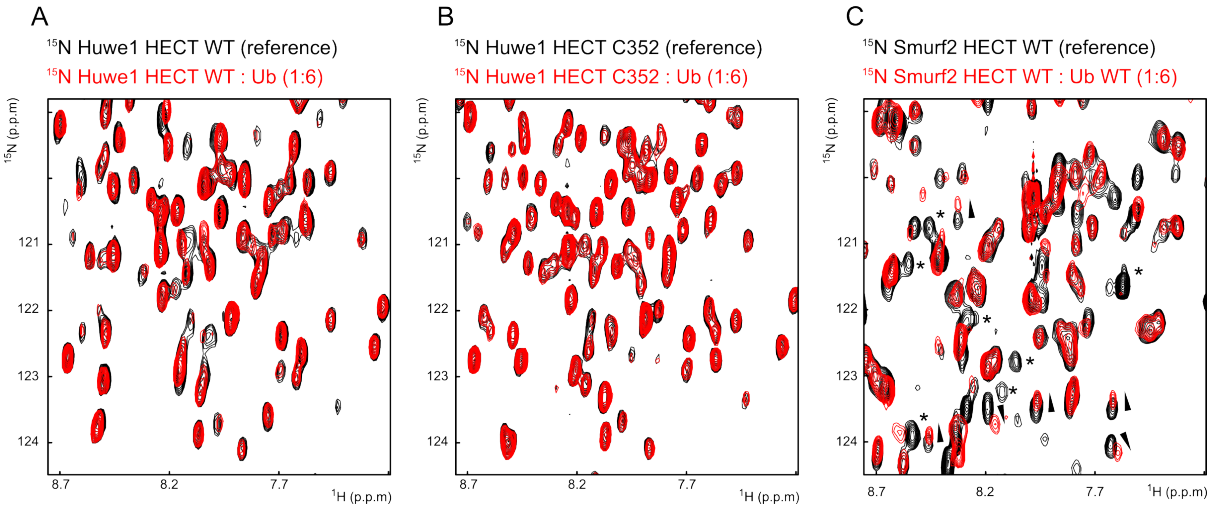

Figure 35: Ubiquitin interacts with the Smurf2 HECT domain (C) from the Nedd4 family but not with the HUWE1 HECT domain (A-B). NMR titration experiments with ^{15}N-labeled HECT domains as indicated. Overlay of a representative region of the ^{1}H,^{15}N-TROSY spectra of the HECT domains in the absence (black) and presence of a 6-fold stoichiometric excess (red) of Ub. Asterisks indicate the disappearance of cross peaks, triangles mark the direction of a chemical shift perturbation of a peak in comparison to the reference spectra (black). The spectrum A was recorded by Timo Strohäker, spectrum C was recorded by Dr. Silke Wiesner.

Moreover, I used the Huwe1 HECT domain mutant that contains the catalytic Cys as sole Cys and is used for disulfide formation, as described in **5.1**, to test whether it has the same function. To this end, I also performed NMR titration experiments with the ^{15}N-labeled C352 only (C1) Huwe1 HECT domain (**Figure 35** B). In both cases, WT Ub was added up to a 6-fold stoichiometric excess to the HECT domains and compared with the reference ^{1}H,^{15}N-TROSY spectra of the HECT domain in absence of Ub (**Figure 35** A, B). In contrast to the Smurf2 HECT domain (**Figure 35** C, **Figure A 5**) the Huwe1 HECT domain shows only very little chemical shift changes even at a large excess of Ub (**Figure 35** A, B, C). Also, the interaction of the C352 only mutant of Huwe1 HECT is similar to the WT Huwe1 HECT domain (**Figure 35** B, C).

The performed NMR titration experiments indecate that the isolated Huwe1 HECT domain does not interact with the Ub in a non-covalent manner in contrast to HECT domains from the Nedd4 family.

5.3.5. The isolated N-lobe of the Huwe1 HECT domain is able to bind Ub in a non-covalent manner

To identify differences between the ubiquitin binding surfaces of different HECT domains that may explain the inability of the Huwe1 HECT domain to interact with monomeric Ub, I performed a multiple sequence alignment of different HECT domains (**Figure 36** A). The key residues for the non-covalent Ub interaction are highly conserved among the HECT domain family [51], [52], [55], [117], [119]. Strikingly, all residues forming the UBS in Nedd4 family members are also found in the Huwe1 HECT domain (**Figure 36** A).

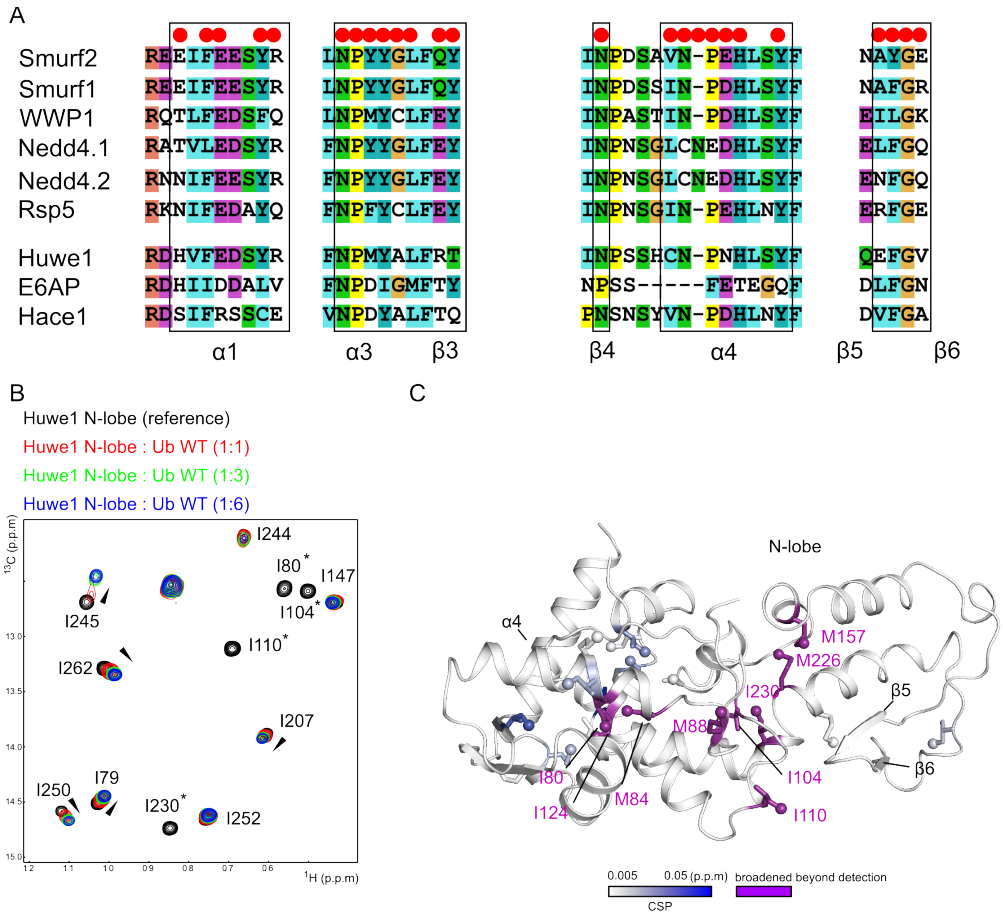

Figure 36: The ubiquitin binding surface (UBS) is highly conserved in the HECT domain family. (A) Multiple sequence alignment of the UBS of different HECT domains. The red dots indicate the conserved residues comprising the UBS which interact with Ub. **(B)** NMR titration experiment with $^{1}H,^{13}C$-methyl IM labelled N-lobe of the Huwe1 HECT domain as indicated. Overlay of a representative region of the $^{1}H,^{13}C$-methyl TROSY (HSQC) spectra of the N-lobe

of the Huwe1 HCT domain in the absence (black) and presence of increasing stoichiometric amounts of Ub as indicated. The triangle indicates the direction of the chemical shift perturbations of a peak in comparison to the reference spectra (black). Peaks broadened beyond detection are indicated with asterisk **(C)** Ub induced CSPs mapped onto the N-lobe of the Huwe1 HECT structure Huwe1 HECT N113C / C352K. The CSPs are coloured from white (CSP ≤ 0.005 p.p.m) to blue (CSP = 0.05 p.p.m). Magenta indicates residues broadened beyond detection. The N-lobe is shown in white cartoon representation. The affected residues are shown in stick representation and the $^{1}H,^{13}C$-labeled methyl groups as spheres.

Therefore, I chose to study the isolated $^{1}H,^{13}C$-methyl IM labelled N-lobe of Huwe1 HECT domain *via* NMR titration experiments to investigate its Ub binding capabilities (**Figure 36** B, **Figure A 6**) To this end, WT Ub was added to the N-lobe of Huwe1 and compared with the reference $^{1}H,^{13}C$-methyl TROSY (HSQC) spectra of the N-lobe (**Figure 36** B). Of note, the N-lobe of Huwe1 was strongly affected by the addition of WT Ub (**Figure 36** B). In order to map the chemical shift perturbations (CSPs) onto the structure of the Huwe1 HECT domain, I assigned the Ile δ_1- and Met ε-methyl resonances of the HECT domain by mutagenesis [92] [103]. The assignment of the methyl Ala β-, Leu δ-and Val resonances was done by Dr. Silke Wiesner by NOE spectroscopy. The observed CPSs of the Ile δ_1- and Met ε-methyl resonances were mapped onto the N-lobe of the crystal structure Huwe1 HECT N113C / C352K (**Figure 36** C). The residues that show the most pronounced CSPs are located in the ubiquitin binding surface, namely I80, M84, M88, I104 and I110. In order to verify the Ub interaction of the UBS in the N-lobe from Huwe1 I compared the CSPs of the before described Huwe1 HECT N113C / C352K : Ub G76C disulfide (**Figure 27** B) with the obtained CSPs of the Huwe1 N-lobe. Indeed, the same residues I80, M84, M88, I104 and I110 of the N-lobe are affected in the Huwe1 HECT N113C / C352K : Ub G76C disulfide (**Figure 37** A, B). In addition, the non-covalent Ub mimic of the Huwe1 HECT N113C / C352K : Ub G76C complex is placed directly in the UBS of the Huwe1 HECT domain (**Figure 37** C), where the observed CSPs occur in the Huwe1 N-lobe (**Figure 37** A) and the Huwe1 HECT N113C / C352K : Ub G76C disulfide NMR experiments (**Figure 37** A, B and C). Therefore, the N-lobe of the Huwe1 HECT domain possesses a ubiquitin binding surface that is equivalent to the members of the Nedd4 family.

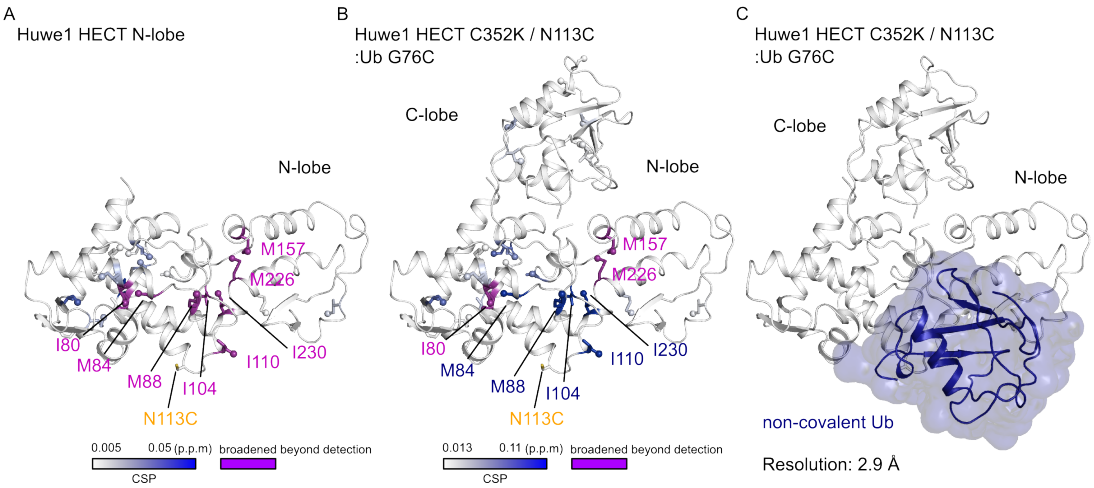

Figure 37: Comparison of the obtained Huwe1 N-lobe CSP with the Huwe1 HECT C352K / N113C:Ub G76C complex. (A) Ub induced CSPs mapped onto the N-lobe of the Huwe1 HECT structure Huwe1 HECT N113C / C352K. The CSPs are coloured from white (CSP ≤ 0.005 p.p.m) to blue (CSP = 0.05 p.p.m). **(B)** Ub induced CSPs mapped onto the Huwe1 HECT C352K / N113C : Ub G76C complex. The CSPs are coloured from white (CSP ≤ 0.013 p.p.m) to blue (CSP = 0.11 p.p.m). **(C)** Ribbon representation of the Huwe1 HECT N113C / C352K : Ub G76C disulfide mimicking non-covalent Ub binding with the HECT domain in white and the non-covalent bound Ub mimnic in blue.

In order to get insights into the interaction strength of the UBS in the N-lobe of Huwe1 with Ub, 2D line shape fitting was performed using TITAN [100] with NMR titration data obtained for the isolated N-lobe of Huwe1 and Ub (WT) (**Table 5**).

Table 5: Dissociation constants (K_D values) determined by NMR titration experiments with monomeric Ub and subsequent line shape analysis for the isolated Huwe1 HECT N-lobe. K_D values were determined by line shape fitting of the NMR CSP experiments with TITAN [100]. Standard deviation was estimated with bootstrapping statistics of 100 replicas (Figure A 13)

Protein	Domain	Ligand	K_D [µM]	± STD
Huwe1	N-lobe	Ub WT	38.5	1.5

The calculated K_D value for NMR titration experiments show that the N-lobe has a high affinity for Ub. The obtained data for the N-lobe show that Huwe1 possess a ubiquitin binding surface which is able to bind Ub identical to ubiquitin binding surface of the Nedd4 family HECTs with a high affinity.

5.3.6. Mutations in the ubiquitin binding surface affect Huwe1 activity

To examine whether the ubiquitin binding surface of Huwe1 plays a role in poly-ubiquitination activity, mutants in the Huwe1 UBS were generated to interfere with non-

covalent Ub binding. Therefore, the identified reporter amino acids I80, M88 and I110 (**Figure 36** B, C) were mutated one at a time to Ala. Also, R82 was mutated to Ala because of its proximity to I80. Additionally, F192 was mutated as it is located in the loop between β5 and β6. For Nedd4, it was shown that the mutation of this phenylalanine leads to a deficiency in non-covalent Ub binding (**Figure 38**) [51], [88]. Furthermore, Q190 was mutated to Ala because of its proximity to F192 and because it was suspected to influence the Ub binding to the ubiquitin binding surface. All these mutations in the UBS were introduced to the C352 only mutant of the Huwe1 HECT domain in order to determine their effect on polyubiquitination. In order to, observe the effect on the polyubiquitination of Huwe1, the Ala mutations were tested in an auto-ubiquitination assay and compared with the polyubiquitination activity of Huwe1 HECT C352 (**Figure 38**A, B).

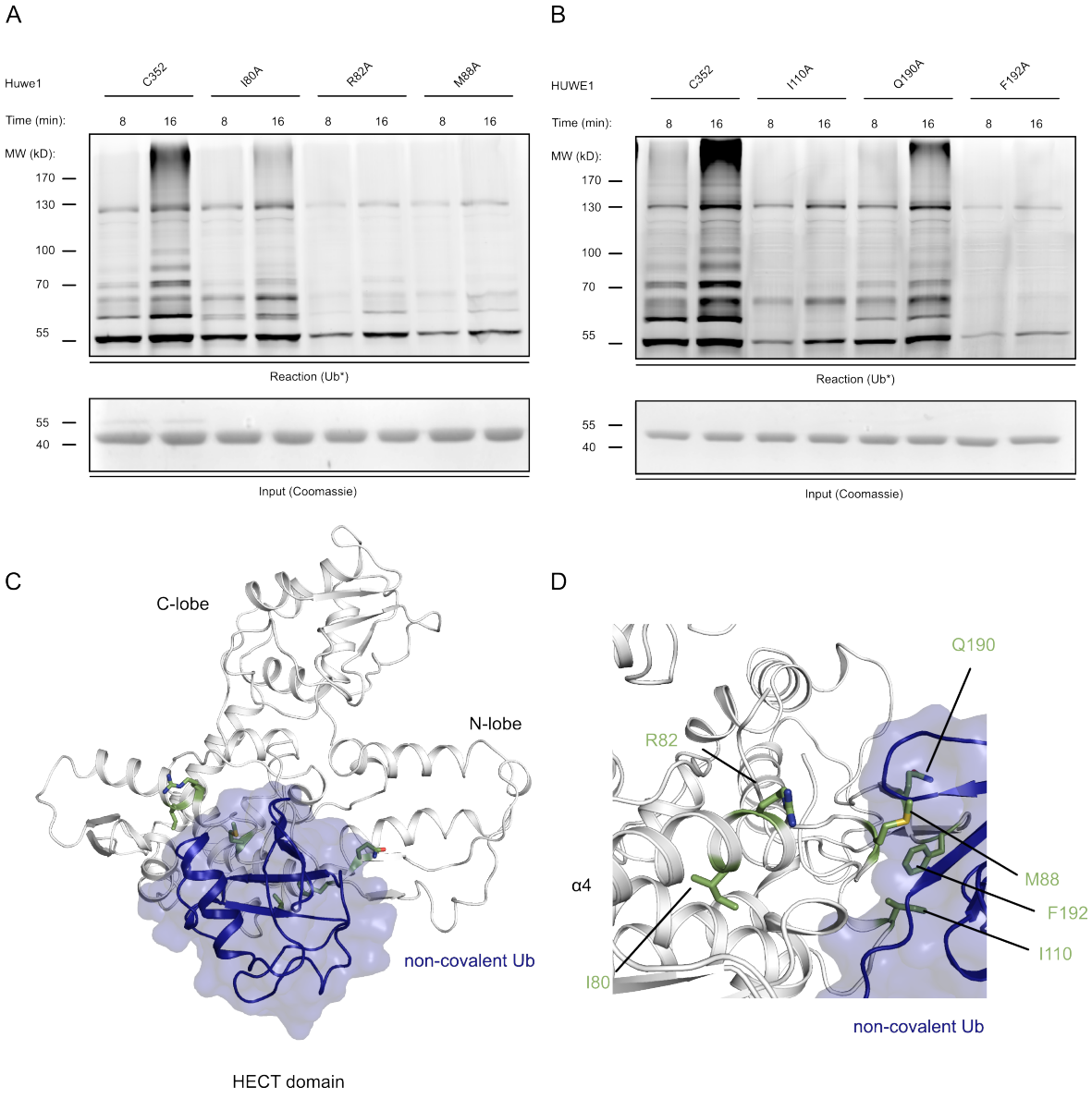

Figure 38: Mutation of the UBS in Huwe1 HECT interferes with ubiquitination activity. (A, B) *In vitro* auto-ubiquitination assays using the Huwe1 C352 mutant and the Huwe1 C352 HECT domain UBS mutants as indicated. Reactions were stopped after 8 and 16 minutes and loaded on an SDS-PAGE to analyse HECT auto-ubiquitination activity with fluorescently labelled Ub (Ub*) (top panels). The input control shows Coomassie stained proteins in the absence of E1 in the bottom panel. **(C)** In white cartoon representation of the Huwe1 HECT N113C / C352K : Ub G76C disulfide with non-covalently bound Ub (blue). Mutated amino acids are shown in stick representation (green). **(D)** As **(C)** but rotated and in a close up of the UBS.

The strongest effect in the polyubiquitination assay could be observed for the F192A mutation which abolishes Huwe1 HECT auto-ubiquitination in comparison toHuwe1 HECT C352 (**Figure 38** B). The other mutants are able to perform the Ub-reaction. Nevertheless, the reactions are considerably slower compared to the Huwe1 C352 HECT domain (**Figure 38** A, B). Only the mutations I80A and Q190A have a comparable polyubiquitination activity with the Huwe1 C352 HECT domain (**Figure 38** A, B). The position of the mutated residues on a Huwe1 HECT N113C / C352K structure reveals the molecular basis for the observations of the assays. M88, I110 and F192 are in close proximity to the ubiquitin associated with the UBS (**Figure 38** C, D) and they show the strongest effects on polyubiquitination in the auto-ubiquitination assays (**Figure 38** A, B). In contrast, the residues I80 and Q190 are more distant from the ubiquitin binding surface (**Figure 38** D). Consequently, these mutations show smaller effects on polyubiquitination activity (**Figure 38** A, B). Of note, the residue R82 has no direct contact to the non-covalent ubiquitin (**Figure 38** D). Nevertheless, it seems to play an important role for polyubiquitination because the Huwe1 HECT domain UBS mutant shows a reduced activity in the auto-ubiquitination assays in comparison to Huwe1 C352 HECT (**Figure 38** A).

In summary, the data of the NMR titration experiments (**Figure 36**) as well as the auto-ubiquitination assays (**Figure 38** A, B) clearly show that the Huwe1 HECT domain possesses a ubiquitin binding surface which plays a crucial role in polyubiquitination and which can be disrupted by point mutations.

5.3.7. Thioester formation enables monomeric Ub to bind to the Huwe1 UBS

During the ubiquitin transfer from the E2 to the HECT domain, the ubiquitin is bound *via* a thioester to the catalytic cysteine of the HECT E3 ligase [40]. In the result part **5.1** I could show that the thioester can be mimicked by a disulfide between the catalytic

cysteine of the HECT domain and the cysteine of Ub G76C. Here, I performed the disulfide formation between Ub G76C and Huwe1 HECT in order to investigate the influence of the trans-thiolation reaction on the ability of the Huwe1 HECT domain to bind Ub in a non-covalent manner. To this end, I first recorded $^{1}H,^{13}C$-methyl TROSY (HSQC) spectra with $^{1}H,^{13}C$-methyl labelled Huwe1 C352 HECT domain and compared it to the thioester mimic (**Figure 39** A, **Figure A 7**), the Huwe1 HECT C352 ~ Ub G76C disulfide. Next, I mapped the CSPs of the before assigned Ile δ_1-, Met-ε, Ala β-, Leu δ-and γ-Val -methyl resonances of the HECT domain onto a model of the Huwe1 HECT domain generated by MODELLER [118] from the PDB structure 4bbn [50].

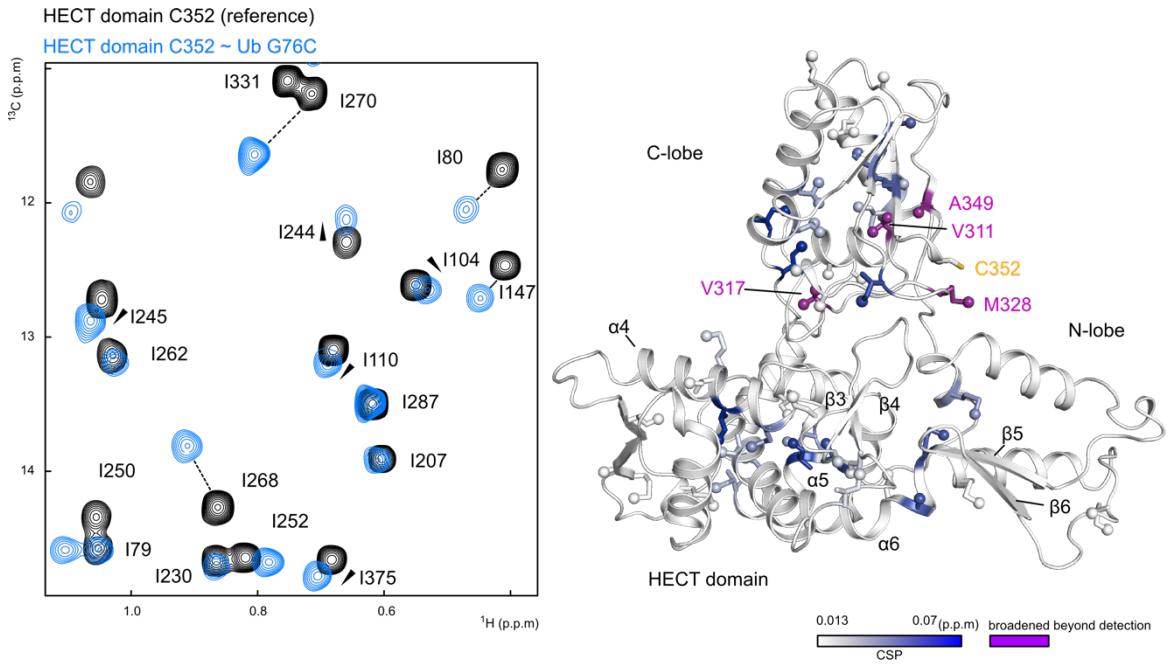

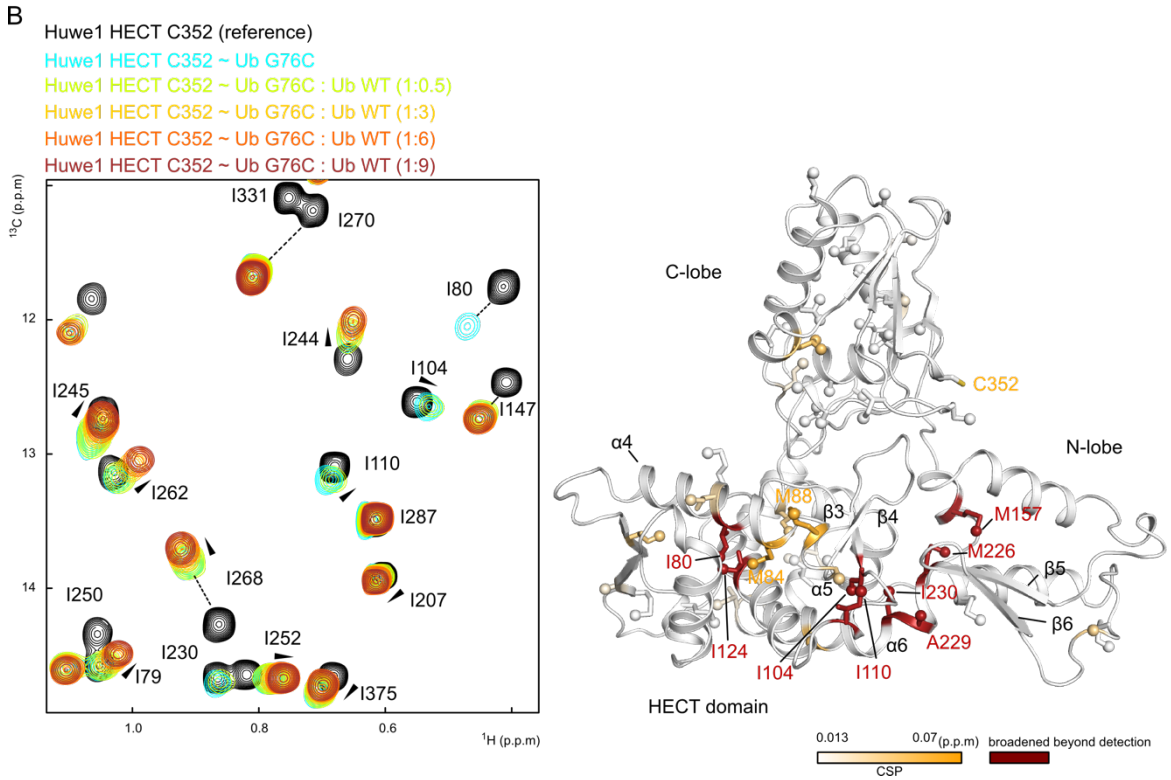

Figure 39: Thioester formation and subsequent Ub titration induces CSPs not only in the C-lobe but also in the N- / C- lobe interface and in the UBS. (A) Overlay of a representative region of the ^{1}H, ^{13}C-methyl TROSY (HSQC) spectra of IMVLA labelled Huwe1 C352 HECT domain (black) and Huwe1 HECT C352 ~ Ub G76C disulfide (cyan) (left side). The triangle indicates the shift of a peak in comparison to the reference spectra (black). On the right side disulfide formation induced CSPs are mapped onto a model of Huwe1 HECT generated by MODELLER [118] from the PDB structure 4bbn [50]. The CSPs are coloured from white (CSP ≤ 0.013 p.p.m) to blue (CSP = 0.07 p.p.m). Magenta indicates residues broadened beyond detection. The Huwe1 HECT domain is shown in white cartoon representation. The affected residues are shown in stick representation and the methyl groups as spheres. (B) NMR titration experiments with ^{1}H,^{13}C-methyl IMVLA labelled Huwe1 C352 HECT as indicated. Overlay of a representative region of

the ^{1}H ^{13}C-methyl TROSY (HSQC) spectra of Huwe1 C352 HECT (black), the Huwe11 HECT C352 ~ Ub G76C disulfide (cyan) and increasing stoichiometric amounts of Ub as indicated (left side). The triangle indicates the shift of a peak in comparison to the Huwe1 HECT C352 ~ Ub G76C disulfide spectrum (cyan). CSPs induced by the addition of Ub to the Huwe1 HECT C352 ~ Ub G76C disulfide are mapped onto a model of Huwe1 HECT generated by MODELLER [118] from the PDB structure 4bbn [50] on the left. The CSPs are coloured from white (CSP ≤ 0.013 p.p.m) to orange (CSP = 0.07 p.p.m). Red indicates residues broadened beyond detection. The Huwe1 HECT domain is shown in white cartoon representation. The effected amino acids are shown in stick representation and the methyl groups as spheres.

Noteworthy, the strongest CSPs are located in the C-lobe of the HECT domain where the Ub is bound to the catalytic Cys (Fig. 28D) (**Figure 39** A). Moreover, CSPs are present in the N-lobe (M84, I124, I147, M157, M226, I250) and in the C-lobe (I268, I270, I331, I336) (**Figure 39** A right panel). The residues M84, I124, I250, I268 and I270 show CSPs even though the residues are far from the binding surface of the donor Ub or the non-covalent binding side in the N-lobe which indicates a domain rearrangement induced by thioester formation. In the next step, I titrated WT Ub up to a 9-fold excess to the ^{1}H,^{13}C-methyl labelled Huwe1 C1 HECT C352 ~ Ub G76C disulfide (**Figure 39** B, **Figure A 7**). I subsequently mapped the observed CSPs onto a structure model of the Huwe1 HECT domain from the Nedd4 HECT domain PDB structure 4bbn [50]. Interestingly, the strongest CSPs are located in the N-lobe of the HECT domain where the non-covalent ubiquitin binding occurs in the UBS (**Figure 39** B right panel). Similar CSPs have been observed in the N-lobe NMR-titration with Ub (**Figure 36** B). To verify that the accessibility of the UBS is due to the thioester and the associated conformational rearrangement of the Huwe1 HECT domain, I added the reducing agent DTT to the titration end point which contained a 9-fold excess of monomeric Ub (**Figure 40**, **Figure A 7**).

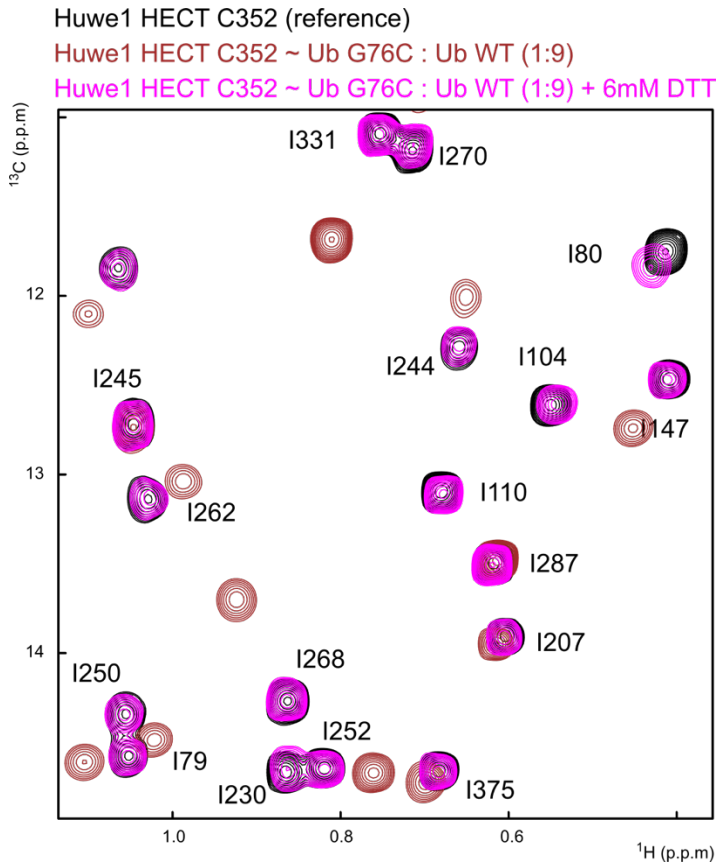

Figure 40: The reorientation of the HECT domain is reversible. Overlay of a representative region of the ^{1}H ^{13}C-methyl TROSY (HSQC) spectra of IMVLA labelled Huwe1 C1 HECT (black), the HUWE1 HECT C352 ~ Ub G76C disulfide at a 9-fold stoichiometric excess of Ub (firebrick) and the Huwe1 HECT C352 ~ Ub G76C disulfide at a 9-fold stoichiometric excess of Ub after addition of 6mM DTT (magenta).

After adding DTT, the chemical shift perturbations reverted to the initial spectrum of the isolated Huwe1 HECT domain (**Figure 40**) due to cleavage of the of the disulfide bond. This experiment confirms my previous observation that the free Huwe1 HECT domain is incapable of interacting with Ub in a non-covalent manner and shows that the C-lobe has to dissociate from the N-lobe to allow non-covalent Ub binding.

Taken together, this indicates that during the thioester formation between the donor Ub and the catalytic Cys in the C-lobe, a rearrangement of the C-lobe w.r.t the N-lobe of the Huwe1 HECT domain occurs. These rearrangements subsequently allow a second Ub to bind in a non-covalent manner to the ubiquitin binding surface.

5.3.8. The free Huwe1 HECT domain adopts a closed conformation in solution

To investigate different orientations of protein domains in solution, paramagnetic relaxation enhancement (PRE) experiments are a commonly used biophysical tool. Thereby conformational changes in proteins or rearrangement of domains upon a binding event can be distinguished [93], [101], [124], [125]. For such experiments, a spin label, containing an unpaired electron, is attached to the protein of interest which induces a paramagnetic relaxation enhancement. This leads to an increase of the R_2 relaxation rate and therefore a reduced peak intensity for peaks which are within a radius of 10-24 Å around the spin label [126]. This reduced intensity can then be mapped onto a known structure or a model of the protein to validate the orientation of the proteins domains or interaction [93], [101], [124]–[126]. To examine the conformation of the C-lobe w.r.t to the N-lobe of the Huwe1 HECT domain I performed PRE-experiments with $^{1}H,^{13}C$-methyl IM labelled Huwe1 HECT domain mutants. To this end, I generated by mutagenesis mutants of the Huwe1 HECT domain were the sole catalytic cysteine (C352) is replaced by an alanine substitution. In this cysteine free mutation background of Huwe1 HECT I replaced the residues Arg9, Arg93 and Asp271 with a Cys. The three Cysteine (R9C, R93C and D271C) mutants of the Huwe1 HECT domain were used to attach the 4-maleimido-tetramethyl-1-piperidinyloxy (TEMPO) spin label to the HECT domain. I recorded spectra for the $^{1}H,^{13}C$-methyl IM labelled Huwe1 HECT mutants R9C, R93C and D271C labelled with TEMPO. The obtained HMQC signal intensities for the TEMPO labelled mutants R9C, R93C and D271 were compared in the oxidised and reduced of the TEMPO labelled HECT domain (**Figure 42** A, B, C, D, **Figure A 8**). The stable TEMPO oxygen radical in the oxidised form was reduced by ascorbate to restore the peak intensity by removing the paramagnetic effect of the spin-label. In addition, I mapped the intensity changes onto the Huwe1 HECT PDB structure 5lp8 [70] (**Figure 41**, **Figure 42** A, B, C, D right panel).

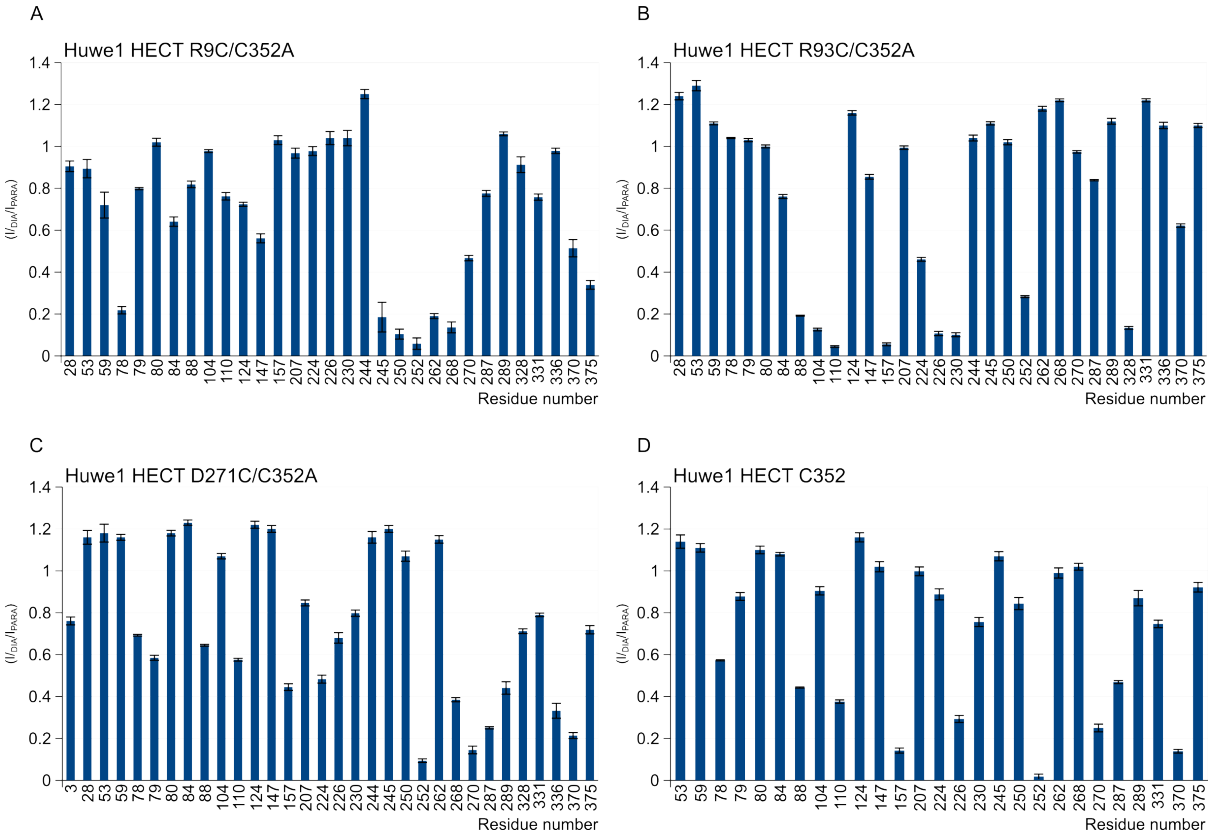

Figure 41: Per-residue quantification of the obtained PREs for the Huwe1 HECT cysteine mutants. The diagrams show the ratio of the PRE-intensities after and before reduction of the spin label. The height of the bar indicates the strength of the obtained intensity and reflects therefore the effect of the PRE on the single residue. **(A)** Per-residue quantification for Huwe1 HECT R9C/C352A **(B**) Per-residue quantification for Huwe1 HECT R93C/C352A **(C)** Per-residue quantification for Huwe1 HECT D271C/C352A **(D)** Per-residue quantification for Huwe1 HECT C352

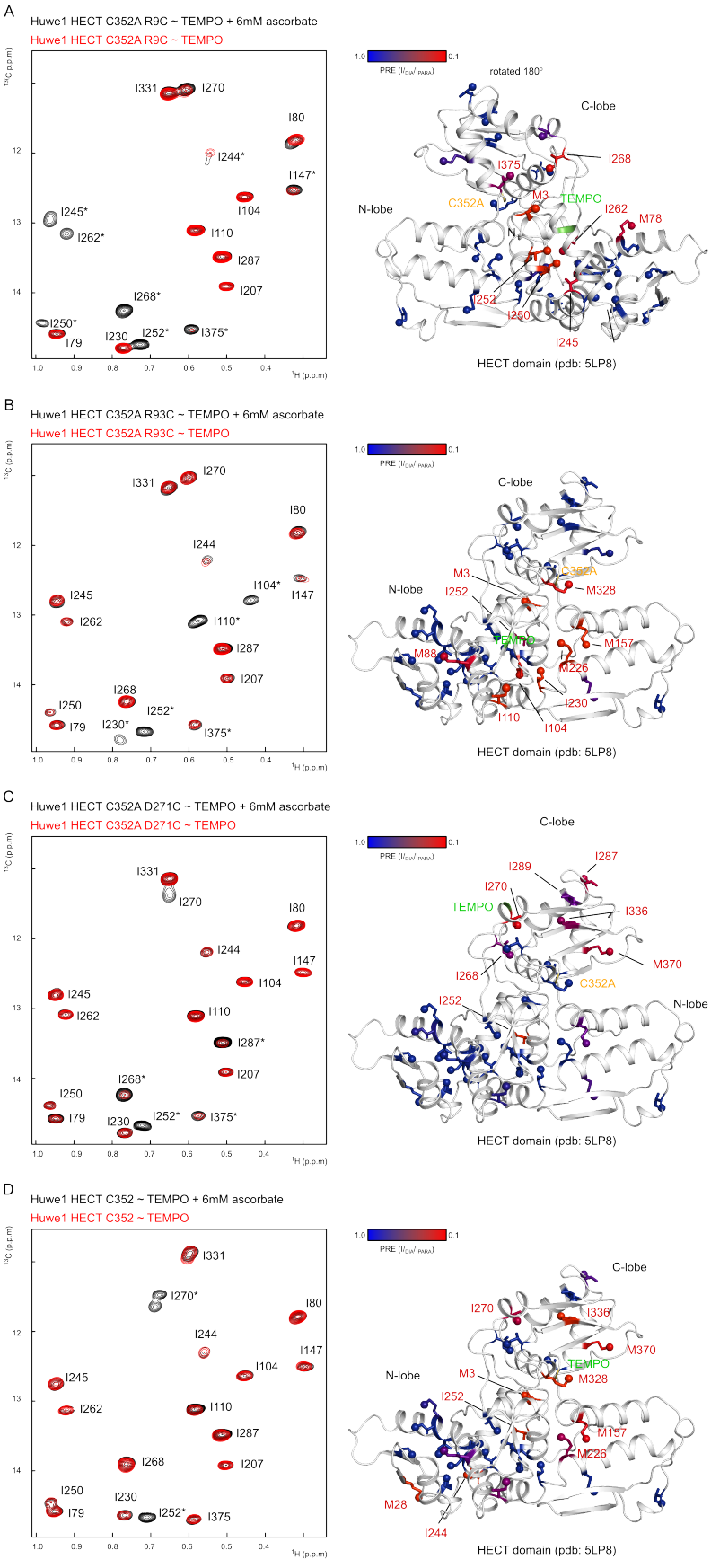
A
Huwe1 HECT C352A R9C ~ TEMPO + 6mM ascorbate
Huwe1 HECT C352A R9C ~ TEMPO
rotated 180°
C-lobe
N-lobe
HECT domain (pdb: 5LP8)
B
Huwe1 HECT C352A R93C ~ TEMPO + 6mM ascorbate
Huwe1 HECT C352A R93C ~ TEMPO
HECT domain (pdb: 5LP8)
C
Huwe1 HECT C352A D271C ~ TEMPO + 6mM ascorbate
Huwe1 HECT C352A D271C ~ TEMPO
HECT domain (pdb: 5LP8)
D
Huwe1 HECT C352 ~ TEMPO + 6mM ascorbate
Huwe1 HECT C352 ~ TEMPO
HECT domain (pdb: 5LP8)

Figure 42: Paramagnetic relaxation enhancement (PRE) experiments to probe the conformation of the C-lobe w.r.t to the N-lobe of the Huwe1 HECT domain. NMR PRE experiments with $^{1}H,^{13}C$-methyl IM labelled Huwe1 HECT mutants R9C, R93C, D271C and C352 containing a sole cysteine residue for spin label attachment as indicated. Left panels: Overlays of a representative region of the $^{1}H,^{13}C$-methyl TROSY (HMQC) spectra of Huwe1 HECT mutant with reduced spin label (black) and presence of the non-reduced spin label (red). On the right side, PRE-induced changes and shifts are mapped onto Huwe1 HECT PDB structure 5lp8 [70]. A linear gradient from blue to red indicates the strength of the PRE, covering the range from 1.0 (no PRE), to 0.1. The Huwe1 HECT domain is shown in white cartoon representation. The affected residues are shown in stick representation and the methyl groups as spheres. The asterisks indicate the affected peaks in the PRE-data in comparison to the reference spectra (black). **(A)** Huwe1 R9C/C352A HECT domain, **(B)** R93C/C352A HECT domain, **(C)** D271C/C352A HECT domain, and **(D)** C352 only HECT domain.

I positioned the first cysteine mutation close to the N-terminus of the HECT domain at position R9 (**Figure 42** A). The peaks that show the most significant relaxation enhancement are M3, M78, I147, I245, I250, I252, I262, I268, I375 and are located in close proximity of the attached spin label of the HECT domain (**Figure 42** A right panel). Next, I attached the TEMPO label at R93 in the ubiquitin binding surface of the HECT domain (**Figure 42** B). The peaks affected by the spin label are M3, M88, I104, I110, M157, M226, I230, I252 and M328. These peaks are located predominantly in the N-lobe of the HECT domain (**Figure 42** B right panel). Interestingly, the residue M328 in the C-lobe is also affected by the relaxation enhancement of the attached spin label which indicates that it is in close proximity to the N-lobe in the Huwe1 HECT PDB structure 5lp8 (**Figure 42** B right panel). Moreover, this suggests that in solution the C-lobe and the N-lobe of the Huwe1 HECT domain are in close proximity to each other. To investigate the orientation of the C-lobe in greater detail a cysteine for the spin label was introduced in the C-lobe (D271C). The observed PREs are located only around the spin label in the C-lobe domain (**Figure 42** C). In the N-lobe, only the I252 peaks was influenced by the relaxation enhancement. For the mutation D271C this might indicate that the $\alpha 1$ helix is either flexible and is therefore influenced by the spin label or that the Huwe1 domain forms a dimeric structure. Both cases are highly speculative because only one PRE was observed and for both cases more peaks should be affected by the PRE of the spin label. Finally, I used the catalytic cysteine to link the spin label to the HECT domain (**Figure 42** D). Of note, attachment of the TEMPO label at the catalytic Cys shows PREs for the residues M3, M28, M157, I244, M226, I252, I270, M328, I336 and M370, occurring in the C-lobe and the N-lobe of the HECT domain (**Figure 42** D right panel). The PREs M157, M226, I270 and I336 occurring in the C- and N-lobe upon attachment of the spin label

onto the C352 mutation of Huwe1 are similar to the CSPs which are obtained due to thioester formation between the Huwe1 C352 HECT and UbG76C. (**Figure 39** A). This suggests that the spin label at the catalytic cysteine induces a conformational change similar to the thioester formation between Huwe1 C352 HECT and UbG76C (**Figure 39** A). Moreover, by attaching the spin label to C352 to the Huwe1 C352 HECT mutant, the N-lobe shows PREs (M28, M157, M226 and I244) which are not affected when the spin label is attached to position D271 in the C-lobe (**Figure 42** C). This also indicates a rearrangement of the C- and N-lobe.

To examine the conformation of the C-lobe w.r.t to the N-lobe of the Huwe1 HECT domain, I performed NMR experiments with $^{1}H,^{13}C$-methyl IM labelled Huwe1 C352 HECT domain, as well as the isolated Huwe1 HECT C- and N-lobe. By comparison of the obtained spectra of the Huwe1 HECT with the isolated C- and N-lobes as well as with the Huwe1 HECT C352~TEMPO and UbG76C disulfide, it became apparent that the residues I147, I230, I252, I268, I270, I331 and I375 show chemical shift changes towards their positions in the spectra of the individual N- and C-lobes (**Figure 43** A, B, C, **Figure A 9**).

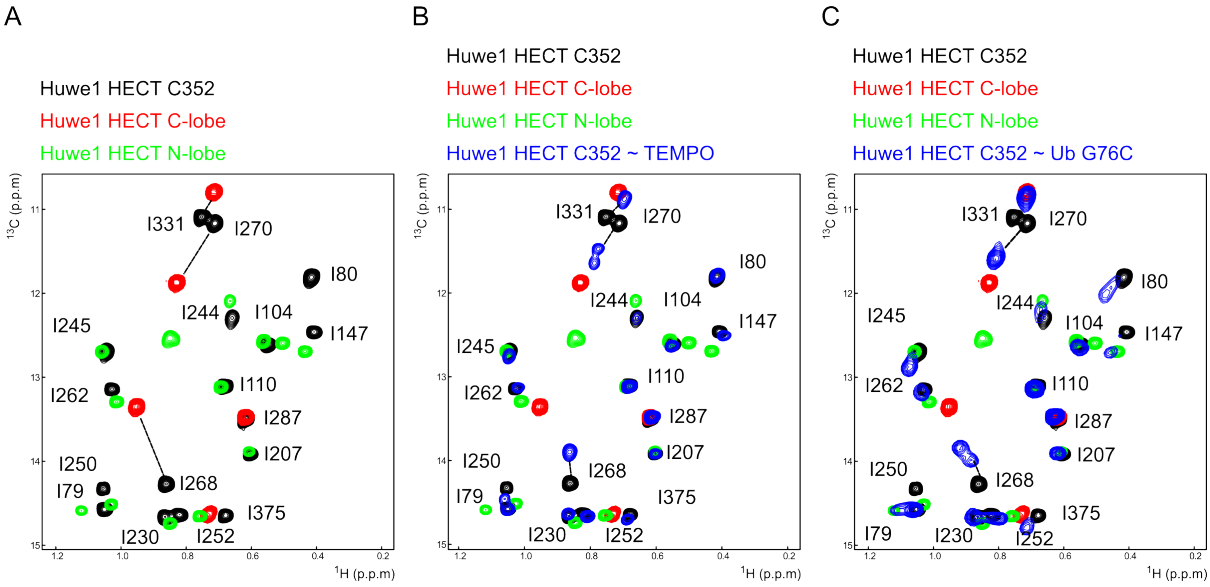

Figure 43: The isolated C- and N-lobe of Huwe1 HECT show similar chemical shift perturbations as the whole HECT domain during the thioester formation at the catalytic cysteine. (A) Overlay of a representative region of the $^{1}H,^{13}C$-methyl TROSY (HSQC) spectra of Huwe1 C352 HECT domain (black) and the isolated C-lobe (red) and N-lobe (green). **(B)** as **(A)**, but with the spin labelled Huwe1 C352 HECT domain (blue). **(C)** as **(A)**, but with the Huwe1 C352 HECT domain ~ UbG76C (blue). The dotted lines indicate the direction of the chemical shift perturbations in comparison to the reference spectra (black).

In summary, the comparison of PREs from the different cysteine mutants indicates that the HECT domain adopts a closed conformation in solution in which the catalytic cysteine is in close contact with the N-lobe. In addition, the isolated C- and N-lobes in comparisons to the Huwe1 C352 HECT ~TEMPO or Ub G76C show that the Ub^D loaded HECT domain of Huwe1 adopts an open conformation in solution. This suggest that, during the Ub transfer from the E2 to the Huwe1 HECT E3 ligase and the formation of the HECT ~ Ub thioester, the interaction of the catalytic cysteine and the N-lobe is disrupted and the HECT domain adopts an open conformation.

5.3.9. The thioester induced rearrangement of the C-lobe can by mimicked by small organic compounds or mutations of the catalytic cysteine

The observed CPSs upon Huwe1 HECT C352 ~ Ub G76C disulfide formation (**Figure 39** A) indicate a reorientation of the C-lobe w.r.t. to the N-lobe. Similar CSPs as in the thioester can also be induced by the attachment of small organic compounds such as a TEMPO spin label to the catalytic cysteine (**Figure 42**). Interestingly, after reduction of the paramagnetic TEMPO radical with 6 mM ascorbate, the spectrum of the $^{1}H,^{13}C$-methyl TROSY (HSQC) spectrum of the Huwe1 HECT C352 ~ TEMPO displayed similar CSPs of the residues I147, I230, I252, I268, I270, I331 and I375 reporting on the C- and N-lobe reorientation upon Huwe1 HECT C352 ~ Ub G76C disulfide formation (**Figure 44** A, B, **Figure A 10**). I270 and I331 are located at the interface between the C- and the N-lobe of the Huwe1 HECT domain and are therefore an indicator of a conformational rearrangement. Also, the residues I147, I245 and I268 show CSPs similar to those observed during the disulfide formation (**Figure 44** A, B).

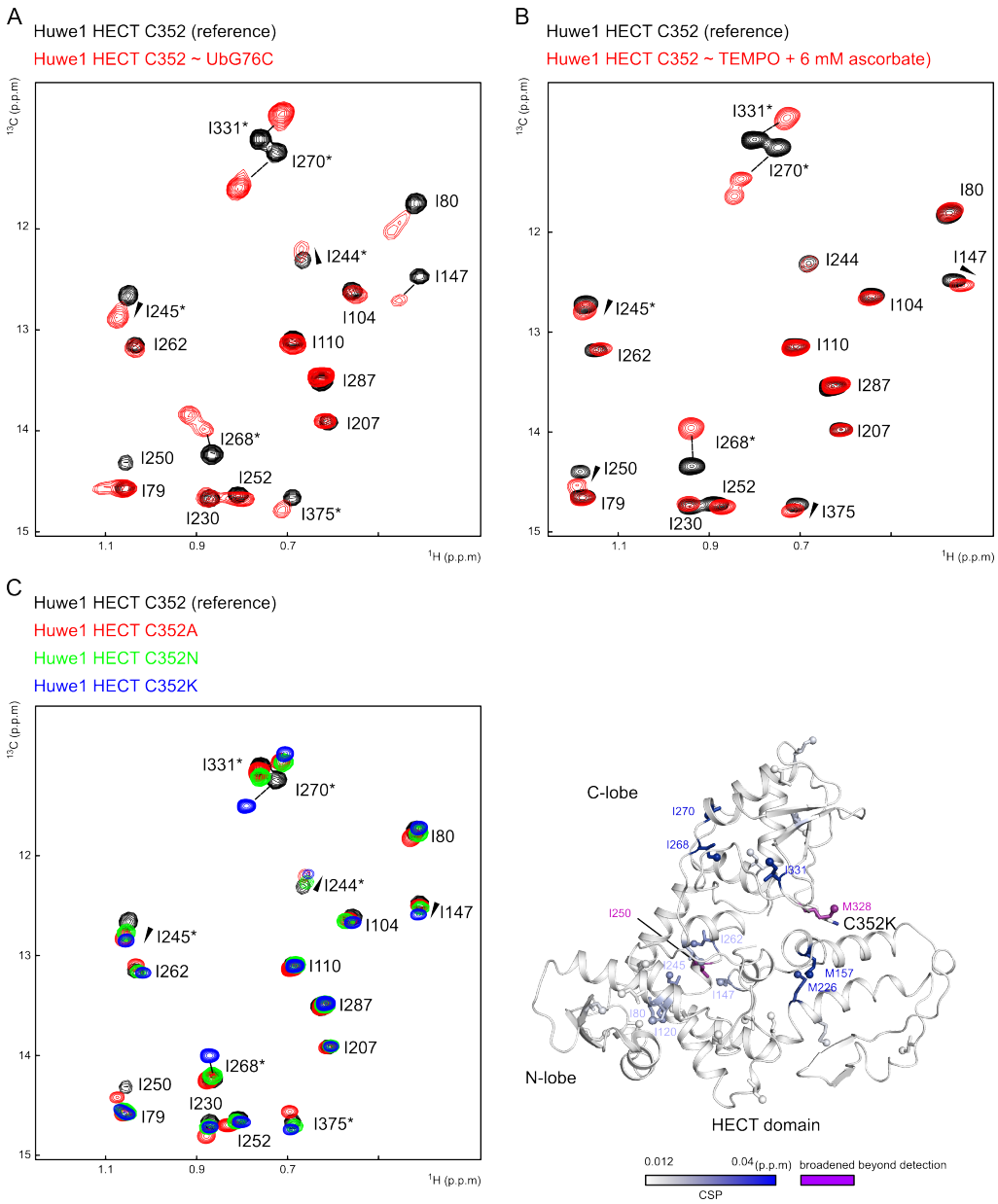

Figure 44: Mutation of the catalytic cysteine induce conformational changes in the Huwe1 HECT domain that are similar to the Huwe1 HECT C352 ~ Ub G76C disulfide. (A) Overlay of a representative region of the ^{1}H,^{13}C-methyl TROSY (HSQC) spectra of Huwe1 C352 HECT domain (black) and the Huwe1 HECT C352 ~ Ub G76C disulfide (red). **(B)** as **(A)**, but with 4-maleimide TEMPO attached to the catalytic cysteine (red). (C) as (A), but with different mutations of C352 of the Huwe1 HECT domain (C352A, red), (C352N, green), (C352K, blue). The triangles and dotted lines indicate the direction of the chemical shift perturbations in comparison to the reference spectra (black). The asterisks show amino acids which show CSPs due the thioester formation. **(C)** as **(A)** but with different mutations of C352 of the Huwe1 HECT domain (C352A, red), (C352N, green), (C352K, blue). The triangles and dotted lines indicate the direction of the chemical shift perturbations in comparison to the reference spectra (black). The asterisks indicate amino acids which are affected by mutation of the catalytic Cys. **(C) right panel:** CSPs induced by the Huwe1 HECT C352K mutation mapped onto the structure Huwe1 HECT N113C / C352K. The CSPs are coloured from white (CSP ≤ 0.012 p.p.m) to blue (CSP = 0.04 p.p.m). Magenta highlights residues that are broadened beyond detection. The Huwe1 HECT domain is shown in white cartoon representation. The affected aa are shown in stick representation and the methyl groups as spheres.

Analogous CSPs as observed for the Huwe1 C352 HECT ~TEMPO and Ub G76C thioester formation occur upon mutation of the catalytic cysteine (**Figure 44** A, C, **Figure A 10**). In essence, the mutation of the catalytic cysteine to lysine also leads to large CSPs of the residues I270 and I331. Therefore, I started to mutate the catalytic cysteine into different amino acids to monitor the effect of the rearrangement of the C- and N-lobe in comparison to the HECT domain with the covalently bound Ub G76C as Ub^D mimic (**Figure 44** A, C). To investigate the effects of the mutations, I recorded $^{1}H,^{13}C$-methyl TROSY (HSQC) spectra of the mutants of the Huwe1 HECT domain and overlaid them with spectra of the Huwe1 C352 HECT domain (**Figure 44** C)

By replacing the catalytic cysteine with amino acids with successively increasing side chain length from Ala to Asn to Lys, the chemical shifts of reporter residues such as I270, I331 and also I147, I245 and I268 show CSPs which progress linearly towards those of the Huwe1 HECT C352 ~ Ub G76C disulfide (**Figure 44** C). Interestingly the amino acid with the longest and positive charged side chain, lysine, induces the strongest CSPs in the reporter residues (**Figure 44** C right panel). Therefore, the population of the Huwe1 HECT domain conformers shifts from a closed state of the free HECT domain towards the thioester conformation with increasing steric hinderance around the catalytic cysteine.

5.3.10. The thioester mimicking mutants interact with Ub in a non-covalent manner

To investigate whether the thioester mimicking mutants can bind ubiquitin in a non-covalent manner, I performed NMR titration experiments with the $^{1}H,^{13}C$-methyl IM labelled C352K mutant of the Huwe1 HECT domain and compared the Ub binding properties with Huwe1 C352 HECT domain (**Figure 45** A, B, **Figure A 11**).

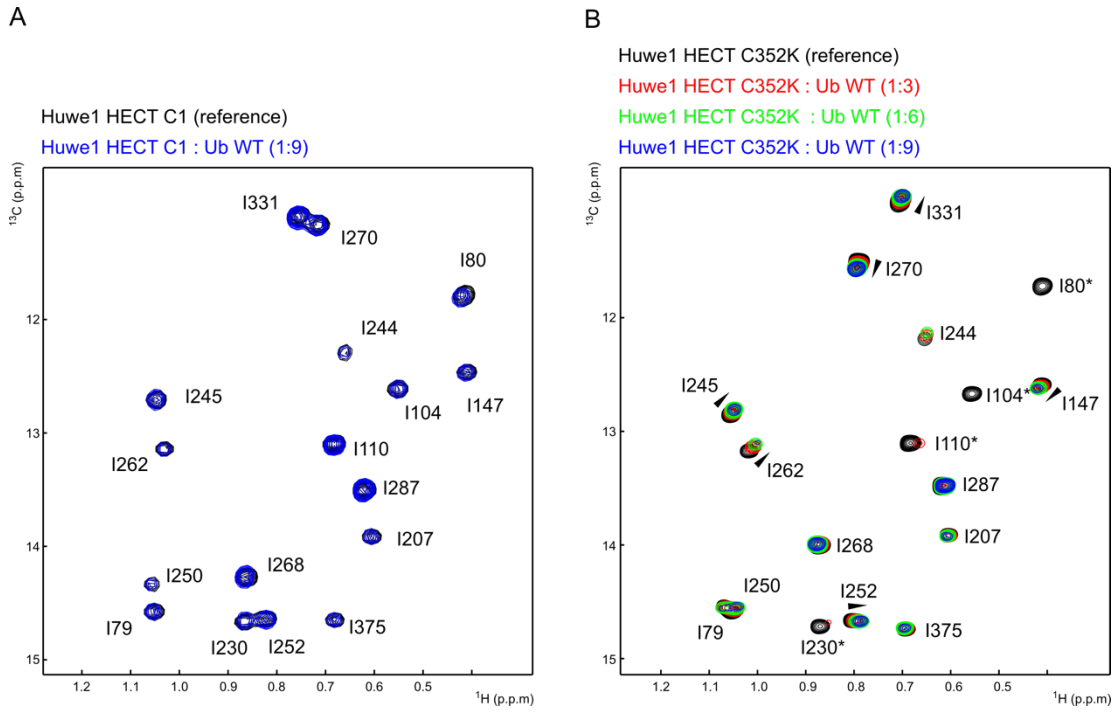

Figure 45: A mutation of the Huwe1 HECT catalytic cysteine mimics the conformational change that occurs upon thioester formation and is able to bind Ub in a non-covalent manner. (A) Overlay of a representative region of the $^{1}H,^{13}C$-methyl TROSY (HSQC) spectra of the Huwe1 C352 HECT domain in the absence (black) and presence of increasing stoichiometric amount of monomeric Ub as indicated. **(B)** As **(A)**, but for the C352K mutant. Triangles indicate peak shifts in comparison to the reference spectrum (black**).** The asterisks indicate amino acids which show CSPs broadened beyond detection, the dotted line and triangle indicate amino acids which show CSPs due to non-covalent Ub binding.

To this end, I added up to a 9-fold excess of unlabelled monomeric Ub to the Huwe1 C352 HECT domain. The C352K mutant was selected since it displays similar CSPs for the residues I270 and I331 as compared to the Huwe1 HECT C352 ~ Ub G76C disulfide (**Figure 44** C), thereby resembling the open conformation of the Huwe1 HECT domain. Upon Ub addition, the methyl labelled Huwe1 C352 HECT domain shows no interaction with Ub (**Figure 45** A). However, the reporter residues for non-covalent Ub binding (I80, I110 and I104) show strong CSPs in the Huwe1 C352K mutant HECT domain upon Ub

addition (**Figure 45** B). This demonstrates that the mutant HECT domain of Huwe1 is able to bind Ub in a non-covalent manner. Furthermore, it shows that the C-lobe of the Huwe1 HECT domain inhibits the ubiquitin binding surface on the N-lobe. This self-inhibition can be abolished by thioester formation with Ub or by the mimicry of this with small organic compounds bound to the catalytic cysteine or by mutations of the catalytic cysteine to lysine.

5.3.11. Structural rearrangement and non-covalent Ub-UBS binding of the Huwe1 HECT domain

To gain additional structural insight into the C-N-lobe interface and the position of the catalytic cysteine relative to the N-lobe, I aligned the Huwe1 HECT N113C / C352K : Ub G76C structure (Ub-UBS binding thioester mimic) with the structure Huwe1 HECT 5lp8 (free HECT domain) and determined the backbone RMSD. The superimposition of the free Huwe1 HECT structure (5lp8) with the structure of the Huwe1 HECT N113C / C352K : Ub G76C complex shows an RMSD of 1.36Å (**Figure 46,** A).

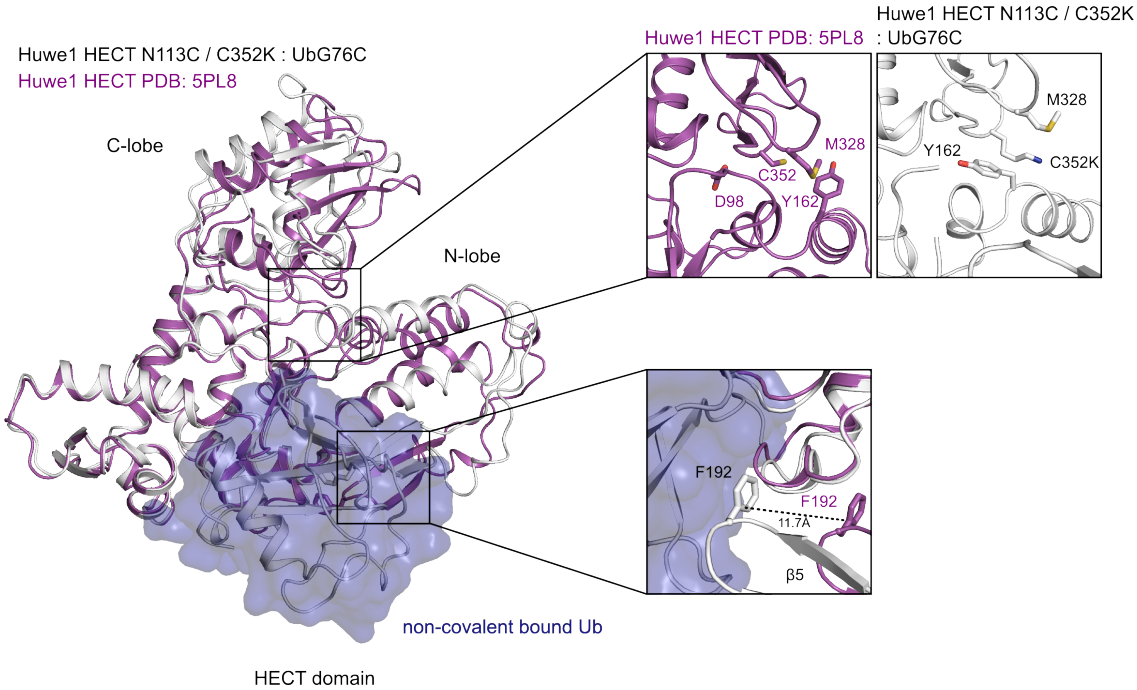

Figure 46: The structure of the Huwe1 HECT N113C / C352K : Ub G76C complex shows differences in the C-N-lobe as well as the Ub-UBS interfaces in comparison to the Huwe1 HECT structure 5lp8. (A) Overlay of the ribbon representation of the crystal structures of the Huwe1 HECT N113C /C352K(white)~UbG76C complex (blue) with Huwe1 HECT (5LP8) (magenta) **(B)** Close up on the **C-lobe - N-lobe** interfaces of the Huwe1 HECT structure 5LP8 and the Huwe1 HECT N113C /C352K structure, residues shown in sticks. In the Huwe1 HECT N113C /C352K structure residue D98 is not visible in the electron density**. (C)** Close up of F192 of the Ub - UBS interaction for the Huwe1 HECT structure 5LP8 and the Huwe1 HECT N113C /C352K structure, residues shown in sticks.

The relatively low RMSD shows a high similarity between the two structures. Nevertheless, the C-N-lobe interface is different between the Huwe1 HECT structure 5lp8 and the Huwe1 HECT N113C /C352K structure. The residues D98, Y162 and M328 are in close proximity to the catalytic cysteine (C352). Of note, M328 shows strong CSPs during the Ub^D binding (**Figure A 7**) in $^{1}H,^{13}C$-methyl IM spectra. In the Huwe1 HECT structure (5lp8) these residues form a pocket like structure and shield the catalytic cysteine of the Huwe1 (**Figure 46** B). Whereas, in the Huwe1 HECT N113C /C352K the C352K is accessible and not shielded by residues Y162 and M328 (**Figure 46** B). Of note, D98 in the Huwe1 HECT N113C / C352K structure is not visible in the electron density and therefore unstructured. Residue F192 has the most notable shift in the Huwe1 HECT N113C / C352K structure with 11.7Å in the direction of the non-covalent Ub in comparison to the solo Huwe1 HECT structure (5lp8). As shown before, this position is crucial for the polyubiquitination reaction (**Figure 38**). This suggests that due to non-covalent Ub binding the loop between the $\beta 5$ and t $\beta 6$ where the F192 is positioned is moved towards the Ub.

To investigate the Ub binding capabilities of the UBS further, I compared the NMR titration experiments of isolated $^{1}H,^{13}C$-methyl IM labelled N-lobe of the Huwe1 HECT domain with the $^{1}H,^{13}C$ -methyl IM labelled C352K mutant of the Huwe1 HECT domain and the $^{1}H,^{13}C$ -methyl IM labelled Huwe1 HECT N113C / C352K : UbG76C that serves as a mimic for an UBS that is fully occupied by Ub (**Figure 47** A, B, C).

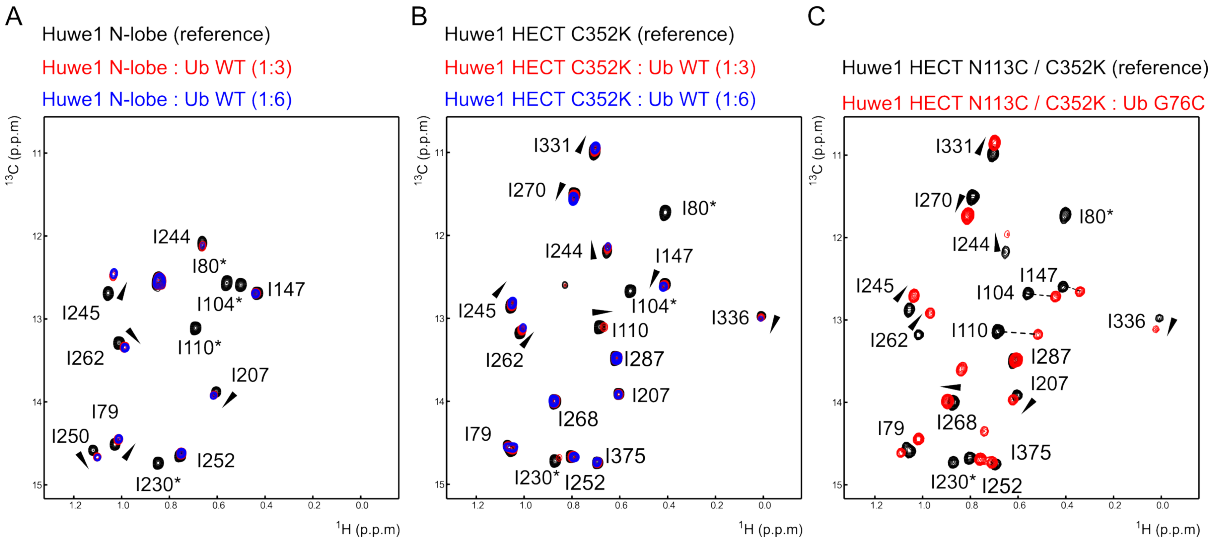

Figure 47: The Huwe1 HECT N113C / C352K : UbG76C mimic, the isolated N-lobe of Huwe1 as well as the mutant Huwe1 C352K HECT are able to bind Ub in a non-covalent fashion. (A) Overlay of a representative region of the $^{1}H,^{13}C$-methyl TROSY (HSQC) spectra of the N-lobe Huwe1 C352 HECT domain in the absence (black) and presence of increasing stoichiometric amount of monomeric Ub as indicated. **(B)** As **(A)**, but for the C352K mutant. **(C)** Huwe1 HECT N113C /C352K as reference (black) overlaid with the Huwe1 HECT N113C /C352K : UbG76C spectrum (red). Huwe1 HECT N113C /C352K : UbG76C serves as a mimic for an UBS that is fully occupied by Ub. Triangles indicate peak shifts in comparison to the reference spectrum (black). The asterisks indicate amino acids which show CSPs broadened beyond detection, the dotted line and triangle indicate amino acids which show CSPs due to non-covalent Ub binding.

The residues I80, M88, M84, I104 and I110 which show CSPs in the N-lobe due to Ub UBS binding are also affected in the Huwe1 C352K HECT mutant and the Huwe1 HECT N113C /C352K : UbG76C UBS occupation mimic. The comparison of the NMR titration experiments of the N-lobe and the Huwe1 C352K HECT with the non-covalent UbG76C mimic Huwe1 N113C / C352K shows that the induced CSPs of the Ub UBS binding are similar in all three cases. This suggests that the crystal structure of the Huwe1 N113C / C352K non-covalent UbG76C mimic is able to represent the Ub UBS binding in solution.

Furthermore, I investigated if the obtained CPSs for Ub UBS binding are present in the Huwe1 N113C / C352 HECT ~UbG76C : UbG76C mimic and which differences appear to

the binding of the Ub^{D} to the C-lobe of the Huwe1 N113C / C352 HECT domain. Therefore, I compared the spectra of the ^{1}H,^{13}C-methyl IM labelled Huwe1 HECT N113C /C352K : UbG76C mimic with the spectra of the Huwe1 N113C / C352 HECT ~UbG76C : UbG76C mimic (**Figure 48** A, B).

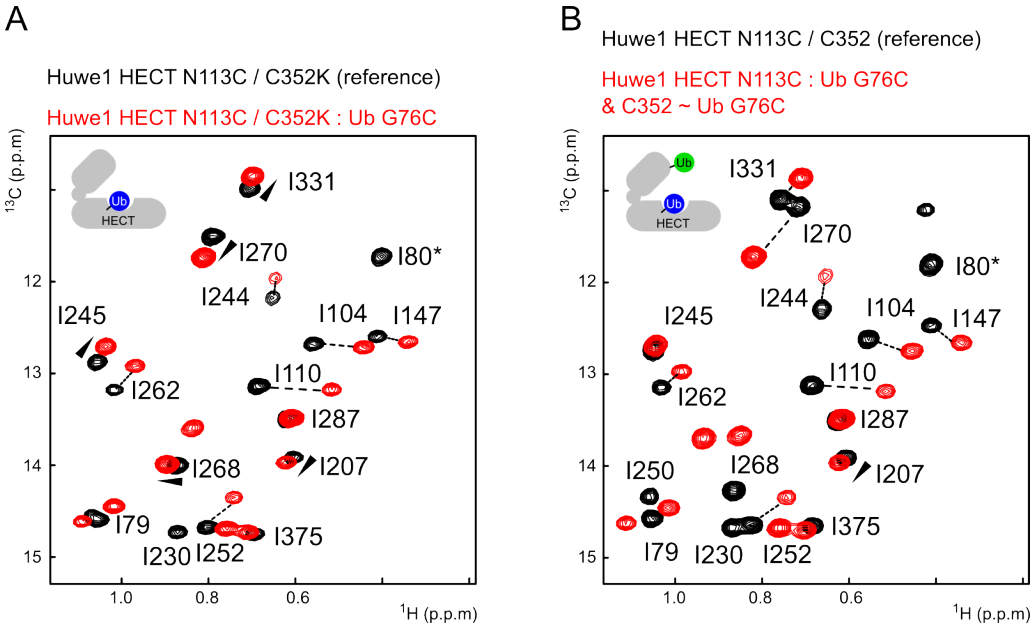

Figure 48: The Huwe1 HECT N113C / C352K : UbG76C mimic shows the similar CSPs in C-N-lobe as the Huwe1 N113C / C352 HECT ~UbG76C : UbG76C mimic. (A) Overlay of a representative region of the ^{1}H,^{13}C-methyl TROSY (HSQC) spectra of the Huwe1 HECT N113C / C352K in the absence (black) and presence non-covalent UbG76C mimic as indicated. **(B)** as in **(A)**, but for the Huwe1 N113C / C352 HECT ~UbG76C : UbG76C mimic. Triangles indicate peak shifts in comparison to the reference spectrum (black). The asterisks indicate amino acids which show CSPs broadened beyond detection, the dotted line and triangle indicate amino acids which show CSPs due to non-covalent Ub binding.

The residues I80, M88, M84, I104 and I110 which indicted UBS binding show similar CSPs in the Huwe1 HECT N113C / C352K : UbG76C mimic and Huwe1 N113C / C352 HECT ~UbG76C : UbG76C complex. Also the CSPs of residues I270 and I331 are comparable between the Huwe1 HECT N113C / C352K : UbG76C mimic and the Huwe1 N113C / C352 HECT ~UbG76C : UbG76C complex. This suggests that the mode of binding to the UBS is identical in both mimics and that the substitution of the catalytic cysteine to a lysine has the similar effects on the C-N-lobe interface of the Huwe1 HECT domain as an Ub^{D} bound to the catalytic cysteine.

All in all, I conclude that the crystal structure of Huwe1 HECT N113C / C352K : UbG76C mimic represents the non-covalent Ub binding in solution and reflects the C-lobe reorientation to the N-lobe in solution.

5.3.12. The open state can be induced by mutations in the N-lobe of the Huwe1 HECT domain

As demonstrated above, the open state can be induced by mutation of the catalytic cysteine in the C-lobe of the Huwe1 HECT domain. To test if the reorientation of the HECT domain can by mutations on the N-lobe I evaluated the residues surrounding the catalytic cysteine in the PDB structure 5lp8 [70]. I was able to identify two residues close to the catalytic cysteine (D98 and Y162), and replaced them with Ala. Next, I recorded $^{1}H,^{13}C$-methyl TROSY (HSQC) spectra of $^{1}H,^{13}C$-methyl IM labelled Huwe1 C352 HECT domain containing either a Y162A or a D98A / Y162A mutation and compared the spectra with the Huwe1 HECT domain and the Huwe1 HECT C352 ~ Ub G76C disulfide (**Figure 49** A, B, **Figure A 12**).

A

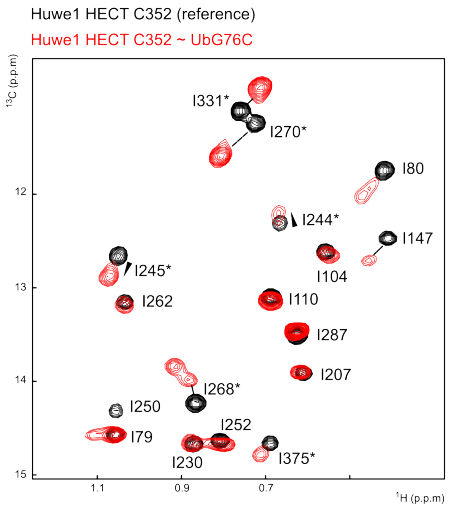
Huwe1 HECT C352 (reference)
Huwe1 HECT C352 ~ UbG76C
I331*
I270*
I80
I244*
I147
I104
I245*
I262
I110
I287
I207
I268*
I250
I252
I79
I230
I375*
^{13}C (p.p.m)
^{1}H (p.p.m)

B

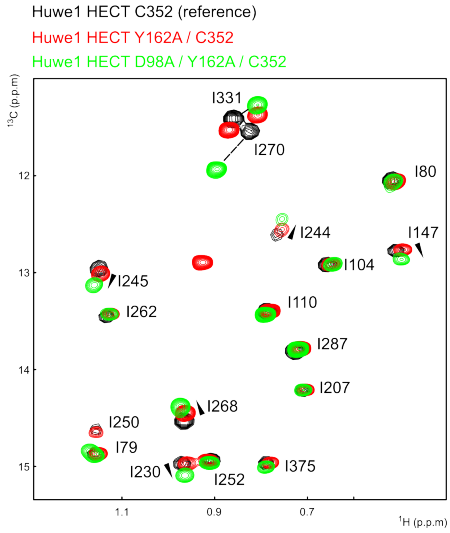
Huwe1 HECT C352 (reference)
Huwe1 HECT Y162A / C352
Huwe1 HECT D98A / Y162A / C352
I331
I270
I80
I244
I147
I104
I245
I262
I110
I287
I207
I268
I250
I79
I230
I252
I375
^{13}C (p.p.m)
^{1}H (p.p.m)

C

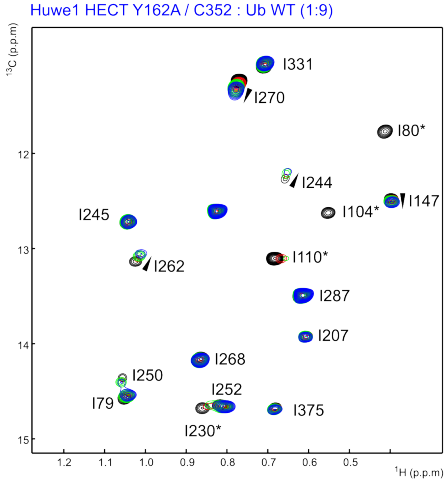
Huwe1 HECT Y162A / C352 (reference)
Huwe1 HECT Y162A / C352 : Ub WT (1:3)
Huwe1 HECT Y162A / C352 : Ub WT (1:6)
Huwe1 HECT Y162A / C352 : Ub WT (1:9)
I331
I270
I80*
I244
I147
I104*
I245
I262
I110*
I287
I207
I268
I250
I252
I79
I375
I230*
^{13}C (p.p.m)
^{1}H (p.p.m)

D

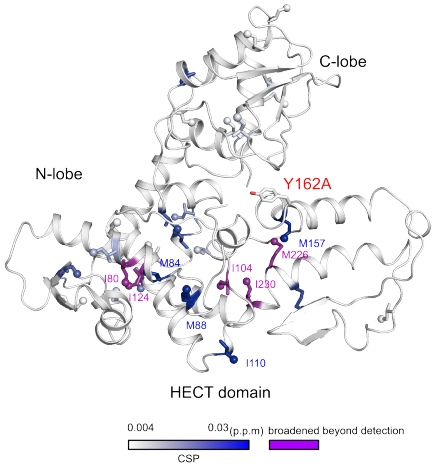
C-lobe
N-lobe
Y162A
M157
M226
M84
I80
I104
I230
I124
M88
I110
HECT domain
0.004
0.03 (p.p.m)
broadened beyond detection
CSP

F

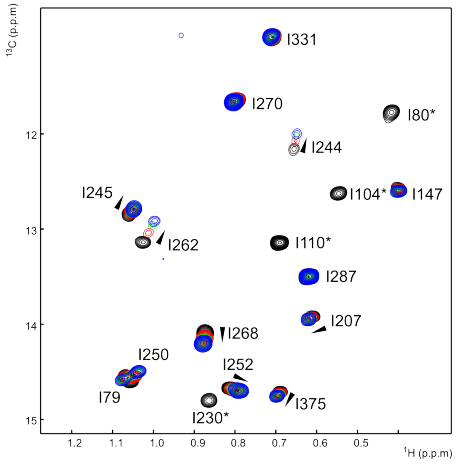
Huwe1 HECT D98A / Y162A / C352 (reference)
Huwe1 HECT D98A / Y162A / C352 : Ub WT (1:3)
Huwe1 HECT D98A / Y162A / C352A : Ub WT (1:6)
Huwe1 HECT D98A / Y162A / C352 : Ub WT (1:9)
I331
I270
I80*
I244
I245
I104*
I147
I262
I110*
I287
I207
I268
I250
I252
I79
I375
I230*
^{13}C (p.p.m)
^{1}H (p.p.m)

G

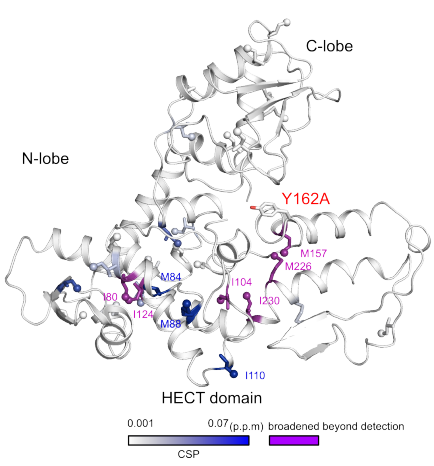
C-lobe
N-lobe
Y162A
M157
M226
M84
I80
I104
I230
I124
M88
I110
HECT domain
0.001
0.07 (p.p.m)
broadened beyond detection
CSP

Figure 49: The open state can also be induced by mutants in the N-lobe (A) Overview of a representative region of the $^{1}H,^{13}C$-methyl TROSY (HSQC) spectra of the $^{1}H,^{13}C$-methyl IM labelled Huwe1 C352 HECT domain (black) and Huwe1 HECT C352 ~ Ub G76C disulfide (red) as indicated. **(B)** as **(A)**, but with the Huwe1 HECT domain mutations Y162A/C352 (red) and D98A / Y162A / C352 (green), The triangle and dotted line indicate the chemical shift perturbations in comparison to the reference spectra (black). **(C)** as **(A)**, but of the Huwe1 HECT Y162A / C352 domain in presence of increasing stoichiometric amount of Ub as indicated. The triangle indicates the shift of a peak in comparison to the reference spectra (black). The asterisk indicates the amino acids which are broadened beyond detection in the N-lobe of Huwe1 by Ub binding. **(D)** Ub induced CSPs as observed in **(C)** were mapped onto the structure of Huwe1 HECT N113C / C352K. The CSPs are coloured from white (CSP ≤ 0.004 p.p.m) to blue (CSP = 0.03 p.p.m) for the Huwe1 HECT Y162A domain and from white (CSP ≤ 0.01 p.p.m) to blue (CSP = 0.07 p.p.m) for the Huwe1 HECT D98A / Y162A domain. Magenta highlights residues that are broadened beyond detection. The Huwe1 HECT domain is shown in white cartoon representation. The affected aa are shown in stick representation and the methyl groups as spheres. **(F)** as **(C)**, but of the Huwe1 HECT D98A / Y162A / C352 domain. **(G)** as **(D)** but with the CSPs observed in **(F).** D98 is not visible in the electron density.

In essence, the Y162A mutation in the N-lobe of the Huwe1 C352 HECT domain shows weak CSPs for the residues I270 and I331 compared to the Huwe1 C352 HECT ~ UbG76C disulfide. Nevertheless, the residues I147, I230, I244, I252, I268 and I375 which indicate a rearrangement of the HECT domain are affected in this single mutant. In contrast, the double mutation D98A / Y162A leads to strong CSPs of the residues I270 and I331 similar to the ones observed for the Huwe1 C352 HECT ~ UbG76C disulfide. This indicates that the double mutation of D98A and Y162A affects the rearrangement of the C-lobe w.r.t to the N-lobe stronger than the single mutation Y162A (**Figure 49** B). Hence, the D98A / Y162A double mutant induces a stronger C-N-lobe reorientation towards the conformation of the thioester.

To investigate whether these mutations enable non-covalent Ub binding, I performed NMR titration experiments with the $^{1}H,^{13}C$-methyl labelled Huwe1 C352 HECT Y162A single mutant and the D98A / Y162A double mutant and added up to 9-fold excess of monomeric Ub (**Figure 49** C, F, **Figure A 12**). As seen for the mutation or modification of the catalytic Cys, I observed CSPs indicating that the N-lobe mutations on the Huwe1 C352 HECT domain cause it to be able to bind Ub. Next, I mapped the observed CSPs onto the Huwe1 N113C / C352K HECT domain structure. When Ub is added I observed that the residues I80, M88, M84, I104 and I110 are affected in the N-lobe mutations of the HECT domain identically to the CSPs of the isolated N-lobe. The strongest CSPs are located in the N-lobe of the HECT domain where the non-covalent ubiquitin binding occurs (**Figure 49** D, G).

These data suggest that there is an interaction surface between the C- and N-lobe of the Huwe1 HECT domain. Hence, mutations in the N-lobe can also lead to a rearrangement of the C-lobe w.r.t to the N-lobe. In addition, the mutations in the N-lobe of the HECT domain allows Ub to bind to the UBS. Furthermore, the degree of conformational change is depending on the substituted residue. The single mutation Y162A in the N-lobe of Huwe1 shows similar CSPs for the residues I270 and I331 as the catalytic cysteine mutation C352A or C352N (**Figure 44**). In comparison, the double mutation D98A / Y192A in the N-lobe and the Lys substitution of the catalytic cysteine of the HECT domain show larger CSPs for the residues I270 and I331 which are comparable with CSPs of the Huwe1 C352 HECT ~ UbG76C disulfide. Therefore, the degree conformational change of the C-lobe w.r.t. to the N-lobe may also influence the interaction of the Ub to the UBS of the Huwe1 HECT domain.

5.3.13. Reorientation of the C-lobe leads to an acceleration of auto-ubiquitination for Y162A single mutant of the Huwe1 HECT domain

The Y162A single mutant and D98A / Y162A double mutant in the Huwe1 C352 HECT domain N-lobe enable me to determine their activity in an auto-ubiquitination assay because the catalytic cysteine has not been mutated as is the case for other open-state inducing mutants such as C352K. It was expected for the auto-ubiquitination assays, that the double mutant, showing stronger non-covalent Ub binding than the single mutant would accelerate the polyubiquitination-reaction even more (**Figure 49**). Surprisingly, the double mutant shows a reduced activity, whereas the single mutant accelerates HECT domain auto-ubiquitination in comparison to the Huwe1 C352 HECT domain (**Figure 50** A).

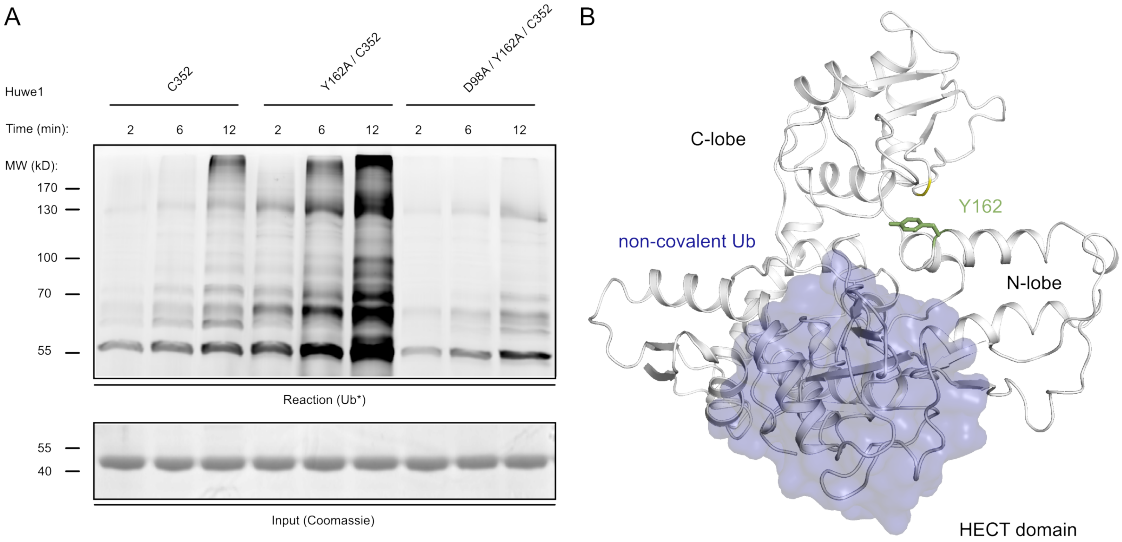

Figure 50: The mutations in the N-lobe can enhance Huwe1 auto-ubiquitination. (A) *In vitro* ubiquitination assays using the indicated Huwe1 C352 HECT domains or the indicated mutations. Reactions were stopped after the indicated time points and loaded on an SDS-PAGE gel to analyse HECT auto-ubiquitination activity with fluorescently labelled Ub (Ub*) (top panel). The bottom panel shows Coomassie stained reaction samples in the absence of E1 as input control. **(B)** In white cartoon representation, of the Huwe1 N113C / C352K HECT domain with Ub present in the UBS (blue) In stick representation the mutation Y162A on the N-lobe (green). D98 is not visible in the electron density.

As shown in Figure 50, the Y162A mutation has a strong influence on the polyubiquitination reaction of Huwe1. Whereas the double mutation D98A / Y162A shows weak polyubiquitination activity in comparison to the Huwe1 C352 HECT domain. Therefore, it is possible that the D98A mutation might be involved in thioester formation during the Ub- transfer reaction from the E2 to the E3. Of note, the mutation D98 is in close proximity to the catalytic cysteine of the Huwe1 HECT domain. Unfortunately, D98 is not visible in the electron density in the Huwe1 N113C / C352K structure. In addition, Carsten Stollmaier could confirm these results for the Y162A and the D98A / Y162A Huwe1 HECT domain mutants in the WT background with all native cysteines. This demonstrates that the mutations introduced to obtain a HECT domain with a single Cys have no effect on the ubiquitination capabilities of the Huwe1 HECT domain. In summary, the data for the single mutant show that the removal of the self-inhibition leads to an accelerated auto-ubiquitination.

5.3.14. Discussion

The regulation of HECT E3s in the cell is important because of the broad impact on the cellular fate [108]. The E3s specifically recognise target proteins and mark them for the degradation *via* the proteasome or the lysosomal pathway. In this way, E3s can alter the outcome of signal transduction pathways. To avoid premature ubiquitination, the activity of E3s is strictly regulated. In the Nedd4 family, different mechanisms inhibit ligase activity [40], [108]. One way to inhibit the E3 HECT ligase is to restrict the protein flexibility. In Smurf2 and Nedd4, auto-inhibition is achieved by an intra-molecular interaction of the C2 domain with the HECT domain close to the catalytic cysteine. In this way, the C2 domain interferes with the transthiolation reaction [42], [81]. A similar mechanism was reported for one member of the SI(ngle) HECT family [70]. In this case, the C-lobe of Huwe1 HECT domain, was locked in a conformation where the catalytic cysteine is not accessible for the transthiolation. This inhibition is achieved by the formation of an asymmetric homo-dimer *via* an helical pointer region N-terminal to the HECT domain [70]. The pointer helix interacts with the C-terminus of the C-lobe of the other HECT domain and locks the C-lobe in a position where the catalytic cysteine is inaccessible for the transthiolation reaction [70]. Here, I present data that show that the Huwe1 HECT domain is already auto-inhibited in the absence of pointer helix on the N-terminus of the HECT domain (**Figure 45** A). In addition, I could show that Huwe1 auto-inhibition can by relieved by the binding of the donor Ub to the catalytic cysteine (**Figure 39**). This auto-inhibition mechanism is distinct from mechanisms known for the Nedd4 family. My findings contribute to the variety of regulation mechanisms in HECT E3 ligases. Of note, Nedd4-family HECT E3 ligases possess a ubiquitin binding surface (UBS) that is located in the N-lobe of the HECT domain. The UBS is essential for the formation of polyubiquitin chains [51]. Furthermore, mutations in the UBS show no effect onto the E2-E3 transthiolation or the monoubiquitination reaction [50]–[53]. I verified that the Huwe1 HECT domain binds Ub at the UBS of the isolated N-lobe like the HECT domains of the Nedd4 family members (**Figure 36** A, B, C). Additionally, my findings show that the thioester formation between the C-lobe of the Huwe1 HECT domain and the donor Ub enables the Huwe1 HECT to bind Ub in the UBS (**Figure 39** A, B). Moreover, the binding of Ub into the UBS of Huwe1 is reversible and Ub can no longer bind to the UBS when the

donor Ub dissociates from the catalytic Cys (**Figure 40**). Of note, the release of the auto-inhibition induced by the thioester formation can be mimicked by alteration of the catalytic cysteine (**Figure 44** B) thereby allowing access of Ub to the UBS (**Figure 45** B).

The conformational rearrangement of the C-lobe relative to the N-lobe of the Huwe1 HECT domain can be probed by comparing PRE-measurements of the isolated C- and N-lobe with the HECT domain. The spin label at the catalytic cysteine induces a conformational change like in the thioester formation between Huwe1 C352 HECT and UbG76C (**Figure 39** A). Moreover, by attaching the spin label to C352 in the Huwe1 C352 HECT mutant, the N-lobe shows PREs (M28, M157, M226 and I244) which are not affected when the spin label is attached to position D271 in the C-lobe (**Figure 42** C). This also indicates a rearrangement of the C- and N-lobe. This rearrangement and therefore open conformation between the C- and N-lobe is also visible by the comparison of the isolated C- and N-lobes with the HECT domain and the HECT∼Ub suggests an open conformation in solution (**Figure 43** A, B, C).

In the closed state the C-lobe and N-lobe interact with each other leading to an inaccessible catalytic cysteine until the thioester formation takes place and opens the Huwe1 HECT domain. This allows the binding of Ub into the UBS (**Figure 42** A, B, C). Furthermore, I was able to introduce mutations in the interface between the C- and N-lobe which lead to a rearrangement of the C-lobe w.r.t. to the N-lobe (**Figure 49** A, B). The mutations Y162A and D98A / Y162A in the N-lobe of Huwe1 HECT also make the UBS accessible for Ub binding (**Figure 49** C, D). Noteworthy, the release of the self-inhibition by the Y162A mutation leads to an acceleration of HECT auto-ubiquitination whereas the D98A / Y162A mutation shows reduced activity (**Figure 50**). The presented data lead to a picture in which the regulation of Huwe1 HECT domain is directly linked to the orientation of the C-lobe relative to the N-lobe (**Figure 51**). This orientation of the C-lobe is modulated by the thioester formation during the Ub binding onto the catalytic cysteine in the C-lobe. During the transthiolation step a β sheet is formed on the Ub side. The reorientation of the C-lobe leads to a conformation where the UBS of Huwe1 is accessible for non-covalent ubiquitin binding (**Figure 51**).

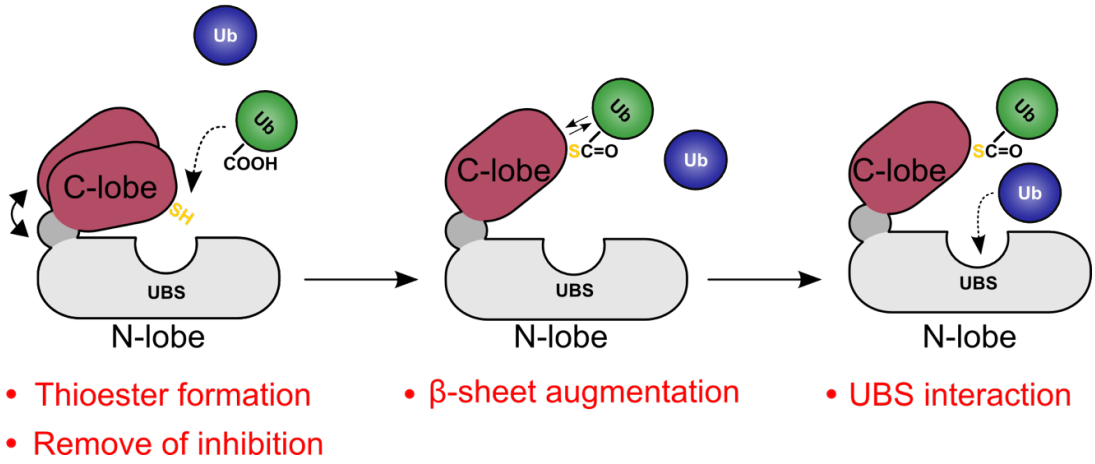

Figure 51: Ubiquitin binding mediated by the Huwe1 HECT domain. Scheme of the Huwe1 HECT domain and the covalent Ub (green) and non-covalent Ub (blue). Right side, Ub is bound to the catalytic cysteine leading to a remove of the self-inhibition state of Huwe1. Middle panel, the covalent Ub interacts with the C-lobe under the formation of the a ***β*** sheet. Left side, the non-covalent Ub is able to access the UBS of Huwe1.

In sum, the obtained data show that Huwe1 HECT possesses a self-inhibition mechanism in which the HECT domain adopts a closed conformation where the C-lobe blocks the UBS in the N-lobe. This is a new regulation mechanism for the SI(ngle) HECT family in comparison to the Nedd4 HECT family such as the Smurf2 HECT domain regulation by the Smurf2 C2 domain [79], [81]. The presented data identify a new mechanism for the HECT domain family, in which the inhibitory elements lie in the HECT domain itself whereas previously known mechanisms depend on interactions with protein regions outside of the HECT domain. Also, the question if Huwe1 possess a functional UBS could be answered. Huwe1 possesses a UBS which is only functional when self-inhibition is relieved by thioester formation. These findings will help to better understand the mechanistic details and of the Ub transfer reaction mediated by the Huwe1 HECT domain.

6. General discussion

The ubiquitin ligases (E3s) catalyse the attachment of the small protein Ub to a target protein. The target protein is recognised based on the Ub linkage and chain type e.g. by the proteasome system. Therefore, the E3 ligases play a crucial role in the cell of eukaryotes [13]. In the HECT-type E3s, the Ub forms a thioester bond exclusively with the catalytic cysteine located in the C-lobe of the HECT-domain [55]. In the next step Ub is linked to the lysine of a target protein or a preceding Ub *via* an isopeptide bond. The HECT E3s possess a UBS which is known to interact in a non-covalent manner with Ub and is essential for polyubiquitin chain elongation [40], [51].

The Ub transfer mediated by the HECT E3s is involved in many regulatory processes of the cell, especially their function in the degradation of proteins by the proteasome or lysosome. Therefore, it is crucial to understand the mechanism of the Ub transfer mediated by the HECT E3s [13], [127]. The obstacle to study HECT E3 Ub intermediates is their transient nature and inherent instability. Several strategies are known to overcome the instable thioester through a mimic of this bond with similar chemical properties [107]. One strategy is the replacement of the thioester or the stabilisation of a transient interaction by disulfide cross-linking [50], [110].

In my thesis, I was able to establish a method which uses disulfide formation to mimic the thioester of the HECT~Ub intermediate, the attack of the catalytic Cys by a donor Ub and non-covalent Ub binding. The advantage of this method is the selective chemical activation of Ub in combination with the disulfide formation *in situ* on a Ni-NTA resin. Therefore, a specific reaction between the thiol group of the HECT domain and activated Ub is achieved. In addition, this method is time-saving since it does not rely on long reaction times (**Figure 23**). Hence, this developed method allows the fast production of a variety of HECT reaction intermediates and their study by biophysiological techniques like crystallography or NMR-spectroscopy (**Figure 25**, **Figure 27**). Moreover, the chemical activation of Ub and the subsequent formation of a disulfide bridge are not limited to the HECT E3s as it can also be applied to E1 and E2 enzymes or substrates (**Table 4**). This technique enabled me to study the HECT~Ub intermediates on a structural and functional level.

During the Ub transfer, Ub is transferred from the E2~Ub thioester to the catalytic cysteine of the C-lobe from the HECT domain [40], [50]. Until now only two structures

from the Nedd4 family members show the donor Ub (Ub^D) bound onto the C-lobe of the HECT domain. In order to gain insights into the Huwe1 HECT domain thioester intermediate, I used the thioester formation method mentioned above to investigate the reaction intermediates of the Huwe1 HECT domain (**Figure 25**, **Figure 27**).

Here, my co-authors and I discovered an additional β strand which is formed during the thioester reaction of the C-lobe and the Ub^D (**Figure 29**). Furthermore, we could show that this additional β stand on the Ub^D side is conserved among the different HECT families by mutations of the crucial interaction residues on the C-lobe of Smurf2 and Huwe1 (**Figure 30**). Together these data strongly suggest that the first step in the transthiolation reaction, where the Ub is linked to the catalytic cysteine is conserved between the different HECT families. We also observed that a substitution of the last 4 residues of the C-terminus of Smurf2 and Huwe1 has an effect on the poly Ub chain reaction but does not influence the transthiolation reaction (**Figure 33**, **Figure 34**). Taken together the analysed data of the truncation and substitution of the last 4 residues for Smurf2 and Huwe1 reflect the non-conserved C-terminus of the HECT and suggest that the C-terminus may play a role in selecting the chain specificity in the Ub reaction (**Figure 30**). It was shown before that mutations of the C-terminal residues are tolerated for Huwe1, Rsp5 and E6AP but decrease Ub ligation activity [50], [53], [54]. However, isopeptide formation in Nedd4 was abolished by mutations of the C-terminal residues [50], [53], [54]. Therefore, it is still under discussion what part the C-terminus plays in the Ub reaction.

We could also answer the question about the Ub chain specificity of Huwe1. The linkage type of the attached Ub defines the signal outcome of the ubiquitinated substrate [7]. For Huwe1 a SI(ngle) HECT family member the linkage type was defined as mixed or unspecific [12]. Based on the observations that Huwe1 is involved in the proteasomal degradation of Mcl-1, Huwe1 has to produce K48 and K11 Ub chains [76]. In this thesis my colleagues and I were able to show that Huwe1 forms mainly K48 linked Ub chains (**Figure 28**).

The UBS of the HECT E3s plays a crucial role in the Ub chain formation since mutations in this surface abolish Ub chain elongation (**Figure 38**) [51]. The residues which are required for Ub binding in the UBS are conserved in all HECT domains, including Smurf2 and Huwe1 (**Figure 36**). For Nedd4 family members, I was able to show that the HECT domain indeed interacts with Ub (**Figure 35**). Surprisingly, Huwe1 a member of the

SI(ngle) HECT family is unable to bind Ub (**Figure 28**, **Figure 35**). In my thesis, I was able to shed light on the regulation mechanism of the UBS in Huwe1 (**Figure 39**, **Figure 40**, **Figure 42**). For the Smurf1, Smurf2, and Nedd4 members of the Nedd4 family it was shown that the UBS is regulated by an auto inhibition mechanism [108] in which the C2 domain of the N-terminus blocks the UBS and prevents the Ub-reaction [79]. The C2 domain can be released from the UBS e.g. by Ca^{2+}, allowing the Ub to bind onto the UBS of the HECT domain [81]. Recently, a self-inhibition mechanism was reported for Huwe1 in which an N-terminal extension forms a asymmetric dimeric structure with a second Huwe1 HECT domain and locks the C-lobe in a catalytically incompetent position in which the catalytic cysteine cannot perform the transthiolation reaction [70].

For Huwe1, I was able to show that Ub interacts with the UBS of the isolated N-lobe and furthermore that thioester formation allows access to the UBS. Hence, in presence of the thioester intermediate, Ub is able to bind in a non-covalent manner to the UBS of the Huwe1 HECT domain (**Figure 36**, **Figure 39**). Moreover, I was able to show by PRE NMR-experiments that the Huwe1 C-lobe w.r.t. the N-lobe adopts a closed conformation in solution (**Figure 42**). In the absence of the thioester the C-lobe is in close proximity to the UBS of the N-lobe thereby hindering Ub binding (**Figure 42**). In addition, I was also able to show by NMR experiments with the isolated C- and N-lobe and comparison with the Huwe1 HECT domain that the Huwe1 C-lobe w.r.t. the N-lobe adopts an open conformation in solution (**Figure 43**). Furthermore, any alteration of the catalytic cysteine leads to a reorientation of the C-lobe w.r.t. the N-lobe (**Figure 44**). Subsequently, these reorientations allow Ub to bind into the UBS (**Figure 45**). This reorientation could also be induced by mutations on the N-lobe (**Figure 49**). The removal of the self-inhibition by mutations and consequently reorientation of the C-lobe w.r.t. N-lobe leads to an acceleration of ubiquitination (**Figure 50**). This clearly shows that the self-inhibition of Huwe1 is modulated by the strength of the interaction between the C- and N-lobe of the Huwe1 HECT domain. This leads to a rearrangement of the C-lobe w.r.t. the N-lobe. The binding of the Ub in the UBS is a reversible process since the cleavage of the thioester intermediate leads to a closing of the Huwe1 HECT domain (**Figure 40**). Of note, the data presented in 5.3 “The Huwe1 HECT domain is auto-inhibited through interactions of the N- and C-lobe” show a self-inhibition mechanism independent from the N-terminal pointer helix identified recently [70] since all experiments were performed in its absence. In sum, the presented data show a self-inhibition mechanism

for the Huwe1 HECT domain where the binding of Ub to the UBS solely relies on the C-lobe orientation w.r.t. the N-lobe.

Overall, I showed that the chemical activation of Ub is a powerful tool to study the Ub transfer reaction of different Ub enzymes. In essence, I was able to show that the transthiolation reaction leads to an interaction surface between the C-lobe and the Ub^D which appears to be highly conserved among different HECT domains. Additionally, I showed that the regulation of the Huwe1 HECT domain is unique in comparison to the Nedd4 family because of the self-inhibition character which lies within the HECT domain itself (**Figure 52**).

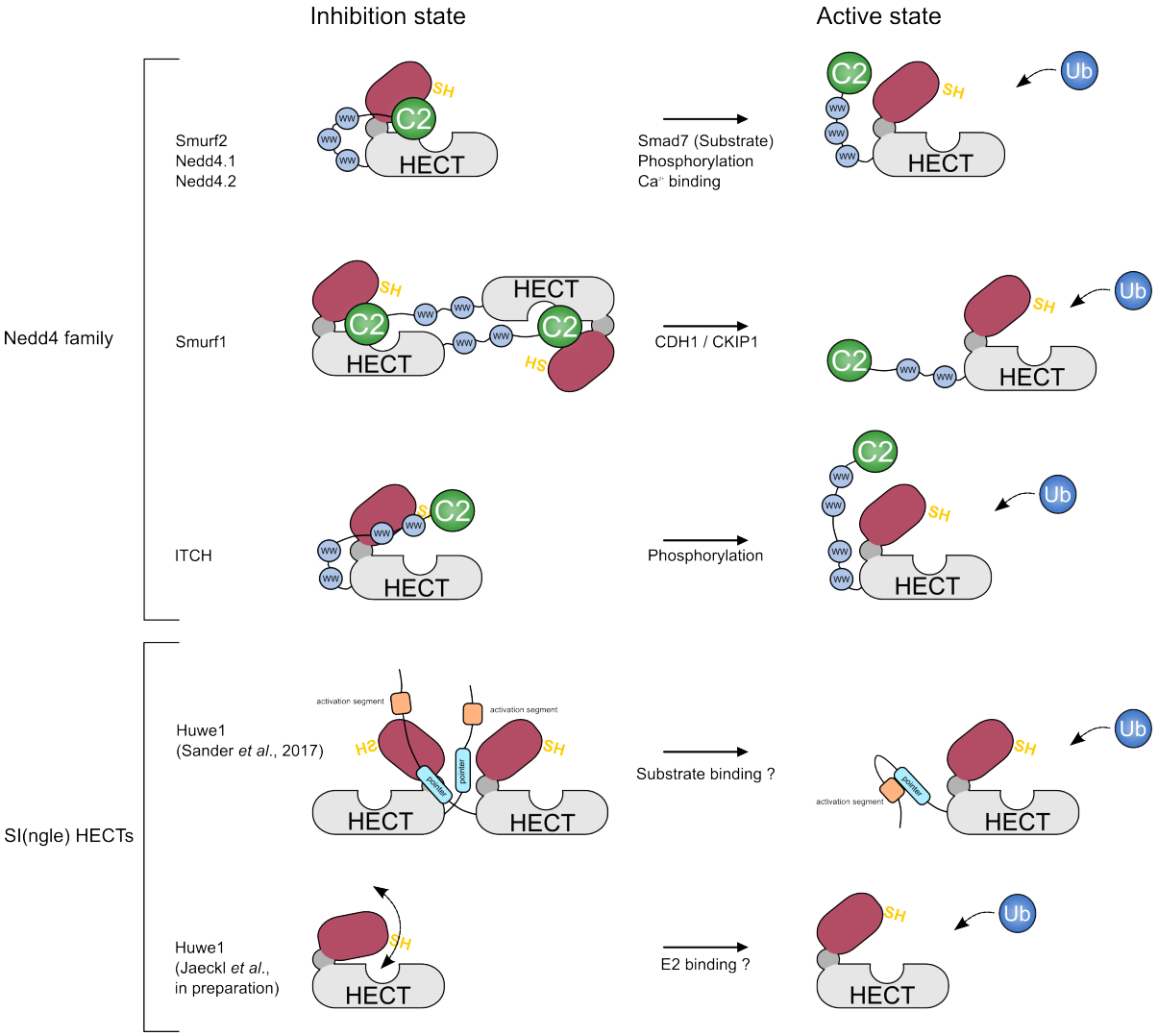

Figure 52: Inhibition of the Nedd4 family in comparison to Huwe1. Shema of the regulations mechanism of the Nedd4 family. The auto- inhibition for Smurf2 is removed by the binding of Smad7 to the WW domain which enhances E2 binding. For Nedd4.1 a Tyr in the C2 is phosphorylated relieving the auto-inhibition state. Whereas, in Nedd4.2 Ca2+ binds to the C2 domain and enables the C2 to bind onto the plasma membrane and remove the inhibition state. In the case of Smurf1 a homodimer is formed, and the inhibition is removed by the binding of CDH1 (Cadherin1) to the C2 domain and the binding of CKIP1 (Casein kinase-2 interaction protein1) onto the linker region between the WW

domains. A serine/threonine phosphorylation of ITCH between the C2 and WW domain activates the ligase. For Huwe1 the first describe inhibition mechanisms is the formation of an asymmetric dimer through an interaction of the pointer helix with the another Huwe1 domain. The of Huwe1 is removed by an activation segment. Which signal triggers the remove is still not known [70]. In addition, the regulation of the Huwe1 HECT domain from the data obtained in this thesis. In this case the C-lobe of Huwe1 HECT modulates the inhibition by the relative orientation to the N-lobe. This rearrangement of the C-lobe is accomplished during the thioester formation which suggests that the binding of the E2~Ub removes the self-inhibition state of the Huwe1 HECT domain. Adopted from Distel *et al*., 2018 [108]

In case of the inhibition of members from the Nedd4 family they rely on an external signal which releases the C2 domain from the HECT domain. Here, I could show that the inhibition of Huwe1 is independent of an external signal and only needs the formation of the thioester bond to activate Huwe1. This connects Huwe1 directly to the E2~Ub binding and subsequently to the transthiolation reaction. Furthermore, Nedd4 and the HERC family show a clearly defined domain structure at the N-terminus, whereas members of the SI(ngle) HECTs show considerable variability in their overall domain arrangement at the N-terminus (**Figure 13**). This may also reflect the evolution of different inhibition mechanisms for the HECT E3s.

There are multiple known genetic alterations positioned in the Huwe1 HECT domain [128], [129] (**Figure 53** A).

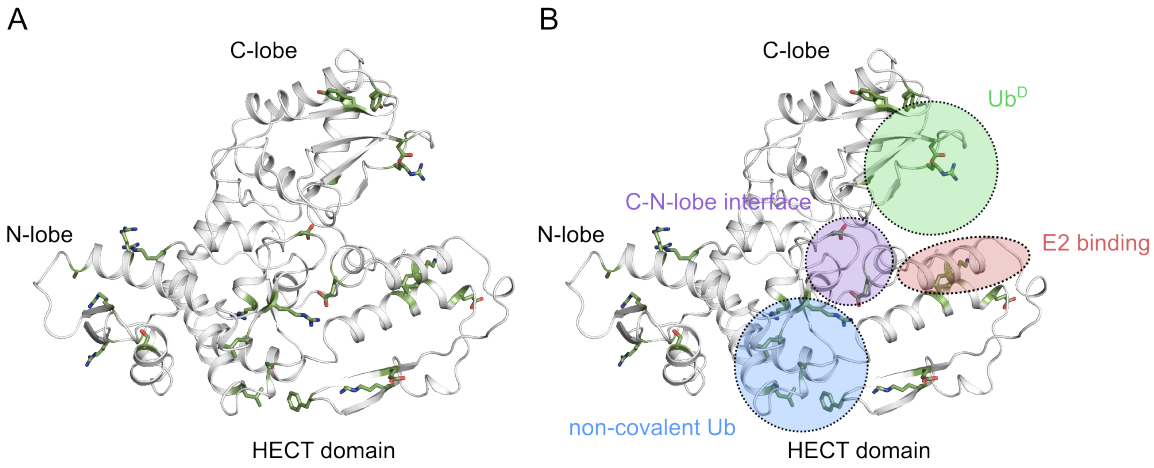

Figure 53: Known genetic alterations in the HECT domain of Huwe1. (A) Cartoon representation of Huwe1 HECT (white) of the PDB structure 5PL8. Sticks (green) represent the position of known genetic alterations in the Huwe1 HECT domain [128], [129]. **(B)** as **(A)** but with interaction regions of Ub, E2 and C-N-lobe as indicated.

Several of them are located in regions of the HECT domain crucial for interactions with either the Ub, the E2 or between the C- and N-lobes (**Figure 53** B). In case of the UBS the amino acids Ser108, Leu91, Arg93, Ser108 and Leu115 have known genetic alterations

[128], [129]. Therefore, it can be speculated that these alterations might influence the polyubiquitination in the same way as shown for the mutation I110 in the HECT domain of Huwe1 in this thesis (**Figure 38**). Also, the thioester formation could be affected by the genetic alterations of the residues 339 and 345 in the C-lobe. Similar to the here presented data for the proline substitution which abolish the thioester formation because the β-strand between the C-lobe and the Ub^D is affected. The residues Leu168, Val218 and Lys215 show genetic alterations [128], [129] and are in the region where the E2~Ub binds for the transthiolation reaction from E2 to E3. Alterations in this region could influence E2 binding and therefore the transthiolation reaction and may lead to a reduced polyubiquitination. Another genetic alteration is positioned in the interface between the C- and N-lobe where the residues Asp98 and Glu160 with a negative charge are altered to Asn with a polar uncharged side chain and to Lys with a positive side chain. The effect of this alterations could be similar to the induced single and double mutation D98A / Y162A in the Huwe1 HECT domain used in this thesis. These mutations influence the interaction between the C-and N-lobe which leading to a rearrangement of the C-lobe w.r.t. the N-lobe allowed binding of Ub into the UBS (**Figure 49**). The effect on the polyubiquitination reaction is more severe, in the case of the Y162A mutation this leads to an acceleration polyubiquitination whereas in the case of the double mutation the polyubiquitination is reduced (**Figure 50**).

Overall, this study will help to understand the Ub transfer mechanism in greater detail and provide insides into the function of the Huwe1- and HECT domains in general. These findings are starting points for drug development in disease caused by the dysfunction of Huwe1.

7. Materials

7.1. Equipment

Table 6: Equipment.

Instrument	Manufacturer
37 °C plate incubator	Hereaus
37 °C shaker incubator, HT Multitron Standard and HT Ecotron	Infors
Acculab-balance	Sartorius
Advanced Primus 25 Thermocycler	Peqlab
Advanced Primus 96 Thermocycler	Peqlab
Agarose gel chamber, HE 99X	Amersham Biosciences
Avance AVIII (600 MHz) spectrometer	Bruker
Avance AVIII (800 MHz) spectrometer	Bruker
Avanti J-26 XP centrifuge	Beckmann Coulter
Amersham™ Imager 600	GE Healthcare
Bio-5000 Scanner	Microtek
Centrifuge 5424 + 5417C	Eppendorf
Centrifuge bucket, 1 L	Beckmann Coulter
Centrifuge bucket, 50 mL	Beckmann Coulter
Digital Sonifier 450	Branson
DNA sequencer (3730XL)	Applied Biosystems
dragonfly	ttp labtech
E-Box 1000/26M system	Vilbert Lormat
Electrophoresis power supply, EP 301	GE Healthcare
EmulsiFlex-C3	AVESTIN, Inc.
FPLC Äkta prime plus	GE Healthcare
FPLC NGC	BioRad
freezer (-20 °C)	Liebherr
freezer (-80 °C)	Liebherr
French press Emulsiflex-C3	Avestin
Gyro-Rocker SSL3	Stuart
Heating block	VWR
HERAEUS multifuge 3SRü centrifuge	Thermo Scientific
Hi Load 16/600, Superdex 75, preg grade (120 ml)	GE Healthcare
Hi Load 26/600, Superdex 75, preg grade (320 ml)	GE Healthcare
HisTrap HP, 1 x 1 ml	GE Healthcare
HisTrap HP, 1 x 5 ml	GE Healthcare
HiTrap Q HP	GE Healthcare
HiTrap SP HP	GE Healthcare
JA-25.50 rotor	Beckmann Coulter
JLA-8.100 rotor	Beckmann Coulter
Light box prolite Basic 2	Kaiser

Magnetic stirrer, MR hei-Mix L and MR Hei-Mix S	Heidolph
Microwave	Bosch
Mighty small II gel caster	GE Healthcare
NanodropTM 100 spectrometer	Thermo Scientific
PD-10 Desalting Columns	GE Healthcare
Peristaltic Pump P1	GE Healthcare
pH meter HI 2221	HANNA Industries
Photometer, bio photometer plus	Eppendorf
Pipetman neo P1000, P200, P100, P20, P10, P2	Gilson
Precision balance 440-47N	Kern
SDS-PAGE unit, SE 250	Amersham Biosciences
Sonoplus sonifier	Bandelin
Thermomixer comfort	Eppendorf
Typhoon 5 Imager	GE Healthcare
Vortex Genie 2	Scientific Industries

7.2. Consumable

Table 7: Consumables.

Product	**manufacturer**
5 mm NMR tubes	Norell
96 well plate	Greiner
96-3 low profile INTELLI-PLATE®	Art Robbins Instruments
Concentrator Vivaspin 20	Sartorius
Cuvettes (plastic)	Roth
Dialysis membrane, MWCO 3500	Spectrum Laboratories
Falcon tubes (15 mL and 50 mL)	Greiner
Inoculation loop	Greiner
Inoculation spreader	Sarstedt
Membrane filters	Millipore
NucleoSpin® Gel and PCR Clean-up	Machery-Nagel
NucleoSpin® Plasmid EasyPure	Machery-Nagel
Parafilm	Pechney
Pasteur piptes	Willmad Lab Glass
PCR plastic tubes	Greiner
Pipet tips	Greiner
Pipets (single use, sterile)	Simport
Plastic cups (1.5 mL and 2 mL)	Eppendorf
Plastic cups (1.5 mL capless)	Fisher Scientific
Snap cap inoculation tubes	Simport
Syringe filter (0.22 µm, 0.45 µm)	Millex
Syringes (6, 20 and 60 mL)	Fisher Scientific
UV cuvettes (plastic)	Eppendorf
Vacuum sterile filter	Millipore

7.3. Chemicals

Table 8: Chemicals.

Chemical	Supplier
$^{1}H,^{12}C$-D-Glucose (99%)	Sigma-Aldrich
Acrylamide-bis solution (29:1), 40 % (w/v)	Roth
Agarose	Sigma-Aldrich
Ammonium chloride	Alfa Aesar
Ammonium chloride ($^{15}NH_4Cl$)	Sigma-Aldrich
Ammonium persulfate (APS)	AppliChem
Ampicillin sodium salt	Roth
BigDye Terminator v3.1 Sequencing reagents	ABI
Biotin	Roth
Boric acid	Sigma-Aldrich
Bradford protein assay reagent (5x)	Serva
Bromophenol blue 0.04 % (w/v)	Alfa-Aesar
Calcium chloride ($CaCl_2$ x 2 H_2O)	Merck
Chloramphenicol	Sigma-Aldrich
Cobalt chloride ($CoCl_2$ x 6 H_2O)	Sigma-Aldrich
Coomassie Brilliant Blue G250	Fisher Scientific
Copper (II) chloride	Alfa Aesar
Copper (II) sulfate ($CuSO_4$ x 5 H_2O)	VWR
D_2O	Sigma-Aldrich
D-Glucose	Baker
Disodium hydrogen phosphae (Na_2HPO_4)	Merck
Dithiothreitol (DTT)	Enzo Life Science
DNA loading dye (6x)	Thermo Scientific
dNTPs	Thermo Scientific
EDTA disodium salt	Promega
Ethanol	Sigma-Aldrich
Gene ruler 100bp DNA ladder	Fermentas
Gene ruler 1kbp DNA ladder	Fermentas
Glycerol	Roth
GSH (reduced)	Sigma-Aldrich
HEPES	Roth
Hydrochloric acid (HCl), 6M	Roth
Imidazole	Roth
IPTG (Isopropyl β-D-1-thiogalactopyranoside)	Roth
Iron (III) chloride ($FeCl_3$ x 6 H_2O)	Alfa Aesar
6-Iodacetamidofluorescein	Thermo Scientific
Kanamycin sulfate	Roth
L-Arginine	SAFC
L-Methionine (methyl-labeled)	CIL
Magnesium chloride	Acros Organics

Manganese (II) sulfate ($MnSO_4$ x 4 H_2O)	VWR
MOPS	Sigma-Aldrich
N,N,N‘,N‘,-tetramethylethylenediamine (TEMED)	Sigma-Aldrich
Ni^{2+}-NTA-agarose beads	Quiagen
PageRuler prestained protein ladder	Thermo Scientific
Potassium phosphate, monobasic (KH_2PO_4)	CalBiochem
Protino® Glutathione Agarose 4B	Macherey-Nagel
Rotiphorese® 50x TAE buffer	Roth
SafeView nucleic acid stain	Applied biological materials Inc.
SDS, 20 % (w/v) solution	AppliChem
SDS-PAGE buffer 10x (Tris, glycine, SDS)	National Diagnostics
Sodium azide (NaN_3)	Sigma-Aldrich
Sodium chloride (NaCl)	Merck
Sodium dihydrogen phosphate monohydrate	Merck
Sodium hydroxide 10N (NaOH)	Alfa-Aesar
Sodium L-glutamate monohydrate	Merck
TEMED (N,N,N',N'-tetramethylethylene diammine)	Sigma-Aldrich
Thiamine hydrochloride	Sigma-Aldrich
Tris-HCl	Roth
Triton X-100	Sigma-Aldrich
Zinc sulfate ($ZnSO_4$ x 7 H_2O)	VWR
4-Maleimido-TEMPO (Tetramethyl-1-piperidinyloxy)	ASLA biotech

7.4. Enzymes

Table 9: Enzymes.

Enzyme	Supplier
DN*ase*I	AppliChem
D*pn*I	NEB
KAPA HiFi DNA polymerase	Roche
Lysozyme	Fluka
Tobacco etch virus (TEV) protease	Production of AG Wiesner

7.5. Buffers and Media

Table 10: Composition of buffers and media

Buffer	Ingredients
Agarose (1 %) stock solution	5 g of agarose is dissolved in 500 mL heated 1x Rotiphorese TAE-buffer and stored at 65 °C
Ampicillin (1,000x)	2.5 g / 25 mL H2O (100 mg/mL)
APS (10 %)	1 g / 10 mL (0.1 g/mL)
Biotin (1,000x)	20 mg / 20 mL H_2O (1 mg/mL; add some 1M NaOH to dissolve)
Chloramphenicol (1,000x)	0.85 g / 25 mL pure EtOH (34 mg/mL)

Coomassie stain solution	0.5 g Coomassie Brilliant Blue G250 (0.025%) in 30 mM HCl, 10% EtOH
DTT (1 M)	3.1 g DTT / 20 mL (155 mg/mL)
DTT (5 M)	7.7 g DTT / 10 mL (770 mg/mL)
Disulfide formation:	
Buffer A	20 mM $NaPO_4$, pH 7.8 150 mM NaCl, 1 mM DTT
Buffer B	20 mM $NaPO_4$, pH 7.8 150 mM NaCl, 50 mM Ellman's reagent (5,5`dithiobis-(2-nitrobenzoic acid))
Buffer C	20 mM $NaPO_4$, pH 7.8, 150 mM NaCl; degassed; Argon purged
Buffer D	20mM $NaPO_4$, pH 6.4, 150mM NaCl; degassed; Argon purged
Fluorescein buffer	50 mM Tris, pH 7.8, 150 mM NaCl, 1 mM DTT
IPTG (1 M)	4.8 g / 20 mL (240 mg/mL)
Kanamycin (1,000x)	1.25 g / 25 mL H2O (50 mg/mL)
LB	10 g bactotryptone, 5 g yeast extract, 10 g NaCl in 1 l of H2O, pH 7.4, autoclaved
LB-Agar	5 g bactotryptione, 2.5 g yeast extract, 5 g NaCl, 7.5 g agar (1.5 %) in 500 ml H_2O, pH 7.4, autoclaved
lysis buffer	NaP buffer with 10 mM Imidazol, 1 mM DTT, pH 7.5
lysis buffer +	lysis buffer with Lysozyme, RNAse, Triton X-100
M9 (10x)	60 g Na2HPO4, 28.6 g KH2PO4, 5g NaCl dissolved in 1 L H2O, pH 7.4
M9 (1x, D2O)	1 L D2O, 6 g Na_2HPO_4, 2.86 g KH_2PO_4, 0.5 g NH_4CL (unlabelled or 15N), pH 7.4, 4 g glucose unlabelled or 2g glucose labelled (1H,13C or 2H,13C or 2H,12C), 1 mL trace elements (1,000x), 0.1 mL trace elements (10,000x), 1 mL $MgSO_4$ (1M), 1 mL biotin (1000x), 1 mL thiamine (1000x), 1 mL of each antibiotic (1000x), 0.3 mL CaCl2 (1M)
M9 (1x, H2O)	100 mL M9 (10x) in 1 L of H_2O, pH 7.4, 0.5 g NH_4CL (unlabelled or 15N), 4 g glucose unlabelled or 2g glucose labelled (^1H,^{13}C or ^2H,^{13}C or 2H,12C), 1 mL trace elements (1,000x), 0.1 mL trace elements (10,000x), 1 mL MgSO4 (1M), 1 mL biotin (1000x), 1 mL thiamine (1000x), 1 mL of each antibiotic (1000x), 0.3 mL CaCl2 (1M)
MOPS pH 7.5 (1 M)	209.26 g MOPS in 1 L H_2O, adjust pH
NaP (10x)	87.6 g/L NaCl, 71 g/L Na_2HPO_4, pH 7.1
NaP (1x)	50 mM NaP, 150 mM NaCl, pH 7.5
NMR:	
Standard	20mM $NaPO_4$, pH 6.4, 150mM NaCl, 1mM DTT
Disulfide	20mM $NaPO_4$, pH 6.4, 150mM NaCl; degassed; Argon purged
nonreducing SDS loading buffer (5x)	3 mL Tris-HCl (1 M, pH 6.8), 2.5 mL glyercol (25 % final), 4.5 mL 20% SDS, 1 mg bromophenol blue (0,01% final)
reducing SDS loading buffer (5x)	3 mL Tris-HCl (1 M, pH 6.8), 2.5 mL glyercol (25 % final), 4.5 mL 20% SDS, 1 mg bromophenol blue (0,01% final), 1 mL of DTT (5 M)
Thiamine (1000x)	20 mg / 20 mL H_2O (1 mg/mL)
Trace elements (1,000x)	5 g EDTA in 100 mL H_2O (adjust to pH 7.5); 0.833 g $FeCl_3$ x 6 H2O, 84 mg ZnCl2, 13 mg $CuCl_2$ x 2 H_2O, 10 mg $CoCl_2$ x 6 H_2O, 10 mg H_3BO_3
Trace elements (10,000x)	3.37 g $CuSO_4$ x 5 H_2O, 3.0 g $MnCl_2$ x 4 H_2O, 0.43 g $ZnSO_4$ x 7 H_2O, 0.5 CoCl2 x 6 H2O in 100 mL H_2O

Tris-HCl pH 6.8 (1 M)	60.5 g Tris-HCl in 500 mL H_2O, pH 6.8
Tris-HCl pH 8.0 (1 M)	121 g Tris-HCl in 1 L H_2O, pH 8
Tris-HCl pH 8.8 (1.5 M)	90.75 g Tris-HCl in 500 mL H_2O, pH 8.8
X-Tals:	
Huwe1 HECT and mutants	25mM HEPES 150mM NaCl pH 6.4
Smurf2 HECT and mutants	50mM Tris 150mM NaCl pH 7.4 5% Glycerol

8. Methods

8.1. Molecular biology

8.1.1. PCR amplification

The here used PCRs (polymerase chain reactions) were used for the modification and verification of the plasmid DNA. For all PCR based reactions like site-directed mutagenesis and RF Cloning the polymerases KapaHiFi (peqlab) were used. The primers were order from Sigma-Aldrich.

A standard PCR reaction mix contains, a thermostable DNA-polymerase, a DNA template, oligonucleotide primers, puffer and nucleotides. The PCR-reaction are classified into 3 steps: denaturation step, the annealing step and the elongation step. In the denaturation step the double stranded template DNA is denatured into a single stranded DNA at 94C°. In the annealing step the oligonucleotide primers hybridises with the single stranded DNA. The temperature of this step depends on the GC content of the used oligonucleotide primers (usually the temperature of the oligonucleotide primers lies between 50-65C°). After the hybridises the elongation step takes place at 72C° in this step the DNA-polymerase use the oligonucleotide primers as start point for the elongation of the single stranded DNA to a double stranded DNA. These 3 steps are repeated in a cycle to duplicate the template DNA. All generated plasmid and used primers are listed in the appendix Table 21.

Table 11: Standard Kapa-HiFi PCR-protocol.

Step	Temperature in °C	Time in seconds	Cycle
	95	180	
Denaturation	98	30	30 x
Annealing	50-65	20	
Elongation	72	210	
	72	600	
Storage	8	Infinite	

8.1.2. QuikChange™ mutagenesis

To introduce multiple or single point mutations into the protein coding sequence, the QuikChange strategy (Stratagene) was used. The primes for the QuikChange were designed using the PrimerX online tool [130]. The PCR reaction was carried out as described Table 11. A typically QuikChange 25 µL reaction contained: 50-100 ng of template DNA, 1 µL of each Fw and Rv primers (10 µM), 5X buffer, 0,5 µL dNTPs (100 mM), 0,25 µL polymerase and MilliQ-water. The PCR program included 20 cycles, using annealing temperatures between 50-65C° according to each set of primers.

8.1.3. Restriction free cloning

Restriction free (RF) cloning allowed the insertion or deletion of large DNA fragments. This technique is an PCR based cloning approach without the need for restriction site and therefore no restriction enzymes [131].

As first step of a RF cloning, a so called “mega or super primer” has to be generated by a linear amplification PCR. This “mega primer” bears the coding DNA sequence of interest and is flanked by a ~25 bp overlapping region with the sequence of the target vector. The primers were designed with the help of the online tool http://www.rf-cloning.org/. An RF reaction contained: ~40 ng of vector, ~200 ng of agarose gel purified mega primer, 5x buffer, 0.5 µL dNTPs (100 mM), 0.25 µL polymerase and Millipore water added up to a total volume of 25 µL. For the PCR programmes a temperature gradient from 60-65°C with ~30 cycles during the annealing phase was used. More detailed information of the set up is describe in [132].

5.1.4. Digestion with DpnI

To digest the methylated template DNA of the QuikChange or RF-cloning PCR reaction was treated with the methylation-specific DpnI restriction enzyme (Thermo Fisher Scientific). For this reaction 0.5 µL DpnI were added to the PCR reaction mix and incubated at 37 °C for 30 min. The DpnI was inactivated at 80 °C for 20 min.

8.1.5. Transformation into chemically competent *E. coli* cells

The isolated plasmid DNA or the with DpnI treated QuikChange or RF reaction was transformed into chemically competent DH5α *E. coli* cells or into BL21-CodonPlus(DE3)-RIL *E. colis* for protein expression. For this purpose, 5 to 10 µL of the PCR product was added to 50 µL of competent *E. coli* cell and incubated 15 min on ice. After this a heat-shock of 42 °C for 1 min was conducted. The cells were then recovered with 200 µL of LB-media and incubated for 60-90 min at 37 °C and shaken at 600 rpm. After this treatment, the cells were plated on agar plates and incubated overnight at 37 °C.

8.1.6. Isolation of plasmid DNA

For the plasmid DNA isolation, according to the NucleoSpin Plasmid EasyPure protocol from Macherey-Nagel, single colonies were picked from agar plates after transformation and inoculated in 7 mL of LB media with the addition of the required antibiotic and grown overnight at 37 °C. The precultures were centrifuged and the pellet was treated according to the NucleoSpin Plasmid EasyPure protocol from Macherey-Nagel. The elution step of the plasmid DNA from the column was done with 30 µL instead of 50 µL elution buffer.

8.1.7. DNA sequencing

The isolated plasmid DNA was analysed in the in-house sequencing facility. The facility uses the next-generation sequencing approach based on the dideoxy method invented by Frederick Sanger. The reaction setup contains: between 25~75 ng of isolated plasmid DNA, 1 µL of primer according to the used vector, 5x sequencing buffer, 0.5 µL of BDT-mix (BigDye™ Terminator, ThermoFischer), and Millipore water added up to a total volume of 10 µL. The obtained data from the in-house sequencing facility were then analysed with the BioEdit Sequence Alignment Editor [133].

8.2. Protein biochemistry

8.2.1. Sodium dodecyl sulfate polyacrylamide gel electrophoresis (SDS-PAGE)

Proteins are unique in their sequence and therefore in their physical properties. The molecular weight (MW) is one of those properties which is calculated from the sum of all amino acids in the sequence of a protein. This characteristic trait can be used to separate proteins according to their MW. One of the used methods for this is the SDS-PAGE. For this technique, the protein is denatured by the detergent SDS that is present in the loading buffer. The SDS forms a negatively charged complex with the protein. As a next step the sample is loaded onto a polyacrylamide gel. When current is applied across the gel the protein will move towards the positively charged cathode because of the negatively charged SDS During this movement across the electrical field the protein-SDS complex is separated based on the size of the protein. Large protein are retained stronger by the polyacrylamide gel and therefore move slower than small proteins. Proteins mixtures with known MW are run on the same gel as a marker. With this marker proteins, the MW of the loaded sample can be estimated after the staining with Coomassie. The SDS-PAGE was running with 180 – 220V. In the Table 12 and Table 13 the commonly cast SDS-polyacrylamide gels are listed.

Table 12: Gel recipe for polyacrylamide separating gels.

Gel % / separation range	8% / 30 - 250 kDa	12% / 14 - 150 kDa	16% / 5 - 70 kDa
40% acrylamide (29:1)	**14 mL**	**21 mL**	**28 mL**
H_2O	**37.5 mL**	**30.5 mL**	**23.5 mL**
1.5M Tris-HCl pH 8.8 (0.375 M)	**17.5 mL**	**17.5 mL**	**17.5 mL**
20% SDS (0.1%)	**0.35 mL**	**0.35 mL**	**0.35 mL**
10% APS (0.1%)	**0.35 mL**	**0.35 mL**	**0.35 mL**
TEMED (0.5 uL / mL)	**35 µL**	**35 µL**	**35 µL**

Table 13: Gel reipe for polyacrylamide stacking gel.

Gel %	4%
40% acrylamide (29:1)	**3.5 mL**
H_2O	**26.5 mL**
1.0M Tris-HCl pH 6.6 (0.125 M)	**4.35 mL**
20% SDS (0.1%)	**0.175 mL**
10% APS (0.1%)	**0.175mL**
TEMED (0.5 uL / mL)	**12.5 µL**

8.2.2. Coomassie staining

One common way to detect proteins which have been separated by SDS-PAGE is to stain the gel with Coomassie Brilliant Blue G250. This dye is bright blue and interacts via hydrophobic interactions with proteins in a nonspecific manner. To stain the gel with Coomassie Blue rinse the gel three to four times in water and boil it for around 1 minute in the microwave. Rinse again with water and add Coomassie staining solution (**Table 14**). Boil the gel in the staining solution. Incubate 15 minutes shaking on room temperature (RT). For better staining results stain, overnight. Remove the staining solution and destained with water. Before scanning the gel rinse in 100% ethanol and wash 2 times with VE water. With this step precipitated Coomassie on the gel surface will be removed, thus increasing contrast.

Table 14: Coomassie staining solution

Coomassie Brillant Blue G250	0.8 g
Ethanol (100%)	**100 mL**
H_2O	**900 mL**
6 M HCl	**5 mL**
	Stir o/n

8.2.3. Recombinant protein expression

For the structural and functional characterisation of proteins, a variety of biophysical techniques are suitable. Two of them are X-ray crystallography and NMR spectroscopy but in all cases the method usually requires vast amounts of pure protein. Therefore, bacterial cells such as *E. coli* are used to overexpress high amounts of recombinant proteins. After the expression, subsequent purification steps are necessary to receive the pure proteins. All used constructs in for protein expression are listed in the appemdix Table 20.

8.2.4. Unlabelled protein expression

For unlabelled proteins Luria-Bertani medium (LB) was used. For standard expression, *E. coli* BL21-CodonPlus (DE3)-RIL cells carrying the desired protein expression construct were inoculated in 50mL of LB with the respective antibiotics and grown over night at 37 °C. With this pre-culture, the 500 to 800 mL LB with the respective antibiotics are inoculated at a starting OD_{600} of 0.02 – 0.04. This culture is grown at 37 °C until it reaches

an OD_{600} of 0.7 – 0.8 and then shifted to 17°C. Once the desired expression temperature is reached the protein expression is induced by addition of IPTG in a concentration of 0.5 to 1 mM. After 14 – 16 hours the cells are harvest by centrifugation at 4000g for 15min at 17°C.

8.2.5. Isotopic labelling

NMR spectroscopy is a technique that requires the labelling of the proteins to be investigated with isotopes. The bioavailable isotopes such as $^{15}NH_4Cl$ as sole nitrogen source or $^{13}C_6$-Glucose as sole carbon source are added to the M9 minimal media for the protein expression. NMR studies on larger proteins (≥ 25 kDa) can require different label schematics and are grown in deuterium oxide in order to minimize hydrogen mediated T_2-relaxation. For HECT domains either the Met- [ε $^{13}CH_3$]- and the Ile-[δ1 $^{13}CH_3$]- or in special cases also Leu-[δ $^{13}CH_3$]-; Val-[γ $^{13}CH_3$]-; and Ala-[β $^{13}CH_3$]- were labelled. In those cases, the culture was inoculated with labelled amino acids like L-methionine-methyl-$^{1}H^{13}C$ or L-alanine-3-$^{2}D^{13}C$ or precursors like Ile: 2-Ketobutyric acid-4-^{13}C and Val-Leu: 2-Keto-3-methyl-^{13}C-butyric-4-^{13}C acid. For a minimal medium expression, a pre-culture was grown in LB overnight. The M9 media was prepared according to the experimental needs e.g. in deuterium oxide. The M9 media was then inoculated with in M9 resuspended pre-culture to an OD_{600}=0.4 and grown at 37 °C. When the culture reached an OD_{600} of around 0.8 the cells were either shifted to 20 °C in the case of ^{15}N and induced with IPTG or in case of Methyl labelling the desired precursors were added. After these cells reached again an OD_{600} of around 0.8 the cells were induced with IPTG and shifted to 25 °C. The cells were then grown around 12 to 16 hours and harvest by centrifugation at 4000g for 15min at 25°C.

8.2.6. Protein purification by affinity chromatography

To obtain sufficient amounts of pure protein for structural biophysical methods like X-ray crystallography or NMR spectroscopy the expressed proteins have to be purified. Depending on the need, different purification strategies are applied. One strategy is the purification of recombinant proteins with 6 to 8 histidines followed by a TEV cleavage site cloned to the N- or C- terminus. After the cells are harvest the cell pellet is lysed. Therefore, the pellet is resuspended in cold lysis buffer and the suspension is sonicated

3 times for 1 minute with an 40% amplitude. The suspension is centrifuged at 4 °C with 40.000 * g for 30 minutes. After this step, the supernatant is loaded onto a with lysis–buffer equilibrated Ni^{2+}-NTA-column. The His_6–tag forms a Histidine-Ni^{2+}-complex with the Ni^{2+}-NTA-beads of the column thus, the histidine-tag of the N- or C-terminus of the protein binds onto the Ni^{2+} -NTA-column. Through washing steps all the impurities are removed. In the finale step the protein is removed from the column by addition of 350 mM imidazole into the buffer. The Imidazole competes with the Histidine about the Ni^{2+}-Ion and displaces due to the high excess the His_6-tag protein. After SDS-PAGE analysis with Coomassie staining different strategies were chosen either to improve the purity of the sample here SEC was chosen or TEV-cleavage to remove the His_6-tag of the protein.

8.2.7. Dialysis and TEV protease cleavage

Each conducted experiment requires specific buffer conditions either to ensure proper separation of the purified protein or the experimental conditions. For example, ion exchange chromatography requires a low buffer conductivity (< 5 mS/cm), reverse Ni^{2+}-NTA-affinity chromatography requires an imidazole concentration below 5 mM. To remove the imidazole a buffer change by dialysis was performed and the sample thereby transferred into the required buffer conditions for the experiment.

The protein solution is filled into a semi-permeable membrane with a 5 kDa cut-off and placed into an appropriate volume of the buffer with the desired characteristics. This step takes place o/n at 4°C. Simultaneously, the expression tag can be removed by the protease from tobacco etch Virus (TEV). This protease recognizes the aa sequence ENLYFQ/G. All used expression constructs possessed the TEV protease recognition site between the C-terminus of the expression His_6-tag and the N-terminus of the protein. For TEV cleavage, 1 aliquot of TEV protease (1 mL, 0.5 mg/mL) was mixed into the dialysed tube which contained the protein solution.

8.2.8. Gel filtration chromatography

One method in protein purification besides affinity chromatography is the separation of proteins by gel filtration (GF) or size exclusion chromatography (SEC). Both methods are based on the separation of molecules according to their size. For this the GF or SEC column contains a porous polymeric matrix. Therefore, smaller proteins have a larger

volume to diffuse then big ones. Thus, large proteins migrate faster and therefore, elute at first in an elution profile. Hence, small and large proteins are separated from each other. The resolution of the separation depends on the column material. Two different columns from GE Healthcare were used S75 16/600 for proteins between 3 kDa and 70 kDa or S75 26/600 for proteins between 10 kDa and 600 kDa columns. For the separation of proteins, the column is equilibrated with an appropriate buffer e.g. NMR buffer for NMR measurements or assay buffer for ubiquitination assays and run on an NGC system (BioRad) or an ÄKTAprime plus (GE Healthcare). Absorptions was monitored at 280 nm and 215 nm to identify protein containing fractions. The purity of the protein containing fractions were analysed by SDS-PAGE and Coomassie staining.

8.2.9. Chemical induced disulfide formation

For studying the interaction between the HECT-domain and ubiquitin, disulfides between mutants of the HECT-domain were formed. Therefore, only the catalytic cysteine of the HECT domain remains and the C-terminal Gly of Ub was mutated to a cysteine.

A 4-fold excess of UbG76C with an N-terminal His-tag in comparison to the used HECT domain was loaded on a Ni-affinity chromatography column. The UbG76C was then fully reduced with 2 column volumes of disulfide buffer A containing fresh DTT. Then the immobilized UbG76C was flushed with disulfide 4 column volumes buffer B, important is here the different pH of the buffers and no DTT therefore the buffer B contains Ellman's reagent. The Ellman's reagent attacks the free thiol group of the Ub G76C and forms a 2-nitro-5-thiobenzoate-UbG76C (TNB). The side product of this reaction is 2-nitro-5-thiobenzoate (TNB) which has a yellow colour and is an indicator if the reaction was successful. The column was then washed with disulfide 2 column volumes buffer C which contains no DTT and is degassed and Argon purged. In the next step the formation between the HECT-domain and the 2-nitro-5-thiobenzoate-UbG76C is performed. Therefore, the DTT containing buffer of the HECT-domain of was exchanged using a PD-25 column. Therefore, 4 times less HECT domain in comparison to the used UbG76C was then loaded onto the column with the 2-nitro-5-thiobenzoate-UbG76C. The disulfide is then eluted with increasing imidazole concentrations in buffer D. Therefore, the imidazole concentration was evaluated stepwise e.g. 20mM ½ column volumes, 40mM ½ column volumes, 80mM ½ column volumes, 120mM ½ column volumes and 300mM ½

column volumes. In a final step, the HECT-Ub disulfides are purified by size exclusion chromatography (SEC). From each step, a sample was loaded on an SDS-PAGE with and without DTT in the loading Dye to validate the disulfide formation between the proteins. The composition of all used buffers is listed in the media and buffer section.

8.2.10. Labelling of ubiquitin with Fluorescein

To enable specific fluorescein labelling onto ubiquitin, an additional cysteine was added at the N-terminus in front of the first methionine of ubiquitin. This engineered ubiquitin* was stored in 50 mM Tris, pH 7.8, 150 mM NaCl, 1 mM DTT.

Before the fluorescein labelling the DTT was removed with 50 mM Tris, pH 7.8, 150 mM NaCl buffer by using a PD-10 column. In 100% DMSO a 4-times molar excess of 6-Iodoacetamidofluorescein (Thermo Scientific) in comparison to 0.5mM ubiquitin was dissolved and added to the ubiquitin. After 3 hours at RT all free fluorescein was removed from the reaction mixture with a second PD-10 and in this step also the buffer was exchanged to 50 mM Tris, pH 7.5, 150 mM NaCl, 1 mM DTT. As a final purification step, size exclusion chromatography was performed to yield the pure ubiquitin*. As a quality control from each step a sample was loaded onto an SDS-PAGE and checked for impurities by using fluorescence imaging and Coomassie G-250staining.

8.3. Functional assays

8.3.1. Ubiquitylation assays

The *in vitro* auto-ubiquitination assays help to analyse the function of an HECT-domain and validate the infuence of inserted mutations in the HECT-domain. The assays were performed in ubiquitination buffer containing 25 mM Tris, pH 7.5, 5 mM $MgCl_2$, 100 mM NaCl 0.2 mM DTT and 2.5 mM ATP. For the Huwe1 HECT reaction a temperature of 30°C and for the Smurf2 HECT reaction of 25°C were chosen. Each 20µl reaction contains the following purified enzymes 0.5 µM E1 (Ube1), 10 µM E2 (UbcH7), 3 µM E3 (Huwe1 HECT or Smurf2 HECT mutants) and 60 µM fluorescein labelled ubiquitin*. All reactions were stopped at indicated time points by addition of 10 µl 3xLaemmli buffer containing 0.5M DTT and 6 M urea. All samples were boiled for 10 minutes at 95°C and loaded according to the expected molecular weight of the reaction outcome either an 8%; 10%; 12% or

16% polyacrylamide gel for SDS-PAGE. The detection took place by fluorescence measurement at 488nm using an Amersham™ Imager 600 from GE Healthcare Life Science.

8.3.2. Thioester assays

With the thioester assay the thioester bond is confirmed that is formed between the Ubiquitin and the HECT-domain in the step of the ubiquitin transfer from the E2 to the E3. The *in vitro* thioester assays were performed in ubiquitination buffer containing 25 mM Tris, pH 7.5, 5 mM $MgCl_2$, 100 mM NaCl 0.2 mM DTT, 2.5 mM ATP. For the Huwe1 HECT reaction a temperature of 30°C and for Smurf2 HECT reaction at 22°C was chosen. Each of the 20µl reactions contains the following concentration of purified enzymes: 0.3 µM E1 (Ube1), 10 µM E2 (UbcH7), 3 µM E3 (Huwe1 HECT or Smurf2 HECT mutants). Fluorescein labeled ubiquitin* in a concentration of 60 µM was used. The reactions were stopped at indicated time points. 10µl Laemmli without DTT was added to the reaction mixture to stop the reaction and to preserve the formed thioester. To determine the amount of formed isopeptide bond 3xLaemmli buffer containing 0.5 M DTT was used. The added DTT in the 3xLaemmli loading buffer will cleave the formed thioester and leaving the isopeptide intact. The samples were loaded on a 12% polyacrylamide gel for SDS-PAGE. The detection was performed by fluorescence measurement at 488nm using an Amersham™ Typhoon 5 (GE Healthcare Life Science).

8.4. Structural biology and biophysics

8.4.1. NMR spectroscopy

All spectra were collected on an 800 MHz Bruker or 600 MHz Avance-III spectrometers. Both spectrometers are equipped with a room temperature probe heads. To setup the experiments the Bruker Topspin 2.1 software was used. To processes the spectrometer data NMRPipe [134] was used. Processed data was visualised with NMRview [135].

8.4.2. Sample labelling and preparation

The NMR samples where labelled according to their experimental need either with ^{15}N isotope or methyl-group specific. To label the protein at the amine position ^{15}N

ammonium chloride was added to the overexpression culture. To label the different methyl-groups of the protein, precursors of the amino acid biosynthesis pathway are added to the overexpression culture [96]. After the protein was purified the sample is filled into a 5 mm NMR tube (Norell) and 10% D_2O is added to a final volume of 400µl between 80 and 100 µM. For the methyl labelled proteins, a $^{1}H,^{13}C$-methyl TROSY (HSQC) NMR-spectra and for the ^{15}N-labelled proteins a $^{1}H,^{15}N$-TROSY NMR-spectra was recorded.

8.4.3. Methyl assignment procedure

To identify the residue of the protein to the corresponding peak on an NMR spectrum it is necessary to assign the peaks of the spectra. In this thesis an IM methyl labelled approach was used. Therefore, the single residues of Met or Ile were stepwise mutated to an NMR-invisible residue like Ala. By comparison of the Huwe1 C352 HECT with the mutant spectra e.g. Huwe1 M88A / C352 the residue number can be identified because the M88A will not give a peak in the mutant spectrum in comparison to the Huwe1 C352 HECT spectra. Therefore, all Met and Ile in the Huwe1 C352 HECT domain were step wisely replaced by mutagenesis. Dr. Silke Wiesner did the assignment of the Ala β-, Leu δ-and Val resonances by NOE NMR-spectroscopy

8.4.4. Chemical shift perturbation experiments and analysis

NMR titration is a powerful experiment in NMR-spectroscopy to study protein-ligand interaction. The basis of this experiment lies in the change of the unique chemical environment of a nucleus during an interaction. The change of the chemical environment leads to the chemical shift perturbation which can be observed by NMR-spectroscopy.

In this thesis methyl labelled mutants and wild type of the Huwe1 HECT domain were used to perform NMR titration experiments. For the NMR titration experiments unlabelled ubiquitin was added to the HECT domain in a defined molar ratio.

The observed CSP data were semi-quantitative analysis to map the interaction surface according to the strength of the CSP. Therefore, the average of the CSPs are used and calculated in ppm:

Equation 5:

$$CSP = \sqrt{\Delta\delta_{1H}{}^2 + \left(\frac{\Delta\delta_{13C}}{4}\right)^2}$$

In this equation $\Delta\delta_{1H}$ is the difference in proton chemical shift between the reference spectra and the spectra of another state e.g. a disulfide, mutation or titration point and $\Delta\delta_{13C}$ is the difference in carbon chemical shift. For analysis of NMR titration experiments, the CSPs between reference and 1:9 titration point were quantified. The chemical shifts of the respective peaks were extracted by Sparky [136]. By using of the equation 6 the CSPs were quantified and mapped colour coded onto structures HECT domains from the PDB using pymol.

8.4.5. Two-dimensional line shape fitting analysis to determine the K_d of a protein ligand interaction

Line shape fitting is a method to extract data about the chemical environment of the observed nucleus and the change of this over time. With the Matlab script TITAN two dimensional line shape fitting is performed [100]. TITAN simulates the spectra with the experimental parameters and fits this simulation on the experimental data.

In this thesis TITAN was used in $^{1}H,^{13}C$-CSP titration experiments for the N-lobe of then Huwe1 HECT domain to determine the K_D of non-covalent binding interaction of Ub (WT) with the UBS of the HECT domain.

TITAN was used according to instructions and online documentation (http://www.nmr-titan.com and https://bitbucket.org/cwaudby/titan/wiki/Home). The spectra were processed with an exponential window function and the errors are estimated with bootstrap analysis on 100 replicas. The shown line shape figures were also prepared with TITAN. To fit the K_D value of the Huwe1 HECT N-lobe the residues M53, I79, M84, M88, I110, I124, I230, I245, I250 and I262 were used. For the analysed residues the titration step with an excess of 9-fold Ub (1:9) was used to calculate the K_D value of the Huwe1 HECT N-lobe (**Figure A 13**).

8.4.6. PRE-experiments

In NMR-spectroscopy, paramagnetic relaxation enhancement (PRE) can be induced by linkage of a spin label to the protein. The induced PREs contain information about the domain orientation of the protein. In this thesis different mutants of the Huwe1 HECT

domain were linked to the spin label 4-maleimido-TEMPO. Before the labelling reaction the DTT in the buffer was removed using a PD-25 column. Thereafter, a 10-fold excess of 150mM stock solution 4-maleimido-TEMPO dissolved in 100% ethanol was added to 500µL protein (250µM) and incubated for 2h at room temperature. After the incubation time the unreacted spin label was removed by SEC. The fractions containing protein were pooled and concentrated. The influence of the nitroxide radical of the spin label to the protein was then measured by $^{1}H,^{13}C$-methyl TROSY (HMQC) NMR-spectroscopy. To obtain the reduced state of the spin label 1 mM ascorbate (5M stock solution 20mM NaP, pH 6.4, 150mM NaCl) as a final concentration was added to the sample. Through the comparison of the intensities of the cross peaks in the spectra of the diamagnetic state (I_{dia}), that is the reduced spin label, with the paramagnetic (I_{para}) state to the spin label the residues which are in close proximity of the spin label can be identified.

The intensities of the I_{dia} and I_{para} state of the PREs were extracted by using CARA (http://cara.nmr.ch/doku.php). The intensities ratios (I_{dia}/I_{para}) between the paramagnetic and the diamagnetic spectra were quantified, and mapped colour coded onto structures of HECT domains of the PDB using pymol.

Table 15: Constructs which were used for NMR experiments.

Construct / experiment	Buffer	Concentration	Spectra	Temp.
Huwe1 C352 HECT ~Ub I44A / G76C	NMR disulfide Buffer	80µM	^{1}H ^{13}C TROSY (HMQC)	303K
Huwe1 N113C / C352K HECT ~UbG76C	NMR disulfide Buffer	180µM	^{1}H ^{13}C TROSY (HMQC)	303K
Huwe1 N113C / C352 HECT ~UbG76C:UbG76C	NMR disulfide Buffer	100µM	^{1}H ^{13}C TROSY (HMQC)	303K
Huwe1 C352 HECT ~Ub K48C	NMR disulfide Buffer	65µM	^{1}H ^{13}C TROSY (HMQC)	303K
Smurf2 HECT C-lobe	Standard NMR Buffer pH 6.5	100µM	^{1}H,^{15}N-TROSY	298K
Smurf2 L710P HECT C-lobe	Standard NMR Buffer pH 6.5	100µM	^{1}H,^{15}N-TROSY	298K
Smurf2 A713P HECT C-lobe	Standard NMR Buffer pH 6.5	150µM	^{1}H,^{15}N-TROSY	298K
Huwe1 HECT C-lobe	Standard NMR Buffer pH 6.4	120µM	^{1}H,^{15}N-TROSY	303K
Huwe1 L346P HECT C-lobe	Standard NMR Buffer pH 6.4	200µM	^{1}H,^{15}N-TROSY	303K
Huwe1 A349P HECT C-lobe	Standard NMR Buffer pH 6.4	217µM	^{1}H,^{15}N-TROSY	303K
Huwe1 C352 HECT : Ub (WT)	Standard NMR Buffer pH 6.4	100µM	^{1}H,^{15}N-TROSY	303K
Huwe1 HECT N-lobe : Ub(WT)	Standard NMR Buffer pH 6.4	75µM	^{1}H ^{13}C TROSY (HMQC)	303K
Huwe1 C352 HECT	Standard NMR Buffer pH 6.4	100µM	^{1}H ^{13}C TROSY (HMQC)	303K
Huwe1 C352 HECT ~ Ub G76C : Ub (WT)	NMR disulfide Buffer	100µM	^{1}H ^{13}C TROSY (HMQC)	303K
Huwe1 HECT C-lobe	Standard NMR Buffer pH 6.4	100µM	^{1}H ^{13}C TROSY (HMQC)	303K
Huwe1 R9C / C352A HECT	Standard NMR Buffer pH 6.4	200µM	^{1}H ^{13}C TROSY (HMQC)	303K
Huwe1 R93C / C352A HECT	Standard NMR Buffer pH 6.4	100µM	^{1}H ^{13}C TROSY (HMQC)	303K
Huwe1 D271C / C352A HECT	Standard NMR Buffer pH 6.4	200µM	^{1}H ^{13}C TROSY (HMQC)	303K
Huwe1 C352 HECT .: Ub (WT)	Standard NMR Buffer pH 6.4	100µM	^{1}H ^{13}C TROSY (HMQC)	303K
Huwe1 C352A HECT	Standard NMR Buffer pH 6.4	510µM	^{1}H ^{13}C TROSY (HMQC)	303K
Huwe1 C352N HECT	Standard NMR Buffer pH 6.4	183µM	^{1}H ^{13}C TROSY (HMQC)	303K
Huwe1 C352K HECT : Ub (WT)	Standard NMR Buffer pH 6.4	100µM	^{1}H ^{13}C TROSY (HMQC)	303K
Huwe1 Y162A / C352 HECT : Ub (WT)	Standard NMR Buffer pH 6.4	100µM	^{1}H ^{13}C TROSY (HMQC)	303K
Huwe1 D98A / Y162A / C352 HECT : Ub (WT)	Standard NMR Buffer pH 6.4	100µM	^{1}H ^{13}C TROSY (HMQC)	303K

NMR disulfide Buffer: 20mM NaP, pH 6.4, 150mM NaCl, 10% D_2O, degassed; Argon purged, Standard NMR Buffer: 20mM NaP, 150mM NaCl, 1mM DTT, 10% D_2O and Temprature (Temp.) in kelvin.

8.4.7. Protein crystallization

In order to use X-ray crystallography, the soluble protein has to form a crystalline lattice. This can be accomplished through a slow supersaturation of a protein solution. The supersaturation state is generated through the addition of mild precipitants like salts or polymers and the manipulation of different parameters e.g. temperature, ionic strength and the pH [106]. In the process of protein crystallization, the water is withdrawn out of the protein solution by the precipitate agents leading to a slow increase of the protein concentration. This process is called salting-in. Metal ions which coordinate with residues of the protein or alcohols lowering the permittivity of the protein water shell are added to the precipitate solution. The added precipitates help the proteins to arrangement into

a crystal structure. The conditions in which a crystalline lattice is formed are different for every protein construct.

The vapor diffusion method is developed to get to the supersaturated state overtime. The system which was used is the siting drop process. Here, the protein solution is mixed in a ration of 1:1 with the precipitant mix. The system contains a reservoir part containing the precipitant mix. The protein mix is detached from the precipitant reservoir. The system is then sealed leading to a two liquid phase system which is connected by a gas phase. To form an equilibrium in the system water diffusion from the protein mix to the precipitant reservoir takes place leading to a slow increase of the protein concentration in the protein mix. Under the right conditions and parameters during this process crystallization of the protein occurs.

In this thesis all protein constructs where mixed in a ratio of 0.3µl:0.3µl with the precipitant solution. The crystallization screening was performed in 96-well plates (96-3 low profile INTELLI-PLATE®, Art Robbins Instruments) with the sitting drop method. For screening, commercially available precipitant solutions were used. The crystallization process was observed for up to 30 days at 20 °C. The grown crystals where then fished and cryoprotected with 25% glycerol to avoid ice formation during the shock freezing of the crystal. After this the crystals were measured at the Swiss Light Source (SLS) of the Paul Scherrer Institute.

8.4.8. Data acquisition

All diffraction data were collected at the Swiss Light Source (SLS) of the Paul Scherrer Institute at the PXII beamline. For detection a PILATUS 6M pixel detector was used and a wavelength of λ=1 Å. The crystals were cryostream protected at 100K.

8.4.9. Data processing

The obtained data has to be processed and indexed. This is accomplished by XDS [137]. resulting in the Miller indices h, k and l. Here, each spot in the diffraction pattern is assigned to its coordinates in the reciprocal space. In the next step the space group has to be determined. Therefore, all possible diffraction patterns and their corresponding space groups are listed according to their score and the space group with the highest score is chosen. Thereafter, the intensity of the single reflection spot is integrated. In the last step

the data are scaled. Here, all the data are merged into one file and the R_{free}- set of reflections is generated [138].
All obtained data was processed using XDS [137]. The space group was calculated by pointless [139].

8.4.10. Phase determination by molecular replacement

The obtained X-ray data contain only the intensities and not the phase information. Without the phase information the electron density map cannot be transferred from the reciprocal into the real space. In order to obtain the phase information molecular replacement was used in this thesis. Here, homologue structures of the HECT domain and Ub were available in the PDB database was used as a search model. The search model was prepared by superimposing of the PDB structure 4bbn from Nedd4 and PDB structure 3h1d from Huwe1 HECT or PDB structure 1zvd from Smurf2 HECT. The Ub^D and non-covalent Ub from the PDB structure 4bbn then added to the PDB structure 3h1d and 1zvd. For C-lobe~Ub^D of Smurf2 and Huwe1 the N-lobe with the non-covalent Ub was removed and only the C-lobe and the Ub^D was used for the molecular replacement and phasing. In the case of the Huwe1 N113C / C352K : UbG76C complex the Ub^D of the before described search model of 4bbn and 3h1d was removed and the used for the molecular replacement and phasing. For all structures PHASER which uses the log-likelihood methods was used [140].

8.4.11. Structural refinement

During structural refinement the model and the phases are improved. Here, the model is built into the density map leading to improvement of the phase and subsequent to a better density map. This cycle is monitored by the R-factor (R_{work}):

Equation 6:

$$R = \frac{\sum ||F_{obs}| - |F_{calc}||}{\sum |F_{obs}|}$$

The R-factor is a way to validate the data quality. Therefore, the observed structure factor F_{obs} is compared with the back-calculated structure factor F_{calc} of the used model. During the refinement steps the R-factor has to decline. This means the model fits better to the data. To avoid overfitting of the model to the data 5% of the observed reflexes are not

included in the refinement. Those reflections are considered for the calculation of the R_{free}-factor, which is another indicator for the model quality. The R_{free}-factor has also to decrease during refinement. Both factors are indicators of the model quality.

In this thesis after the initial model was found with PHASER. the refinement was done in alternating circles of phase improvement with Phenix [141] using anisotropic B-factors and model building in Coot [142]. All the shown figures of the structures were prepared in PyMOL (www.pymol.org).All finale refinement statistics for the solved structures and the crystallization conditions are provided in Table 16, Table 17, Table 18 and Table 19.

Table 16: Buffer and crystallization conditions of the X-ray constructs.

Construct	**Buffer**	**Crystallization Condition**	**Protein Concentration**
Huwe1 C352 HECT C-lobe~Ub G76C	25mM HEPES 150mM NaCl pH 6.4	0.8 $ZnSO_4$, 1M Sodium-Acetat pH 4	22mg/ml
Smurf2 C716 HECT C-lobe~Ub G76C	50mM Tris 150mM NaCl pH 7.4 5% Glycerol	1.36M Tri-Sodium citrat pH 6.5, 15% (v/v) Glycerol	15mg/ml
Huwe1 N113C / C352K : UbG76C	25mM HEPES 150mM NaCl pH 6.5	0.1M HEPES pH: 6.5, 10% (w/v) PEG 6000	12mg/ml

Table 17: Statistics of X-ray data collection and model refinement for the Huwe1 HECT N113 / C352K : Ub G76C complex[1]

Data collection:	
Resolution (Å)	44.33-2.704 (2.801-2.704)[2]
Completeness (%)	96.30 (99.39)
No. of unique reflections	19289 (1960)
Redundancy	13.1 (12.4)
CC1/2* (%)	1 (0.722)
$I/\sigma I$	18.41 (1.70)
Wilson B-Factor (Å^2)	71.69
FreeR (% of reflections)	5
Crystal properties:	
Space group	P 21 21 21
Unit cell dimensions:	
a, b, c (Å)	63.51 66.72 166.02
α, β, γ (°)	90 90 90
Solvent content (%)	64.33
Refinement:	
Resolution (Å)	44.33-2.704 (2.801-2.704)
R_{work} (%) / R_{free} (%)	26.77 / 32.16
R.m.s.d. bond lengths (Å)	0.001
R.m.s.d. bond angles (°)	0.35
B-Factor (Å^2) (Overall)	106.33
No. of atoms (Total)	4200
Ramachandran (%) (Favoured / allowed / outliers)	95.31 / 4.46 / 0.22

[1]Number of crystals equals one.

[2]Values in parentheses are for highest-resolution shell.

X-tal condition : 0.1M HEPES pH: 6.5, 10% (w/v) PEG 6000

Table 18: Statistics of X-ray data collection and model refinement for the Smurf2 C-lobe~Ub G76C complex[1]

Data collection:	
Resolution (Å)	19.57 – 2.5 (2.589 – 2.5)[2]
Completeness (%)	98.28 (97.76)
No. of unique reflections	14674 (1484)
Redundancy	3.5 (3.6)
CC1/2* (%)	0.98 (0.656)
$I/\sigma I$	6.31 (1.91)
Wilson B-Factor (Å^2)	28.93
FreeR (% of reflections)	5
Crystal properties:	
Space group	P 1
Unit cell dimensions:	
a, b, c (Å)	38.63 45.95 70.46
α, β, γ (°)	108.921 94.43 106.753
Solvent content (%)	42.92
Refinement:	
Resolution (Å)	19.57 – 2.5 (2.589 – 2.5)
R_{work} (%) / R_{free} (%)	18.73 / 23.89
R.m.s.d. bond lengths (Å)	0.002
R.m.s.d. bond angles (°)	0.57
B-Factor (Å^2) (Overall)	39.18
Protein / Ligands / Solvent	39.37 / 40.48 / 31.99
No. of atoms (Total)	3204
Protein / Ligands / solvent	3108 / 12 / 84
Ramachandran (%) (Favoured / allowed / outliers)	99.20 / 0.80 / 0

[1]Number of crystals equals one.

[2]Values in parentheses are for highest-resolution shell.

X-tal condition: 1.36M Tri-Sodium citrat pH 6.5, 15% (v/v) Glycerol

Table 19: Statistics of X-ray data collection and model refinement for the Huwe1 HECT C-lobe~Ub G76C complex[1]

Data collection:	
Resolution (Å)	41.12 - 2.906 (3.01 - 2.906)[2]
Completeness (%)	99.64 (97.28)
No. of unique reflections	114772 (10657)
Redundancy	16.7 (16.5)
CC1/2* (%)	0.999 (0.857)
$I/\sigma I$	21.43 (3.09)
Wilson B-Factor (Å^2)	67.16
FreeR (% of reflections)	5
Crystal properties:	
Space group	P 43 21 2
Unit cell dimensions:	
a, b, c (Å)	82.234 82.234 85.852
α, β, γ (°)	90 90 90
Solvent content (%)	59.06
Refinement:	
Resolution (Å)	41.12 - 2.906 (3.01 - 2.906)[2]
R_{work} (%) / R_{free} (%)	22.96 / 26.61
R.m.s.d. bond lengths (Å)	0.002
R.m.s.d. bond angles (°)	0.46
B-Factor (Å^2) (Overall)	60.65
Protein / Ligands / Solvent	60.51 / 80.45 / 40.53
No. of atoms (Total)	1522
Protein / Ligands / solvent	1501 / 16 / 5
Ramachandran (%) (Favoured / allowed / outliers)	94.12 / 4.81 / 1.07

[1]Number of crystals equals one.

[2]Values in parentheses are for highest-resolution shell.

X-tal condition: 0.8 $ZnSO_4$, 1M Sodium-Acetat pH 4

8.4.12. Iterative-build OMIT map

The crystallographic phases are calculated during the refinement from the building model. This is done in cycles where the previously used model is used for the next refinement step and therefore phase calculation. However, during this process e.g. incorrectly placed atoms can lead to model bias. An effective way to obtain, validate and remove this model bias is the iterative-build OMIT maps [116]. Here, model building, density modifications and refinements are carried out by omit parts of the model. To this end, an OMIT region and map is generated which is bias free. All generated OMIT maps and regions can be combined leading to a bias free overall OMIT map.

In this thesis the iterative-build OMIT map was used on the solved crystal structures to validate the disulfide bond of the HECT Ub complex.

9. Appendix

9.1. Huwe1 C352 HECT domain disulfides ^{1}H ^{13}C-methyl TROSY spectra

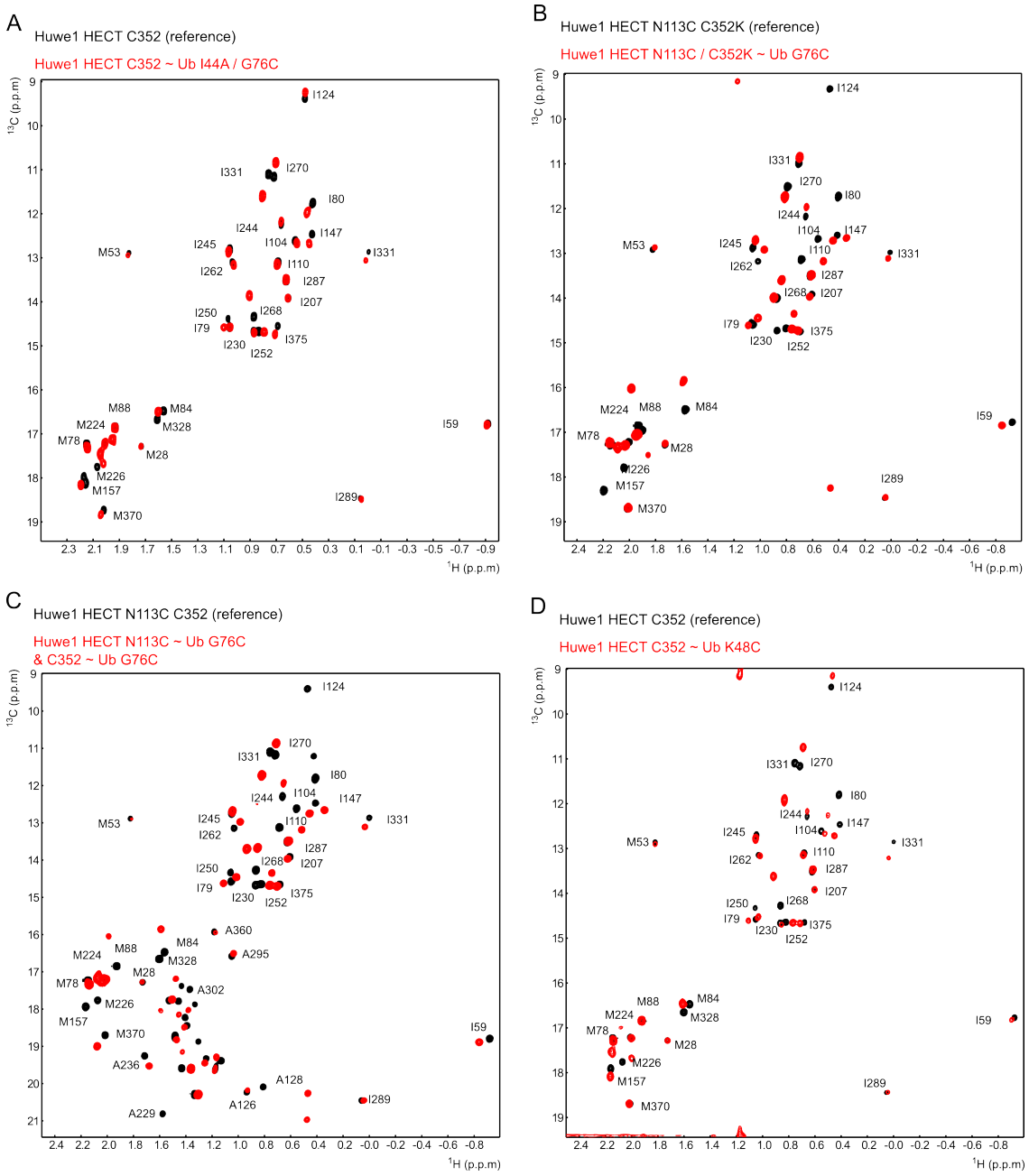

Figure A 1: Complete spectra of the ^{1}H ^{13}C-methyl labelled Huwe1 HECT domain disulfides. (A) Overlay of the ^{1}H ^{13}C-methyl TROSY spectra of the Huwe1 C352 HECT domain (black) and the Huwe1 C352 HECT ~ Ub I44A / G76C disulfide (red) that represents the thioester state during Ub transfer. **(B)** as in **(A)** but with ^{1}H ^{13}C-methyl IM labelled Huwe1 N113C / C352K HECT domain **(C)** as in **(A)** but with ^{1}H,^{13}C-methyl IMA labelled HECT domain from Huwe1 N113C / C352 domain. **(D)** as in **(A)** but with ^{1}H,^{13}C-methyl IM labelled HECT domain from Huwe1 C352 domain ~ UbK48C.

9.2. Superimpose of Smurf2 C-lobe ~UbG76C

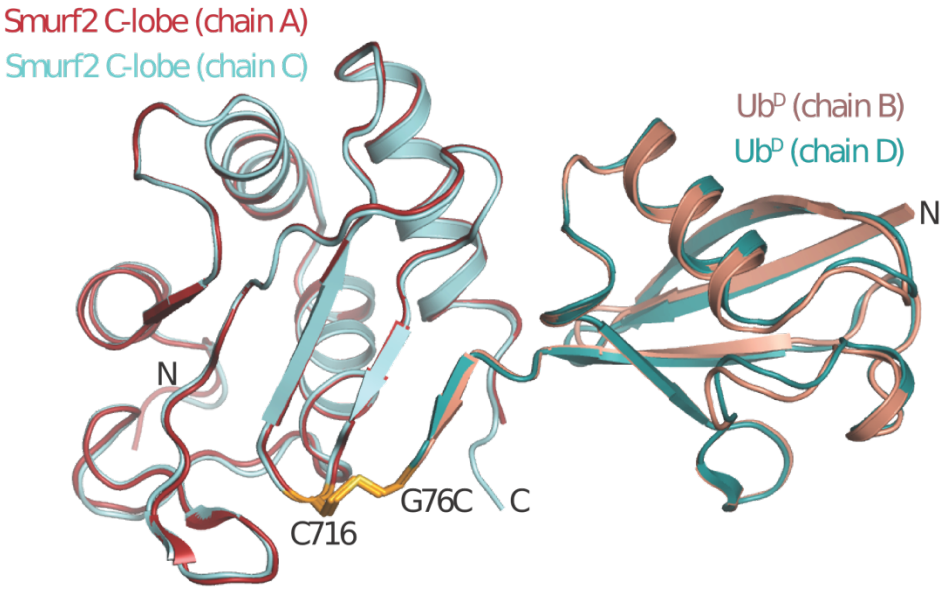

Figure A 2: Structure overlay of the two copies of Smurf2 C-lobe ~UbG76C form the asymmetric unit. The complex is shown as ribbon representation. The disulfide linkage is highlighted as stick and shown in orange.

9.2. Huwe1 HECT domain (WT) $^{1}H,^{15}N$-TROSY NMR titration experiments

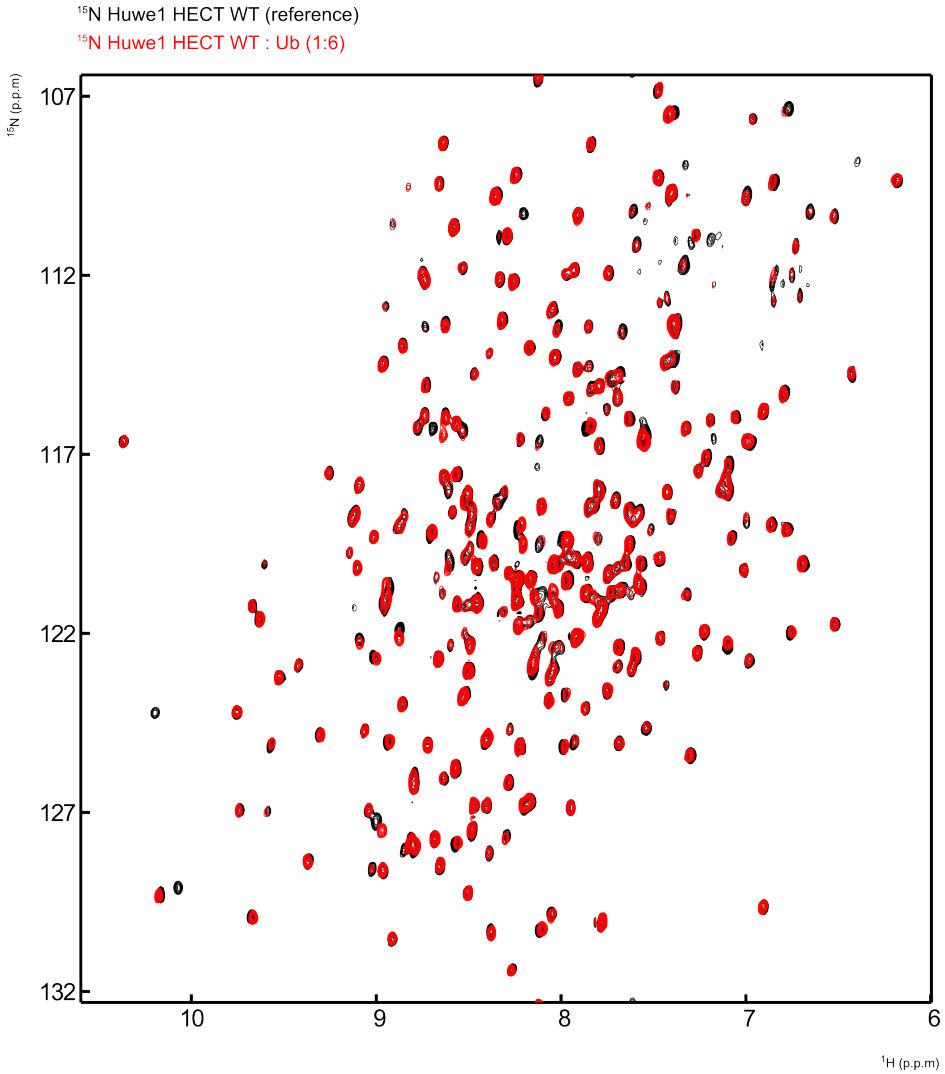

Figure A 3: NMR titration experiments with ^{15}N-labeled Huwe1 HECT WT domains and Ub. Overlay the complete $^{1}H,^{15}N$-TROSY spectra of the HECT domains in the absence (black) and presence of a 6-fold stoichiometric excess (red) of Ub. The spectrum was recorded by Timo. Strohäker.

9.3 Huwe1 C352 HECT domain $^{1}H,^{15}N$-TROSY NMR titration experiments

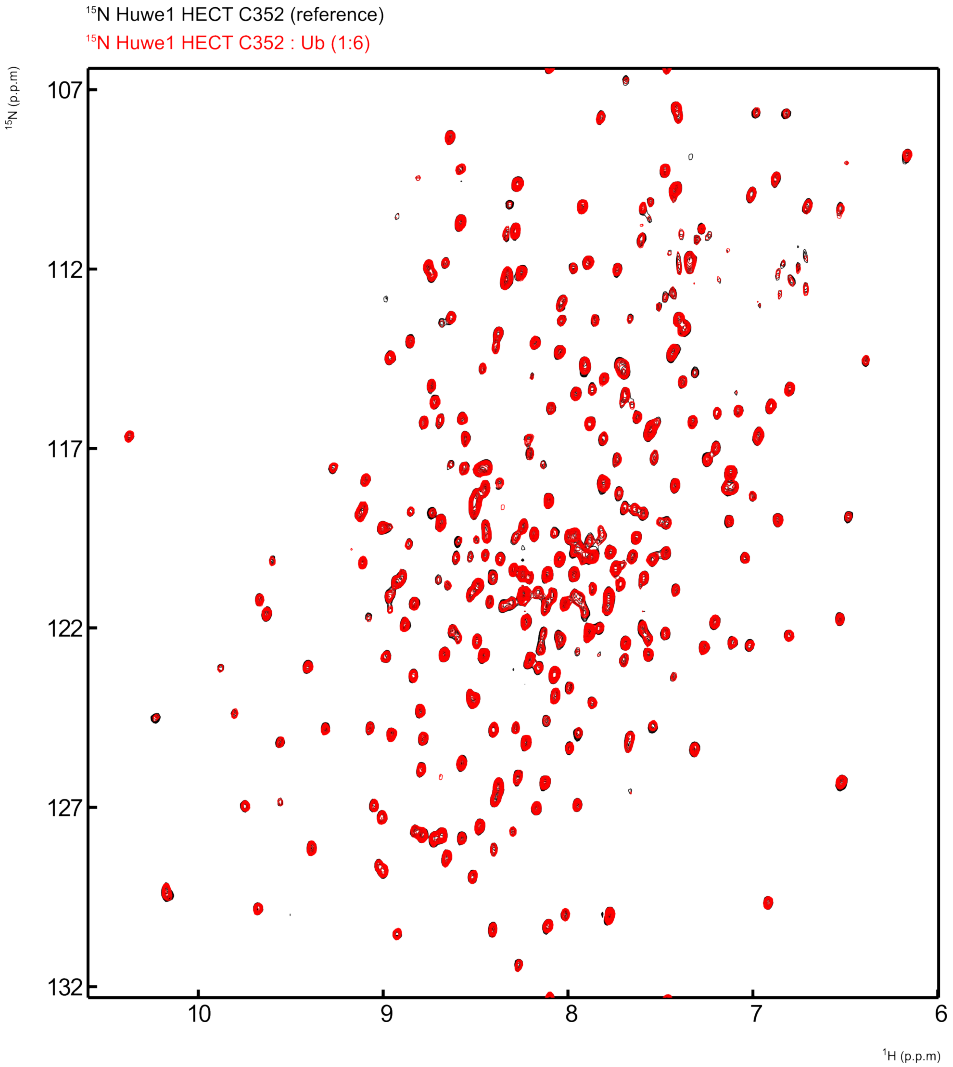

Figure A 4: NMR titration experiments with ^{15}N-labeled Huwe1 HECT C352 domains and Ub. Overlay the complete $^{1}H,^{15}N$-TROSY spectra of the HECT domains in the absence (black) and presence of a 6-fold stoichiometric excess (red) of Ub.

9.4. Smurf2 (WT) HECT domain $^{1}H,^{15}N$-TROSY NMR titration experiments

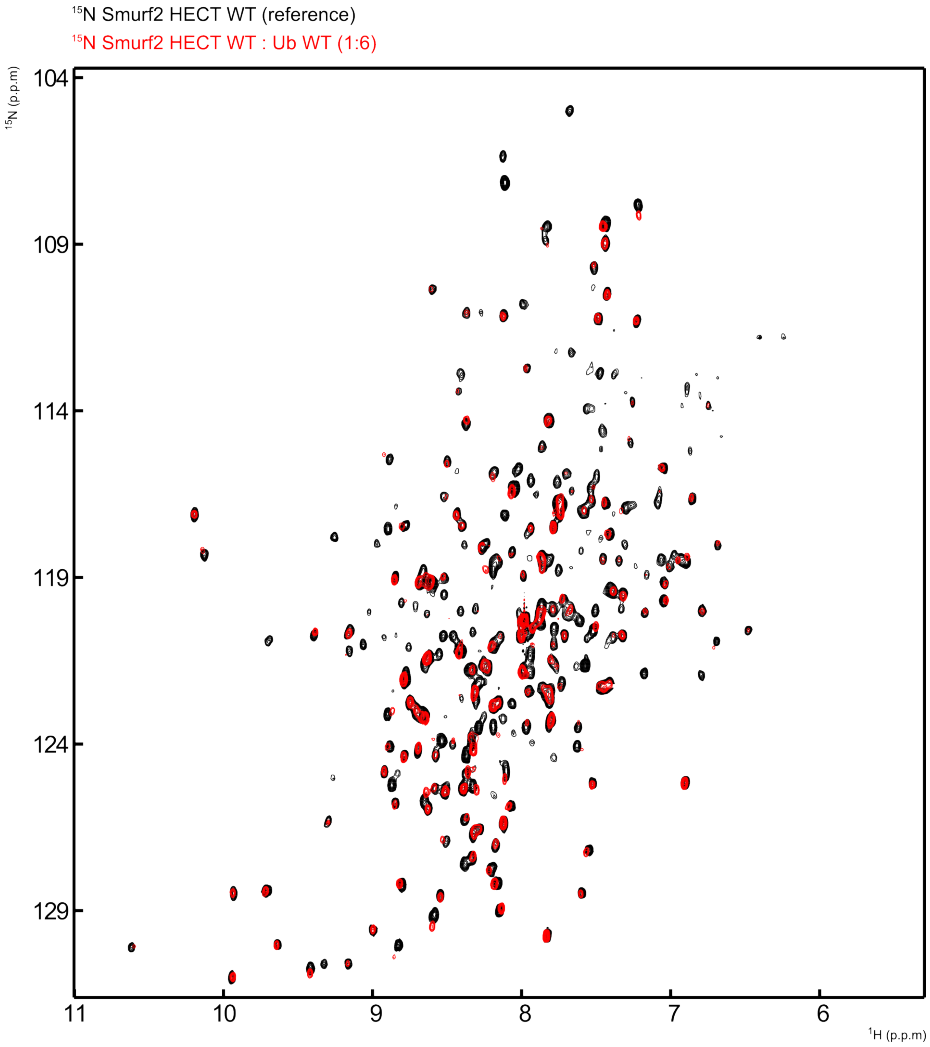

Figure A 5: NMR titration experiments with ^{15}N-labeled Smurf2 HECT WT domains and Ub. Overlay the complete $^{1}H,^{15}N$-TROSY spectra of the HECT domains in the absence (black) and presence of a 6-fold stoichiometric excess (red) of Ub. The spectrum was recorded by Dr. Silke Wiesner.

9.4. Huwe1 N-lobe ^{1}H ^{13}C-methyl TROSY NMR titration experiments

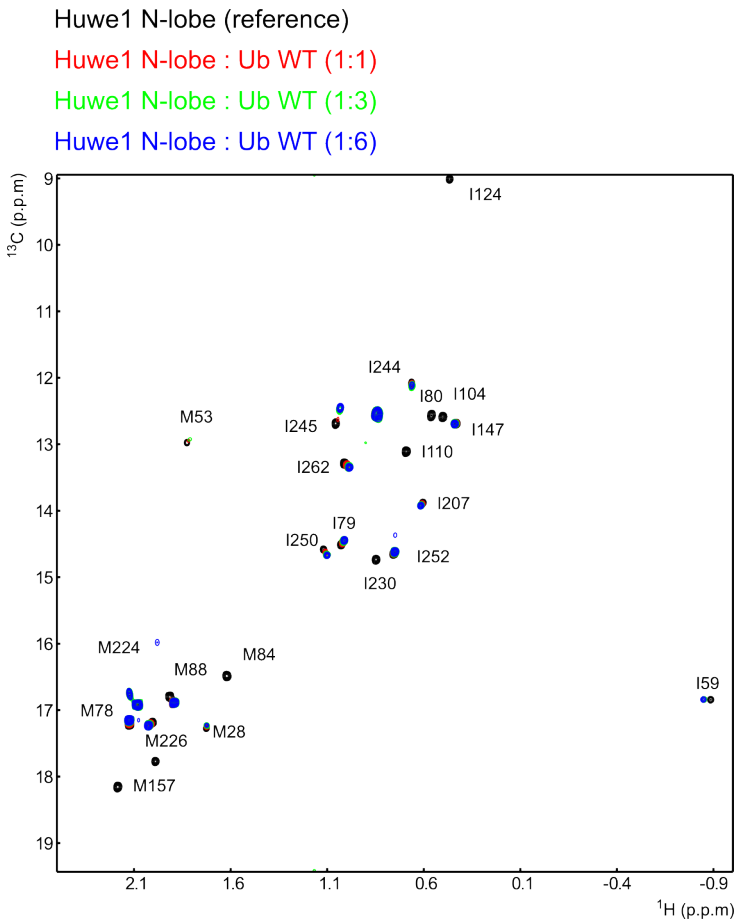

Figure A 6: NMR titration experiments with IM-labelled Huwe1 HECT N-lobe and Ub. Overlay the complete ^{1}H ^{13}C-methyl TROSY spectra of the N-lobe in the absence (black) and presence of an increasing stoichiometric amount of Ub as indicated.

9.5. Huwe1 C532 HECT ~Ub G76C and Ub ^{1}H ^{13}C-methyl TROSY NMR titration experiments

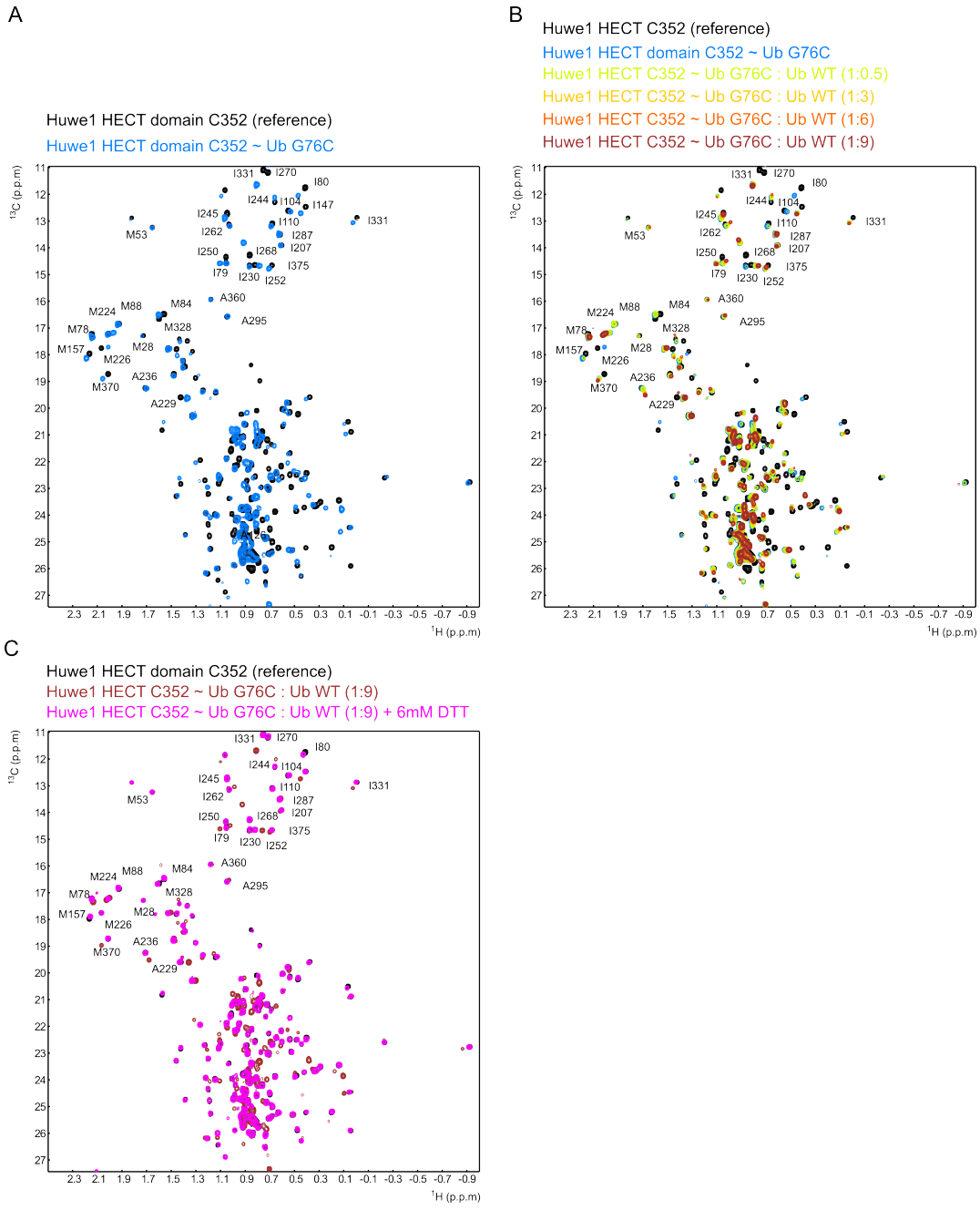

Figure A 7: NMR titration experiments with IMVLA-labelled Huwe1 C 352 HECT ~Ub G76C and Ub. (A) Complete spectra of the ^{1}H, ^{13}C-methyl TROSY (HSQC) spectra of IMVLA labelled Huwe1 C352 HECT domain (black) and Huwe1 HECT C352 ~ Ub G76C disulfide (cyan). **(B)** NMR titration experiments with ^{1}H,^{13}C-methyl IMVLA labelled Huwe1 C352 HECT as indicated. Complete spectra n of the ^{1}H ^{13}C-methyl TROSY (HSQC) spectra of Huwe1 C352 HECT (black), the HUWE1 HECT C352 ~ Ub G76C disulfide (cyan) and increasing stoichiometric amounts of Ub as indicated. **(C)** Complete spectra of the ^{1}H ^{13}C-methyl TROSY (HSQC) spectra of IMVLA labelled Huwe1 C1 HECT (black), the HUWE1 HECT C352 ~ Ub G76C disulfide at a 9-fold stoichiometric excess of Ub (firebrick) and the HUWE1 HECT C352 ~ Ub G76C disulfide at a 9-fold stoichiometric excess of Ub after addition of 6mM DTT (magenta).

9.6. Paramagnetic relaxation enhancement (PRE) experiments with Huwe1 HECT mutants.

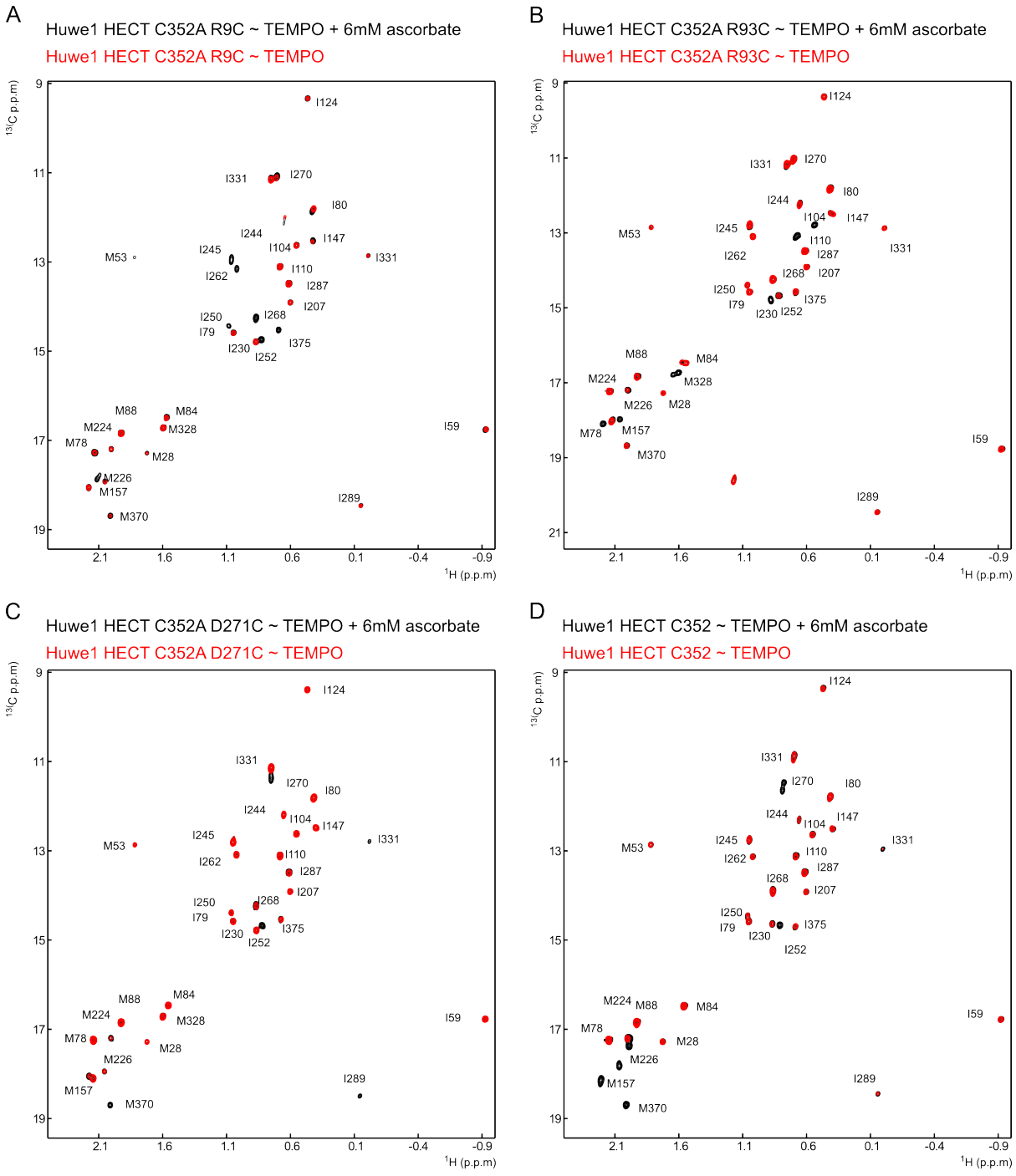

Figure A 8: Paramagnetic relaxation enhancement (PRE) experiments to probe the conformation change of the Huwe1 HECT domain. NMR PRE experiments with ^{1}H,^{13}C-methyl IM labelled Huwe1 HECT mutations R9C, R93C, D271C and C352 containing a sole cysteine residue for spin label attachment as indicated. Overlays of the complete spectra of the ^{1}H,^{13}C-methyl TROSY (HSQC) spectra of Huwe1 HECT mutant as indicated with reduced spin label (black) and presence of the non-reduced spin label (red). **(A)** Huwe1 R9C/C352A HECT domain, **(B)** R93C/C352A HECT domain, **(C)** D271C/C352A HECT domain, and **(D)** C352 only HECT domain.

9.7. ^{1}H ^{13}C-methyl TROSY NMR spectra of the Huwe1 C352 HECT and the isolated C- and N-lobe of Huwe1.

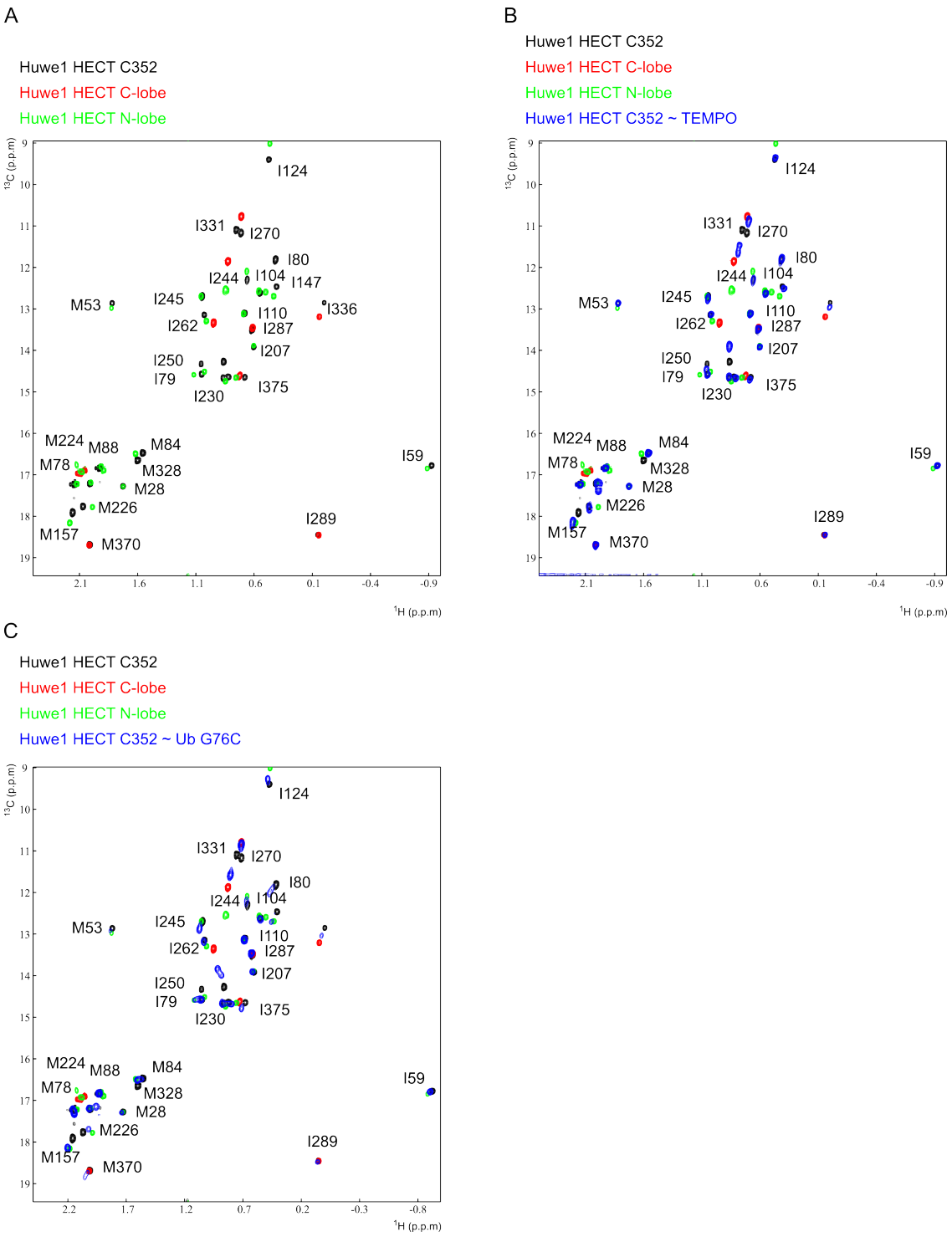

Figure A 9: **The isolated C- and N-lobe of Huwe1 HECT show similar chemical shift perturbations during the thioester formation. (A)** Overlay of the complete region of the ^{1}H,^{13}C-methyl TROSY (HSQC) spectra of Huwe1 C352 HECT domain (black) and the isolated C-lobe (red) and N-lobe (green). **(B)** as **(A)**, but with the spin labelled Huwe1 C352 HECT domain (blue). **(C)** as **(A)**, but with the Huwe1 C352 HECT domain ~ UbG76C (blue).

9.8. Spectra of Huwe1 C352 HECT ~UbG76C and different mutation of the catalytic cysteine in the Huwe1 HECT domain.

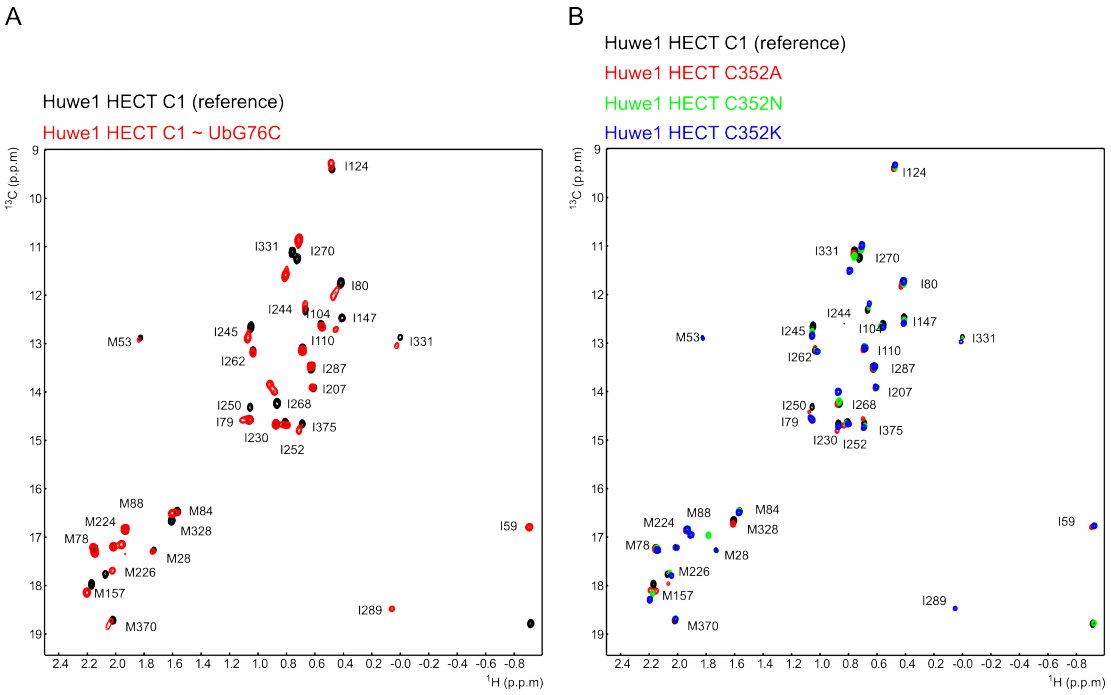

Figure A 10: Mutation of the catalytic cysteine induce conformational changes in the Huwe1 HECT domain that are similar to the Huwe1 HECT C352 ~ Ub G76C disulfide. (A) Overlay of the complete region of the ^{1}H,^{13}C-methyl TROSY (HSQC) spectra of Huwe1 C352 HECT domain (black) and the Huwe1 HECT C352 ~ Ub G76C disulfide (red). **(B)** as **(A)** but with different mutations of C352 of the Huwe1 HECT domain (C352A, red), (C352N, green), (C352K, blue).

9.9. Huwe1 C352K HECT NMR titration experiments

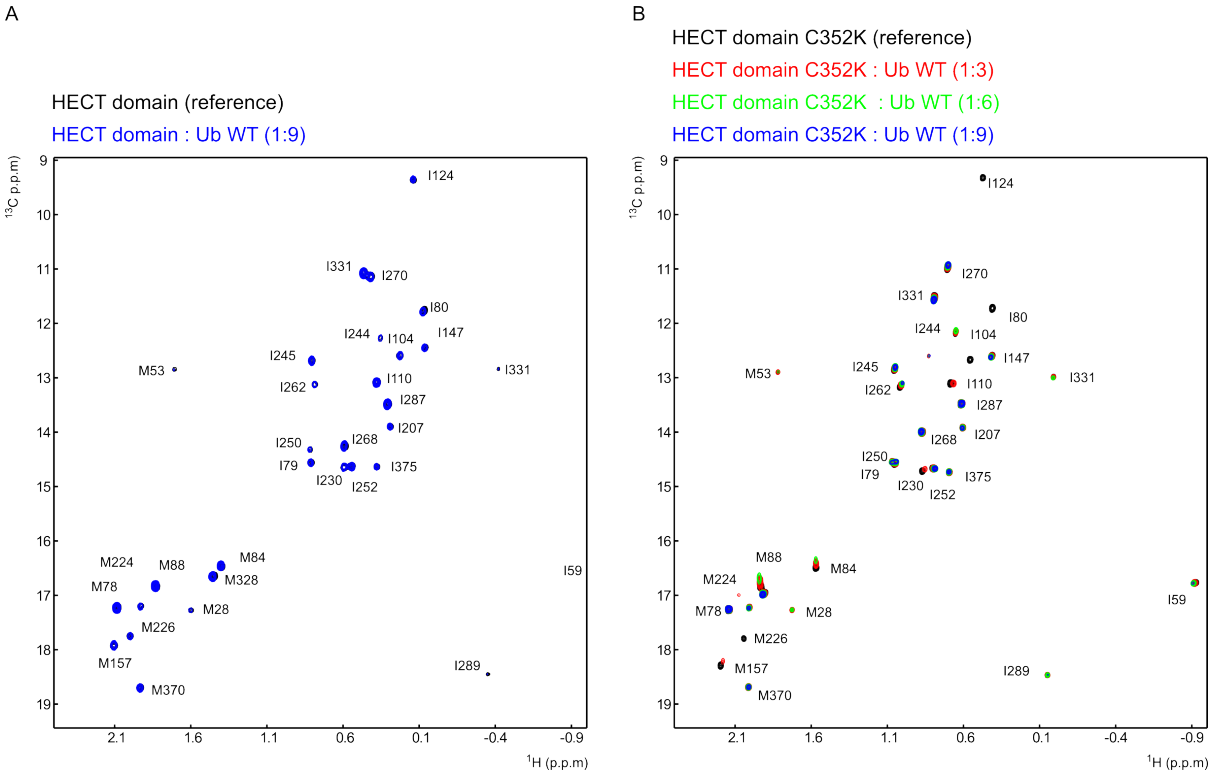

Figure A 11: The mutations of the Huwe1 HECT mimic the conformational change that occurs upon thioester formation and are able to bind Ub in a non-covalent manner. **(A)** Overlay of the complete region of the $^{1}H,^{13}C$-methyl TROSY (HSQC) spectra of the Huwe1 C352 HECT domain in the absence (black) and presence of increasing stoichiometric amount of monomeric Ub as indicated. **(B)** As **(A)**, but for the C352K mutant of Huwe1 HECT.

9.10. NMR titration experiments with mutations of the Huwe1 HECT in the N-lobe

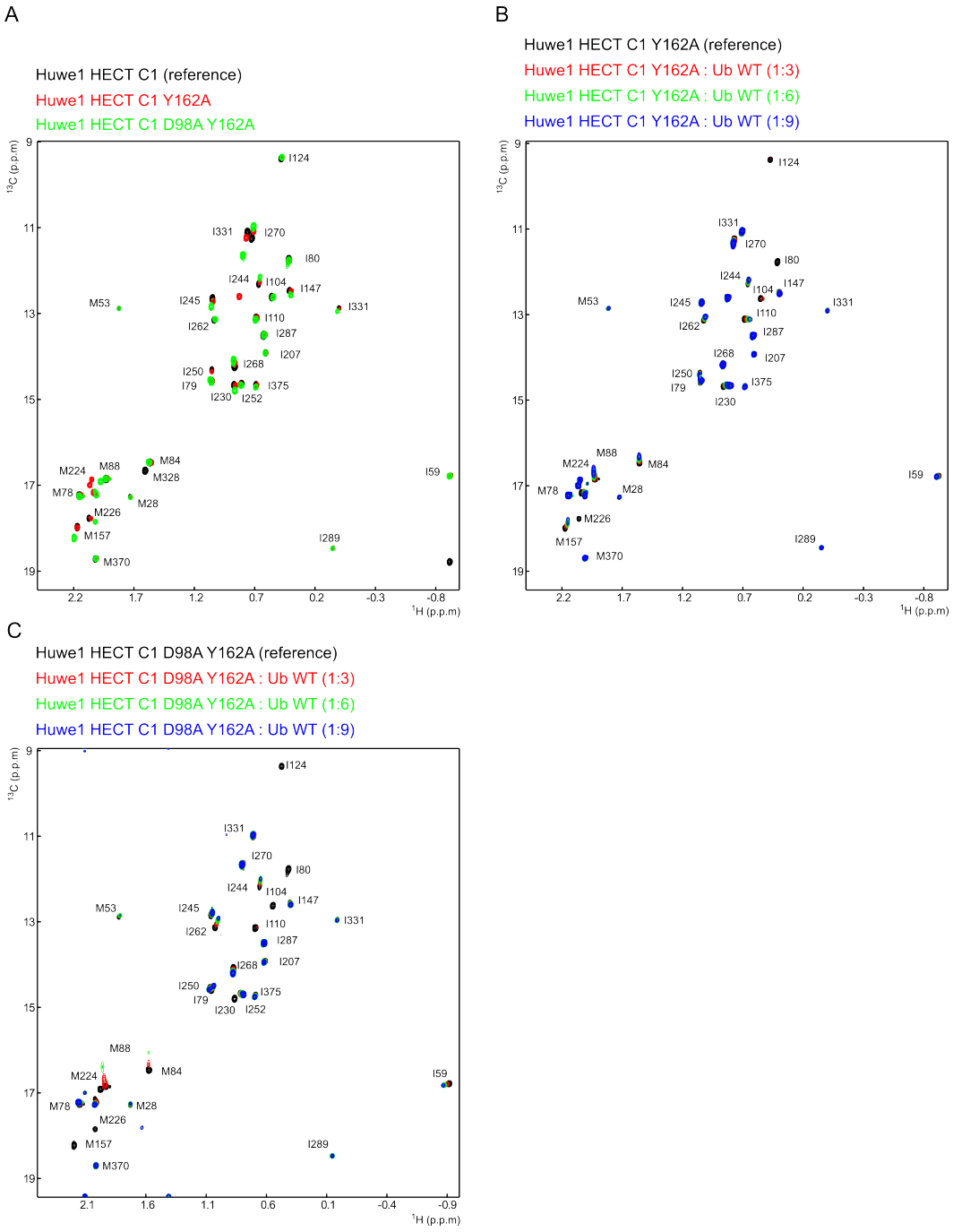

Figure A 12: **Titration experiments with Huwe1 HECT mutants in the N-lobe and Ub. (A)** Overview of complete region of the $^{1}H,^{13}C$-methyl TROSY (HSQC) spectra of the $^{1}H,^{13}C$-methyl IM labelled Huwe1 C352 HECT domain (black) and the Huwe1 HECT domain mutations Y162A / C352 (red) and D98A / Y162A / C352 (green). **(B)** as **(A)**, Overview of complete spectra of the Huwe1 HECT Y162A / C352 domain in presence of increasing stoichiometric amount of Ub as indicated. **(C)** as in **(A)**, Overview of complete spectra of the Huwe1 HECT D98A / Y162A / C352 domain in presence of increasing stoichiometric amount of Ub as indicated

9.11. Line shape fitting analysis of Huwe1 HECT N-lobe

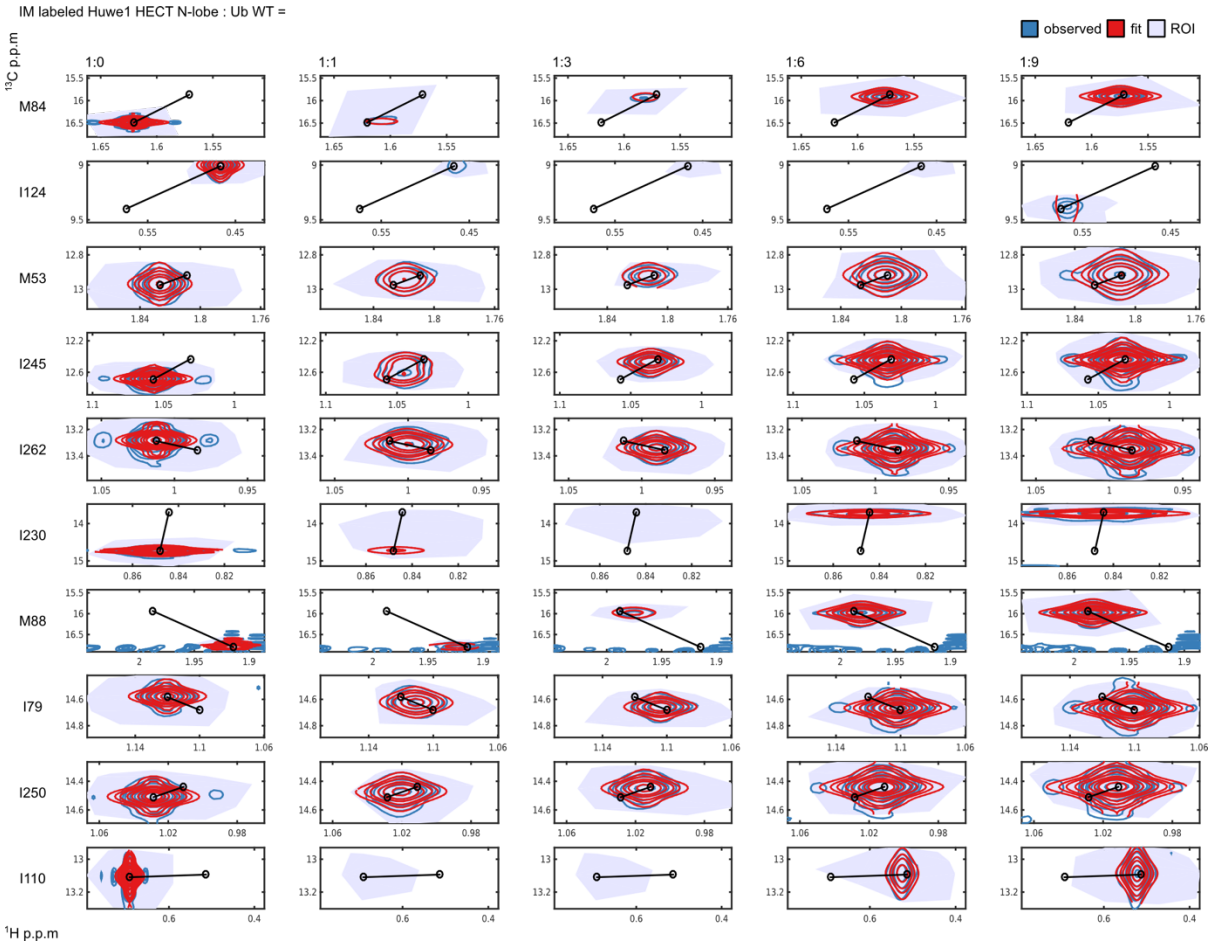

Figure A 13: Line shape fitting analysis of the Huwe1 HECT N-lobe interaction with the Ubiquitin. Contour plots of $^{1}H,^{13}C$-HSQC spectra of each cross peak used in TITAN line shape fitting analysis [100] at each titration point are shown. In blue cross peaks whereas fits are shown in red. Black lines indicate the course of the titration between the reference point and an estimated saturation point of the fit CSPs. The grey area around the cross peaks indicates the region of interest selected to fit the data in TITAN. Titration points are indicated above each column. Plots were generated by TITAN.

9.12. Plasmids

Table 20: Submitted plasmids into the local database related to this thesis. Plasmids listed with the database number, protein name, domain, mutation, vector and depositor. The C352 refers to the Huwe1 HECT domain which contain only the catalytic cysteine in the C-lobe of Huwe1 HECT.

Database entry	Protein	Domain	Mutation	Vector	Depositor
393	hHuwe1	HECT	C107I C134A C192N C219A C349A C375N	pET M11	K.Hyz
394	hHuwe1	HECT	C107I C134A C192N C219A C349A C375N R9C	pET M11	K.Hyz
397	hHuwe1	HECT	C107I C134A C192N C219A C349A C375N E83C	pET M11	K.Hyz
398	hHuwe1	HECT	C107I C134A C192N C219A C349A C375N R93C	pET M11	K.Hyz
399	hHuwe1	HECT	C107I C134A C192N C219A C349A C375N S159C	pET M11	K.Hyz
414	hHuwe1	N-lobe	WT	pET M11	K.Hyz
586	hHuwe1	N-lobe	C107I+C134A+C192N+C219A	pET M11	T.Strohäker
587	hHuwe1	C-lobe	C352	pET M11	T.Strohäker
594	hUbiquitin	full length	G76C	pET M11	T.Strohäker
719	hHuwe1	HECT	M153V	pET M11	M.Jäckl
720	hHuwe1	HECT sub N1	C107I	pET M11	M.Jäckl
721	hHuwe1	HECT sub N1	C107I C134A	pET M11	M.Jäckl
722	hUbiquitin	full length	I44A G76C	pET M11	M.Jäckl
819	hHuwe1	HECT	M0V C352	pET M11	M.Jäckl
820	hHuwe1	HECT	M0V M84V C352	pET M11	M.Jäckl
821	hHuwe1	HECT	M0V M88V C352	pET M11	M.Jäckl
822	hHuwe1	HECT	M0V I104L C352	pET M11	M.Jäckl
823	hHuwe1	HECT	M0V M157V C352	pET M11	M.Jäckl
824	hHuwe1	HECT	M0V I230V C352	pET M11	M.Jäckl
825	hHuwe1	HECT	M0V M224V C352	pET M11	M.Jäckl
826	hHuwe1	HECT	M0V M328V C352	pET M11	M.Jäckl
827	hHuwe1	HECT	M0V I331V C352	pET M11	M.Jäckl
828	hHuwe1	HECT	M0V C352 M370V	pET M11	M.Jäckl
829	hHuwe1	HECT	M0V C352 I375V	pET M11	M.Jäckl
843	hHuwe1	HECT	M0V I59V C352	pET M11	M.Jäckl
844	hHuwe1	HECT	M0V I79V C352	pET M11	M.Jäckl
845	hHuwe1	HECT	M0V I80 C352	pET M11	M.Jäckl
846	hHuwe1	HECT	M0V I147V C352	pET M11	M.Jäckl
847	hHuwe1	HECT	M0V I207V C352	pET M11	M.Jäckl
848	hHuwe1	HECT	M0V I244V C352	pET M11	M.Jäckl
849	hHuwe1	HECT	M0V I245V C352	pET M11	M.Jäckl
850	hHuwe1	HECT	M0V I250V C352	pET M11	M.Jäckl
851	hHuwe1	HECT	M0V I252VC352	pET M11	M.Jäckl
852	hHuwe1	HECT	M0V I262V C352	pET M11	M.Jäckl
853	hHuwe1	HECT	M0V I287V C352	pET M11	M.Jäckl
854	hHuwe1	HECT	M0V I336V C352	pET M11	M.Jäckl
855	hHuwe1	HECT	M0V M28V C352	pET M11	M.Jäckl
856	hHuwe1	HECT	M0V M53V C352	pET M11	M.Jäckl
857	hHuwe1	HECT	M0V M226V C352	pET M11	M.Jäckl
861	hHuwe1	HECT	M0V I124V C352	pET M11	M.Jäckl
989	hHuwe1	HECT	M0V R43C C352K	pET M11	M.Jäckl
990	hHuwe1	HECT	M0V N113C C352K	pET M11	M.Jäckl
991	hHuwe1	HECT	M0V R84A C352	pET M11	M.Jäckl
992	hHuwe1	C-lobe	A349F C352	pET M11	M.Jäckl
993	hHuwe1	HECT	M0V E75A C352	pET M11	M.Jäckl
994	hHuwe1	HECT	M0V G167S C352	pET M11	M.Jäckl
995	hHuwe1	HECT	M0V D182M C352	pET M11	M.Jäckl
996	hHuwe1	HECT	M0V L384M C352	pET M11	M.Jäckl
997	hHuwe1	HECT	M0V M78V C352	pET M11	M.Jäckl

998	hHuwe1	HECT	M0V M84V C352	pET M11	M.Jäckl
999	hHuwe1	HECT	M0V M88V C352	pET M11	M.Jäckl
1000	hHuwe1	HECT	M0V M157V C352	pET M11	M.Jäckl
1001	hHuwe1	HECT	M0V M157L C352	pET M11	M.Jäckl
1002	hHuwe1	HECT	M0V M224V C352	pET M11	M.Jäckl
1003	hHuwe1	HECT	M0V M226V C352	pET M11	M.Jäckl
1004	hHuwe1	HECT	M0C M226L C352	pET M11	M.Jäckl
1005	hHuwe1	HECT	M0V M328V C352	pET M11	M.Jäckl
1006	hHuwe1	HECT	M0V C352K	pET M11	M.Jäckl
1007	hHuwe1	HECT	M0V R34A C352	pET M11	M.Jäckl
1008	hHuwe1	HECT	M0V D35A C352	pET M11	M.Jäckl
1009	hHuwe1	HECT	M0V A348F C352	pET M11	M.Jäckl
1011	hHuwe1	HECT	M0V Y117C C352K	pET M11	M.Jäckl
1077	hSmurf2	C-lobe	C716	pET M30	C. Stollmaier
1119	hHuwe1	HECT	V0H C352	pETM11	M.Jäckl
1120	hHuwe1	HECT	M0V R34A C352	pETM11	M.Jäckl
1121	hHuwe1	HECT	M0V G63A C352	pETM11	M.Jäckl
1122	hHuwe1	HECT	M0V I110A C352	pETM11	M.Jäckl
1123	hHuwe1	HECT	M0V F192A C352	pETM11	M.Jäckl
1124	hHuwe1	HECT	M0V N195M C352	pETM11	M.Jäckl
1125	hHuwe1	HECT	M0V D182M N195M C352	pETM11	M.Jäckl
1126	hHuwe1	HECT	M0V G167S D182M N195M C352	pETM11	M.Jäckl
1134	hSmurf2	HECT	K716C E87C	pProEx HTb	M.Jäckl
1145	hHuwe1	HECT	M0V Δα1 C352	pETM11	J.Tholen
1146	hHuwe1	HECT	M0V 1/2Δα1 C352	pETM11	J.Tholen
1151	hUbiquitin	full length	G76C M-1H	pETM11	J.Tholen
1253	hHuwe1	HECT	M0V A137C C352A	pETM11	J.Tholen
1255	hHuwe1	HECT	M0V C352N	pETM11	J.Tholen
1262	hUbiquitin	FL	K48C	pETM11	J.Tholen
1280	hHuwe1	HECT	M0V C352A G381C	pETM11	J.Tholen
1284	hHuwe1	HECT	L346P	PET M30-HA	J.Tholen
1285	hHuwe1	HECT	Δ-1aa	PET M30-HA	J.Tholen
1286	hHuwe1	HECT	Δ-2aa	PET M30-HA	J.Tholen
1287	hHuwe1	HECT	Δ-3aa	PET M30-HA	J.Tholen
1288	hHuwe1	HECT	Δ-4aa	PET M30-HA	J.Tholen
1291	hHuwe1	HECT	A348P	PET M30-HA	J.Tholen
1292	hHuwe1	C-lobe	M0V A348P C352	pETM11	J.Tholen
1308	hHuwe1	HECT	C351A	pETM11	J.Tholen
1357	hUbiquitin	FL	WT, Sumo-C-hUb	pET M11-SUMO	C. Stollmaier
1403	hHuwe1	HECT	M0V N113C C352K	pETM11	M.Jäckl
1404	hHuwe1	HECT	M0V E83C C351K	pETM11	M.Jäckl
1405	hHuwe1	HECT	M0V S159C C351	pETM11	M.Jäckl
1408	hHuwe1	HECT	M0V Y162A C352	pETM11	I.Holdermann
1409	hHuwe1	HECT	HA-tag, WT, cterm Chimera AVE	PET M30-HA	I.Holdermann
1410	hHuwe1	HECT	HA-tag, WT, cterm Chimera VE	PET M30-HA	I.Holdermann
1411	hHuwe1	HECT	HA-tag, WT, cterm Chimera E	PET M30-HA	I.Holdermann
1412	hHuwe1	HECT	M0V D98A Y162A C352	pETM11	M.Jäckl
1413	hHuwe1	C-lobe	L346P C352	pETM11	I.Holdermann
1414	hHuwe1	HECT	WT Y162A D98A	pETM11	M.Jäckl
1415	hHuwe1	HECT	WT Y162A	pETM11	M.Jäckl

9.13. Protein sequences

NP_113584.3 E3 ubiquitin-protein ligase HUWE1 [Homo sapiens]

*hs*HUWE1 HECT-domain	3993-4375	(Internal 0 to 385)
*hs*HUWE1 C-lobe	4255-4375	(Internal 267 to 385)

Sequences Huwe1 HECT catalytic Cysteine only:

GAMGDFDVKR KYFRQELERL DEGLRKEDMA VHVRRDHVFE DSYRELHRKS PEEMKNRLYI VFEGEEGQDA GGLLREWYMI ISREMFNPMY ALFRTSPGDR VTYTINPSSH CNPNHLSYFK FVGRIVAKAV YDNRLLECYF TRSFYKHILG KSVRYTDMES EDYHFYQGLV YLLENDVSTL GYDLTFSTEV QEFGVCEVRD LKPNGANILV TEENKKEYVH LVCQMRMTGA IRKQLAAFLE GFYEIIPKRL ISIFTEQELE LLISGLPTID IDDLKSNTEY HKYQSNSIQI QWFWRALRSF DQADRAKFLQ FVTGTSKVPL QGFAALEGMN GIQKFQIHRD DRSTDRLPSA HTCFNQLDLP AYESFEKLRH MLLLAIQECS EGFGLA

NP_073576.1 E3 ubiquitin-protein ligase SMURF2 [Homo sapiens]

*hs*Smurf2 HECT-domain	366-748
*hs*Smurf2 Clobe	610-748

Sequences Smurf2 HECT catalytic Cysteine only:

PRYKRDLVQK LKILRQELSQ QQPQAGHCRI EVSREEIFEE SYRQVMKMRP KDLWKRLMIK FRGEEGLDYG GVAREWLYLL SHEMLNPYYG LFQYSRDDIY TLQINPDSAV NPEHLSYFHF VGRIMGMAVF HGHYIDGGFT LPFYKQLLGK SITLDDMELV DPDLHNSLVW ILENDITGVL DHTFCVEHNA YGEIIQHELK PNGKSIPVNE ENKKEYVRLY VNWRFLRGIE AQFLALQKGF NEVIPQHLLK TFDEKELELI ICGLGKIDVN DWKVNTRLKH CTPDSNIVKW FWKAVEFFDE ERRARLLQFV TGSSRVPLQG FKALQGAAGP RLFTIHQIDA CTNNLPKAHT CFNRIDIPPY ESYEKLYEKL LTAIEETCGF AVE

9.14. Primers

Table 21: List of primes used during these projects. Primer listed with the database number, mutations, protein name, domain, and sequence.

#	Mutation	Protein	Domain	Sequence
883	M0V	hHuwe1 C352	HECT	CTTTATTTTCAGGGCGCCGTGGGGGACTTTGATGTC
885	M84V	hHuwe1 M0V C352	HECT	GATCATCTCTCGAGAGGTGTTTAACCCTATG
887	M88V	hHuwe1 M0V C352	HECT	GAGATGTTTAACCCTGTGTATGCCTTGTTCC
889	I230V	hHuwe1 M0V C352	HECT	AGAATGACAGGAGCCGTGCGCAAGCAGTTGGC
891	I331V	hHuwe1 M0V C352	HECT	CCCTCGAAGGCATGAATGGCGTGCAGAAGTTTCAG
897	I375V	hHuwe1 M0V C352	HECT	CACATGCTACTGTTGGCTGTGCAGGAGAACTCTGAAGGC
901	M53V	hHuwe1 M0V C352	HECT	CATCGCAAATCCCCCGAAGAAGTGAAGAATCGATTGTATATAG
905	M226V	hHuwe1 M0V C352	HECT	GTAGCACAGATGAGAGTGACAGGAGCCATC
907	I79V	hHuwe1 M0V C352	HECT	CTCCTGCGGGAGTGGTATATGGTGATCTCTCGAGAGATGTTTAAC
909	I80V	hHuwe1 M0V C352	HECT	CGGGAGTGGTATATGATCGTGTCTCGAGAGATGTTTAAC
913	I147V	hHuwe1 M0V C352	HECT	CGATCCTTTTACAAACACGTGTTGGGCAAGTCAGTCAG
915	I44A	hUb G76C	FL	GATTGGCGTTTGCCGGTAGACAGCTCGAGGACGGTAG
917	I207V	hHuwe1 M0V C352	HECT	CCCAATGGGGCCAACGTGTTGGTAACAGAGGAG
919	I244V	hHuwe1 M0V C352	HECT	CTTAGAAGGCTTCTATGAGGTGATTCCAAAGCGCCTCATTTC
921	I245V	hHuwe1 M0V C352	HECT	GAAGGCTTCTATGAGATCGTGCCAAAGCGCCTCATTTC
923	I250V	hHuwe1 M0V C352	HECT	CATTCCAAAGCGCCTCGTGTCCATCTTCACTGAGC
925	I252V	hHuwe1 M0V C352	HECT	CCAAAGCGCCTCATTTCCGTGTTCACTGAGCAGGAGTTAG
927	I262V	hHuwe1 M0V C352	HECT	GAGTTAGAGCTGCTTGTGTCAGGACTGCCCACC
929	I278V	hHuwe1 M0V C352	HECT	CAGGACTGCCCACCGTGGACATCGATGATCTG
933	I59V	hHuwe1 M0V C352	HECT	GACCAGCAGAGGTTGGCGTTTGCTGGGAAACAGC
937	I44A	hUb (WT)	FL	GACCAGCAGAGGTTGGCGTTTGCTGGGAAACAG
941	I124V	hHuwe1 M0V C352	HECT	CAAGTTTGTCGGACGCGTGGTGGCCAAAGCTGTAT
945	M224V	hHuwe1 M0V C352	HECT	CACCTGGTAGCACAGGTGAGAATGACAGGAG
949	M328V	hHuwe1 M0V C352	HECT	CTGCCCTCGAAGGCGTGAATGGCATTCAG
951	M370V	hHuwe1 M0V C352	HECT	CTTTGAGAAGCTCCGCCACGTGCTACTGTTGGCTATCCAG
963	M78V	hHuwe1 M0V C352	HECT	CTGCGGGAGTGGTATGTGATCATCTCTCGAG
965	M157V	hHuwe1 M0V C352	HECT	CAGTCAGATATACAGATCTGGAGAGTGAAGATTAC
969	N113C	hHuwe1 M0V C352K	HECT	CTTCCCACATCAACCCCTGCCACCTCAGCTACTTC
971	Y117C	hHuwe1 M0V C352K	HECT	CAACCACCTCAGCTGCTTCAAGTTTGTCG
1099	E75A	hHuwe1 M0V C352	HECT	GCTCCTGCGGGCGTGGTATATGATC
1101	R34A	hHuwe1 M0V C352	HECT	GCTGTGCATGTCCGTGCGGACCATGTGTTTGAAG
1103	D35A	hHuwe1 M0V C352	HECT	GCATGTCCGTCGTGCGCATGTGTTTGAAGAC
1105	G167S	hHuwe1 M0V C352	HECT	GAAGATTACCACTTCTACCAAAGCCTGGTTTATCTGCTGG
1107	D182M	hHuwe1 M0V C352	HECT	ACACTAGGCTATATGCTCACCTTCAGCACTGAGGTC
1109	C351K	hHuwe1 M0V C352	HECT	CCTGCCTTCAGCTCACACAAAATTTAATCAGCTGGATCTG
1111	R43C	hHuwe1 M0V C352K	HECT	GTGTTTGAAGACTCCTATTGCGAGCTGCATCGCAAATC
1113	A349F	hHuwe1 M0V C352	HECT	CACAGATCGCCTGCCTTCATTTCACACATGTTTTAATCA
1115	F382Stops	hHuwe1 M0V C352	HECT	CAGGAGAACTCTGAAGGCTAAGGGCTGGCC
1117	C75Stop	hUb G76C	FL	CTTAAGACTTCGTGGTTAATAAGGTACCGGATCC
1121	A385E	hHuwe1 M0V C352	HECT	CTGAAGGCTTTGGGCTGGAA
1123	D68E	hHuwe1 M0V C352	HECT	GAAGAAGGGCAGGCGGCTGGCGGGCTC
1125	R82A	hHuwe1 M0V C352	HECT	GAGTGGTATATGATCATCTCTGCGGAGATGTTTAACCCTATG
1127	L384M	hHuwe1 M0V C352	HECT	GAGAACTCTGAAGGCTTTGGGATGGCC
1129	N195M	hHuwe1 M0V C352	HECT	GTCCAAGAGTTTGGAGTTATGGAAGTTCGTGACCTCAAAC
1133	N113C	hHuwe1 n-lobe pET M11	N-lobe	CTTCCCACATCAACCCCTGCCACCTCAGCTACTTC
1135	R48C	hUb (WT)	FL	GATTGATCTTTGCCGGTTGCCAGCTCGAGGACGGTAG
1139	I110A	hHuwe1 M0V C352	HECT	CAATCCATCTTCCCACGCGAACCCCAACCACCTC
1141	F192A	hHuwe1 M0V C352	HECT	CACTGAGGTCCAAGAGGCGGGAGTTAACGAAGTTC
1151	C716K	Smurf2 C716	HECT	CCTGCCGAAAGCCCACACTAAATTCAATCGAATAGACATTC
1153	E87C	Smurf2 C716	HECT	GGTTGTATCTCTTGTCACATTGCATGTTGAATCCATACTATGGC
1155	E83C	hHuwe1 M0V C352K	HECT	GGTATATGATCATCTCTCGATGCATGTTTAACCCTATGTATGCC
1157	A-2H	hHuwe1 M0V C352	HECT	GAGAATCTTTATTTTCAGGGCCATATGGGGGACTTTGATGTCAAG
1179	M-1H	hUbG76C	FL	CTTTATTTTCAGGGCGCCCATGGAATGCAGATCTTCGTC
1181	M-1H	hHuwe1 M0V C352	HECT	CTTTATTTTCAGGGCGCCCATGGGGACTTTGATGTCAAG

1183	C76G	hUb G76C	FL	CTTAAGACTTCGTGGTGGTTAAGGTACCGGATG
1192	GAVGDF to GSGF	hHuwe1 M0V C352	HECT	GAGAATCTTTATTTTCAGGGCAGCGGCTTTGATGTCAAGCGCAAA
1194	Δ α1 helix	hHuwe1 M0V C352	HECT	GAGAATCTTTATTTTCAGGGCAGCGGCCTCCGGAAAGAAGACATG
1196	Δ 1/2α1 helix	hHuwe1 M0V C352	HECT	GAG AAT CTT TAT TTT CAG GGC AGC GGC TTC CGC CAA GAG CTG
1202	M0H	hUbG76C	FL	CTTTATTTTCAGGGCGCCCATGGAATGCAGATCTTCGTC
1236	K352C	hHuwe1 M0V N113C C352	HECT	CTGCCTTCAGCTCACACATGCTTTAATCAGCTGGAT
1717	D98A	hs HUWE1 (WT)	HECT	CTCACCTGGTGCGCGAGTCACCTAC
1719	chimera AVE C-terminus	hs HUWE1 (WT)	HECT	GCTCTGAAGGCTTTGCGGTGGAATAAGGTACCGGATCC
1721	chimera VE C-terminus	hs HUWE1 (WT)	HECT	CTGAAGGCTTTGGGGTGGAATAAGGTACCGGATC
1723	chimera E C-terminus	hs HUWE1 (WT)	HECT	GCTTTGGGCTGGAATAAGGTACCGG
1725	G193A	hs HUWE1 (WT)	HECT	GAGGTCCAAGAGTTTGCGGTTTGTGAAGTTCGTG
1727	L346P	hHuwe1 C352	C-lobe	GTCCACAGATCGCCCGCCTTCAGCTCACAC
1729	E160V	hHuwe1 M0V C352	HECT	ATACAGATATGGAGAGTGTGGATTACCACTTCTACC
1731	Y162V	hHuwe1 M0V C352	HECT	CAGATATGGAGAGTGAAGATGCGCACTTCTACCAAGG
1733	D98A	hHuwe1 M0V C352	HECT	CTCACCTGGTGCGCGAGTCACCTAC
1739	C110A	hs HUWE1 (WT)	HECT	CAATCCATCTTCCCACGCGAACCCCAACCACCTC
1741	Q189A	hs HUWE1 (WT)	HECT	CTTCAGCACTGAGGTCGCGGAGTTTGGAGTTTGTG
1743	F192A	hs HUWE1 (WT)	HECT	CACTGAGGTCCAAGAGGCGGGAGTTTGTGAAGTTC

10. References

[1] A. Ciechanover, "Tracing the history of the ubiquitin proteolytic system: The pioneering article," *Biochem. Biophys. Res. Commun.*, vol. 387, no. 1, pp. 1–10, 2009.

[2] A. Ciechanover, "The unravelling of the ubiquitin system," *Nat. Rev. Mol. Cell Biol.*, vol. 16, no. 5, pp. 322–324, May 2015.

[3] A. Hershko and A. Ciechanover, "THE UBIQUITIN SYSTEM," *Annu. Rev. Biochem.*, vol. 67, no. 1, pp. 425–479, Jun. 1998.

[4] R. Yau and M. Rape, "The increasing complexity of the ubiquitin code," *Nat. Cell Biol.*, vol. 18, no. 6, pp. 579–586, 2016.

[5] K. E. Sloper-Mould, J. C. Jemc, C. M. Pickart, and L. Hicke, "Distinct Functional Surface Regions on Ubiquitin," *J. Biol. Chem.*, vol. 276, no. 32, pp. 30483–30489, 2001.

[6] B. M. Kessler, "Ubiquitin - omics reveals novel networks and associations with human disease," *Curr. Opin. Chem. Biol.*, vol. 17, no. 1, pp. 59–65, 2013.

[7] D. Komander and M. Rape, "The ubiquitin code.," *Annu. Rev. Biochem.*, vol. 81, no. 1, pp. 203–29, 2012.

[8] A. Varshavsky, "The ubiquitin system, an immense realm.," *Annu. Rev. Biochem.*, vol. 81, no. 1, pp. 167–76, 2012.

[9] R. Suryadinata, S. N. A. Roesley, G. Yang, and B. Šarčević, "Mechanisms of generating polyubiquitin chains of different topology," *Cells*, vol. 3, no. 3, pp. 674–689, 2014.

[10] M. J. Clague, C. Heride, and S. Urbé, "The demographics of the ubiquitin system," *Trends Cell Biol.*, vol. 25, no. 7, pp. 417–426, 2015.

[11] D. Morimoto and M. Shirakawa, "The evolving world of ubiquitin: Transformed polyubiquitin chains," *Biomol. Concepts*, vol. 7, no. 3, pp. 157–167, 2016.

[12] K. N. Swatek and D. Komander, "Ubiquitin modifications.," *Cell Res.*, vol. 26, no. 4, pp. 399–422, Apr. 2016.

[13] D. Rotin and S. Kumar, "Physiological functions of the HECT family of ubiquitin ligases.," *Nat. Rev. Mol. Cell Biol.*, vol. 10, no. 6, pp. 398–409, Jun. 2009.

[14] M. A. Rodgers *et al.*, "The linear ubiquitin assembly complex (LUBAC) is essential for NLRP3 inflammasome activation," *J. Exp. Med.*, vol. 211, no. 7, pp. 1333–1347, 2014.

[15] R. Budhidarmo, Y. Nakatani, and C. L. Day, "RINGs hold the key to ubiquitin

transfer," *Trends Biochem. Sci.*, vol. 37, no. 2, pp. 58–65, Feb. 2012.

[16] K. Haglund and I. Dikic, "Ubiquitylation and cell signaling," *EMBO J.*, vol. 24, no. 19, pp. 3353–3359, 2005.

[17] M. Akutsu, I. Dikic, and A. Bremm, "Ubiquitin chain diversity at a glance.," *J. Cell Sci.*, vol. 129, no. 5, pp. 875–80, Mar. 2016.

[18] M. Scheffner and S. Kumar, "Mammalian HECT ubiquitin-protein ligases: Biological and pathophysiological aspects," *Biochim. Biophys. Acta - Mol. Cell Res.*, vol. 1843, no. 1, pp. 61–74, Jan. 2014.

[19] Y. Kulathu and D. Komander, "Atypical ubiquitylation — the unexplored world of polyubiquitin beyond Lys48 and Lys63 linkages," *Nat. Rev. Mol. Cell Biol.*, vol. 13, no. 8, pp. 508–523, Aug. 2012.

[20] E. B. Dammer *et al.*, "Polyubiquitin linkage profiles in three models of proteolytic stress suggest the etiology of alzheimer disease," *J. Biol. Chem.*, vol. 286, no. 12, pp. 10457–10465, 2011.

[21] M. A. Michel, K. N. Swatek, M. K. Hospenthal, and D. Komander, "Ubiquitin Linkage-Specific Affimers Reveal Insights into K6-Linked Ubiquitin Signaling," *Mol. Cell*, vol. 68, no. 1, p. 233–246.e5, Oct. 2017.

[22] G. L. Grice and J. A. Nathan, "The recognition of ubiquitinated proteins by the proteasome," *Cell. Mol. Life Sci.*, vol. 73, no. 18, pp. 3497–3506, Sep. 2016.

[23] Y. Kazansky, M.-Y. Lai, R. K. Singh, and D. Fushman, "Impact of different ionization states of phosphorylated Serine-65 on ubiquitin structure and interactions," *Sci. Rep.*, vol. 8, no. 1, p. 2651, Dec. 2018.

[24] C. Grabbe, K. Husnjak, and I. Dikic, "Europe PMC Funders Group The spatial and temporal organization of ubiquitin networks," vol. 12, no. 5, pp. 295–307, 2013.

[25] K. Husnjak and I. Dikic, "Ubiquitin-Binding Proteins: Decoders of Ubiquitin-Mediated Cellular Functions," *Annu. Rev. Biochem.*, vol. 81, no. 1, pp. 291–322, Jul. 2012.

[26] C. Heride, S. Urbé, and M. J. Clague, "Ubiquitin code assembly and disassembly," *Curr. Biol.*, vol. 24, no. 6, pp. R215–R220, 2014.

[27] D. C. Rubinsztein, "The roles of intracellular protein-degradation pathways in neurodegeneration.," *Nature*, vol. 443, no. 7113, pp. 780–6, Oct. 2006.

[28] J. C. Christianson and Y. Ye, "Cleaning up in the endoplasmic reticulum: ubiquitin in charge.," *Nat. Struct. Mol. Biol.*, vol. 21, no. 4, pp. 325–35, Apr. 2014.

[29] I. Livneh, V. Cohen-Kaplan, C. Cohen-Rosenzweig, N. Avni, and A. Ciechanover, "The life cycle of the 26S proteasome: from birth, through regulation and function and onto its death," *Cell Res.*, vol. 26, no. 8, pp. 869–885, Aug. 2016.

[30] L. Lemus and V. Goder, "Regulation of Endoplasmic Reticulum-Associated Protein Degradation (ERAD) by Ubiquitin.," *Cells*, vol. 3, no. 3, pp. 824–47, Aug. 2014.

[31] X. Wu and T. A. Rapoport, "ScienceDirect Mechanistic insights into ER-associated protein degradation," *Curr. Opin. Cell Biol.*, vol. 53, pp. 22–28, 2018.

[32] D. Voges, P. Zwickl, and W. Baumeister, "The 26S Proteasome: A Molecular Machine Designed for Controlled Proteolysis," *Annu. Rev. Biochem.*, vol. 68, no. 1, pp. 1015–1068, Jun. 1999.

[33] D. Finley, X. Chen, and K. J. Walters, "Gates, Channels, and Switches: Elements of the Proteasome Machine," *Trends Biochem. Sci.*, vol. 41, no. 1, pp. 77–93, Jan. 2016.

[34] D. Popovic, D. Vucic, and I. Dikic, "Ubiquitination in disease pathogenesis and treatment," *Nat. Med.*, vol. 20, no. 11, pp. 1242–1253, Nov. 2014.

[35] R. Krajmalnik-Brown, Z.-E. Ilhan, D.-W. Kang, and J. K. DiBaise, "Effects of gut microbes on nutrient absorption and energy regulation.," *Nutr. Clin. Pract.*, vol. 27, no. 2, pp. 201–14, Apr. 2012.

[36] J. Luo, H. Kamata, and M. Karin, "IKK / NF-κB signaling : balancing life and death — a new approach to cancer therapy," *J. Clin. Invest.*, vol. 115, no. 10, pp. 2625–2632, 2005.

[37] Y. Ben-Neriah and M. Karin, "Inflammation meets cancer, with NF-κB as the matchmaker.," *Nat. Immunol.*, vol. 12, no. 8, pp. 715–23, Jul. 2011.

[38] H.-C. Tai, A. Serrano-Pozo, T. Hashimoto, M. P. Frosch, T. L. Spires-Jones, and B. T. Hyman, "The synaptic accumulation of hyperphosphorylated tau oligomers in Alzheimer disease is associated with dysfunction of the ubiquitin-proteasome system.," *Am. J. Pathol.*, vol. 181, no. 4, pp. 1426–35, Oct. 2012.

[39] S. Keck, R. Nitsch, T. Grune, and O. Ullrich, "Proteasome inhibition by paired helical filament-tau in brains of patients with Alzheimer's disease.," *J. Neurochem.*, vol. 85, no. 1, pp. 115–22, Apr. 2003.

[40] S. Lorenz, "Structural mechanisms of HECT-type ubiquitin ligases," *Biol. Chem.*, vol. 399, no. 2, pp. 127–145, Jan. 2018.

[41] C. E. Berndsen and C. Wolberger, "New insights into ubiquitin E3 ligase mechanism.," *Nat. Struct. Mol. Biol.*, vol. 21, no. 4, pp. 301–7, Apr. 2014.

[42] L. Buetow and D. T. Huang, “Structural insights into the catalysis and regulation of E3 ubiquitin ligases.,” *Nat. Rev. Mol. Cell Biol.*, vol. 17, no. 10, pp. 626–42, Oct. 2016.

[43] R. J. Deshaies and C. A. P. Joazeiro, “RING Domain E3 Ubiquitin Ligases,” *Annu. Rev. Biochem.*, vol. 78, no. 1, pp. 399–434, Jun. 2009.

[44] K. K. Dove and R. E. Klevit, “RING-Between-RING E3 Ligases: Emerging Themes amid the Variations,” *J. Mol. Biol.*, vol. 429, no. 22, pp. 3363–3375, Nov. 2017.

[45] K. Rittinger and F. Ikeda, “Linear ubiquitin chains: enzymes, mechanisms and biology,” *Open Biol.*, vol. 7, no. 4, p. 170026, Apr. 2017.

[46] K. K. Dove and R. E. Klevit, “RING-between-RINGs-keeping the safety on loaded guns,” *EMBO J.*, vol. 31, no. 19, pp. 3792–3794, Oct. 2012.

[47] J. J. Smit and T. K. Sixma, “RBR E3-ligases at work.,” *EMBO Rep.*, vol. 15, no. 2, pp. 142–54, Feb. 2014.

[48] J. M. Huibregtse, M. Scheffner, S. Beaudenon, and P. M. Howley, “A family of proteins structurally and functionally related to the E6-AP ubiquitin-protein ligase.,” *Proc. Natl. Acad. Sci.*, vol. 92, no. 7, pp. 2563–2567, 1995.

[49] H. B. Kamadurai *et al.*, “Insights into Ubiquitin Transfer Cascades from a Structure of a UbcH5B∼Ubiquitin-HECTNEDD4L Complex,” *Mol. Cell*, vol. 36, no. 6, pp. 1095–1102, Dec. 2009.

[50] E. Maspero *et al.*, “Structure of a ubiquitin-loaded HECT ligase reveals the molecular basis for catalytic priming.,” *Nat. Struct. Mol. Biol.*, vol. 20, no. 6, pp. 696–701, Jun. 2013.

[51] E. Maspero *et al.*, “Structure of the HECT:ubiquitin complex and its role in ubiquitin chain elongation,” *EMBO Rep.*, vol. 12, no. 4, pp. 342–349, Mar. 2011.

[52] A. A. Ogunjimi *et al.*, “The ubiquitin binding region of the Smurf HECT domain facilitates polyubiquitylation and binding of ubiquitylated substrates.,” *J. Biol. Chem.*, vol. 285, no. 9, pp. 6308–15, Feb. 2010.

[53] H. B. Kamadurai *et al.*, “Mechanism of ubiquitin ligation and lysine prioritization by a HECT E3.,” *Elife*, vol. 2, no. 2, p. e00828, Aug. 2013.

[54] C. Salvat, G. Wang, A. Dastur, N. Lyon, and J. M. Huibregtse, “The -4 phenylalanine is required for substrate ubiquitination catalyzed by HECT ubiquitin ligases.,” *J. Biol. Chem.*, vol. 279, no. 18, pp. 18935–43, Apr. 2004.

[55] H. C. Kim, A. M. Steffen, M. L. Oldham, J. Chen, and J. M. Huibregtse, “Structure and function of a HECT domain ubiquitin-binding site,” *EMBO Rep.*, vol. 12, no. 4, pp.

334–341, 2011.

[56] S. Sánchez-Tena, M. Cubillos-Rojas, T. Schneider, and J. L. Rosa, “Functional and pathological relevance of HERC family proteins: A decade later,” *Cell. Mol. Life Sci.*, vol. 73, no. 10, pp. 1955–1968, 2016.

[57] S. Bekker-Jensen *et al.*, “HERC2 coordinates ubiquitin-dependent assembly of DNA repair factors on damaged chromosomes,” *Nat. Cell Biol.*, vol. 12, no. 1, pp. 80–86, 2010.

[58] F. Bernassola, M. Karin, A. Ciechanover, and G. Melino, “The HECT Family of E3 Ubiquitin Ligases: Multiple Players in Cancer Development,” *Cancer Cell*, vol. 14, no. 1, pp. 10–21, Jul. 2008.

[59] Z. Chen *et al.*, “A Tunable Brake for HECT Ubiquitin Ligases.,” *Mol. Cell*, vol. 66, no. 3, p. 345–357.e6, May 2017.

[60] X. Zou, G. Levy-Cohen, and M. Blank, “Molecular functions of NEDD4 E3 ubiquitin ligases in cancer,” *Biochim. Biophys. Acta - Rev. Cancer*, vol. 1856, no. 1, pp. 91–106, Aug. 2015.

[61] N. A. Boase and S. Kumar, “NEDD4: The founding member of a family of ubiquitin-protein ligases,” *Gene*, vol. 557, no. 2, pp. 113–122, Feb. 2015.

[62] F. R. Garcia-Gonzalo and J. L. Rosa, “The HERC proteins: functional and evolutionary insights,” *Cell. Mol. Life Sci.*, vol. 62, no. 16, pp. 1826–1838, Aug. 2005.

[63] V. Fajner, E. Maspero, and S. Polo, “Targeting HECT-type E3 ligases - insights from catalysis, regulation and inhibitors.,” *FEBS Lett.*, vol. 591, no. 17, pp. 2636–2647, 2017.

[64] H. C. Kim and J. M. Huibregtse, “Polyubiquitination by HECT E3s and the Determinants of Chain Type Specificity,” *Mol. Cell. Biol.*, vol. 29, no. 12, pp. 3307–3318, 2009.

[65] M. Scheffner, U. Nuber, and J. M. Huibregtse, “Protein ubiquitination involving an E1–E2–E3 enzyme ubiquitin thioester cascade,” *Nature*, vol. 373, no. 6509. pp. 81–83, 1995.

[66] M. A. Michel, K. N. Swatek, M. K. Hospenthal, and D. Komander, “Ubiquitin Linkage-Specific Affimers Reveal Insights into K6-Linked Ubiquitin Signaling,” *Mol. Cell*, vol. 68, no. 1, p. 233–246.e5, Oct. 2017.

[67] Z. Hao *et al.*, “K48-linked KLF4 ubiquitination by E3 ligase Mule controls T-cell proliferation and cell cycle progression,” *Nat. Commun.*, vol. 8, 2017.

[68] X. Zhao *et al.*, "The HECT-domain ubiquitin ligase Huwe1 controls neural differentiation and proliferation by destabilizing the N-Myc oncoprotein," *Nat. Cell Biol.*, vol. 10, no. 6, pp. 643–653, Jun. 2008.

[69] Y. A. Kristariyanto *et al.*, "Assembly and structure of Lys 33 -linked polyubiquitin reveals distinct conformations," *Biochem. J.*, vol. 467, no. 2, pp. 345–352, Apr. 2015.

[70] B. Sander, W. Xu, M. Eilers, N. Popov, and S. Lorenz, "A conformational switch regulates the ubiquitin ligase HUWE1," *Elife*, vol. 6, pp. 1–32, Feb. 2017.

[71] R. K. Pandya, J. R. Partridge, K. R. Love, T. U. Schwartz, and H. L. Ploegh, "A structural element within the HUWE1 HECT domain modulates self-ubiquitination and substrate ubiquitination activities," *J. Biol. Chem.*, vol. 285, no. 8, pp. 5664–5673, 2010.

[72] S. V. Khoronenkova and G. L. Dianov, "The emerging role of Mule and ARF in the regulation of base excision repair," *FEBS Lett.*, vol. 585, no. 18, pp. 2831–2835, Sep. 2011.

[73] Q. Zhong, W. Gao, F. Du, and X. Wang, "Mule/ARF-BP1, a BH3-Only E3 Ubiquitin Ligase, Catalyzes the Polyubiquitination of Mcl-1 and Regulates Apoptosis," *Cell*, vol. 121, no. 7, pp. 1085–1095, Jul. 2005.

[74] M. R. Warr and G. C. Shore, "Unique biology of Mcl-1: therapeutic opportunities in cancer.," *Curr. Mol. Med.*, vol. 8, no. 2, pp. 138–47, Mar. 2008.

[75] D. Nijhawan *et al.*, "Elimination of Mcl-1 is required for the initiation of apoptosis following ultraviolet irradiation.," *Genes Dev.*, vol. 17, no. 12, pp. 1475–86, Jun. 2003.

[76] A. Shmueli and M. Oren, "Life, Death, and Ubiquitin: Taming the Mule," *Cell*, vol. 121, no. 7, pp. 963–965, Jul. 2005.

[77] F. X. Schaub and J. L. Cleveland, "Tipping the MYC-MIZ1 balance: targeting the HUWE1 ubiquitin ligase selectively blocks MYC-activated genes.," *EMBO Mol. Med.*, vol. 6, no. 12, pp. 1509–11, Dec. 2014.

[78] S. Peter *et al.*, "Tumor cell-specific inhibition of MYC function using small molecule inhibitors of the HUWE1 ubiquitin ligase," *EMBO Mol. Med.*, vol. 6, no. 12, pp. 1525–1541, 2014.

[79] S. Wiesner *et al.*, "Autoinhibition of the HECT-Type Ubiquitin Ligase Smurf2 through Its C2 Domain," *Cell*, vol. 130, no. 4, pp. 651–662, Aug. 2007.

[80] A. A. Ogunjimi *et al.*, "Regulation of Smurf2 ubiquitin ligase activity by anchoring

the E2 to the HECT domain.," *Mol. Cell*, vol. 19, no. 3, pp. 297–308, Aug. 2005.

[81] S. Mari *et al.*, "Structural and functional framework for the autoinhibition of Nedd4-family ubiquitin ligases.," *Structure*, vol. 22, no. 11, pp. 1639–49, Nov. 2014.

[82] S. Huang *et al.*, "Activation of Smurf E3 ligase promoted by smoothened regulates hedgehog signaling through targeting patched turnover.," *PLoS Biol.*, vol. 11, no. 11, p. e1001721, Nov. 2013.

[83] R. Dunn and L. Hicke, "Domains of the Rsp5 ubiquitin-protein ligase required for receptor-mediated and fluid-phase endocytosis.," *Mol. Biol. Cell*, vol. 12, no. 2, pp. 421–35, Feb. 2001.

[84] L. Huang *et al.*, "Structure of an E6AP-UbcH7 complex: insights into ubiquitination by the E2-E3 enzyme cascade.," *Science*, vol. 286, no. 5443, pp. 1321–6, Nov. 1999.

[85] V. Vittal, M. D. Stewart, P. S. Brzovic, and R. E. Klevit, "Regulating the Regulators: Recent Revelations in the Control of E3 Ubiquitin Ligases.," *J. Biol. Chem.*, vol. 290, no. 35, pp. 21244–51, Aug. 2015.

[86] K. Zhu *et al.*, "Allosteric auto-inhibition and activation of the Nedd4 family E3 ligase Itch," *EMBO Rep.*, vol. 18, no. 9, p. e201744454, 2017.

[87] D. David, S. A. Nair, and M. R. Pillai, "Smurf E3 ubiquitin ligases at the cross roads of oncogenesis and tumor suppression," *Biochim. Biophys. Acta - Rev. Cancer*, vol. 1835, no. 1, pp. 119–128, 2013.

[88] M. Jäckl *et al.*, "β-Sheet Augmentation Is a Conserved Mechanism of Priming HECT E3 Ligases for Ubiquitin Ligation," *J. Mol. Biol.*, Jun. 2018.

[89] A. H. Kwan, M. Mobli, P. R. Gooley, G. F. King, and J. P. Mackay, "Macromolecular NMR spectroscopy for the non-spectroscopist.," *FEBS J.*, vol. 278, no. 5, pp. 687–703, Mar. 2011.

[90] J. CAVANAGH, W. J. FAIRBROTHER, A. G. PALMER, M. RANCE, and N. J. SKELTON, "CHAPTER 1 - CLASSICAL NMR SPECTROSCOPY," in *Protein NMR Spectroscopy (Second Edition)*, Second Edi., J. CAVANAGH, W. J. FAIRBROTHER, A. G. PALMER, M. RANCE, and N. J. SKELTON, Eds. Burlington: Academic Press, 2007, pp. 1–28.

[91] F. J. . M. van de Ven, *Multidimensional NMR in Liquids - Basic Principles and Experimental Methods*, 1st ed. John Wiley & Sons, 1995.

[92] S. Wiesner and R. Sprangers, "Methyl groups as NMR probes for biomolecular interactions," *Curr. Opin. Struct. Biol.*, vol. 35, pp. 60–67, Dec. 2015.

[93] C. Göbl, T. Madl, B. Simon, and M. Sattler, "NMR approaches for structural analysis

of multidomain proteins and complexes in solution," *Prog. Nucl. Magn. Reson. Spectrosc.*, vol. 80, pp. 26–63, Jul. 2014.

[94] K. Pervushin, R. Riek, G. Wider, and K. Wüthrich, "Attenuated T2 relaxation by mutual cancellation of dipole-dipole coupling and chemical shift anisotropy indicates an avenue to NMR structures of very large biological macromolecules in solution.," *Proc. Natl. Acad. Sci. U. S. A.*, vol. 94, no. 23, pp. 12366–71, Nov. 1997.

[95] R. Riek, K. Pervushin, and K. Wüthrich, "TROSY and CRINEPT: NMR with large molecular and supramolecular structures in solution.," *Trends Biochem. Sci.*, vol. 25, no. 10, pp. 462–8, Oct. 2000.

[96] R. Kerfah, M. J. Plevin, R. Sounier, P. Gans, and J. Boisbouvier, "Methyl-specific isotopic labeling: a molecular tool box for solution NMR studies of large proteins," *Curr. Opin. Struct. Biol.*, vol. 32, pp. 113–122, Jun. 2015.

[97] J. E. Ollerenshaw, V. Tugarinov, and L. E. Kay, "Methyl TROSY: explanation and experimental verification," *Magn. Reson. Chem.*, vol. 41, no. 10, pp. 843–852, Oct. 2003.

[98] R. Rosenzweig and L. E. Kay, "Bringing Dynamic Molecular Machines into Focus by Methyl-TROSY NMR," *Annu. Rev. Biochem.*, vol. 83, no. 1, pp. 291–315, Jun. 2014.

[99] F. A. Renschler *et al.*, "Structural basis for the interaction between the cell polarity proteins Par3 and Par6," *Sci. Signal.*, vol. 11, no. 517, 2018.

[100] C. A. Waudby, A. Ramos, L. D. Cabrita, and J. Christodoulou, "Two-Dimensional NMR Lineshape Analysis.," *Sci. Rep.*, vol. 6, no. 1, p. 24826, Jul. 2016.

[101] J. P. Wurm, I. Holdermann, J. H. Overbeck, P. H. O. Mayer, and R. Sprangers, "Changes in conformational equilibria regulate the activity of the Dcp2 decapping enzyme," *Proc. Natl. Acad. Sci.*, vol. 114, no. 23, pp. 6034–6039, 2017.

[102] T. K. Mal, M. Ikura, and L. E. Kay, "The ATCUN domain as a probe of intermolecular interactions: Application to calmodulin-peptide complexes," *J. Am. Chem. Soc.*, vol. 124, no. 47, pp. 14002–14003, 2002.

[103] M. A. Cvetkovic, J. P. Wurm, M. J. Audin, S. Schütz, and R. Sprangers, "The Rrp4-exosome complex recruits and channels substrate RNA by a unique mechanism," *Nat. Chem. Biol.*, vol. 13, no. 5, pp. 522–528, 2017.

[104] M. C. Stoffregen, M. M. Schwer, F. A. Renschler, and S. Wiesner, "Methionine scanning as an NMR tool for detecting and analyzing biomolecular interaction surfaces," *Structure*, vol. 20, no. 4, pp. 573–581, 2012.

[105] B. Rupp, *Biomolecular Crystallography: Principles, Practice, and Application to Structural Biology*. 2009.

[106] A. McPherson and J. A. Gavira, "Introduction to protein crystallization.," *Acta Crystallogr. Sect. F, Struct. Biol. Commun.*, vol. 70, no. Pt 1, pp. 2–20, Jan. 2014.

[107] G. T. Debelouchina and T. W. Muir, "A molecular engineering toolbox for the structural biologist," *Q. Rev. Biophys.*, vol. 50, 2017.

[108] J. Sluimer and B. Distel, "Regulating the human HECT E3 ligases," *Cell. Mol. Life Sci.*, no. 123456789, pp. 1–21, Jun. 2018.

[109] C. P. R. Hackenberger and D. Schwarzer, "Chemoselective ligation and modification strategies for peptides and proteins," *Angew. Chemie - Int. Ed.*, vol. 47, no. 52, pp. 10030–10074, 2008.

[110] S. Lorenz, M. Bhattacharyya, C. Feiler, M. Rape, and J. Kuriyan, "Crystal Structure of a Ube2S-Ubiquitin Conjugate.," *PLoS One*, vol. 11, no. 2, p. e0147550, 2016.

[111] S. K. Olsen and C. D. Lima, "Structure of a ubiquitin E1-E2 complex: insights to E1-E2 thioester transfer.," *Mol. Cell*, vol. 49, no. 5, pp. 884–96, Mar. 2013.

[112] N. Merkley, K. R. Barber, and G. S. Shaw, "Ubiquitin manipulation by an E2 conjugating enzyme using a novel covalent intermediate.," *J. Biol. Chem.*, vol. 280, no. 36, pp. 31732–8, Sep. 2005.

[113] G. L. Ellman, "A colorimetric method for determining low concentrations of mercaptans," *Arch. Biochem. Biophys.*, vol. 74, no. 2, pp. 443–450, Apr. 1958.

[114] A. F. Habeeb, "[37] Reaction of protein sulfhydryl groups with Ellman's reagent.," *Methods Enzymol.*, vol. 25, no. C, pp. 457–64, 1972.

[115] L. Chen, I. Annis, and G. Barany, "Disulfide bond formation in peptides.," *Curr. Protoc. protein Sci.*, vol. Chapter 18, p. Unit18.6, May 2001.

[116] T. C. Terwilliger *et al.*, "Iterative-build OMIT maps: map improvement by iterative model building and refinement without model bias.," *Acta Crystallogr. D. Biol. Crystallogr.*, vol. 64, no. Pt 5, pp. 515–24, May 2008.

[117] W. Zhang *et al.*, "System-Wide Modulation of HECT E3 Ligases with Selective Ubiquitin Variant Probes," *Mol. Cell*, vol. 62, no. 1, pp. 121–136, Apr. 2016.

[118] B. Webb and A. Sali, *Protein Structure Prediction*, vol. 1137. New York, NY: Springer New York, 2014.

[119] M. E. French, J. L. Klosowiak, A. Aslanian, S. I. Reed, J. R. Yates, and T. Hunter, "Mechanism of ubiquitin chain synthesis employed by a HECT domain ubiquitin

ligase," *J. Biol. Chem.*, vol. 292, no. 25, pp. 10398–10413, 2017.

[120] D. S. Kirkpatrick, S. A. Gerber, and S. P. Gygi, "The absolute quantification strategy: a general procedure for the quantification of proteins and post-translational modifications.," *Methods*, vol. 35, no. 3, pp. 265–73, Mar. 2005.

[121] T. Mund, M. Graeb, J. Mieszczanek, M. Gammons, H. R. B. Pelham, and M. Bienz, "Disinhibition of the HECT E3 ubiquitin ligase WWP2 by polymerized Dishevelled.," *Open Biol.*, vol. 5, no. 12, p. 150185, Dec. 2015.

[122] A. Escobedo, T. Gomes, E. Aragón, P. Martín-Malpartida, L. Ruiz, and M. J. Macias, "Structural basis of the activation and degradation mechanisms of the E3 ubiquitin ligase Nedd4L.," *Structure*, vol. 22, no. 10, pp. 1446–57, Oct. 2014.

[123] J. Wang, Q. Peng, Q. Lin, C. Childress, D. Carey, and W. Yang, "Calcium activates Nedd4 E3 ubiquitin ligases by releasing the C2 domain-mediated auto-inhibition.," *J. Biol. Chem.*, vol. 285, no. 16, pp. 12279–88, Apr. 2010.

[124] Z. Liu, Z. Gong, X. Dong, and C. Tang, "Transient protein–protein interactions visualized by solution NMR," *Biochim. Biophys. Acta - Proteins Proteomics*, vol. 1864, no. 1, pp. 115–122, Jan. 2016.

[125] N. J. Anthis and G. M. Clore, "Visualizing transient dark states by NMR spectroscopy.," *Q. Rev. Biophys.*, vol. 48, no. 1, pp. 35–116, Feb. 2015.

[126] G. M. Clore, "Exploring sparsely populated states of macromolecules by diamagnetic and paramagnetic NMR relaxation," *Protein Sci.*, vol. 20, no. 2, pp. 229–246, Feb. 2011.

[127] N. Zheng and N. Shabek, "Ubiquitin Ligases: Structure, Function, and Regulation," *Annu. Rev. Biochem.*, vol. 86, no. 1, pp. 129–157, Jun. 2017.

[128] C. Rubio-Perez *et al.*, "In silico prescription of anticancer drugs to cohorts of 28 tumor types reveals targeting opportunities.," *Cancer Cell*, vol. 27, no. 3, pp. 382–96, Mar. 2015.

[129] Cancer Genome Atlas Research Network *et al.*, "The Cancer Genome Atlas Pan-Cancer analysis project.," *Nat. Genet.*, vol. 45, no. 10, pp. 1113–20, Oct. 2013.

[130] G. Y. Lapid C, "PrimerX-Automated design of mutagenic primers for site-directed mutagenesis." 2003.

[131] T. Unger, Y. Jacobovitch, A. Dantes, R. Bernheim, and Y. Peleg, "Applications of the Restriction Free (RF) cloning procedure for molecular manipulations and protein expression.," *J. Struct. Biol.*, vol. 172, no. 1, pp. 34–44, Oct. 2010.

[132] F. van den Ent and J. Löwe, “RF cloning: a restriction-free method for inserting target genes into plasmids.,” *J. Biochem. Biophys. Methods*, vol. 67, no. 1, pp. 67–74, Apr. 2006.

[133] T. A. Hall, “Symposium on RNA Biology. III. RNA, Tool and Target. Research Triangle Park, North Carolina, USA. October 15-17, 1999. Proceedings.,” *Nucleic Acids Symp. Ser.*, vol. 41, no. 41, pp. 1–218, 1999.

[134] F. Delaglio, S. Grzesiek, G. W. Vuister, G. Zhu, J. Pfeifer, and A. Bax, “NMRPipe: A multidimensional spectral processing system based on UNIX pipes,” *J. Biomol. NMR*, vol. 6, no. 3, pp. 277–293, 1995.

[135] B. A. Johnson and R. A. Blevins, “NMR View: A computer program for the visualization and analysis of NMR data,” *J. Biomol. NMR*, vol. 4, no. 5, pp. 603–614, 1994.

[136] W. Lee, M. Tonelli, and J. L. Markley, “NMRFAM-SPARKY: enhanced software for biomolecular NMR spectroscopy.,” *Bioinformatics*, vol. 31, no. 8, pp. 1325–7, Apr. 2015.

[137] W. Kabsch, “XDS.,” *Acta Crystallogr. D. Biol. Crystallogr.*, vol. 66, no. Pt 2, pp. 125–32, Feb. 2010.

[138] A. T. Brünger, “Free R value: A novel statistical quantity for assessing the accuracy of crystal structures,” *Nature*, vol. 355, no. 6359, pp. 472–475, 1992.

[139] P. Evans, “Scaling and assessment of data quality.,” *Acta Crystallogr. D. Biol. Crystallogr.*, vol. 62, no. Pt 1, pp. 72–82, Jan. 2006.

[140] A. J. McCoy, R. W. Grosse-Kunstleve, P. D. Adams, M. D. Winn, L. C. Storoni, and R. J. Read, “Phaser crystallographic software,” *J. Appl. Crystallogr.*, vol. 40, no. 4, pp. 658–674, 2007.

[141] P. D. Adams *et al.*, “PHENIX: a comprehensive Python-based system for macromolecular structure solution.,” *Acta Crystallogr. D. Biol. Crystallogr.*, vol. 66, no. Pt 2, pp. 213–21, Feb. 2010.

[142] P. Emsley, B. Lohkamp, W. G. Scott, and K. Cowtan, “Features and development of Coot.,” *Acta Crystallogr. D. Biol. Crystallogr.*, vol. 66, no. Pt 4, pp. 486–501, Apr. 2010.

11. Acknowledgments

Since I am not able to mention everyone, I would like to thank everyone who isn't in the acknowledgments for the support during these years of my PhD thesis.

I gratefully thank my supervisor Dr. Silke Wiesner for the opportunity to work on such an interesting project. Moreover, I am very glad for the scientific support and discussions that Dr. Silke Wiesner was given me during this time.
I want to thank my TAC committee for following my progress over time, especially Prof. Dr. Thilo Stehle for agreeing to be my university PhD supervisor and his support over this last years.

Special thanks to my examiner Prof. Dr. Dirk Schwarzer, not only for being an examiner, but also for the collaboration on the Sortase project together with Dr. Lena Schmohl.

In addition, I would like to thank Prof. Dr. Frank Böckler who agreed to be my examiner and the nice conversation in his office about my thesis.

I would also like to thank everyone who was involved in generating the data for this thesis:

- Dr. Simona Polo and Dr. Elena Maspero for the successful collaboration.
- Dr. Luisa Ströh not only for the X-ray support ☺.
- Dr. Ancilla Neu for X-ray and lab support.
- Dr. Iris Holdermann for X-ray and lab support.
- Dr. Marcus D. Hartmann for X-ray and SAXS support.
- Dr. Vincent Truffault for NMR support.

Also, I want to mention the help that I received from Dr. Dagmar Sigurdardottir for the discussions and advice. Moreover, Dr. Andrei Lupas for financial support during the last 6 months and allowed me to stay in the MPI until this thesis was finished.

Furthermore, I thank all the members of the group from Remco Spranges and Silke Wiesner for the help that I received and the familiar and cooperative atmosphere.

- Mira and Samira for the lab support.
- Carsten for all the very big favors in the last 9 month and for continuing the project ☺.
- Philip (Der Kleine) for the discussions, talks and prove reading.
- Philip for the help with the NMR, PRE-data and all the other stuff, also the legendary evenings with Maxime ☺.
- Maxime ……. Jacques I think I do not have to say more.
- Anna, Stefan, Jan for all the comments and discussions either job-related or private.
- Jonas thx for the cloning and lab work, you did an awesome job!

Finally, thanks to the "coffee gang" Daniela and Fabi.
They helped me over the last 6 months with …… a lot and coffee. THANK YOU GUYs*innen.
The Schrödinger Coffee: The coffee can be hot or not hot until you try you will not know.

Thanks to all of you for the support, help and time we spent together.

##########

Hier möchte ich meiner Familie danken, für deren Unterstützung, die weit bevor diese Arbeit ihr Ende fand, begann.
Vielen lieben Dank an meine Eltern für die Nerven, die Ihr gebraucht habt. Ich hoffe es wird jetzt besser. Danke an meine Brüder Valentin und Felix für…. dass Ihr meine Brüder seid und mir bei jedem „Scheiß“, den ich gemacht habe, geholfen habt, auch wenn es noch so bescheuert war.
Danke an Kerstin für die legendären Abende im Familienkreis (ich sag nur: der Waschmaschinenkalender).
An meinen Neffen: Lieber Benno, danke, dass du da bist! ich freu mich riesig darauf, dir alles möglich beizubringen, was mein Bruderherz nicht so toll findet ☺ zB. -Wäsche, Müll Recycling- oder -Wir sollten ins Krankenhaus und das nähen lassen, aber es wächst sicher auch so zusammen- nach den großen Philosophen in der Familie Jäckl.

An Helen + Nick & Jona, Julia, Christian + the Kids, Daniel, Deike, Kilian, Jacqui, die Sport Gang: Dennis, Felix, Valentin, Michi, Iki, Stephi, ….. , die Wein Tasting Crew: Nadine, Daniela, Philip, Martina, Maxime, Aoifa, Annamaria ….. die Schwarzer Gruppe: Julia, Jan, Sören, Julian, Niki (jup, ich weiß, zähl dich aber mal zu den Schwarzers)…. Danke für die Zeit, die Gespräche, den Sport und die Hilfe in jeder Lebenslage.

Zuletzt möchte ich einer Person danken, die mir in den letzten 3 oder 4 Jahren (so einig sind wir uns da nicht ☺) zu einem entscheidenden Teil meines Lebens geworden ist. Ohne sie wäre das hier alles sicher anders verlaufen. Es ist für mich immer noch unfassbar und ich kann es nicht wirklich in Worte fassen, wie glücklich ich bin, dich Teil meines Lebens nennen zu dürfen.

-Vielen lieben Dank, Lena-